Cysteine proteases and their inhibitors in microbe - maize root interactions

Inaugural-Dissertation

zur
Erlangung des Doktorgrades
der Naturwissenschaften
(Dr. rer. nat)

der Mathematisch-Naturwissenschaftlichen Fakultät
der Universität zu Köln
vorgelegt von

Jan Schulze Hüynck
aus Stevede

Köln, 2019

Cysteine proteases and their inhibitors in microbe - maize root interactions

Inaugural-Dissertation

zur
Erlangung des Doktorgrades
der Naturwissenschaften
(Dr. rer. nat)

der Mathematisch-Naturwissenschaftlichen Fakultät
der Universität zu Köln
vorgelegt von

Jan Schulze Hüynck
aus Stevede

Köln, 2019

Die Untersuchungen zur vorliegenden Arbeit wurden von Oktober 2015 bis Juni 2019 am Lehrstuhl für Terrestrische Mikrobiologie an der Universität zu Köln unter der Betreuung von Herrn Prof. Dr. Gunther Döhlemann durchgeführt.

He that breaks a thing to find out what it is
has left the path of wisdom.
J.R.R. Tolkien (1892-1973)

All fungi are edible.
Some fungi are not edible more than once.
Terry Pratchett (1948-2015)

Zusammenfassung / Abstract

Zusammenfassung

Pflanzen sind dauerhaft in Kontakt mit einem breiten Spektrum von Mikroben, die zu gutartiger Symbiose oder desaströsen Krankheiten führen können. Proteasen agieren als Regulatoren in vielen Prozessen der Pflanzenzelle, wie der Samenentwicklung, Immunreaktion, Seneszenz und programmierten Zelltod (PCD). Apoplastische Papain-ähnliche Cysteine Proteasen (PLCPs) sind Knotenpunkte in der Pflanzen-Mikroben Interaktion. Der Apoplast wird unter anderem von sogenannten Endophyten bevölkert und stellt eine entscheidende Grenzfläche für Interaktionen zwischen Pflanzen und Mikroben dar. Bisher wurden hauptsächlich apoplstische Mais PLCPs in oberirdischen Pflanzenteilen beschrieben.

Um zu ergründen, ob PLCPs in organspezifischen Immunreaktionen involviert sind, konzentriert sich diese Studie auf PLCPs des Wurzel-Apoplasten. Mittels eines proteomischen Ansatzes wurden PLCPs nach Salizylsäure (SA) -Behandlung verglichen um Unterschiede zwischen den enthaltenen apoplastischen PLCPs von Blättern und Wurzeln zu untersuchen. Hierbei wurden mehrere wurzel-spezifische PLCPs identifiziert. Biochemische Charakterisierung zeigte, dass sich diese PLCPs aufgrund ihrer Substratspezifität und Inhibitor Anfälligkeit unterscheiden. Mittels Aktivitäts-basierter Protein Markierung (ABPP) konnten drei SA-assoziierte PLCPs identifiziert werden. Diese Ergebnisse lassen vermuten, dass PLCPs eine organspezifische Rolle in der SA-assoziierten Immunantwort spielen.

In einem weiteren Ansatz wurden endophytische Maiswurzel-Bakterien und -pilze untersucht und vier Bakterien identifiziert, die einen PLCP Inhibitor sekretieren. Eines dieser Bakterien ist nötig für die Stabilität einer kleinen synthetischen Bakterien-Gemeinschaft, was eine stabilisierende Funktion für PLCPs in der Gemeinschaft vermuten lässt. Weitere Tests zeigten, dass es sich bei dem Inhibitor wahrscheinlich um ein Protein handelt. Um diesen Inhibitor zu identifizieren, wurde eine Blast-Suche nach Homologen zu bekannten PLCP Inhibitoren und Motiven durchgeführt. Hierbei konnte kein Homolog identifiziert werden, allerdings wurden Kandidaten entdeckt, die ein Inhibitor-Motiv enthalten.

In dieser Studie wurden Wurzel-spezifische PLCPs charakterisiert und Unterschiede zwischen der SA-assoziierten Aktivierung von PLCPs in Blättern und Wurzeln aufgezeigt, was eine organspezifische Rolle der PLCPs in der Immunreaktion implizieren könnte. Außerdem deuten unsere Ergebnisse darauf hin, dass bakterielle PLCP Inhibitoren nicht nur eine wichtige Rolle für die Interaktionen zwischen Pflanzen und Mikroben, sondern auch für die Ausprägung und Stabilität von Pflanzen assoziierten bakteriellen Gemeinschaften spielen.

Abstract

Plants are associated with a broad spectrum of microbes and the outcome in plant-microbe interactions ranges from beneficial symbiosis to destructive diseases. Plant proteases are key regulators of plant cell processes such as seed development, immune responses, senescence and programmed cell death (PCD). Apoplastic papain like cysteine proteases (PLCPs) are hubs in plant-microbe interactions. The apoplast can be inhabited by so-called endophytic microorganisms and displays a crucial interface for the interaction between plant and microbes. So far, apoplastic maize PLCPs and their function have been mostly described for aerial plant parts.

This study focused on PLCPs in the root apoplast of maize and aims to investigate whether PLCPs are involved in organ specific defense processes. A proteomics approach was used to study differences in PLCP content after salicylic acid (SA) treatment between leaf and root apoplast. This approach identified nine additional root specific PLCPs. Biochemical analysis of recombinant PLCPs revealed different substrate specificities and inhibitor affinities between these proteases. Using activity-based protein profiling (ABPP), three root-specific SA-activated PLCPs were identified. This result suggests organ-specific involvement of single PLCPs in SA-associated defense responses.

We hypothesise that PLCPs are involved in the first steps of plant defense and need to be overcome by endophytes to develop a mutualistic interaction with the host plant. To address this hypothesis, a screening of bacteria and fungi from maize root-endophytes able to inhibit PLCPs was performed. Four bacteria were identified that secrete inhibitors of maize PLCPs. One of these bacteria is known for its hub function to stabilize a small synthetic community of root bacteria, suggesting that PLCPs are involved in stabilizing this community. Further tests indicate that the secreted inhibiting compounds to be effector proteins. To identify these inhibitors, a blast search for putative PLCP inhibitor motifs and homologs to known PLCP inhibitors was performed. This blast search did not identify sequence homologs to known PLCP-inhibitors, but revealed putative inhibitors containing an inhibitor motif.

This study characterized maize root-specific PLCPs and determined differences between SA-dependent activation of PLCPs in roots and leaves, suggesting PLCPs to be involved in organ specific SA-related defense responses. Additionally, our results suggest that bacterial PLCP inhibitors play a role in plant-microbe interactions and might also be involved in shaping and stabilizing of plant associated microbe communities.

List of abbreviations

°C	Degree Celsius
aa	Amino acid
Arg	Arginine
ATP	Adenosine triphosphate
bp	Base pairs
BSA	Bovine serum albumin
Carb	Carbenicillin
cDNA	Complementary DNA
CDS	Coding sequence
CV	Column volume
Cys	Cysteine
DAMP	Damage-associated molecular pattern
DMSO	Dimethylsulfoxid
DNA	Deoxyribonucleic acid
dai	days after infiltration
dpi	days post infection
DTT	Dithiotreitol
EDTA	Ethylenediaminetetraacetic acid
EGB	Early golden bantam
ETI	Effector-triggered immunity
EtOH	Ethanol
ETS	Effector-triggered susceptibility
f.c.	Final concentration
Gent	Gentamycin
Gln	Glutamine
$H_2O_{bid.}$	Double distilled water
His	Histidine
hpi	hours post infection
HR	Hypersensitive response
IPTG	Isopropyl-B-D-thiogalactopyranoside
JA	Jasmonic acid

kb	Kilobases
kDA	Kilodalton
LAF	Leaf apoplastic fluid
LRR	Leucine rich repeat
mA	Milliampere
MAMP	Microbe-associated molecular pattern
MeOH	Methanol
MgCl$_2$	Magnesium chloride
min	Minute(s)
ml	Millilitre
MoClo	Modular cloning
NLR	Nucleotide-binding/leucine rich repeat
nm	Nanometer(s)
OD	Optical density
OD$_{600}$	Optical density at 600 nM
O/N	over night
PAGE	Polyacrylamide gel electrophoresis
p	Statistical probability value of false positive results
PAMP	Pathogen-associated molecular pattern
Pit2	Protein involved in tumours 2
PLCP	Papain-like cysteine protease
PTI	Pattern-triggered immunity
qRT-PCR	Quantitative real-time polymerase chain reaction
R protein	Resistance protein
RAF	Root apoplastic fluid
Rif	Rifampicin
RNA	Ribonucleic acid
ROS	Reactive oxygen species
RE	Root exudates
rpm	Rounds per minute
SA	Salicylic acid
SAR	Systemic acquired resistance
SEC	Size exclusion chromatography
SDS	Sodium dodecyl sulfate
TE-buffer	Tris-EDTA buffer solution

TEMED	Tetramethylethylenediamine
U	Unit of enzyme activity
V	Volt
v/v	Volume/volume
w/v	Weight/volume
X-Gal	5-bromo-4-chloro-3-indolyl-β-D-galactopyranoside
$\times g$	$\times$ Gravitational acceleration on earth $(9.81 \frac{m}{s^2})$
µg	Microgram
µl	Microliter
µM	Micromolar
µm	Micrometer
Clm	Chloramphenicol
g	Gram
h	Hour
HR	Hypersensitive response
HRP	Horseradish peroxidase
NTA	Nitrilotriacetic acid
mm	Millimetre
s	Second(s)
Strep	Streptavidin
M	Molar
PCR	Polymerase chain reaction
DMF	Dimethylformamid
YT	Yeast extract tryptone
RT	Room temperature
A	Ampere
SDS-PAGE	Sodium dodecyl sulfate polyacrylamide gel electrophoresis
APS	Ammonium persulfate

Table of content

List of Figures

List of Tables

1 Introduction

1.1 The plant immune system

Animals and plants are in constant contact with microorganism including pathogens but differ in their lifestyles. Animals are motile and possess an immune system based on antibodies and mobile immune cells. They are able to redirect immune related cells to the side of pathogen attacks. Plants on the other hand are sessile and do not possess mobile immune cell components. Therefore, plants rely on innate defense mechanisms. The first physical barriers plants developed to prevent unwanted interactions are spikes, leaf hair and a cell wall reinforced by lignin deposition. A waxy cuticula, solemnly built of epidermal cells, does not only provide protection towards microbial colonization but also provides protection towards drought stress and other abiotic stresses (Dangl et al., 2001; Hückelhoven, 2007; Koeck et al., 2011). Apart from these physical protection mechanisms, plants also offer a wide repertoire of antimicrobial secondary metabolites, saponins, glucosinolates, cyanogen glycosides and unsaturated lactones as chemical defense agents against unwanted microbial interactions to inhibit microbial growth (Osbourn, 1996).

Due to their lack of mobile immune cells, each plant cell on its own needs to be able to identify pathogens as such and elicit appropriate immune responses. Plant immunity therefore consists of an innate, multi-layered inducible immune system. The first layer is based on recognition of evolutionary highly conserved molecular structures associated to microbes, herbivores and damage. The so-called microbe-associated molecular patterns (MAMPs), herbivore-associated molecular patterns (HAMPs) and damage-associated molecular patterns (DAMPs) are recognized by specific receptor like proteins and receptor like kinases (1.1) (Boller et al., 2009a; Dodds et al., 2010; Zipfel, 2014; Couto et al., 2016). This first recognition of microbes by MAMPs, HAMPs and DAMPs with the associated first immune reaction is called the PAMP-triggered immunity (PTI) (Jones et al., 2006).

Two well-known and -described examples of PTI elicitors of the model plant *Arabidopsis thaliana* are flg22, which is part of the flagellin of the bacterial flagellum, and elf18, which is a part of the bacterial elongation factor elongation factor thermos unstable (EF-Tu). Both molecules are sensed by the leucine-rich repeat receptor like kinases (LRR-RLKs) flagellin sensing 2 (FLS2) and EF-Tu receptor (EFR), respectively (Gomez-Gomez et al., 2000; Zipfel et al., 2006).

Yet, other membrane-bound receptors are responsible for the perception of DAMPs, which are endogenous plant signal molecules (Chisholm et al., 2006; Boller et al., 2009a; Boller et al., 2009b). DAMPs are released upon pathogen attack or damages induced by herbivory attacks. Cytoplasmic

proteins as well as cell wall components can act as DAMPs and elicit a non-infectious immune response. For example, the DAMP-receptor wall-associated kinase 1 (WAK1), which contains an epidermal growth factor-like (EGF) ecto-domain, can sense oligogalacturonat, the main component of pectin (Brutus et al., 2010). Besides, perception of the endogenous peptides ATPep1-6 which are released upon pathogen attacks leads to an amplification of the plant immune reaction (Huffaker et al., 2011).

PTI mechanisms can be divided into two differing parts. The so far described part represents fast mechanisms occurring within minutes and includes H^+- and Ca^{2+}- influx through the plasma membrane (1.1). Ca^{2+} acts as an intracellular secondary messenger and activated calcium-dependent protein kinases (CDPKs) and mitogen activated protein kinase (MAPK) cascades that regulate innate immunity of the cell (Doehlemann et al., 2008; Cheval et al., 2013; Seybold et al., 2014; Lee et al., 2015; Couto et al., 2016). MAPKs are also responsible for direct activation of reactive oxygen species (ROS) producing NADPH-oxygenases (Seybold et al., 2014). Signals released upon PTI can be amplified by phytohormones to enhance immunity (Pieterse et al., 2012; Couto et al., 2016). This is done mainly by salicylic acid (SA), jasmonic acid (JA) and ethylene (Et) (Conrath et al., 2015). SA and JA induce the production of antimicrobial secondary metabolites, accumulation of pathogenesis related (PR) proteins, like chitinases and glucanases as well as the induction of callose and lignin synthesis to enhance cell wall stability (Gómez-Gómez et al., 1999; van Loon et al., 2006; Conrath et al., 2015).

During co-evolution and through tight contact with their host, pathogens specialized and gained the ability to overcome the first line of defense responses by production of the so-called effector proteins. Effectors are secreted into the apoplastic space, passively taken up or directly injected into the host plant (1.1) (Panstruga et al., 2009; Stergiopoulos et al., 2009; Di et al., 2016). Pathogens use their effector repertoire to manipulate immune responses and to suppress PTI. This immune repression results in the so-called effector-triggered susceptibility (ETS) of the host plant. Plants, on the other hand, established mechanisms to tackle ETS by developing resistance proteins (R-proteins) that sense effectors which are then referred to as avirulence proteins (Avrs). R-proteins target to neutralize Avr effects and induce a secondary improved immune reaction, the effector triggered immunity (ETI) (Jones et al., 2006). This ETI is usually a stronger immune response compared to PTI and recent studies suggest it to be a reactivated and enhanced PTI reaction (Kadota et al., 2019). This amplification of the PTI leads in many cases to a hypersensitive response (HR) and local programmed cell death (PCD) of infected tissue. Apart from local effects, an infection can lead to systemic acquired resistance (SAR) in tissues and organs distant to the place of infection. This SAR primes plants for attacks of pathogens of the same type as the SAR inducer throughout the plant and enhances resistance (de Wit, 2007; Klessig et al., 2018).

The biggest class of R-proteins are the nucleotide-binding site leucine-rich repeat receptors (NB-LRRs) (Dangl et al., 2001; Cui et al., 2015). They contain a nucleotide binding site, a leucine-rich repeat showing similarity to RLKs and variable N- and C-termini. NB-LRRs can be divided into two large subfamilies which are defined upon their N-terminal domains (Dangl et al., 2001). The presence of a dicotyledonous specific toll/interleuin-1-receptor (TIR) domain at the N-terminus brands them as TIR-NB-LRRs (TNLs) while presence of a coiled-coil (CC) -domain, which can be found among dicotyledons as well as monocotyledons, labels them as CC-NB-LRRs (CNLs) (Dangl et al., 2001; Gay et al., 2007; Jacob et al., 2013). Plants and animals contain intracellular immune NOD-like-receptors (NLRs) which sense pathogens and lead to local PCD (Duxbury et al., 2016). Recently, the formation of the "resistosome" by the *A. thaliana* NLR receptor Hopz-activated resistance 1 (ZAR1) was reported. In an ATP-dependent manner ZAR1 oligomerized into a pentameric wheel-like structure, forming the "resistosome" which localizes to the plasma membrane where it might create pores in membranes (1.1) (Wang et al., 2019a; Wang et al., 2019b).
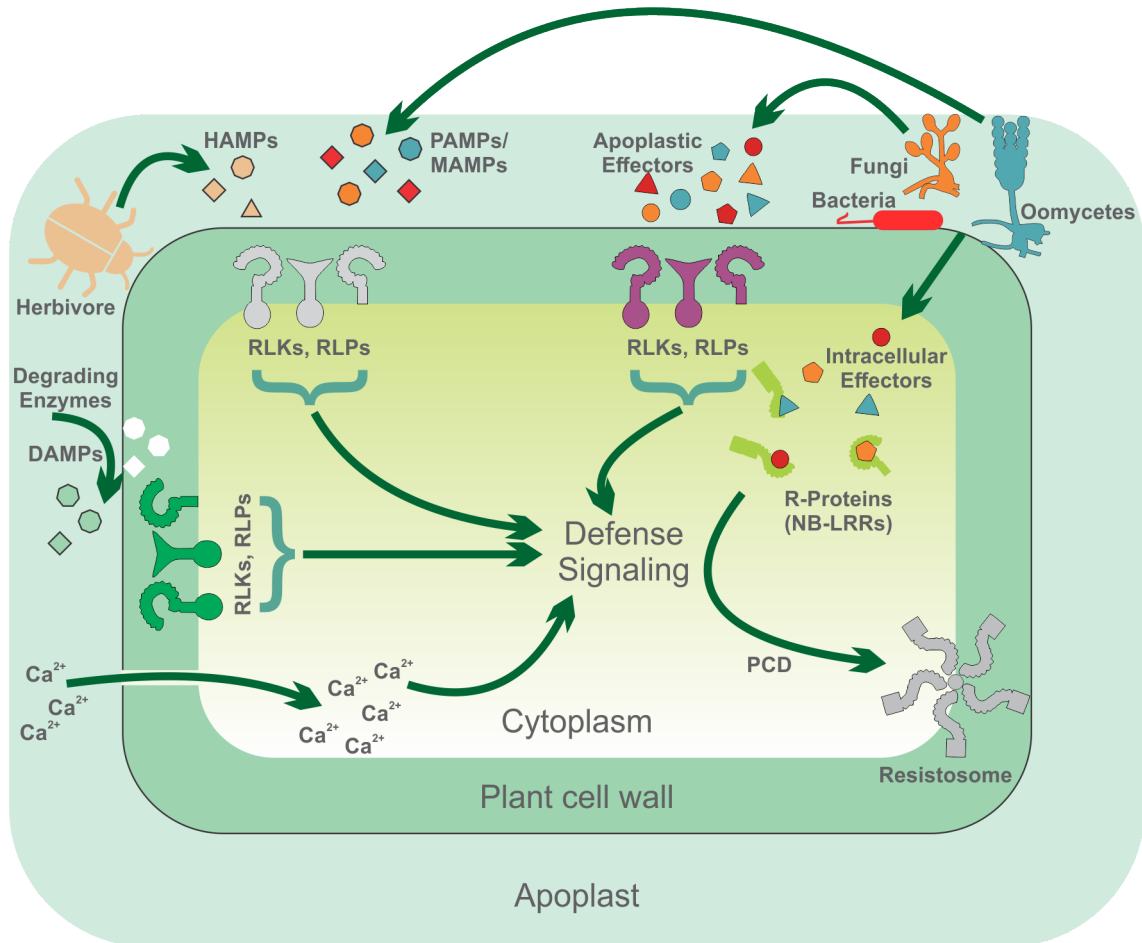
Figure 1.1: **General mechanisms and components of plant immunity.**
Damage-, herbivore-, pathogen-, and microbe-associated patterns (DAMPs, HAMPs, PAMPs, MAMPs, respectively) and effectors are sensed by plants and associated to threats. Perception via receptor-like kinases (RLKs), receptor-like proteins (RLPs) and Ca^{2+} influx induces downstream defense signaling. Pathogen perception via nucleotide-binding-site-leucine-rich repeat (NB-LRRs) resistance (R) proteins leads to formation of the resistosome and associated PCD. (modified from Boller et al., 2009a)

Perception of pathogens with the plant immune system was long based on the gene-for-gene hypothesis (Flor, 1971) that postulates a direct interaction of an Avr with a corresponding R-gen (Jia et al., 2000). This hypothesis was proven inaccurate for various plant-pathogen interactions. It has been described that effector proteins can also be indirectly targeted by NBS-LRRs, which is referred to as the guard-model. The guard-model describes the interaction of an effector with a guard-protein that is recognized by a receptor inducing a downstream immune reaction after recognition (Dangl et al., 2001). As a consequence of high stress through effectors, the plant effector targets are under a high selective pressure which lead to gene duplications (Plissonneau et al., 2017; Rajaraman et al., 2018). These duplicated genes do not fulfill their intrinsic function but act as a bait for the effectors preventing them to interact with their initial target and thereby hinder effectors in plant immunity manipulation. This mechanism was described in the decoy-hypothesis (van der Hoorn et al., 2008; Bernoux et al., 2014; Wu et al., 2015). One well-studied example for the decoy-model is the cysteine protease Rcr3 from tomato plant, *Solanum lycopersicum*. Rcr3 is a PR-protein that is translocated into the apoplast upon infection of various pathogens or SA application (Rooney et al., 2005; Shabab et al., 2008; Song et al., 2009). The Avr2 effector of the fungal pathogen *Cladosporium fulvum* targets and inhibits Rcr3 as well as the *S. lycopersicum* cysteine protease PIP1. Interestingly, it was found that the inhibition of Rcr3 through Avr2 itself does not enhance the virulence of the pathogen. It was shown that the interaction of Rcr3 and Avr2 is monitored by the tomato protein Cf-2 (Rooney et al., 2005) which then transmits an immune response. In this case, Rcr3 acts as a decoy for Avr2, which interaction is monitored by Cf-2 followed by the identification of the pathogen and respective immune activation (Dixon et al., 2000).

The previously described repertoire of immunity related proteins as well as the complexity of interaction and the guard-decoy-examples emphasize the continuous strife between host and pathogen. This competition and the resulting development of always novel effector proteins on the pathogen side to enhance virulence as well as the development of corresponding R-proteins to counter virulence is described as an evolutionary "arms race" and visualized by the Zig-Zag-model (Jones et al., 2006).

1.2 Hormonal control of immunity

Phytohormones are plant derived organic compounds playing crucial regulatory functions and acting as signal transmitter in growth, plant development, reproduction, maturation and immunity. The most prominent and important pythohormones are absisic acid (ABA), auxin, brassinosteroids (BR), cytokines, JA, SA, Et as well as gibberellic acid which are involved in various developmental processes (Mok et al., 2001; Fujioka et al., 2003; Rai et al., 2011; Rodrigues et al., 2012; Li et al., 2016). As well as for SA, JA and Et studies stated important functions in immunity for gibberilic acid, ABA, auxine, cytoxines and BRs (Robert-Seilaniantz et al., 2011). Flg22 and the brassinosteroid brassinolid (BL), that is sensed by interaction with the receptor brassinosteroid insensitive 1 (BRI1), elicit distinct, non-overlapping immune reactions. If wild-type plants of the host *A. thaliana* are treated simultaneously with flg22 and BL, one can observe a reduced PTI-reaction compared to a single treatment with flg22 (Lozano-Durán et al., 2013). These results suggest a one-sided negative crosstalk between PTI and BRs, which leads to the so-called trade-off between growth and immunity. The molecular background of this cross-talk remains elusive, but it could be shown to be independent of the shared co-receptor bri1-associated receptor kinase 1 (BAK1) and direct phosphorylation of fls2 (Albrecht et al., 2012). These independencies indicate that the cross-talk takes place downstream of BAK1 in the signal cascades (Lozano-Durán et al., 2013; Lozano-Durán et al., 2015).

The crosstalk between different plant signaling pathways allows plants to react fast, highly specific and energy efficient to a pleiotropy of combinations of biotic- and abiotic stresses. Tight communication between defense responses for specific types of biotic stresses with each other as well as with other traits, like plant growth offers the plant an enormous and fast regulatory capacity to fine-tune resources used for immunity and growth depending on specific biotic and abiotic situations. The two main actors in fine-tuning of specific immune reactions are SA and JA (Pieterse et al., 2012; Yang et al., 2015).

Jasmonic acid and several of its derivatives are lipid-based compounds fast synthesized upon herbivore and necrotrophic pathogen attack via the oxylipin-synthesis signal pathway (Gfeller et al., 2010). Jasmonate can be metabolized to various isoforms of which the conjugation to the amino acid isoleucine, JA-Ile, is one of the biologically most potent enantiomers (Pieterse et al., 2012). The F-box protein coronate insensitive 1 (COI1) is a molecular key regulator of JA-signaling together with proteins of the jasmonate zim (JAZ) family. Both are part of the E4 ubiquitin ligase SKP1-cullin-F-Box-complex SCF1COI1 and JA-Ile receptors (Yang et al., 2009; Sheard et al., 2010). JAZ proteins are transcriptional repressors that bind to and negatively regulate JA-transcription factors. JA-Ile can disrupt the direct interaction between JAZ proteins and the transcription factors which leads to positive regulation of transcription. JA-mediated COI1-recruitment of JAZ towards the SKP1-complex causes to ubiquitin-mediated proteasome-degradation, which in turn leads to an

activation of several known JA marker genes (Pieterse et al., 2012). Among these marker genes are PDF1.2 and ERF1, which gene products exhibit anti-fungal activity (Penninckx et al., 1996; Lorenzo et al., 2003). JA accumulation in the plant cell occurs mostly as a response towards the presence of necrotrophic pathogens (Kunkel et al., 2002; Glazebrook, 2005). As necrotrophic pathogens need dead plant material as a nutrient source they are known for their secretion of enzymes and toxins aiming to kill host plants and mobilize nutrients (Hancock et al., 1981; Glazebrook, 2005). In contrast to this lifestyle, biotrophic pathogens are constrained to living host tissue to fulfill their life cycle. This contrasting lifestyle from necrotrophic pathogens makes it necessary for the plant to use different defense mechanisms aiming to locally kill host cells in order to constrain biotrophic infections.

The JA antagonistic phytohormone SA and downstream signaling pathway are necessary components of effective defense against biotrophic pathogens (Hancock et al., 1981; Glazebrook, 2005). SA is a phenolic phytohormone that mediates host responses to microbial pathogens. SA can be synthesized via two distinct pathways both based on the precursor metabolite chorismate. Phenylalanine ammonia lyases (PALs) are involved in one of these synthesis pathways located in the cytosol while the other pathway relays on isochorismate synthase (ICS) (Wildermuth et al., 2001; Garcion et al., 2008; Pieterse et al., 2012). 90% of defense-related SA is derived from the plastid located ICS pathway (Garcion et al., 2008). Just recently, it was found that only two additional enzymes to ICS are required to generate cytosolic SA. Enhanced disease susceptibility 5 (EDS5) exports isochorismate from the plastid and the aminotransferase avrPphB susceptible 3 (PBS3) generates isochorismate-9-glutamate which then spontaneously decomposes to SA and 2-hydroxy-acryloyl-N-glutamate (Rekhter et al., 2019). Pathogen attack induces an increase of intracellular Ca^{2+}, which is a crucial sensor for activation of SA synthesis and SA signaling cascades (Du et al., 2009). The SA signal cascade is mainly regulated through non-expressor of PR genes 1 (NPR1) which is responsible for SAR and other SA-related processes (Cao et al., 1997; Kinkema et al., 2000; Dong, 2004; Ali et al., 2018). NPR1 is located in the cytoplasm as an oligomer which is formed by intermolecular, redox-sensitive disulfide bridges (Tada et al., 2008). SA-induced changes of the redox-potential inside the cell lead to monomerization of NPR1 which then diffuses inside the nucleus and acts as a transcription coactivator for many PR-genes with antimicrobial capacity like PR3 and PR5 (Dong, 2004; van Loon et al., 2006; Moore et al., 2011; Dolezal et al., 2014). Albeit direct interaction between SA and NPR1 could not be shown so far it was proposed that two paralogs, NPR3 and NPR4, are responsible for SA concentration dependent degradation of NPR1 oligomers (Fu et al., 2012). Recently, opposite roles as SA receptors were proposed for NPR1 and its paralogs NPR3 and NPR4 in transcriptional regulation of plant immunity. NPR1 functions as a transcriptional co-activator while NPR3/NPR4 function as transcriptional co-repressors and are inhibited by SA to promote downstream expression (Ding et al., 2018). Upon ETI, SA synthesis is locally activated leading to a SA-gradient from the infection

site towards adjacent tissues. High SA concentrations at the infection site promt an HR related cell death whereas lower SA levels in adjacent cells leads to the activation of SAR related genes, limiting the cell death to the infection site and increasing resistance in adjacent cells (Fu et al., 2012).

1.3 Plant proteases

Proteases determine a variety of biological processes ranging from meiosis, organ maturation, embryogenesis, storage and mobilization of storage compounds, senescence and programmed cell death (van der Hoorn et al., 2004a; van der Hoorn, 2008). Therefore, plant genomes contain hundreds of varying proteases. Besides the mentioned functions, proteases are key players in local and systemic immunity upon pathogen infections (van der Hoorn, 2008). Albeit their diversity and various strict regulatory mechanisms, all proteases perform the same cleavage of substrates into small fragments by catalyzing the hydrolysis of the peptide bond. The half-time of hydrolysis of a peptide bond in neutral aqueous solution takes several years and is reduced to milliseconds in the presence of a good protease (Drag et al., 2010). However, additional non-proteolytic functions such as the production of diverse cyclic peptides by asparaginyl endopeptidases (AEPs) were recently discussed (James et al., 2018). To prevent uncontrolled proteolytic activity at the site of enzyme production, proteases are produced as inactive zymogens (Beers et al., 2004). These are inactive enzymes that are only activated through maturation processes at specific locations or through specific triggers. Proteases can be divided into exopeptidases and endopeptidases, where the former only cleaves at the borders of proteins and where the latter cleaves peptide bounds inside of proteins. Proteases are classified into main classes according to their catalytic site, which performs the nucleophilic attack on the substrates carbonyl carbon: cysteine proteases, serine proteases, threonine proteases (forming covalent enzyme intermediates), aspartic proteases, and metalloproteases (not forming covalent enzyme intermediates) (van der Hoorn, 2008; Rawlings et al., 2018). Cysteine proteases are further subdivided into 14 super families, each using the catalytic triad or dyad in a different structural fold, representing convergent evolution of the catalytic mechanism (Rawlings et al., 2018). In this study we are focusing on papain-like cysteine proteases (PLCP).

1.3.1 PLCP activity and regulation

PLCPs are classified into clan CA based on their structural similarity to papain and conserved catalytic residues (Rawlings et al., 2018). They are divided into family C1B (cytosolic) and C1A (apoplastic) and further subdivided into nine subfamilies based on phylogeny (Richau et al., 2012). PLCPs are known to be involved in growth-related senescence (Noh et al., 1999a; McLellan et al., 2009), programmed cell death (Gilroy et al., 2007; Coll et al., 2011; Lampl et al., 2013), predicted to be important for resource acquisition (Adamczyk et al., 2010) and act as hubs in plant immunity, where they are involved in the perception of microbes, initiation of signaling cascades and activation of responses against pathogens (Misas-Villamil et al., 2008; Jashni et al., 2015; Misas-Villamil et al., 2016). PLCPs display several specific features (1.2A). They carry a signal peptide important for their transport to the apoplast as well as an inhibitory prodomain prior to the active C1-protease domain which is removed upon post-translational activation of the PLCP (Groves et al., 1996). In several subfamilies PLCPs carry the ERFNIN motif in the prodomain which provides the core structure of the prodomain (Karrer et al., 1993). The active site in the protease domain consists of the catalytic triad Cys, His, Asn and a N-terminal Gln. Some AALP-like proteases additionally carry an N-terminal NPIR sequence for vacuolar localization whether members of the CEP1-like subfamily might carry a C-terminal KDEL motif for endoplasmic reticulum (ER) localization. Some members of the subfamily 1 (RD21-like) and 4 (XBCP3-like) contain a proline-rich domain followed by a granulin domain sharing homology with granulins / epithelin, which are growth hormones in animals, released after wounding (Bateman et al., 1998; Bateman et al., 2009; Richau et al., 2012). PLCP cleavage preferentially occurs at peptide bonds C-terminally of hydrophobic amino acids as well as Arg at the P1 position bound to the enzymes S1 site (1.2B) (Schechter et al., 1967; Niemer et al., 2016; Paireder et al., 2017). Additionally the residue at the N-terminal P2-position has been previously identified to be crucial for PLCP cleavage efficiency (Turk et al., 1995; Paireder et al., 2016; Paireder et al., 2017).

A

B
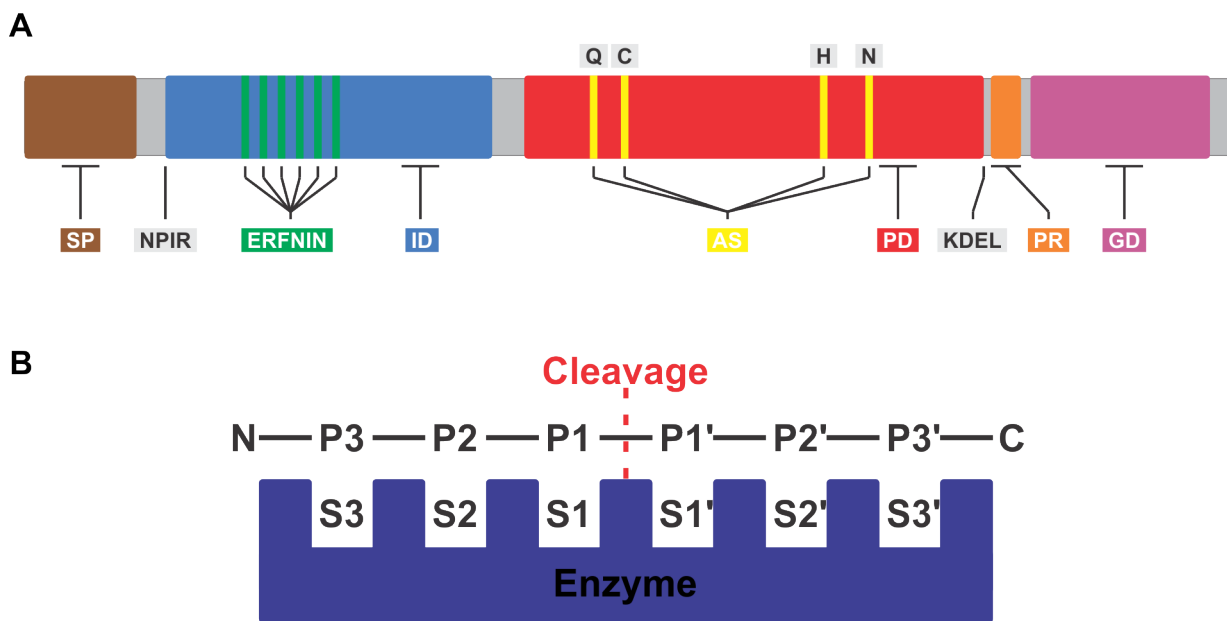
Figure 1.2: **Schematic structure of PLCP components.**
(A) Signal peptide (SP, brown), ERFNIN motif (green), inhibitory domain (ID, blue), protease domain (PD, red), active site (AS, yellow), proline-rich domain (PR, orange) and granulin domain (GD, purple) are shown in their relative position in PLCPs. NPIR and KDEL motifs indicating specific localization are indicated.
(B) S3-S3'-substrate binding sites within the enzyme active site. P3-P3'-substrate residues binding to the respective substrate binding sites. Cleavage occurs between P1 and P1'-substrate residues. Substrates N- and C-terminus are labelled respectevly. (modified from Schechter et al., 1967)

The general proteolysis mechanism can be divided into three steps. The first is the association of enzyme and substrate to form the enzyme-substrate complex. The second part is the actual cleavage of the peptide bound and the last part is composed of the dissociation of the complex and regeneration of the active enzyme (Michaelis et al., 1913). PLCPs contain the conserved catalytic triad Cys, His, Asn for proteolysis. The first step of their general enzymatic activity is a proton transfer from the thiol-group (acid) of the Cys to the imidazole-ring (base) of the His. The now de-protonated thiol-group of the Cys performs a nucleophilic attack at the substrate carbonyl-carbon and the double bond between the carbon and the oxygen converts to a single bond forcing the oxygen to accept an electron (1.3A). This forms the first tetrahedral intermediate. The oxyanion is stabilized by the Cys backbone and the NH-group of a Gln N-terminal of the Cys forming an oxyanion hole (Menard et al., 1991; Ménard et al., 1995; Otto et al., 1997) (1.3B). The protonated His is stabilized by the sidechain of an adjacent Asn and transfers a proton from the imidazole group via rotation to the N of the peptide bond which leads to hydrolysis and cleavage of the peptide bond. The new amine of the substrate is connected to the His through a hydrogen bridge (1.3C). In the next step, the substrate with an amino terminus is released and replaced by a water molecule. The acyl-enzyme complex is formed by a thioester bound between the thiol-group of the CYS and the carboxyl-terminus of the substrate. This thioester bond is hydrolyzed upon a nucleophilic attack of the oxygen of free water at the carboxyl-terminus carbon of the substrate (1.3D) generating a second tetrahedral intermediate (1.3E). This intermediate resolves in generation of a carboxyl-acid on the substrate and releases it while regenerating the thiol-group of the free enzyme (Menard et al., 1991; Otto et al., 1997) (1.3F).
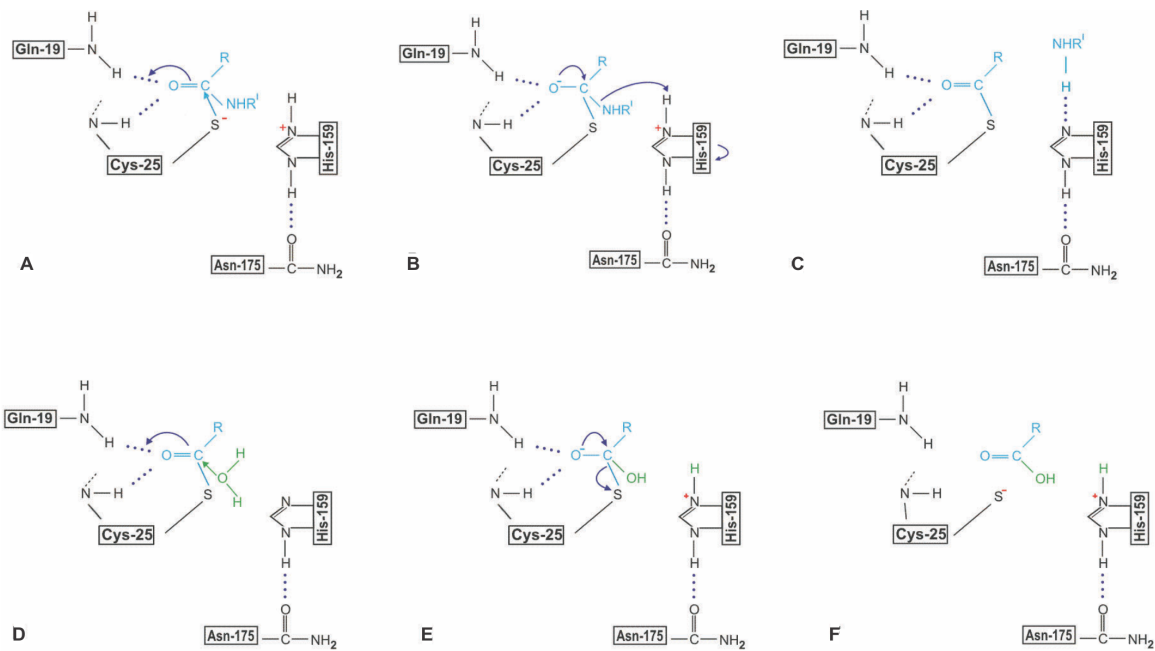
Figure 1.3: **Catalytic mechanism of cysteine proteinases.**
Description in text, (Rzychon et al., 2004)

Imbalanced and excessive activity of endogenous cysteine proteases is known to cause severe pathologies, such as osteoporosis and multiple sclerosis in humans or growth deficiencies in plants (Berdowska et al., 2000). Due to this danger of uncontrolled proteolytic activity and their crucial roles in the regulation of various cellular processes in plants, PLCP activity is tightly controlled at different levels. Regulation ranges from protease expression, secretion, and maturation through specific post-translational modifications, to blockage of the active site by endogenous inhibitors (Martinez et al., 2008; Ochieng et al., 2010; Martínez et al., 2012; van der Linde et al., 2012a; Lampl et al., 2013). Several mechanistically different groups of protease inhibitors evolved and serve various biological functions. Protease inhibitors are grouped by the MEROPS-database in inhibitor families named I1 – I93 (Rawlings et al., 2018). The prodomain inhibitors of PLCPs belong to the I29 inhibitor group and interact via their C-terminal segment with the mature enzyme (Rawlings et al., 2018). The C-terminal segment binds between the two domains of the enzyme by a short α-helix and their backbone covers the substrate binding site. This binding occurs in reverse order compared to the binding modes of substrates which leads to a blockage of the active site while preventing cleavage of the inhibitor (Fox et al., 1992; Coulombe et al., 1996; Wiederanders et al., 2003). Contrasting to this reversible mechanism, serpins (I4) bind covalently and distort the catalytic center of the protease. Serpins are known to inhibit serine proteases as well as cysteine proteases (Rawlings et al., 2018). Upon binding of the protease to a surface located target of the serpin, a conformational change occurs leading to a partial denaturation of the protease and disruption of its

catalytic center which inactivates the protease (Huntington et al., 2000; Stennicke et al., 2002). The inhibitory mechanism of serpins is therefore often referred to as the "mouse trap type" (Grosse-Holz et al., 2016). Another group of important cysteine protease inhibitors are the cystatins which are divided into the families of stefins, cystatins and kininogens (Otto et al., 1997; Grzonka et al., 2001). Cystatins are exocite binding inhibitors. They do not bind at the active site but adjacent to it and obstruct the access of the substrate to the enzyme without direct interaction with the catalytic center (Bode et al., 2000). Cystatins bind in a substrate-like manner but pointing away from the enzyme active site and thereby avoiding cleavage. Thus the cystatin remains intact and unprocessed bound to the enzyme (Stubbs et al., 1990).

Numerous biological processes in plants require cysteine proteases. Among them especially PLCPs serve crucial functions in different aspects and subcellular localizations during plant defense reactions. PLCPs are key players in microbe perception (Shindo et al., 2008; Misas-Villamil et al., 2016). They initiate signaling cascades and activate defense responses against a vast range of pathogens including herbivores (van der Linde et al., 2012a). For Papain, which is abundant in the latex of *Carica papaya*, it was shown that it gets activated upon wounding and inhibited the growth of lepidopteran larvae (Konno et al., 2004; Azarkan et al., 2006). The apoplast as one of the first interaction zones between plants and pathogens is an important organelle for effector perception and extracellular defense signalling. Cysteine proteases are one of the most abundant classes of proteases found in the plant apoplast. One example of an apoplastic PLCP is CathB which is a positive regulator of HR and contributes to basal resistance in *A. thaliana* (McLellan et al., 2009). In *N. benthamiana*, CathB is secreted into the apoplast where it is activated. A deficiency of CathB in *N. benthamiana* restricts PCD triggered by bacterial pathogens like *Pseudomonas syringae* and hydrogen peroxide (Gilroy et al., 2007; Cai et al., 2018). The role of PLCPs in plant defense is not restricted to the apoplast. The Arabidopsis PLCP RD21 is located in the vacuole, active in developmental senescence in leaves and released into the cytoplasm during PCD. *rd21* null mutant lines show reduced resistance to the necrotrophic fungal pathogen *Botrytis cinerea* (Shindo et al., 2012). Its activity is tightly controlled by the cytoplasmic serpin-like suicide inhibitor AtSERPIN1 by forming of a covalent complex with RD21 (Lampl et al., 2013). In addition, it was recently reported that RD21 acts as a negative regulator of a specific type of sphingolipid-induced cell death (Ormancey et al., 2019). AtCEP1 is a PLCP containing a C-terminal KDEL motif leading to an endoplasmic reticulum (ER) localisation and contributes to basal resistance upon infection with the fungal obligate biotroph *Erysiphe cruciferarum*. A putative cleavage site that would result in the loss of the KDEL motif was identified and may indicate an activity of AtCEP1 apart from ER-localisation (Howing et al., 2014; Howing et al., 2017). Just recently, HvPAP14, a *hordeum vulgare* PLCP was found to be ER, vesicular bodies and chloroplast localized, closely associated to the thylakoid membrane. HvPAP14, which was reported to cleave the large subunit of Rubisco, is proposed to be involved in normal turnover of chloroplasts and during leaf senescence (Frank et al., 2019). These

diverse functions of PLCPs in various cellular compartments during plant immunity underline their importance.

Due to their involvement in defense related processes, PLCPs are also feasible targets of plant pathogen effectors to hamper plant immunity. A striking example is the earlier mentioned Rcr3 which is targeted by unrelated plant pathogens. The fungal pathogen *Cladosporium fulvum* secretes Avr2 which inhibits Rcr3 in *S. lycopersicum* (Luderer et al., 2002). Rcr3 is also the target of other effectors such as the cystatin-like effectors EPIC1 and EPIC2B from the oomycete *Phytophthora infestans* (Song et al., 2009) or the allergen-like effector Gr-VAP1, secreted by the nematode *Globodera rostochiensis* (Lozano-Torres et al., 2012). The *S. lycopersicum* PLCP Pip1, which is closely related to Rcr3 is inhibited by EpiC2B and Avr2 (Tian et al., 2007; Shabab et al., 2008). Another target for inhibition of EPIC1 and EPIC2B is the *S. lycopersicum* PLCP C14 which is additionally targeted by the *P. infestans* effector AvrBlb2, preventing secretion of C14 into the apoplast presumably blocking its defense function (Kaschani et al., 2010; Bozkurt et al., 2011). Notably, also bacterial effectors interfering with plant PLCPs have been identified. The RD19 protease from Arabidopsis is relocated from mobile vacuole-associated compartments to the nucleus upon interaction with the bacterial type III effector PopP2 from *Ralstonia solanacearum* (Bernoux et al., 2008). Recently, SDE1 from *Candidatus liberibacter asiaticus*, the causative agent of citrus greening disease was shown to interact with various citrus PLCPs and displayed *in vitro* PLCP inhibition (Clark et al., 2018). The fact, that various kinds of microbes secrete effectors to target plant PLCPs underlines the importance of PLCPs in plant immunity to orchestrate interactions with microbes.

1.4 PLCPs in maize immunity

Maize belongs to one of the most important crop plants. It does not only play an important role for human consumption but also for the feeding of livestock and the production of biofuels as an alternative to petrol (FAO, 2012; Ranum et al., 2014). Different models predict that - due to climate - change the yield of maize might decrease up to 10% in some areas like Africa by 2055 (Jones et al., 2003). This loss has to be compensated by improvements in plant breeding and pest control. To be able to cope with pests, we need a better understanding of the interaction between plants and their associated microbes both, in the phyllosphere and the rhizosphere. Maize associates with a variety of microbes, which might lead to beneficial effects on plant growth such as the interaction with arbuscular mycorrhizal fungi (Subramanian et al., 2013; Bárzana et al., 2014). On the other side, interaction with microorganisms can result into tremendous damage on the plant such as the interaction with the biotrophic fungus *Ustilago maydis*, the causative agent of the corn smut which infects all aerial part of the plant (Christensen, 1963; Brefort et al., 2009) or the necrotrophic pathogen *Fusarium verticillioides*, the causative agent of maize ear- and kernel rot (Nayaka et al., 2009; Duncan et al., 2010; Picot et al., 2010). Most plants and microbes first interact via the apoplast, which contains different types of defense components such as proteases and toxic metabolites (Ökmen et al., 2016). The importance of maize apoplastic leaf PLCPs for plant immunity and during *U. maydis* infection in aerial part have been demonstrated in the past (1.4) (van der Linde et al., 2012a; Mueller et al., 2013; Ziemann et al., 2018). In maize, the basidiomycete fungus *U. maydis* suppresses an immune reaction by the production of Pit2, a secreted effector that inhibits the C14 related PLCPs CP1A and CP1B (Mueller et al., 2013). For this interaction, Pit2 is treated like a substrate by the PLCPs and acts as a molecular mimicry. Upon cleavage of Pit2, the underlying conserved microbial inhibitor of proteases (cMIP) is released which in turn yield an even enhanced inhibition of apoplastic maize PLCPs (Misas Villamil et al., 2019). These observations lead to the hypothesis that also root endophytes might use effector proteins containing motifs similar to cMIP to avoid the activation of PLCPs and overcome plant immune responses (Misas Villamil et al., 2019). Additionally, the endogenous cystatin CC9 acts as a compatibility factor through fungal activation of JA-related signaling pathways and thus inhibiting antagonistic SA-related signaling pathways including direct apoplastic PLCP inhibition (van der Linde et al., 2012a; van der Linde et al., 2012b). Further stressing the central role of apoplastic PLCPs in plant immunity was the identification of the endogenous peptide Zip1. This apoplastic peptide is released after cleavage of the propeptide PROZIP1 which needs the active PLCPs CP1 and CP2 after activation of SA-related immunity. Zip1 in turn leads to further activation of PLCPs and SA neogenesis (Ziemann et al., 2018).
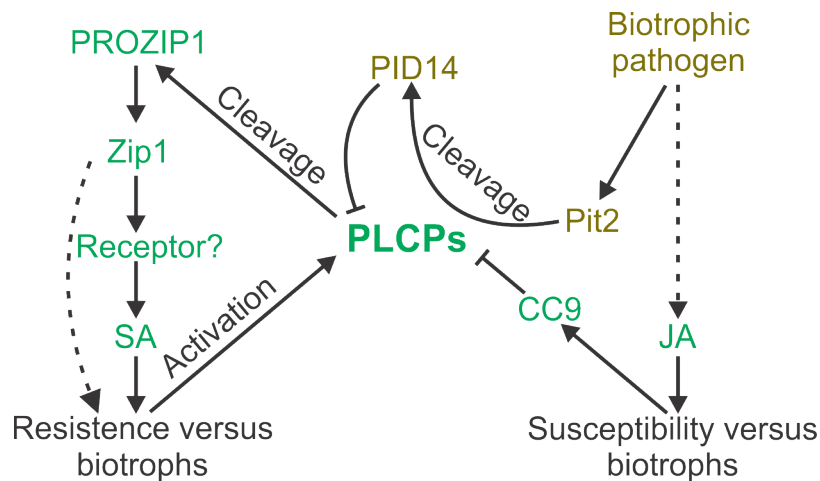
Figure 1.4: **Regulation of immunity in maize through modulation of PLCP activity.**
Induction of SA defense signaling activates apoplastic PLCPs which in turn release Zip1 from its pro-peptide PROZIP1. Zip1 binds to an unknown receptor and leads to an accumulation of SA which induces SA-signaling and enhances PLCP activity. The biotrophic pathogen U. maydis activates JA-signaling which leads to an induction of the endogenous PLCP inhibiting cystatin CC9. Additionally, the effector Pit2 is secreted by the fungus. Pit2 acts as a molecular mimicry and releases upon cleavage through PLCPs the inhibitory peptide PID14 inactivating plant PLCPs. (modified from (Eitzen et al., 2019))

In maize, PLCPs were also found to be involved in processes apart from the described SA-related defense responses. The maize PLCP Mir1 accumulates in vascular tissues upon herbivory wounding and increases resistance to caterpillars, root-feeding herbivores and aphids (Pechan et al., 2002; Gill et al., 2011; Louis et al., 2015). Most recently, the highly similar Mir1 paralog Mir3 was found to be active in leaf senescence (Pechan et al., 2002; Gill et al., 2011; Louis et al., 2015; Sekhon et al., 2019).

1.5 Plant-microbe interactions

In natural conditions, plants are in constant contact with a plethora of organisms that occupy important roles in plant growth and health. Plants form complex, intimate and dynamic communities with microorganisms above- and below ground, which have a strong impact on survival and fitness of all interacting partners. The plant-associated microbe collective (archeae, bacteria, fungi, protists and viruses) is termed as the microbiota while the term microbiome incorporates all microbial genomes (Bordenstein et al., 2015). The "holobiont" theory states that those host-microbe systems, being complex assemblages of diverse organisms, act as unique biological entities and are defined as "metaorganisms" or holobionts (Margulis et al., 1991; Rosenberg et al., 2007; Rosenberg et al., 2016). Studies on the functionality of plant-microbe interactions and factors involved in community assembly and maintenance will lead to a better understanding of plant-microbe holobionts and how plants benefit from their microbial partners.

Vascular plants host a variety of fungi. Plant roots are colonized by soil-borne pathogenic fungi but also by non-pathogenic or mutualistic fungi like arbuscular mycorrhizae (AM) or ectomycorrhizae (EM) which are mostly associated to woody plants (Osonubi et al., 1991). Mycorrhizal fungi solubilize nutrients from the soil to make them accessible for the plant and sequester harmful heavy metal ions to benefit the plant (Jakobsen et al., 1992; Fomina et al., 2005). In the past, fungi have been less studied as members of the microbiome whereas many studies have been carried out in human biology targeting especially the gut-microbiome (Garrett, 2017). These approaches have been transferred to other disciplines including plant biology. Plants offer microbiota several supportive micro-environments where it can be distinguished between the ectosphere and the endosphere. The ectosphere includes plant outer surfaces while the endospere consists of the inner plant tissues (Berg et al., 2014; Vandenkoornhuyse et al., 2015). Taking plant anatomy into consideration, it can be discriminated between above-ground and below-ground micro-environments. The aerial parts consist of the leaf phyllosphere, the fruit carposphere, the flower anthosphere and the seed spermosphere. Below ground level the root-microbiota complex forms the rhizospere, which is located at the interface between plant root and soil (Berg et al., 2014). Together with the rhizosphere, the phyllosphere is one of the most studied plant microbiota (Berg et al., 2014).

Plant bacterial microbiota comprise pathogenic, neutral and beneficial microorganisms. Some bacteria can cause disease symptoms through the production of phytohormones and phytotoxic compounds. *P. syringae* is a well-known example of a pathogen infecting a variety of hosts including tomato, olive, green bean and tobacco. Other examples for bacterial pathogens infecting crops as potato and banana are *Xanthomonas* and *Ralstonia solanacearum* and *Xylella fastidiosa* (Mansfield et al., 2012). The success and severity of plant disease depends on multiple factors, such as the plant resistance, environmental conditions, pathogen population size and biotic factors such as bacterial microbiota (Brader et al., 2017).

Above- and belowground microbiota have been shown to reduce disease severity either by commensal-pathogen interactions or by modulation of plant defense responses (Rudrappa et al., 2008; De Vrieze et al., 2018). Many examples are known for biocontrol activities against pathogen infection involving the production of antibiotics, lytic enzymes, volatiles and siderophores (Hopkins et al., 2017; Berg et al., 2018). Other biocontrol effects rely on modulation of the host hormone levels and induction of systemic resistance. Studies have shown that particularly bacteria of specific genera such as *Pseudomonas*, *Streptomyces*, *Bacillus*, *Enterobacter*, and *Burkholderia* have been involved in biocontrol and pathogen suppression (Gómez Expósito et al., 2017; Schlatter et al., 2017). It was also found that the invasion of *Fusarium* wilt, caused by *Fusarium oxysporum*, is controlled by three bacteria belonging to the taxa of Acidobacteria, Actinobaceria and Firmicutes (Trivedi et al., 2017).

Apart from protection from pathogenic infections, plant microbiota can also promote plant growth either directly or indirectly. Some bacteria are known for their production of phytohormones such as auxin, cytokinin or gibberellin which affect plant growth through modulation of plant hormonal levels. Additionally, strains of *Pseudomonas spp.*, *Arthrobacter spp*, *Bacillus spp.* and others have been reported to enhance plant growth through secretion of the enzyme 1-aminocyclopropane-1-carboxlate (ACC) deaminase (Glick et al., 1998; Compant et al., 2019). This enzyme reduces the concentration of the plant stress hormone Et, which can be produced from ACC and in turn lowers ethylene's negative effect on plant growth (Honma et al., 1978). In wheat and soybean several bacteria, including *Pseudomonas spp.*, have been identified to promote plant growth by phosphate solubilization, nitrogen fixation and other so far unclear mechanisms improving nutrient uptake and stress tolerance (Rascovan et al., 2016).

Above-ground plant tissues offer unique environments for endophyte and epiphyte interactions. Most endophytes spread systemically via the xylem to distinct plant compartments, like leaves, stem or fruit, although it was also shown that they can enter plant tissue through aerial compartments such as flowers or fruits (Compant et al., 2010; Compant et al., 2011). It was shown that phyllosphere bacteria are also recruited from the surrounding soil and shaped by the plant and environmental parameters (Vorholt, 2012; Zarraonaindia et al., 2015). As a consequence, it was observed that the microorganisms in the endosphere and phyllospere differ on the genus and the species level although an overlap of genera like *Pseudomonas* and *Bacillus* was reported (Campisano et al., 2014; Zarraonaindia et al., 2015). A recent study of the leaf microbiome across 300 maize lines found that the dominant taxa were sphingomonads and methylobacteria (Wallace et al., 2018). Additionally, they reported that the composition of phyllosphere bacteria is mainly driven by environmental factors. Several studies found the taxa of Pseudomonas as being predominant in the anthosphere of apple, almond, pumpkin, grapefruit and tobacco (Aleklett et al., 2014). Apart from Pseudomonas, the taxa of Enterobacteriaceae was found to be also dominant in the apple anthosphere (Steven et al., 2018). The spermosphere is not only related to the anthospere and carposphere but also to soil microbiota (Compant et al., 2010; Mitter et al., 2017; Glassner et al., 2018). Recently, the composition of seed microbiota has been revealed to be mainly comprised of Proteobacteria, Actinobacteria, Bacteroidetes and Firmicutes (Johnston-Monje et al., 2011; Liu et al., 2012; Barret et al., 2015). Generally, the members of the above-ground microbiota are derived from the soil, seeds and air and adapt to an endophytic or epiphytic life. This adaptation is mainly driven by environmental conditions.

At the root level, microbiota have strong impact on modulation of plant physiology and metabolism under various environmental conditions. Understanding the mechanisms underlying these modulations from the microbiota could be a breakthrough in sustainable agriculture for enhancing crop yield and quality (Berendsen et al., 2012). Due to these reasons, microbial diversity of root associated microbiota have been extensively studied after the definition of the core root bacterial microbiome of *A. thaliana* by Bulgarelli et al. (2012) and Lundberg et al. (2012).

Root microbiota are actively recruited by plants from surrounding microbial reservoirs. The main sources are the soil and the rhizosphere but also the phyllosphere, spermosphere and carposphere (Hardoim et al., 2015). Unlike the human gut microbiota, which is inherited from mothers to children, the root microbiota is mainly re-formed for each plant and each generation (Bai et al., 2015; van der Heijden et al., 2015). The source is mainly the soil environment, which is dominated by Proteobacteria, Actinobacteria, Bacteroidetes, Acidobacteria, Verrucomicrobacteria and Planctomycetes (Fierer, 2017). However, recent studies revealed the existence of seed bacterial microbiota that might be transferred vertically across plant generations (Liu et al., 2012; Shade et al., 2017). Unfortunately, knowledge about this vertically transferred microbiota remains limited.

The complex plant root system provides unique ecological niches for soil bacteria to colonize. Root associated microbes can be classified depending on their location relative to the root. Microbes of the rhizosphere are located outside of the root, including a narrow soil layer surrounding the roots. This area is considered a hot spot of microbial activity and one of the most complex ecosystems (Hiltner, 1994). Microbes of the rhizoplane directly inhabit the root surface and the endorhiza hosts the so-called endophytes living inside the root tissue (Berg et al., 2014). It has been shown for several plant models, including rice, maize and Arabidopsis, that the selection of plant root bacteria occurs at these locations (Peiffer et al., 2013; Schlaeppi et al., 2014; Edwards et al., 2015). An enrichment in microbial density was observed from bulk soil to rhizosphere with a loss of microbial diversity (Bulgarelli et al., 2012). The composition and density of the microbiome of each compartment is shaped by various effects to a different extend. Soil bacteria are the main source of the rhizosphere bacteria and have a huge impact on the composition of the rhizosphere members (Bonito et al., 2014; Vandenkoornhuyse et al., 2015). Additionally, abiotic factors such as pH, humidity and availability of minerals in the soil influence the rhizosphere bacteria (Fierer, 2017). The effect of the soil and soil bacteria is decreasing over the rhizoplane to the endorhiza. On the other hand, the plant is also actively shaping the composition and density of associated bacteria. Root-driven changes in the architecture of the bacterial community was observed for the wheat rhizosphere. A 10-fold higher abundance of Actinobacteria, Pseudomonads, Oligotrophs and Copiotrophs was found in the rhizosphere as compared to the bulk soil. These changes over time were limited to the rhizosphere and rhizoplane, whereas the bacterial composition of the bulk soil remained unchanged (Donn et al., 2015). Another microbe recruitment effect is due to root exudates (RE), which can be sensed by bacteria causing the so-called rhizosphere effect (Glick, 2012;

Mendes et al., 2013). RE are actively secreted molecules from plant roots into the rhizosphere. They consist of various compounds such as organic acids, amino acids, fatty acids, phenolics, plant growth regulators, nucleotides, sugars, sterols and vitamins and are known to affect the composition of root-associated microbiota (Badri et al., 2009). One example of RE sensing was observed for the rhizosphere of *Avena barbata*. It was reported that the combination of root exudate chemistry and bacterial substrate preferences affects the assembly patterns of the bacterial communities in the rhizosphere (Zhalnina et al., 2018). Furthermore, benzoxazinoids (BXs), a group of defense related secondary metabolites released by maize roots alters the composition of the bacterial rhizosphere communities. It was observed that Proteobacteria and Actinobacteria were strongest affected by BXs (Hu et al., 2018).

Besides from bacteria living and interacting with the plant from the outside, the plants inner tissue is also colonized by the so-called endophytic bacteria (Hallmann et al., 1997). Their entry inside the root tissue often occurs via passive processes by wounds or root cracks and emergence points of lateral roots as well as by active mechanisms (Compant et al., 2005; Sørensen et al., 2007). The successful colonization of the endorhiza depends on many factors such as the allocation of plant resources and the adaptions of the endophyte. Some of the most prominent phyla in grapevine roots were Proteobacteria, Actinobacteria, Bacteroidetes, Firmicutes, Acidobacteria and Verrucomicrobia (Burns et al., 2015; Zarraonaindia et al., 2015; Faist et al., 2016; Samad et al., 2017). Comparable to the bacteria in grapevine, the most prominent bacteria found in maize roots were Proteobacteria, Bacteriodetes and Firmicutes although the abundance of these phyla was influenced by the cultivation history of the soil (Correa-Galeote et al., 2018). In general, the phyla of Proteobacteria, Actinobacteria and Firmicutes were reported to be dominant endo-phytes (Hallmann et al., 1997; Marquez-Santacruz et al., 2010; Romero et al., 2014; Shi et al., 2014).

1.6 Aim of this study

Various studies report that PLCPs play a major role in plant immunity. Therefore, we propose that the modulation of PLCPs displays a conserved mechanism during plant-microbe interactions. For a first encounter with the plant, microbes need to overcome plant immunity by modulation of apoplastic PLCP activity. Maize research on plant microbe interactions so far mainly focused on aerial plant parts. Its interaction with the biotrophic fungus *U. maydis* provides a great model system offering methods for fast and easy modifications from the fungal site. However, the discovery of the conserved cMIP across various kingdoms of microbes colonizing aerial as well as below-ground plant parts inspired us to further investigate apoplastic PLCPs in the root. During my PhD-project, I investigated the abundance and activity of apoplastic PLCPs in maize roots. Besides, I studied their role in plant immunity and regulation of microbe community composition.

My first question was, if apoplastic PLCP composition in roots differs from the known PLCPs in leaves (van der Linde et al., 2012a). A proteomics approach together with mass spectrometry was used to identify PLCPs in the maize root apoplast for comparison with leaf PLCPs. It was shown that PLCPs are involved in SA-mediated defense signaling in maize leaves. The second question was, if there is a relation between SA-signaling and root apoplastic PLCPs. We investigated PLCP activity and biochemical characteristics for substrate specificities, pH-stability and inhibitor susceptibility in the context of sequence and structure differences among tested PLCPs. The last question was whether root endophytic microbes need PLCP inhibition as a trait for interaction with the plant. To answer this, I screened root endophytic bacteria and fungi for secretion of PLCP inhibitors.

2 Results

2.1 Organ specific SA-signaling and PLCP activation

2.1.1 PLCP activation through SA-signaling

The maize genome encodes 52 papain-like cysteine proteases localized in different compartments such as cytoplasm, vacuole, vesicles and apoplast (Rawlings et al., 2018). In leaf proteomes, salicylic acid (SA) has been described to activate apoplastic PLCPs (van der Linde et al., 2012a). I aimed to investigate root PLCP content and responses to SA-treatment. Changes in root PLCP activity and cleavage specificities upon SA-treatment which may indicate changes in PLCP composition were investigated. To study this, the activity of mock- (2.1A) and SA (2.1B)-treated samples was tested performing substrate cleavage assays using 10 µM of four synthetic substrates coupled to a 7-amino-methyl-coumarin (AMC): Phe-Arg-AMC (FR), Phe-Val-Arg-AMC (FVR), Leu-Arg-AMC (LR) and Arg-Arg-AMC (RR). All these substrates differ in their residue at the P2-position which has been previously identified to be crucial for PLCP activity specificity (D. Turk et al., 1995; Melanie Paireder et al., 2016; M. Paireder et al., 2017). RAF showed a preference for cleavage of the LR-substrate. Additionally, it was observed that in mock samples the FR- as well as the FVR-substrates were 25% efficiently cleaved compared to the LR-substrate and the RR-substrate was 40% efficiently cleaved compared to the LR-substrate (2.1A). These observed relative preferences did not change upon SA-treatment but the overall activity raised about five-fold compared to mock-treated samples (2.1B). It is known that protease activity is sensitive to pH (Beynon et al., 2000). To test if PLCPs with different pH-optima were induced upon SA-treatment the activity of RAF was measured in a pH-range from pH 3 – 10 using the LR-substrate. The optimal pH for root apoplastic fluid (RAF) PLCPs was measured at pH 6 in mock samples and did not change upon SA-treatment (2.1C). The observed pH-optimum correlated to the measured pH 6 for RAF of mock- and SA-samples and apoplastic pH of 5-6.5 as reported in literature (Pfanz et al., 1987; Grignon et al., 1991). A general increased PLCP activity upon SA-treatment was also observed during the pH-range measurements.
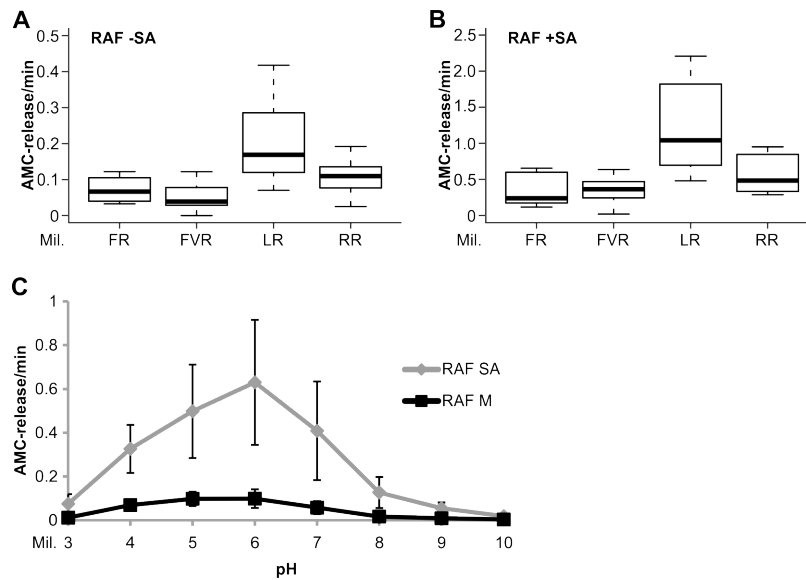
Figure 2.1: **SA-mediated PLCP activation in maize.**
(A-B) Substrate cleavage assays of root apoplastic fluid (RAF) using synthetic substrates. RAF of mock- **(A)** and SA- **(B)** treated maize roots were tested in substrate cleavage assays using 10 µM of the following substrates: Z-FR-AMC (FR), BZ-FVR-AMC (FVR), Z-LR-AMC (LR) and Z-RR-AMC (RR). The release of AMC (relative fluorescent unit = RFU) per minute was calculated and plotted against each substrate. Activity was normalized to samples treated with E-64. The box signifies the upper (Q3) and lower (Q1) quartiles, and the median is represented by a thick black line within the box for each substrate. Lower and upper whiskers represent Q1-1.5 x IQR and Q3+1.5 x IQR, respectively. This experiment was performed using three independent biological replicates each with technical duplicates.
(C) pH stability of RAF-activity. RAF of mock- (RAF M) and SA-treated (RAF SA) plants were tested for their activity at different pH (3 to 10) using 10 µM of the substrate Z-LR-AMC. The release of AMC per minute was measured and plotted against pH. Error bars represent the SEM. Activity was normalized to samples treated with E-64. The experiment was performed in three independent biological replicates using technical duplicates.

2.1.2 Identification of the root specific CP1C

The next aim was to identify the PLCP composition in maize RAF in comparison to PLCPs identified in leaf apoplastic fluids (LAFs) (van der Linde et al., 2012a). RAF of maize seedlings treated with SA were isolated to analyze the effect of SA on the activation of root PLCPs. Fractionation of RAFS by ion exchange chromatography (IEC) followed by an in vitro activity assay using the substrate Z-FR-AMC showed one distinct peak corresponding to leaf apoplastic PLCPs (2.2A) and three distinct peaks representing elevated PLCP activities in roots (2.2B). Pre-treatment of leaf and root apoplastic proteomes with the specific PLCP inhibitor E-64 abolished this activity (2.2A - B). Interestingly, the observed activity pattern of the root apoplast significantly differs from the leaf apoplast since the leaf proteome shows 10-20-fold lower activity compared to RAF (2.2A - B). In a following step, protein fractions corresponding to the three major peaks observed in 2.2B were pooled and active PLCPs were labeled using DCG-04, a probe that binds covalently and irreversible to the active site of PLCPs allowing us to monitor the availability of active sites rather than their abundance (D. Greenbaum et al., 2000; R. A. L. van der Hoorn et al., 2004b). Taking advantage of the biotin tag present in DCG-04, a pull down purification of labeled proteins was performed. Signals corresponding to labelled proteins of different molecular weights, were excised from the gel and subjected to an in - gel digest (IGD) mass spectrometry analysis (2.2C, position A to C). Five apoplastic PLCPs have been identified in maize RAF (2.2D). The two CP1-isoforms, CP1A and CP1B, as well as CP2 and XCP2 were detected in roots, correlated to previous identification in the leaf apoplast (van der Linde et al., 2012a). In addition, a third CP1-like PLCP, CP1C was identified in roots although it has not been previously identified in leaves (2.2D) (van der Linde et al., 2012a). Cathepsin B (CathB) which was identified by IGD only in leaves was later also detected by OBD being present in maize root in this study (2.6) (van der Linde et al., 2012a).

CP1C was the only PLCP found in position A and B of peak 1 and it was additionally found in position A of peak 2. In contrast, CP1A and CP1B were not found in peak 1 but in all positions of peak 2 as well as in position B and C of peak 3. The fact that CP1C was fractionated at different volumes than CP1A and CP1B might indicate distinct biochemical properties of CP1C compared to the other two isoforms and can be attributed to differential charges. CP1C has a higher isoelectric point (pI: 5.55, without signal peptide and prodomain) compared to CP1A and CP1B (pI: 5.09 and 5.10, without signal peptide and prodomain, respectively). A lower pI corresponds to a stronger negative charge at a specific pH. We have performed IEC at pH 6 which results in a stronger binding to the resin of proteins with lower pI and elution at higher salt concentrations. The differences in elution of CP1A, CP1B and CP1C are therefore in line with their respective pI of the mature protein. All identified unique peptides were located in the predicted protease C1 domain (CD) which confirms the success of the DCG-04 pull down targeting solely active proteases (2.2E). Taken together, the comparison of active PLCPs in leaf- and root proteome revealed the presence of the four PLCPs CP1A, CP1B, CP2 and XCP2, previously identified in the leaf apoplast (van der Linde et al., 2012a), as well as one additional root specific PLCP: CP1C.
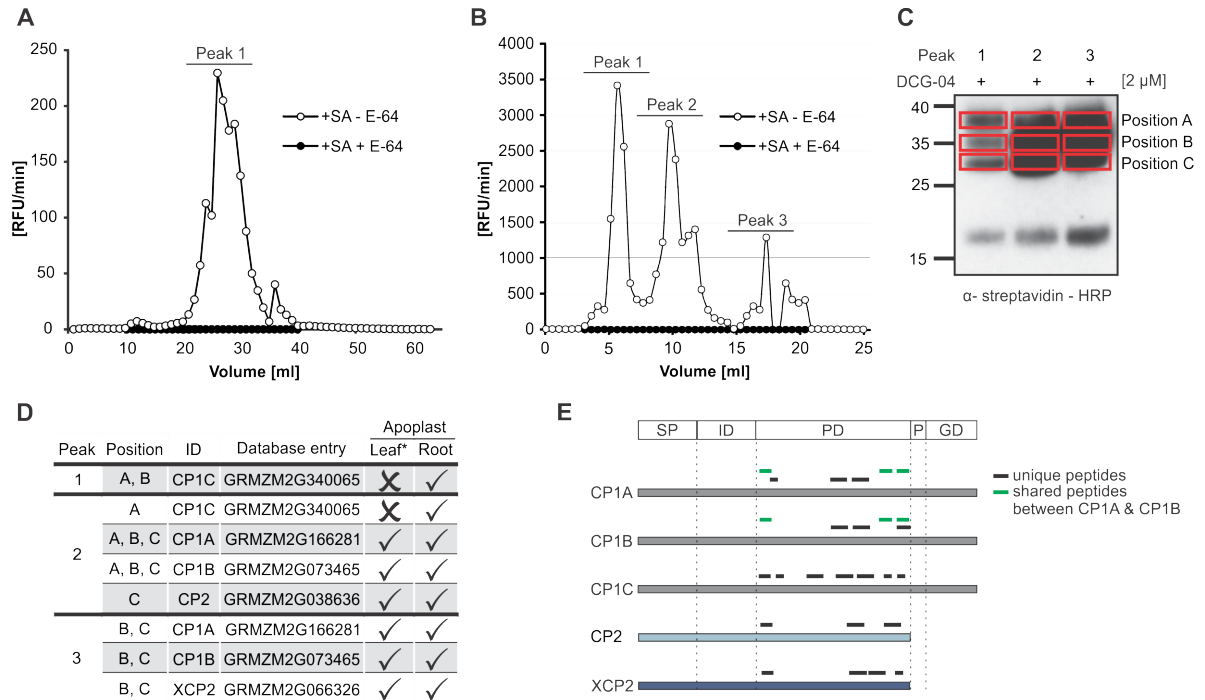
Figure 2.2: **Identification of maize root PLCPs after ion-exchange chromatography.**
(A) Leaf apoplastic fluid (LAF) and **(B)** root apoplastic fluid (RAF) of maize leaves or roots, pre-treated with 2 mM SA (+SA) were isolated and fractionated using ion exchange chromatography (IEC). Fractions were tested for PLCP activity using 10 µM of the substrate Z-FR-AMC with (+) or without (-) 2 µM E-64. The release of AMC (relative fluorescent unit = RFU) per minute was measured and plotted against fraction volume. Peaks represent fractions of higher PLCP activity that were inhibited when using E-64.
(C) DCG-04 labeling of fractions corresponding to different peaks (B) were pooled and labeled with 2 µM DCG-04 for 2 h. Samples were separated by SDS-PAGE and detection of biotinylated proteins was performed using an α-streptavidin-HRP antibody. Red squares mark samples subjected to in gel digest (IGD) and MS analysis. Peaks 1, 2 and 3 correspond to pooled fractions (B) and position A, B and C mark size separated signals of each peak loaded.
(D) Identification of apoplastic root PLCPs and comparison with leaf proteome. Apoplastic root-PLCPs identified by MS analysis were compared to PLCPs previously published in leaf apoplastic fluid by van der Linde et al., 2012a (*). Peak and position (B, C) of PLCPs identified in this study as well as PLCP presence (✓) or absence (✗) is indicated.
(E): Analysis of peptides found by mass spectrometry. Displayed is a schematic representation of the identified PLCPs and the position of peptides found: SP = signal peptide, ID = inhibitory prodomain, PD = protease C1-domain, P = proline-rich domain, GD = granulin domain. Unique peptides are labelled in black and shared peptides are labelled in green.

2.1.3 Expression of identified root PLCPs is unaffected by SA

Previous results in maize showed an increased activity of apoplastic PLCPs after SA-treatment. To examine how this increased abundance is regulated the expression of several root PLCPs was evaluated via qRT-PCR in mock- and SA-treated maize roots (2.3 & 6.1). Expression of the SA-marker PR3 and PR5 increased significantly upon SA-treatment in maize roots confirming a successful SA-treatment (Dolezal et al., 2014; Ray et al., 2016). PR3 was shown to possess chitinase activity explaining its antifungal effects (Dolezal et al., 2014). PR5 on the other hand belongs to the thaumatin-like proteins (TLPs) (J. Yan et al., 2015). PR5 proteins show structural similarity to thaumatin, which is a sweet-tasting protein from *Thaumatococcus daniellii* (van der Wel et al., 1972). Although their exact mechanism of action is often hard to elucidate TLPs are known for their antifungal activity *in vitro* and *in vivo* and can cause leakage of intracellular components of target cells and disrupt the pH gradient across membranes (Roberts et al., 1990; D. Liu et al., 1994; Abad et al., 1996). The expression did not change significantly for any of the tested root apoplstic PLCPs upon SA-treatment (2.3) indicating that transcriptional regulation of the tested PLCPs is not involved in the observed increase in PLCP activity after SA-treatment (2.1A – B).
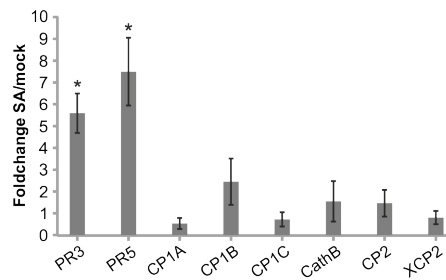
Figure 2.3: **SA-induced root PLCP expression in maize.**
Expression pattern of root apoplastic maize PLCPs. qRT-PCR analysis of root apoplastic maize PLCPs of mock- and SA-treated plants. Fold change of expression in SA/mock samples for the SA-marker genes PR3 and PR5 and the maize PLCPs: CP1A, CP1B, CP1C, CathB, CP2 and XCP2 is displayed. Expression was normalised to expression levels of the housekeeping gene GAPDH. Error bars represent the SEM. P-values were calculated with an unpaired t-test. *$P < 0.05$. The experiment was performed in three independent biological replicates using technical triplicates.

2.1.4 SA-induced changes in protein abundance of root apoplastic fluids

A further aim was to characterize the changes occurring on apoplastic protein abundance upon SA-treatment focusing on PLCPs especially the novel root specific CP1C and potential involvement in SA-signaling. For this, RAF from plants pre-treated with 2 mM SA or mock was labelled using DCG-04. Besides an increase in activity, a shift into lower molecular weight signals was noticed after treatment with SA, suggesting that some PLCPs become less active, while others are activated or post-translationally modified through SA-treatment (2.4A). To investigate the observed root specificity, the expression pattern of CP1C in leaves and roots was compared to the expression of the five maize leaf PLCPs. Using publicly available B73 expression data of untreated maize leaves and roots (maizegdb.org), PLCP expression patterns were displayed using a heat map in which root gene expression was normalized to leaves (2.4B). Overall, apoplastic PLCPs seem to be higher expressed in roots compared to leaves, which correlates with the higher enzyme activity level observed in roots compared to leaves (2.2A - B). CP1B, CP2, XCP2 and CathB show a slightly higher expression level in roots, whereas CP1A expression is slightly stronger in leaves (2.4B). CP1C transcripts are detected in leaves, but its expression is about 6-fold higher in roots (2.4B). Remarkably, of all six PLCPs, CP1C shows the strongest differential expression in roots compared to leaves. To understand if the expression levels found for the PLCPs correlate with their abundance and their activity shot-gun analysis was performed together with a DCG-04 pull down. Abundance is described as the total pool of proteins, active and inactive present in the proteome. Roots of maize seedlings were treated with mock or SA. After two days, RAF was isolated and one part was used for shot-gun analysis while the other part was labeled with DCG-04 (2.4C). A comparison between protein abundance in mock vs. SA-treated samples has been represented using a volcano plot (2.4D). Remarkably, the total abundance of PLCPs did not change after SA-treatment (2.4D, red) suggesting a post-

translational activation to explain the SA-induced increase in RAF PLCP activity (2.1 & 2.4A). The majority of proteins (84.2%) do not change significantly in abundance upon SA-treatment but 7.9% show differential behaviour being significantly more abundant in the apoplast after SA-treatment (2.4E).

Figure 2.4: **Abundance and activity of root apoplastic PLCPs after SA-treatment.**
(A) DCG-04 labeling of root apoplastic fluid (RAF) pre-treated with 2 mM SA or mock. RAF was preincubated for 30 min either with 20 μM E-64 or DMSO. Samples were labeled with 2 μM DCG-04 for 2 h and analyzed with SDS-PAGE. Biotinylated proteins were detected using an α-streptavidin-HRP antibody.
(B) Expression pattern of six apoplastic PLCPs. Relative expression of root apoplastic maize PLCPs in untreated B73 based on publicly available data (Winter et al., 2007; R. S. Sekhon et al., 2011; Carson M. Andorf et al., 2016; Stelpflug et al., 2016). Mean expression of leaves and roots at different developmental stages was calculated and normalized to leaf expression for individual PLCPs. The heat map represents a one – to – one comparison for each PLCP. PLCPs were clustered based on their relative expression pattern to leaves.
(C) Schematic overview of MS experimental setup. Roots of maize plants were treated with 2 mM SA or mock. Apoplastic fluid of four biological replicates was isolated 12 h after treatment. One part of the apoplastic fluid was used for shotgun analysis to investigate protein abundance (I) and the other part was used for a DCG-04 pull down of labelled PLCPs followed by on bead digest (OBD) (II). Both, samples I and II, were subjected to mass spectrometry analysis for protein identification and quantification.

(D) Protein abundance in roots after SA-treatment. A comparison of protein abundance between mock- and SA-treated RAFs is displayed in a volcano plot. Fold change differences between treatments against negative log p-value is plotted. Cysteine proteases are labelled in red and cysteine protease inhibitors are labelled in blue. The black line represents the threshold for significant changes. Proteins above the line have a −Log p > 1.8 and show at least a Log2 = 0.8-fold change between treatments.

(E) Comparison of protein abundance after SA-treatment. Changes in protein abundance after SA-treatment compared to mock-treated plants were displayed using a Venn diagram. Total numbers of identified proteins and percentages are indicated. Proteins significantly less abundant in SA-treated samples compared to mock are labelled in blue. Not differential proteins are labelled in purple and significantly more abundant proteins in SA-treated samples compared to mock are shown in red.

Analysis of the protein abundance after SA-treatment showed an increase of proteins associated with SA-signaling confirming a successful treatment (Schulze Hüynck et al., 2019). An excerpt of SA-induced changes in protein abundance is displayed in 2.5. A strong increase was observed for Thioredoxin. Thioredoxins are involved in the catalysis of oligomer to monomer conversion of NPR1, important for its nuclear localization and function as a positive transcription factor for SA-signaling associated PR-genes (Tada et al., 2008). The pathogen related PR10 is induced upon *Aspergillus flavus* infection in maize seeds and was shown to act antifungal in addition to displaying ribonuclease activity in vitro (Chen et al., 2010). This is in line with the observation of increased protein abundance of the TLP zeamatin in SA-treated samples. Zeamatin leads to leakage of intracellular components of *Neurospora crassa* (Roberts et al., 1990) and inhibits trypsin and α-amylases from insects as well (Schimoler-O'Rourke et al., 2001). Another reaction to pathogen attack is the consolidation of the cell wall to prevent pathogenic penetration trough reposition of lignin in the cell wall (Lange et al., 1995; Cheong et al., 2002). Correlated to the importance of lignin, we found cinnamyl alcohol dehydrogenase, a key enzyme in lignin biosynthesis which was shown to increase disease resistance in *A. thaliana* to be more abundant upon SA-treatment (Tronchet et al., 2010). Interestingly we also found higher abundance of the SA biosynthesis related shikimate biosynthesis protein (D'Maris Amick Dempsey et al., 2011). The plastid localized shikimate pathway leads to a supply of chorismate. This acts mainly as a precursor for the synthesis of aromatic amino acids, such as tryptophan, phenylalanine and tyrosin but also serves as a starting substance for the generation of secondary metabolites and the isochorismatesynthase dependent (ICS) synthesis of SA (D'Maris Amick Dempsey et al., 2011; Maeda et al., 2012). Additionally, we saw an increased abundance of several glutathione-s-transferases (GSTs) and actin-depolimerisation factor 10. GST enzymes are known to be involved in SA-mediated SAR, although the exact mechanisms remain elusive (Chen et al., 1993; Vernooij et al., 1994; Ryals et al., 1995). Stability of the cytoskeleton is an important trait for eukaryotic cells. Studies of plant programmed cell death (PCD) propose an actin-depolimerisation-mediated PCD for example in pollen maturation and embryo-genesis (Smertenko et al., 2003; Thomas et al., 2006; Franklin-Tong et al., 2008). Phenazines, which can be used as a biocontrol agent, are cyclic lipoproteins (CLPs) mostly known to be produced by some archaea and eubacteria like *Pseudomonas fluorescence* and their antagonistic activity against soil-borne

pathogens (Thomashow et al., 1988; Mavrodi et al., 2010). Interestingly, we also found higher amounts of this compound in SA-samples which may be derived from root associated putative beneficial bacteria. SA signaling also involves post-translational activation of the 26S proteasome leading to protein degradation fitting to increased levels of 26S proteasome in our samples (Gu et al., 2010). We observed reduced levels of E3 ubiquitin ligase upon SA-treatment which was recently shown to induce JA-mediated defense through labeling of the JA defense repressor JAV1 for degradation (Ali et al., 2019). Also, in line to an increased SA-signaling we found less vignain and LRR-extensins. Vignain is a PLCP involved in mobilization of stored seed proteins, PCD and is predicted to act in defense responses towards insects like the maize PLCP Mir1 and may therefore be associated to JA/Et-signaling (Helm et al., 2008; Castano-Duque et al., 2018). LRR-extensins are involved in root hair growth which fits to its lower abundance due to a plant trade-off between immunity and growth favoring defense related metabolism for the cost of growth (Ringli, 2005; Draeger et al., 2015). Surprisingly, we found reduced levels of phenylalanine ammonia-lyases (PALs) in SA-treated samples. These enzymes catalyze the first step of the PAL pathway for SA-synthesis (D'Maris Amick Dempsey et al., 2011). Also, we observed a reduction of endochitinase abundance in SA samples, which are known to directly attack fungal pathogens through their fungal cell wall degrading activity (Yan et al., 2015). Interestingly, it was found that the abundance of the cystatin P31726, an endogenous cysteine protease inhibitor, was increased almost fourfold after SA-treatment whereas the abundance of other cysteine protease inhibitors did not change (2.4D, blue & 2.5).

Protein	ID	Foldchange [Log2]	Reference
Thioredoxin	B4FH44	3.51	Tada et al., 2008
PR10	Q29SB6	0.99	Chen et al., 2010
Zeamatin	P33679	1.62	Roberts et al., 1990
Cinnamyl alcohol dehydrogenases	B6U7D8, B4FR97 A0A1D6DYM3	0.25, 3.40, 6.51	Tronchet et al., 2010
Shikimate bio-synthesis protein	B6UCV5	2.53	Dempsey et al., 2011
Glutathione-s-transferases	B6SZY7, A0A1D6PDA0	4.61, 3.86	Chen et al., 1993
Actin-depolimerisation factor 10	B4FSW2	1.80	Smertenko et al., 2003
Phenazine	B6U0C2	2.81	Mavrodi et al., 2010
26S proteasome	B4FR70, A0A1D6IP54	2.37, 2.03	Gu et al., 2010
E3 ubiquitin ligase	A0A1D6K434	-3.11	Kelley et al., 2012
Vignain	A0A1D6KMS8	-1.57	Castano-Duque et al., 2018
LRR-extensins	A0A1D6KXF5, K7UCP0	-1.50, -2.45	Draeger et al., 2015
Phenylalanine ammonia-lyases	A0A1D6E5Z0, A0A1D6HN61	-0.84, -0.86	Dempsey et al., 2011
Endochitinase	A0A1D6N6M0	-2.91	Yan et al., 2015
Corn cystatin 1	P31726	3.11	van der Linde et al., 2012

Figure 2.5: **Changes in abundance of SA-related proteins after SA-treatment.**
Excerpt of SA-related proteins changed in abundance upon SA-treatment from 2.4D. Displayed are the protein, respective database IDs, Log2 fold-change SA/mock and references were the role of these proteins in SA signaling has been described.

To get more insight into the SA-effect on activation of apoplastic PLCPs a DCG-04 pull down of SA-treated and mock plant AFs was performed followed by an on bead digest (OBD) and mass spectrometry analysis. MS/MS counts were plotted against identified proteins (2.6A). The majority of peptides found in this pull down correspond to PLCPs confirming an enrichment of those proteases after DCG-04 labeling (Schulze Hüynck et al., 2019). In agreement with the previously described IGD, performed on samples separated by ion-exchange chromatography (IEC), peptides for CP1A, CP1B, CP1C, CP2 and XCP2 were identified in the OBD-samples (2.6A). Additionally, peptides for CathB were identified, which has not been identified in the previous IGD-MS analysis made for maize root apoplast (2.2D & E; 2.6A) likely, due to its isoelectric point of 5.49 close to the conditions used for the IEC (pH 6). Remarkably, the activities of the previously characterized PLCPs CP1A, CP1B, CP1C, CP2, XCP2 and CathB and five additionally detected PLCPs do not change significantly after SA-treatment compared to mock. One of these five unchanged PLCPs was found to be another member of the CP1-like PLCPs CP1D which shares high sequence similarity with CP1C. In contrast, three other PLCPs were identified with significantly increased active protein abundance, up to 70-fold, after SA-treatment: B4FS65 belonging to the cysteine protease superfamily, B4FYA3 a xylem bark cysteine peptidase and Q10716 a cysteine proteinase 1 (2.6). With these experiments the presence of the previously leaf identified PLCPs, CP1A, CP1B, CP1C, CP2 and XCP2 was demonstrated in the root apoplast and additionally, CathB was identified together with other eight PLCPs, which have not been previously found in the IEC root apoplast analysis. Three of the newly identified PLCPs seem to be activated upon SA-treatment.
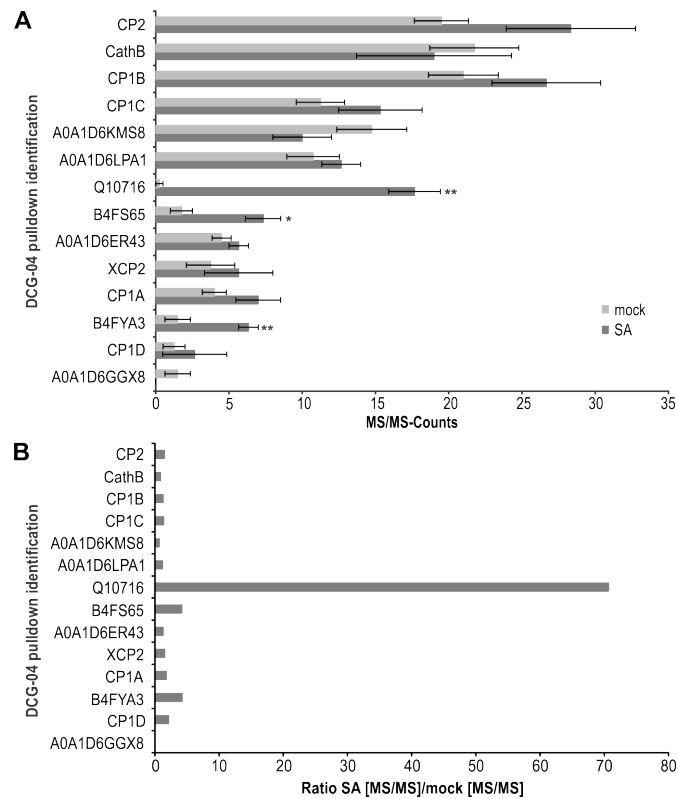
Figure 2.6: **SA-mediated activation of root apoplastic PLCPs.**
DCG-04 labelled and streptavidin pulled down samples were subsequently on bead digested (OBD; trypsin) (2.5). The tryptic peptides were then analyszed by LC-MS/MS and compared between treatments.
(A) MS/MS-counts were plotted against identified PLCPs in both treatments. MS/MS-counts of SA-treatments are labelled in dark grey and MS/MS-counts of mock-treated samples are labelled in light grey. Error bars represent the SEM. P-values were calculated with an unpaired t-test. *P<0.05; **P<0.01.
(B) The ratio of the number of measured MS/MS spectra (MS/MS-counts) after SA-treatment compared against the number of MS/MS counts in a mock-treated sample was calculated and plotted. The experiments were performed using four independent biological replicates.

2.1.5 Phylogeny of maize PLCPs

To get insights into the subfamily classification of the newly identified root apoplastic proteases the sequence similarity of maize apoplastic PLCPs was evaluated using phylogeny. A phylogenetic tree using the maximum likelihood method was generated by Dr. Jasper Depotter using the following sequences: 52 maize PLCP sequences from B73 retrieved from the MEROPS database (Rawlings et al., 2018), the five previous PLCPs identified from Early Golden Bantam (EGB) leaves and the nine newly identified root PLCPs. Additionally, for the subfamily classification, one type member of each PLCP subfamily of *A. thaliana* (Richau et al., 2012) was included. Two serine proteases from *A. thaliana* (AtDGP11 and AtDEGP2) were used as outgroup (Beers et al., 2004; Richau et al., 2012) (2.7). PLCPs were classified into nine subfamilies: RD21-like (1), CEP1-like (2), XCP2-like (3), XBCP3-like (4), THI1-like (5), SAG12-like (6), RD19A-like (7), AALP-like (8) and CTB3-like (9). The largest group of maize PLCPs belongs to the RD21-like subfamily (17 members), followed by members of the SAG12-like subfamily (12 members), the THI1-like subfamily (11 members) and CEP1-like subfamily (8 members). Other PLCP subfamilies are represented by few members (2.7). All identified apoplastic CP1-like PLCPs, CP1A, CP1B, CP1C and CP1D carrying a granulin domain, cluster together into the subfamily 1 of RD21-like together with previously identified apoplastic PLCPs like Mir1-3. CP1C and CP1D are phylogenetically closer to Mir1 (MER0003752), Mir2 (MER0003753) and a pseudotzain whereas CP1A and CP1B are closer to Mir3 although all four CP1-like PLCPs show high sequence and structural similarities (2.7, 2.8, 2.11). It was noticed that CP1A from EGB is highly similar in sequence (91% identity of amino acids) to Mir3 (MER0003754) from B73 indicating that CP1A is the corresponding Mir3 in EGB. CathB, CP2 and XCP2 grouped into the subfamilies CTB3-like, AALP-like and XCP2-like, respectively (2.7). The SA activated PLCP B4FS65 (MER036246) belongs to the THI1-like subfamily, whereas Q10716 (MER0001404) was found to be present in the RD19A-like subfamily (2.7). Sequence alignment of the SA activated PLCP B4FYA3 (MER0137791) showed high sequence similarity to CP14 (MER0137791) belonging to subfamily of XBCP3-like PLCPs. B4FYA3 is homolog to *Nicotiana benthamiana* and *N. tabaccum* CP14 proteins described to be involved in programmed cell death (Zhao et al., 2013; Paireder et al., 2016). The remaining four non SA-responsive PLCPs A0A1D6KMS8, A0A1D6GGX8, A0A1D6LPA1 and A0A1D6ER43 belong to the subfamilies CEP1-like, SAG12-like, RD21-like and AALP-like, respectively. A0A1D6KMS8 was identified as a vignain and A0A1D6LPA1 shows high similarity to Mir2 (MER0003753). Both, vignains and Mir2 are known to be involved in PCD and anti-insect defense (Castano-Duque et al., 2018).
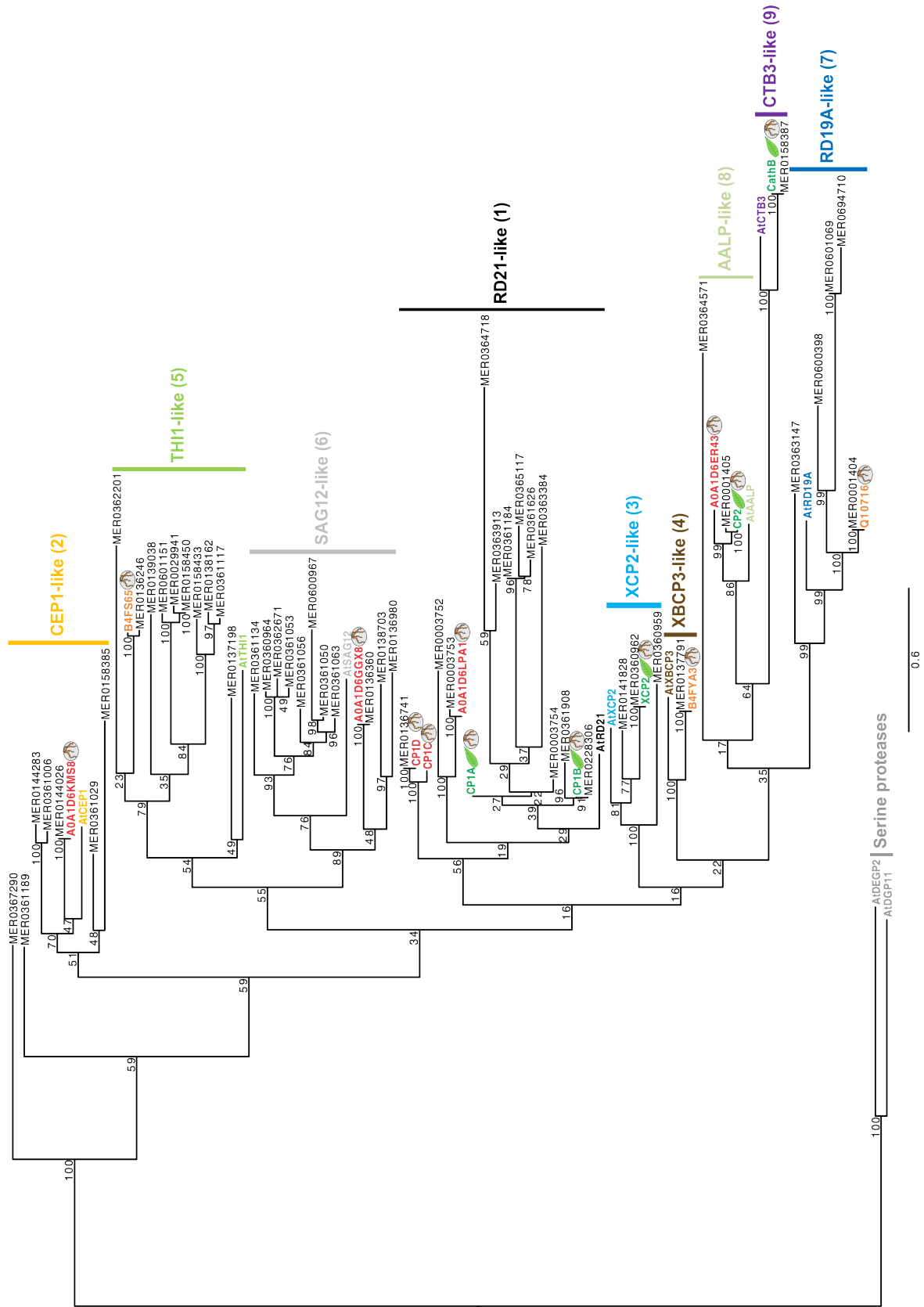
Figure 2.7: **Phylogeny of apoplastic maize-PLCPs.**

52 maize PLCP sequences of the line B73 retrieved from the MEROPS database (Rawlings et al., 2018), the five previously in leaves identified PLCPs from Early golden Bantam (EGB) (van der Linde et al., 2012a) and the nine newly identified root PLCPs were used to generate a phylogenetic tree. Additionally, we included one type member of each PLCP subfamily of *A. thaliana* and two serine proteases DEGP2 and DGP11 from *A. thaliana* as outgroup (Beers et al., 2004; Richau et al., 2012). We used full length sequences including signal peptide, prodomain, protease C1-domain and, if present, proline-rich domain and granulin domain as was used before in Richau et al., 2012. The tree is drawn to scale, with branch lengths measured in the number of substitutions per site. Sequences were aligned using MAFFT (v7.407) (Katoh et al., 2013). RAxML with the GTRGAMMA substitution model (v8.2.0) was used for the construction of the tree (Stamatakis, 2014). The robustness was assessed using 100 bootstrap replicates. Apoplastic EGB maize PLCPs were highlighted according to the organs they were found in: leaves (green) roots (red). The SA-activated root PLCPs (2.6) are highlighted in orange. Numbers indicate the PLCP subfamilies based on Richau et al., 2012.

2.1.6 Biochemical characterization of root specific CP1C

Granulin containing PLCPs of the subfamily 1, such as Mir1 from maize or RD21 from Arabidopsis are known to play crucial roles related to plant defense and senescence (Lopez et al., 2007; Shindo et al., 2012). Here CP1C, a root specific granulin containing PLCP closely related to CP1A and CP1B was identified. Sequence analysis of mature CP1C compared to CP1A and CP1B revealed high similarities, 74% identity, at the amino acid level (2.8A). All three proteases contain a predicted N-terminal secretion signal, an inhibitory prodomain, including the core structure peptide ERFNIN with a substitution of I95V in CP1B and CP1C, and a C-terminal granulin domain (2.8A). CP1C catalytic triad consists of three main residues: C179, H316 and N336, as well as Q173, which was shown to stabilize the oxyanion during the catalytic reaction (2.8A & C) (Menard et al., 1991). Sequence variation was observed between predicted domains e.g. signal peptide and inhibitory prodomain and between inhibitory prodomain and protease C1-domain and at the C-terminal granulin domain (2.8A). To further analyze CP1C at the structural level a three dimensional model was predicted based on the cysteine protease caricain (PDB: 1pciA) (Groves et al., 1996; Kelley et al., 2015). An overlay of the models predicted for the mature CP1A and CP1C was performed. The majority of residue changes appeared to be located on the surface of the proteins (2.8B). Out of 53 different surface residues between CP1A and CP1C, 25 were predicted to cause a minor impact for the structure due to similar biochemical properties. Of all changes, only three differential amino acids were located inside CP1C: D172N, A186S, and K335R. All three amino acids are predicted to be located in close proximity to the active site (2.8C). Interestingly, the catalytic groove seems to be narrower in CP1C compared to CP1A. A different orientation of the basic amino acids K335R close to N336 between CP1A and CP1C might explain the distinct catalytic properties and substrate preferences (2.8C). Altogether, CP1A and CP1C seem to share similar sequence homology and structure although differences on the surface of CP1C might result into different interaction partners.

A

```
                 *         20          *         40          *         60          *         80
CP1A : MAASTTA---AAALLLLLLL-SI------AAAA-DMSIVSYG--------ERSEEEARRMYAEWMAAHGRTYNAVGE----EE :  59
CP1B : MGASTTPLASAAALLLLLLAPL------AAADSMSIVSYG--------ERSEEEARRMYAEWMAAHGRTYNAVGE----EE :  64
CP1C : MAALGRG---LPLLLLLLLLAVSGAANAAAAPGGMSIITYNEEHGARGLERTEPEVRAMYDLWLAEHGRAYNALGEGEGERD :  79
consensus : MaAstt     aaaLLLLLL  6     AAAa  MSI63Yg       ER3EeEaRrMYaeW6AaHGRtYNA6GE    ee
                                                    SP                                 ID
                 *        100          *        120          *        140          *        160
CP1A : RRYQVFRDNLRYIDAHNAAADAGVHSFRLGLNRFADLTNDEYRATYLGARTRE-QRERKLGARY-HAADNEDLPESVDWRAK : 139
CP1B : RRFEVFRDNLRYVDAHNAAADAGVHSFRLGLNRFADLTNDEYRATYLGVRSRE-QRERRLGDRY-LAGDNEDLPESVDWRAK : 144
CP1C : RRELVFWDNLRFVDAHNER--AGARGFRLGMNQFADLTNDEFRAAYLGMVPAARRGAVGERYRTD-CAAPELPESVDWREK  : 159
consensus : RR5 VFrDNLR56DAHNaaadAGvhsFRLG6NrFADLTNDE5RAtYLGar rp qRer 6G RY hagdnEdLPESVDWRaK
                                                    ID
                 *        180          *        200          *        220          *        240
CP1A : GAVAEVKDQGSCGSCWAFSTIAAVEGINQIVTGDLISLSEQELVDCDTS-YNQGCNGGLMDYAFEFIINNGGIDTEKDYPYK : 220
CP1B : GAVAEIKDQGSCGSCWAFSTIAAVEGINQIVTGDMISLSEQELVDCDTS-YNQGCNGGLMDYAFEFIINNGGIDTEDYPYK  : 225
CP1C : GAVAPVKNQCQCGSCWAFSAVSSVESVNQIVTGEMVTLSEQELVECSTDGGNSGCNGGLMDAAFEDFIIKNGGIDTEDDYPYR : 241
consensus : GAVAe6K1QGsCGSCWAFSt6aaVEg6NQIVTGd663LSEQELVdCdTs yNqGCNGGLMDyAFeFIInNGGIDTE DYPY4
                 *        260          *        280          *        300          *        320
CP1A : GTDGRCDVNRKNAKVVTIDSYEDVPANDEKSLQKAVANQPVSVAIEAAGTAFQLYSSGIFTGSCGTALDHGVTAVGYGTENG : 302
CP1B : GTDGRCDVNRKNAKVVTIDSYEDVPANSEKSLQKAVANQPISVAIEAGGRAFQLYNSGIFTGTCGTALDHGVTAVGYGTENG : 307
CP1C : AVDGKCDMNRKNARVVSIDGFEDVPENDEKSLQKAVAHQPVSVAIEAGGREFQLYKSGVFSGSCTINLDHGVVAVGYGAENG : 323
consensus : gtDG4CD6NRKNA4VV3IDs5EDVPaNdEKSLQKAVAnQP6SVAIEAgGraFQLY SG6F3G3CgTaLDHGVtAVGYGtENG
                 *        340          *        360          *        380          *        400
CP1A : KDYWIVKNSWGSSWGESGYVRMERNIKASSGKCGIAVEPSYPLKEGANPPNPGPSPPSPTPAP-AVCDNYYSCPDSTTCCCI : 383
CP1B : KDYWIVKNSWGSSWGESGYVRMERNIKASSGKCGIAVEPSYPLKKGANPENPGPTPPSPTEPP-TVCDNYYSCPDSTTCCCI : 388
CP1C : KDYWIVRNSWGPKWGEAGYIRMERNVNASTGKCGIAMASYPTKKGANPRESPTTPPTEPAAPDNVCDENFSGSAGSTCCCA  : 405
consensus : KDYWIV4NSWGssWGEsGY6RMERN6kAS3GKCGIA6epSYPlKkGANPnPnPgP3PP3PtpaP VCDny5SCpds3TCCCi
                                                    PD                            P
                 *        420          *        440          *        460          *        480          *
CP1A : YEYGKYCFAWGCCPLEGATCCDDHYSCCPHDYPICNVRQGTCLMGKDSPLSLSVKATKRTLAKPHWAFSGNT-ADGMKSSA : 463
CP1B : YEYGKYCFAWGCCPLEGATCCDDHYSCCPHDYPVCNVKQGTCLMGKDSPLSLSVKATKRTLAKPHWAFSGNTA ADGMKSSA : 469
CP1C : FGGRNVCLVWGCCPVEGATCCKDEASCCPGYPVCNVEAGTCSVSKNSPL--SVKALKRTLAKLST-------------A   : 470
consensus : 5e5gkyCfaWGCCP6EGATCCdDHySCCPhdYP6CNV4qGTCl6gK1SPLslSVKAtkRTLAKphwafsgnt adgmkssA
                                                                                     GD
```

B

C

Figure 2.8: **Sequence and structural comparison of maize apoplastic CP1-like PLCPs.**

(A) Sequence homology between CP1-like PLCPs. Amino acid sequences of apoplastic CP1-like PLCPs: CP1A, CP1B, and CP1C of the maize line EGB were aligned to evaluate their sequence conservation. Dark grey background indicates conserved amino acids among all three PLCPs, light grey background indicates similar amino acids among two PLCPs and white background indicates different amino acids. Signal peptide (SP, brown), inhibitory prodomain (ID, blue), protease C1-domain (PD, red), proline-rich domain (P, orange) and granulindomain (GD, purple) were predicted. Amino acids forming the ERFNIN motif are labelled in green and amino acids of the active site C179, H316, N336 and the H316 stabilising Q173 are labelled in yellow.
(B) Structure similarities between CP1A and CP1C. A 3D-model of superimposed mature CP1A and CP1C was generated. CP1A (grey) and CP1C (green) from EGB were modelled without signal peptide, inhibitory prodomain and granulin doman using Phyre2 (Kelley et al., 2015) based on the crystal structure of caricain PDB: 1pciA (Groves et al., 1996). The active site C179, H316, N336 and Q173 are indicated in yellow (CP1A) and red (CP1C), respectively.
(C) Close-up of the active site of superimposed CP1A and CP1C. Differences in the catalytic grooves of CP1A and CP1C (B) were examined. The active site C179, H316, N336 and Q173 are indicated in yellow (CP1A) and red (CP1C), respectively. Amino acid differences D172N, A186S and K335R were modelled from CP1A (grey) to CP1C (green).

To study if CP1C also shares biochemical properties with other apoplastic PLCPs, found in roots and leaves, their substrate specificity was analyzed. CP1A, CP1B, CP1C, XCP2, CP2 and CathB were transiently overexpressed in *N. benthamiana* using Agrobacterium and after three days apoplastic fluids were isolated and tested for their activity using the activity-based probe MV201 (Richau et al., 2012) (2.9A). For CathB and XCP2 a double band was seen in ABPP labelled samples which could be due to different steps of maturation or post-translational modifications, such as glycosilation (2.9A). Additionally, the catalytic inactive mutant CP1A[mut] was used as a negative control, as well as overexpressed cytosolic GFP. Both, CP1A[mut] and GFP were used to differentiate the endogenous activity of *N. benthamiana* PLCPs from the overexpressed maize PLCPs (2.9A & 6.2). Purity of apoplastic fluids from cellular contaminants was ensured by an immunoblot for the exclusively cellular RuBisCo for leaf AF and histone 3 (6.3A & B). An immunoblot to quantify PLCPs was unsuccessful, as the C-terminal His-tag from CP1C as well as the tags of the other PLCPs was cleaved off in *N. benthamiana* (personal note from Dr. J. Misas Villamil) (6.4) leaving ABPP as the best option to quantify active protein content. Apoplastic fluids were tested in a substrate cleavage assay using 10 µM of four synthetic substrates coupled to a 7-amino-methyl-coumarin (AMC) as described before (2.1). Activity was then normalized to the CP1A[mut] and the GFP-control. Based on the literature, hydrophobic amino acids as well as Arg are predicted to be favored by PLCPs (Niemer et al., 2016; Paireder et al., 2017). All tested substrates carried an Arg in the P1-position but differed in their residue at the P2-position which has been previously identified to be crucial for PLCP activity (Turk et al., 1995; Paireder et al., 2016; Paireder et al., 2017). All overexpressed PLCPs show a preferred cleavage activity for the substrate LR (2.9B). The basal PLCP activity of *N. benthamiana* also shows LR cleavage preference although with reduced levels in comparison to the overexpressed samples (6.2). CP1A and CP1B also cleave RR, FR and FVR despite CP1B slightly preference for FR. Strikingly, the root specific CP1C differs in the substrate cleavage preference from CP1A

and CP1B which may be explained by unequal substrate accessibility to their active site. It mostly processes the LR-substrate displaying only trace amounts of activity towards other substrates. This LR unique cleavage preference resembles the cleavage specificities of the phylogenetically distant XCP2 and CathB (PLCP subfamily 3 and 9, respectively) (2.9B). CP2 shows generally very low cleavage activity towards the tested substrates (2.9B), although it is active and highly overexpressed in N. benthamiana using ABPP (2.9A). The low cleavage activity of CP2 in contrast to strong activity signals in ABPP may indicate distinct substrate specificities for this protease in comparison to the other tested apoplastic PLCPs.
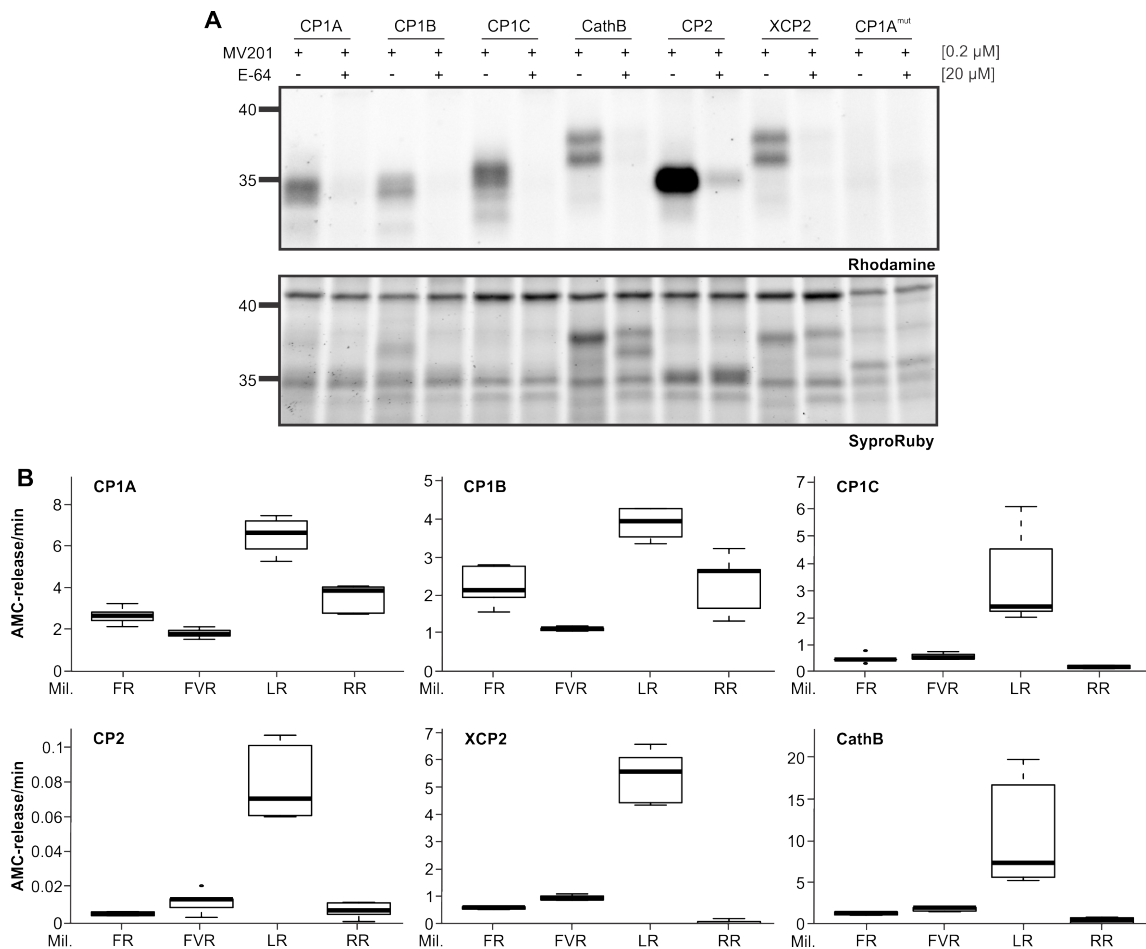
Figure 2.9: **Differential substrate specificities of apoplastic PLCPs.**

(A) Activity of heterologous expressed maize apoplastic PLCPs. Leaf apoplastic fluids of *N. benthamiana* overexpressed PLCPs: CP1A, CP1B, CP1C, Cathepsin B (CathB), CP2, XCP2 and the catalytic inactive CP1A mutant CP1A^{mut} were isolated and labelled with the probe MV201 (Richau et al., 2012). Samples were pre-incubated for 30 min either with 20 µM E-64 (+), a covalent and irreversible PLCP inhibitor (Barrett et al., 1982), or DMSO (-) followed by 2 h labeling with 0.2 µM MV201 (Richau et al., 2012). Labeled PLCPs were visualized by fluorescence scanning (Ex. 532 nm, Em. 580 nm). SyproRuby stain (Ex. 450 nm, Em. 610 nm) was performed for visualization of sample loading.

(B) Substrate cleavage assays of PLCPs using synthetic substrates. Signal quantification from (A) was used to normalize for equal amounts of active PLCPs in this assay. Recombinant PLCPs were tested in substrate cleavage assays using 10 µM of the following substrates: Z-FR-AMC (FR), BZ-FVR-AMC (FVR), Z-LR-AMC (LR) and Z-RR-AMC (RR). The release of AMC (relative fluorescent unit = RFU) per minute was calculated and plotted against each substrate. Activity was normalized to samples treated with E-64. Data was represented in a boxplot as described before. This experiment was performed using three independent biological replicates each with technical duplicates.

As a second approach to the biochemical characterization of CP1C, the inhibitory profile of apoplastic CP1-like PLCPs towards characterized inhibitors was tested: E-64, a covalent and irreversible PLCP inhibitor (Hanada et al., 1978; Barrett et al., 1981; Barrett et al., 1982), CC9, an endogenous cystatin (van der Linde et al., 2012a) and cMIP, a conserved microbial inhibitor of proteases shown to inhibit maize PLCPs (Misas Villamil et al., 2019). To test their inhibitory efficiency towards the CP1-like PLCPs, an inhibitor concentration range using a substrate cleavage assay with Z-LR-AMC was performed. Equal amounts of active PLCPs were used based on signal quantification from MV201 labelled apoplastic fluids (6.5). The cleavage activity of each PLCP in the absence of inhibitors was set to 100% and plotted against Log of inhibitor concentration. E-64 and CC9 show strong inhibition of PLCPs already in the nanomolar-range, with E-64 being a stronger inhibitor for all tested PLCPs than CC9 (2.10A & B). On the contrary, micromolar concentrations of cMIP were needed to reach inhibition (2.10C). CP1C is most susceptible towards E-64 compared to CP1A and CP1B (2.10A) and shows a tendency to be less susceptible towards CC9 (2.10B). Strikingly, cMIP is least effective for CP1B and most effective for CP1A inhibition. CP1C shows an intermediate susceptibility towards cMIP and at lower inhibitor concentrations, between 30 nM and 250 nM, CP1C activity seems to be enhanced. On the contrary, CP1A and CP1B show a gradually, dose-dependent reduction in activity with increasing cMIP concentration (2.10C).
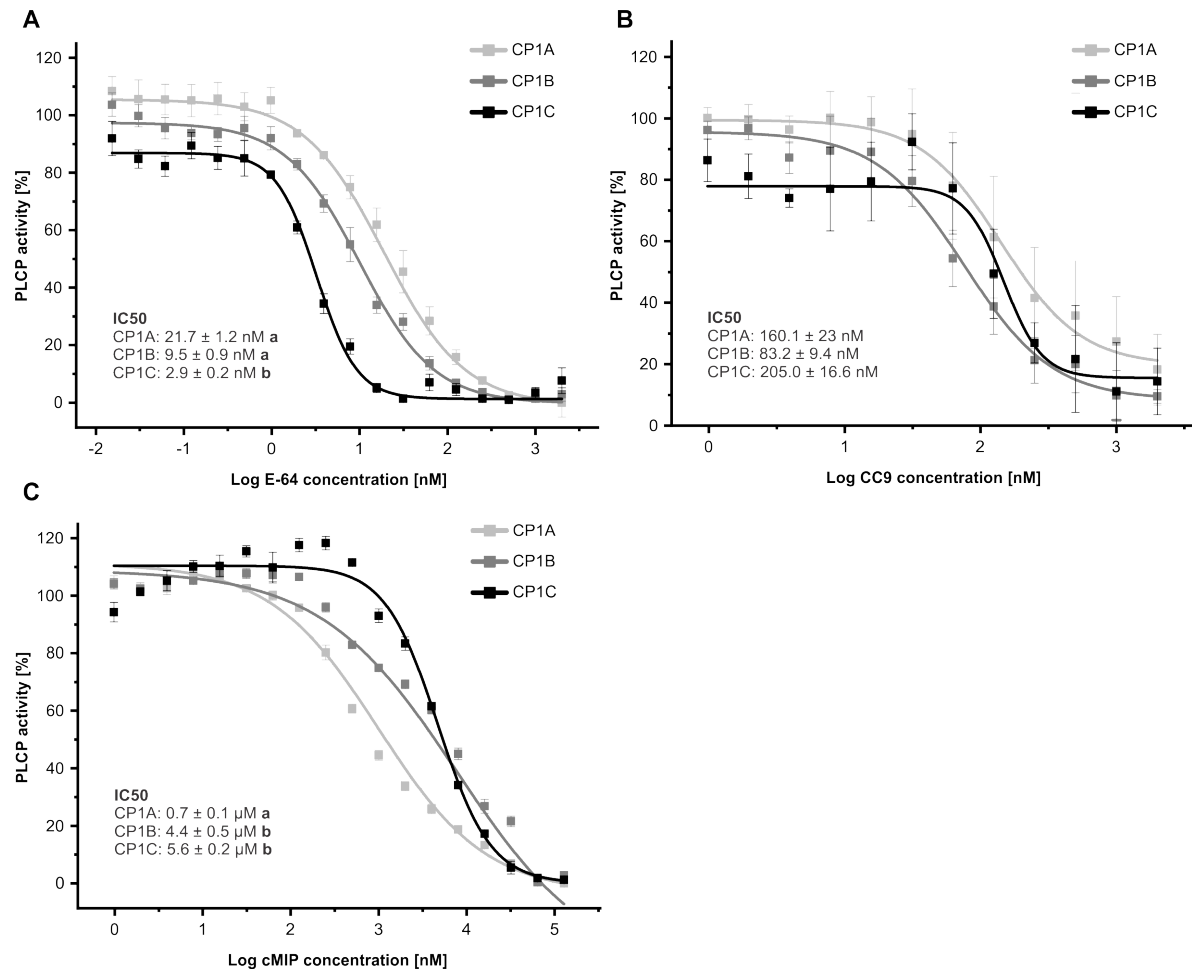
Figure 2.10: **CP1-like proteases show distinct inhibitory profiles.**
Apoplastic fluids of *N. benthamiana* overexpressed CP1A, CP1B and CP1C were evaluated for their activity using 10 µM of the substrate Z-LR-AMC (LR). The inhibitory profile for E-64 **(A)**, CC9, an endogenous cystatin (van der Linde et al., 2012a) **(B)** and cMIP, a conserved microbial inhibitor of proteases (Misas Villamil et al., 2019) **(C)** was tested. We used equal amounts of active PLCPs based on signal quantification from MV201 labeling of apoplastic fluids (6.5). Inhibitor concentrations ranged from 15 pM to 128 µM. Activity was set to 100% in the absence of inhibitor. Normalized values were plotted against Log of inhibitor concentration in nM. The experiment was performed in three independent biological replicates each with technical duplicates. A nonlinear fit based on a dose response function was performed and IC50-values were calculated. Error bars represent the SEM. Significance was calculated using an unpaired t-test and differing letters behind the IC50-values indicate significant differences ($P < 0.05$).

2.1.7 The CP1-like CP1D protease

Together with the previously described novel SA-associated root apoplastic PLCPs the CP1-like PLCP CP1D was identified which displays high sequence similarity to CP1C (92.8%). CP1D, like CP1C and other CP1-like PLCPs consists of a secretion signal for apoplastic localization followed by an inhibitory prodomain, including the core structure peptide ERFNIN with a I91V substitution, and a C1-protease domain. Specific to all CP1-like PLCPs, CP1D also shows a proline-rich motif c-terminal to the protease domain followed by a granulin domain (2.11). CP1D displays high sequence similarity throughout the mentioned domains, only showing small amino acid deletions in the proline-rich motif, the inhibitory domain and the signal peptide. In contrast to the previously described protein alignment in this study (2.8A) even high similarity in the interdomain regions of CP1C and CP1D could be seen (2.11).

Figure 2.11: **Sequence comparison of maize apoplastic CP1-like PLCPs CP1C and CP1D.** Sequence similarity between CP1C and CP1D. Amino acid sequences of CP1C and CP1D of the maize line EGB were aligned to evaluate their sequence conservation. Black background indicates conserved amino acids among both PLCPs, light grey background indicates similar amino acids among the two PLCPs and white background indicates different amino acids or gaps. Signal peptide (SP, brown), inhibitory prodomain (ID, blue), protease C1-domain (PD, red), proline-rich domain (P, orange) and granulin domain (GD, purple) were predicted. Amino acids forming the ERFNIN motif are labelled in green and amino acids of the active site C175, H312, N332 and the H312 stabilising Q169 are labelled in yellow.

Due to the high sequence similarity and the fact that CP1D is localized on chromosome 2 whereas CP1C is localized on chromosome 10 the role of these two PLCPs and their putative redundancy was addressed (Portwood JL II et al., 2018). A three-dimensional model was predicted on the cysteine protease caricain (PDB: 1pciA) to compare the structural characteristics of CP1C and CP1D. An overlay of the models for mature CP1C (grey) and CP1D (green) was performed (2.12A-B). All eleven amino acid changes are located on the surface. Of them, only P337A is located in relative proximity to the catalytic triad C175, H312 and N332 which is conserved in their position in the molecules. Strikingly, the orientation of the H312 imidazole side chain is different for CP1D compared to CP1C. The His side chain in CP1C is oriented inside towards the catalytic triad similar to the orientation seen for CP1A (2.8B-C). In contrast, H312 in CP1D is oriented outward (2.12B).
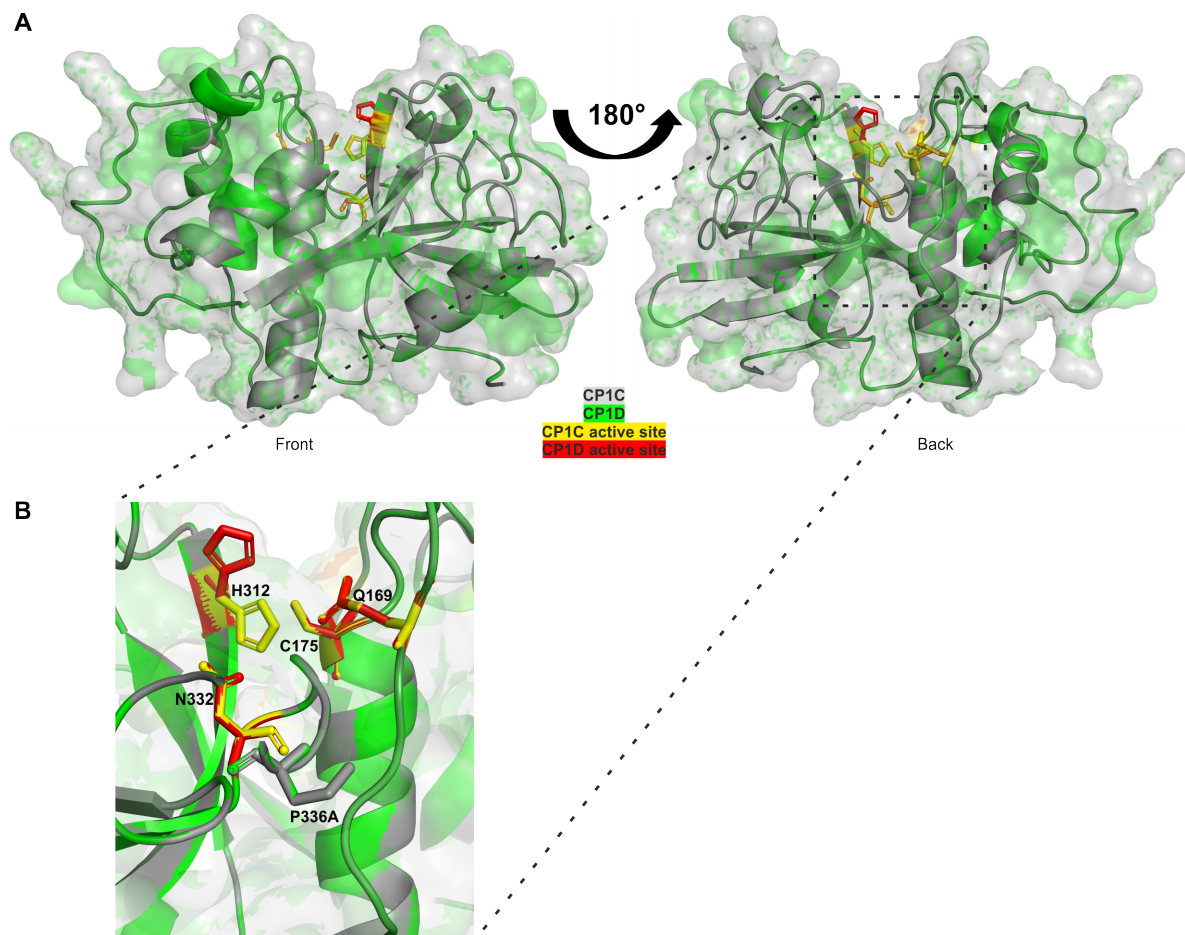
Figure 2.12: **Structural comparison of maize apoplastic CP1D and CP1C.**
(A) Structure similarities between CP1C and CP1D. A 3D-model of superimposed mature CP1C and CP1D was generated. CP1C (grey) and CP1D (green) from EGB were modelled without signal peptide, inhibitory prodomain and granulin doman using Phyre2 (Kelley et al., 2015) based on the crystal structure of caricain PDB: 1pciA (Groves et al., 1996). The active site C175, H312, N332 and Q169 are indicated in yellow (CP1C) and red (CP1D), respectively.
(B) Close-up of the active site of superimposed CP1C and CP1D. Differences in the catalytic grooves of CP1C and CP1D (A) were examined. The active site C175, H312, N332 and Q169 are indicated in yellow (CP1C) and red (CP1D), respectively. Amino acid difference P336A was modelled from CP1C (grey) to CP1D (green).

In addition, CP1D was recombinant expressed in *N. benthamiana* for further biochemical character-ization. A C-terminal mCherry tag was fused to CP1D as well as to CP1A^{mut} which were used as controls together with GFP. mCherry can be detected performing an immunoblot even after cleavage from the protein of interest and acts as a measure for protein expression. Heterologous expression in *N. benthamiana* followed by AF isolation and an immunoblot with α-mCherry antibody showed signal for cleaved, but not full length mCherry in the apoplast for CP1D. No mCherry signals were detectable for CP1A^{mut} and the negative control GFP (2.13A). The observed signals for cleaved mCherry confirmed successful expression of mCherry tagged CP1D. To confirm the presence of active CP1D, an ABPP on the same samples using the probe DCG-04 was performed. A strong signal for active CP1D in contrast to weak signals for CP1A^{mut} and GFP were observed, indicating that these are background signals derived from *N. benthamina* PLCPs (2.13B).
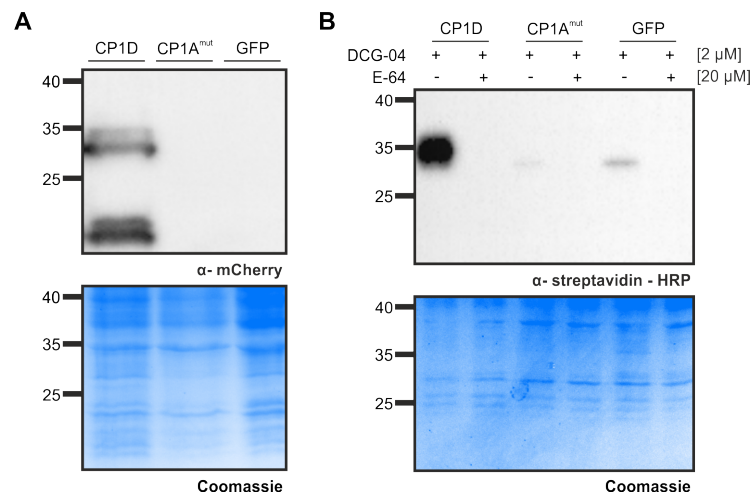
Figure 2.13: **Recombinant overexpression of the maize root PLCP CP1D.**
(A) Immunoblot of heterologous expressed CP1D. CP1D and CP1A^{mut} were fused with a C-terminal mCherry tag and recombinant expressed in *N. benthamiana*. Leaf apoplastic fluids were isolated and samples were analyzed together with leaf apoplastic fluid of heterologous expressed GFP using SDS-PAGE. mCherry-tagged proteins were detected using a primary α-mCherry antibody followed by a secondary α-mouse-HRP antibody. Coomassie stain shows the loading control. This experiment was performed in three independent biological replicates showing similar results. This figure is an excerpt of 2.16B.
(B) DCG-04 labeling of heterologous expressed maize root PLCPs. Leaf apoplastic fluids from (A) were labelled with the probe DCG-04. Samples were pre-incubated for 30 min with (+) or without (-) 20 μM E-64 followed by 2 h labeling with 2 μM DCG-04 and analyzed with SDS-PAGE. Biotinylated proteins were detected using an α-streptavidin-HRP antibody. Coomassie stain shows the loading control. This experiment was performed in three independent biological replicates showing similar results. This figure is an excerpt of 2.16C.

To confirm substrate specificities, substrate cleavage assays were performed as described before (2.1). In line with all so far tested PLCPs, CP1D showed highest cleavage activity for the LR-substrate (2.14A & 2.9B). CP1D did not show cleavage activity for RR and only marginal cleavage for FVR but moderate cleavage activity for the FR substrate in contrast to the substrate specificity pattern observed for CP1C (2.14A & 2.9B). To investigate whether CP1D shows a distinct inhibitory profile the same set of PLCP inhibitors were tested as described before (2.10). The resulting inhibition curves of CP1D were displayed together with the previously described CP1-like PLCPs for clearer distinction (2.14B – D). CP1D shows similar susceptibility as CP1C towards E-64 which is higher than that of CP1A and CP1B while CP1D and CP1C differ strongly in their susceptibility towards CC9 (2.14B & C). Compared to all CP1-like PLCPs, CP1C seems to be least susceptible to CC9 inhibition. In contrast to CP1C, CP1D displays the highest susceptibility to this endogenous cystatin (2.14C). cMIP is showing lowest inhibition towards CP1C whereas CP1B and CP1D are stronger inhibited and CP1A is the strongest. In addition to that, the activation effect that was observed for CP1C at lower concentration is not present for CP1D, like seen for CP1A and CP1B (2.14D).
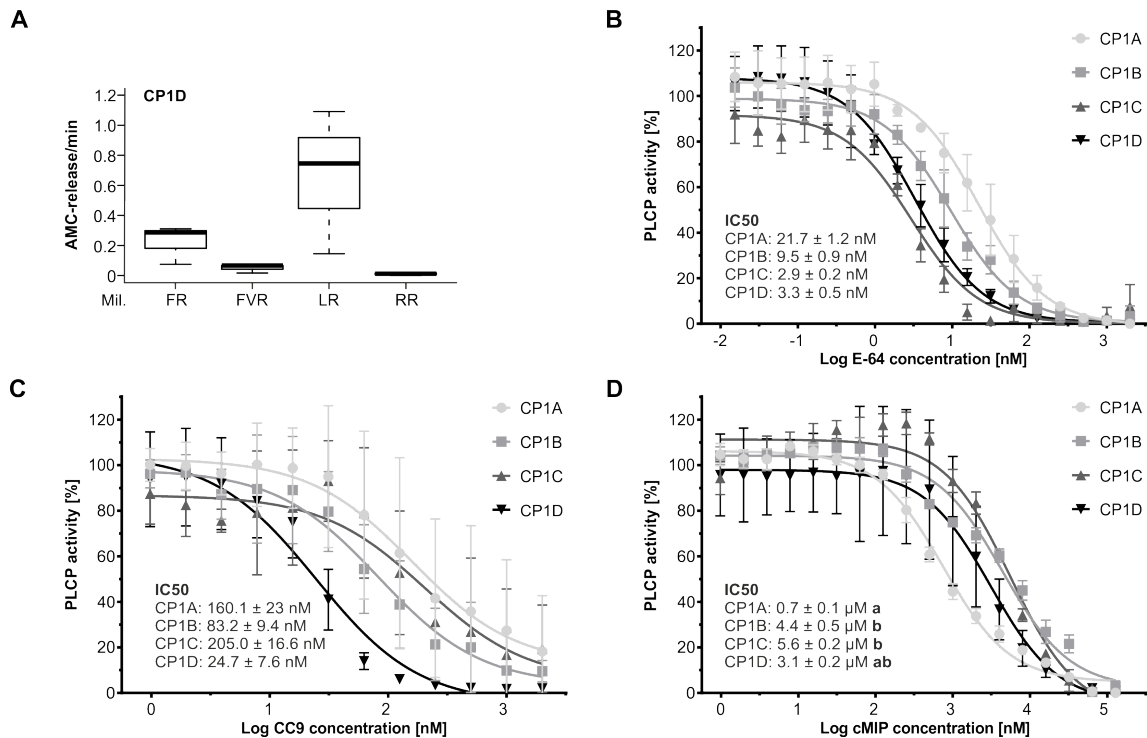
Figure 2.14: Biochemical characterisation of CP1D in relation to previously described apoplastic CP1-like PLCPs.

(A) Substrate cleavage assays of CP1D using synthetic substrates. Recombinant CP1D was tested in substrate cleavage assays using 10 µM of the following substrates: Z-FR-AMC (FR), BZ-FVR-AMC (FVR), Z-LR-AMC (LR) and Z-RR-AMC (RR). The release of AMC (relative fluorescent unit = RFU) per minute was calculated and plotted against each substrate. Activity was normalized to samples treated with E-64. Data was represented in a boxplot as described before. This experiment was performed using three independent biological replicates each with technical duplicates.

(B-D) CP1D protease shows no distinct inhibitory profiles compared to CP1-like PLCPs. Apoplastic fluids of recombinant in *N. benthamiana* produced CP1A, CP1B, CP1C and CP1D were evaluated for their activity using 10 µM of the substrate Z-LR-AMC (LR). The inhibitory profile for E-64 **(B)**, CC9, **(C)** and cMIP **(D)** was tested. Inhibitor concentrations ranged from 15 pM to 128 µM. Activity was set to 100% in the absence of inhibitor. Normalized values were plotted against Log of inhibitor concentration in nM. The experiment was performed in three independent biological replicates each with technical duplicates. A nonlinear fit based on a dose response function was performed and LogIC50-values were calculated. Error bars represent the STDEV. Significance was calculated using an unpaired t-test and differing letters behind the IC50-values indicate significant differences ($P<0.05$).

2.1.8 SA-activated PLCPs

MS analysis of the root apoplast proteome after shotgun and DCG-04 pull down did not only confirm the presence of previously identified PLCPs including the root specific CP1C and the fourth CP1-like PLCP CP1D but also revealed the presence of three SA-activated PLCPs. In contrast to the SA-associated CP1-like PLCPs in the maize leaf apoplast (van der Linde et al., 2012a) which belong to the subfamily 1 (RD21-like) the root SA-associated PLCPs B4FS65, B4FYA3 and Q10716 belong to different subfamilies of PLCPs (subfamily 5, 4 and 7, respectively, 2.4). Sequence analysis of B4FS65, B4FYA3 and Q10716 compared to the PLCP type members from A. thaliana show high variance in different protein domains and interdomain regions with an exception of the C1-protease domain pointing to its importance compared to other domains (2.15). These differences in sequence could be addressed to the different organism, organ and putative specific functions of maize and respective *A. thaliana* PLCP (Krylov et al., 2003). Similar to the respective subfamily type members, all three PLCPs contain a n-terminal signal peptide suggesting a localization in the root apoplast. All PLCPs also contain an inhibitory prodomain (PD) and a C1-protease domain (PD) with a conserved catalytic triad consisting of a Cys, a His and an Asn (2.15). The ERFNIN core structure of the inhibitory prodomain can be found in all six PLCPs. In case of the XBCP3-like PLCPs the motif is mutated to ERFNVN whereas the RD19a-like PLCPs motif is changed to the conserved ERFNAQ (2.15A & B, respectively). Additionally, only B4FYA3 which belongs to the XBCP3-like subfamily contains a prolin-rich motif C-terminal of the protease domain followed by a granulin domain (2.15B) similar to the previously described CP1-like PLCPs of the subfamily RD21-like. Maize PLCPs display only limited sequence similarity to their *A. thaliana* type members. The sequence similarity between B4FS65 and Thi1 is 57.9%, between B4FYA3 and XBCP3 is 71.0% and between Q10716 and RD19A is 76.2%. Notably the sequences differ mostly in the secretion signal, prodomain and in interdomain regions. The C1-protease domain shows the highest sequence similarity to their respective type member for all three PLCPs (2.15).
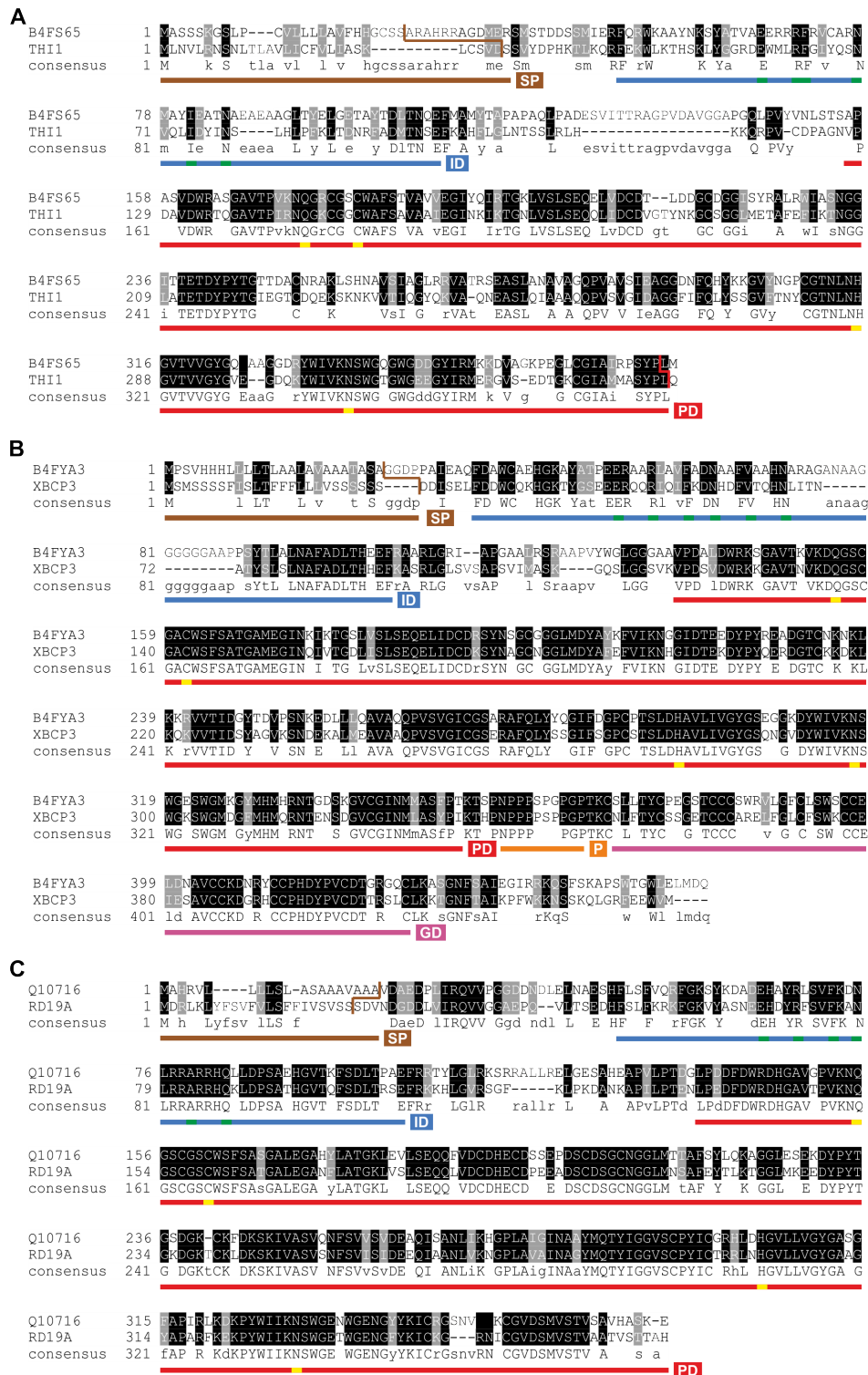
Figure 2.15: **Sequence analysis of SA-activated apoplastic PLCPs.**

Amino acid sequences of SA-activated root PLCPs B4FS65 **(A)**, B4FYA3 **(B)** and Q10716 **(C)** of the maize line B73 were aligned to their respective *A. thaliana* type member to dissect putative domain conservation. Black background indicates conserved amino acids among both PLCPs, light grey background indicates similar amino acids among the two PLCPs and white background indicates different amino acids or gaps. Signal peptide (SP, brown), inhibitory prodomain (ID, blue), protease C1-domain (PD, red) and granulin domain (GD, purple) were predicted. Amino acids forming the ERFNLN motif are labelled in green and amino acids of the active site of B4FS65 (A), B4FYA3 (B) and Q10716 (C) are highlighted in yellow.

2.1.9 Recombinant production and biochemical characterization of SA-induced root PLCPs

To get a better understanding of organ specific defense responses the three SA-activated PLCPs B4FS65, B4FYA3 and Q10716 (2.6) were cloned for recombinant expression in *N. benthamiana*. CP1A was included as a positive control and CP1A^{mut} and GFP as negative controls. AF from *N. benthamiana* leaves heterologous expressing the PLCPs was isolated. To confirm the activation of B4FS65, B4FYA3 and Q10716 after SA-treatment also in *N. benthamina* leaves plants were sprayed with 5 mM SA or mock one day before AF isolation. An ABPP using the probe MV201 was done to quantify active PLCPs content. The PLCP inhibitor E-64 was used as a negative control for each PLCP quantification (6.6). Successful SA-treatment was monitored by an increase of chlorosis and necrosis in SA-treated leaves compared to mock (6.8). Comparing SA-treated and mock samples of CP1A, B4FS65, B4FYA3 and Q10716 did not show striking differences between treatments (2.16A). CP1A which served as a positive control for overall transient expression and activity was also used as a negative control for SA-activation as it was not shown to be induced by SA-treatment. Surprisingly also no differences in activity for the three SA-activated PLCPs were detected (6.6A). Even active recombinant B4FS65 and B4FYA3 could not be detected in contrast to CP1A and Q10716 which gave strong signals in ABPPs with MV201 (6.6A & 6.6). Bands at 26 kDA and 38 kDA correspond to unspecific background signals also present in CP1A^{mut} and GFP control samples (6.6). A substrate cleavage assay as a complementary method to monitor PLCP activity verified that SA-treatment does not improve PLCP activity when overexpressed in *N. benthamiana* indicating a missing downstream signal specific for roots or maize plants (6.9). The observed SA-activation in maize roots could not be reproduced after successful SA-treatment for recombinant expressed B4FS64, B4FYA3 and Q10716 in *N. benthamiana* leaves.

To further improve the heterologous production of SA-activated PLCPs together with CP1D and rule out a problem on the transcriptional level, the PLCPs were C-terminally tagged with mCherry. The C-terminal mCherry tag was fused to B4FS65, B4FYA3, Q10716 and CP1D as well as to CP1A and CP1A^{mut} which were used as controls together with GFP as described before. Heterologous expression in *N. benthamiana* followed by AF isolation and an immunoblot with α-mCherry antibody showed signal for cleaved, but not full length mCherry in the apoplast for B4FYA3, Q10716 and CP1D indicating processing of the mCherry tag in the plant leaf. No mCherry signals were detectable for B4FS65 and the controls CP1A and CP1A^{mut} which might indicate no expression for these constructs. No mCherry signal was detected for the negative control GFP (2.16B). GFP production was confirmed by fluorescence detection (6.7). Performing an ABPP on the same samples using the probe DCG-04, a strong signal of active PLCPs for B4FYA3 and CP1D was visible. Weak signals were seen for B4FS65, Q10716 at similar levels as for CP1A^{mut} and GFP indicating that these are background signals derived from *N. benthamina* PLCPs (2.16C). In contrast to 2.16B, no activity signal was visible for Q10716. A strong activity signal was observed for CP1A contrasting the observations from 2.16B which might indicate that CP1A is involved in degradation of mCherry to undetectable fragments. For B4FYA3 expression and presence of protein could be confirmed using an immunoblot for mCherry and ABPP with DCG-04 but not MV201 while Q10716 protein could be confirmed using an mCherry immunoblot and MV201 labeling but not DCG-04 labeling. This indicates different PLCP binding specificities for MV201 and DCG-04 despite the common E-64-warhead as described for MV202 and DCG-04 (Lu et al., 2015). It may be due to the tags added to the warhead that could influence the tertiary structure and stability of probe-PLCP complexes and influence binding efficiency. No successful recombinant expression of B4FS65 could be detected by ABPP using the probe MV201 (2.16A) or DCG-04 (2.16C) and not by an immunoblot for the C-terminal mCherry tag (2.16B). Thi1-like PLCPs like B4FS65 were shown to be flower specific on expression and protein level and containing a specific flower signal (Richau et al., 2012). They might lack a leaf secretion signal to be transported to the apoplast in *N. benthamina* leaves and therefore may be localized inside the cell. To prove expression of proteins and their localization qRT-PCR, as well as fluorescence microscopy and western blot against mCherry of total leaf extracts should be performed.
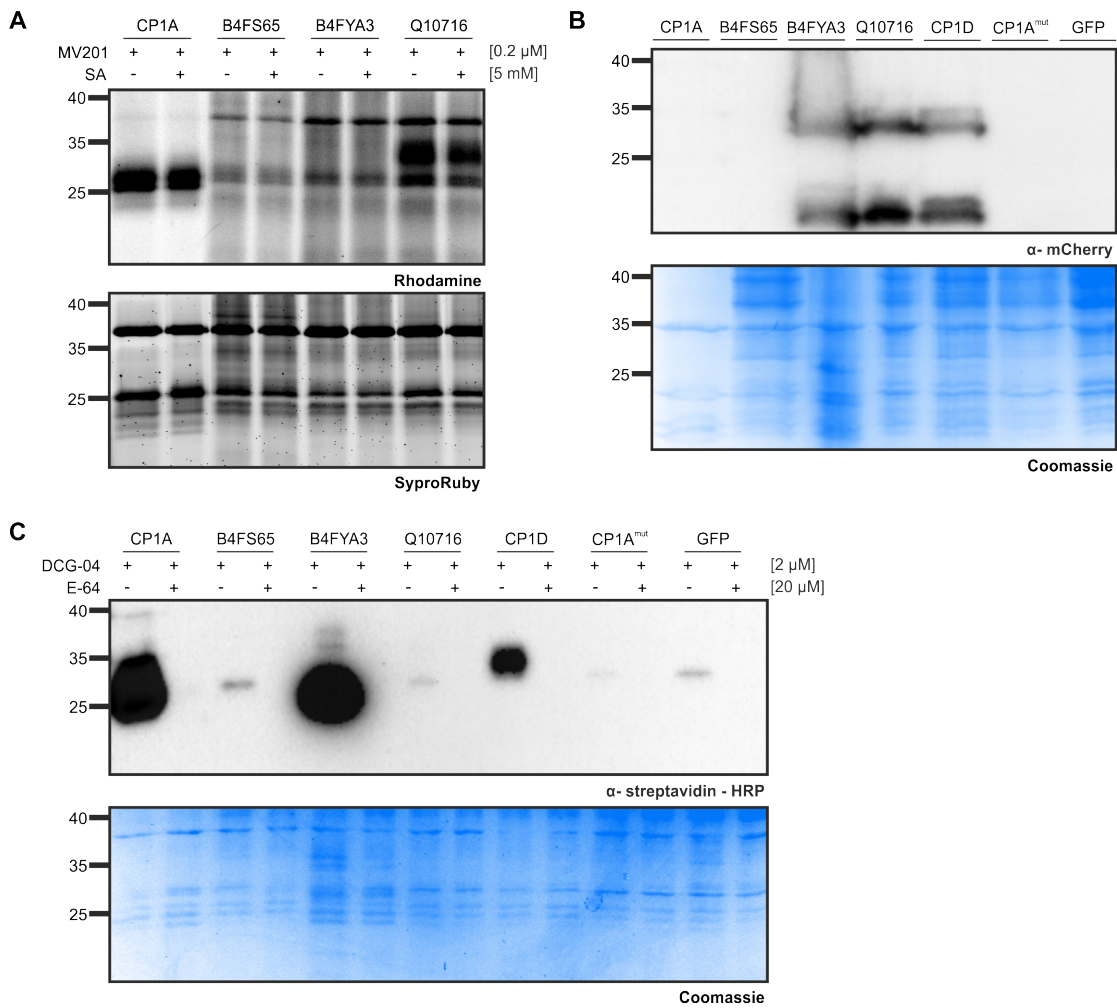
Figure 2.16: **Recombinant overexpression of SA-activated maize root PLCPs.**
(A) Activity of recombinant expressed SA-activated maize root PLCPs with (+) and without (-) SA-treatment. Leaf apoplastic fluids of recombinant PLCPs expressed in *N. benthamiana*: CP1A, B4FS65, B4FYA3 and Q10716 were isolated and labelled for 2 h with 0.2 μM MV201 (Richau et al., 2012). Labeled PLCPs were visualized by fluorescence scanning (Ex. 532 nm, Em. 580 nm). SyproRuby-stain (Ex. 450 nm, Em. 610 nm) was performed for visualization of sample loading. This experiment was performed in three independent biological replicates showing similar results.
(B) Immunoblot of recombinant expressed maize root PLCPs. CP1A, B4FS65, B4FYA3, Q10716, CP1D and CP1A[mut] were fused with a C-terminal mCherry tag and recombinant expressed in *N. benthamiana*. Leaf apoplastic fluids were isolated and samples were analyzed together with leaf apoplastic fluid of recombinant expressed GFP using SDS-PAGE. mCherry-tagged proteins were detected using a primary α-mCherry antibody followed by a secondary α-mouse-HRP antibody. Coomassie stain shows the loading control. This experiment was performed in three independent biological replicates showing similar results.
(C) DCG-04 labeling of recombinant expressed maize root PLCPs. Leaf apoplastic fluids from (B) were labelled with the probe DCG-04. Samples were pre-incubated for 30 min with (+) or without (-) 20 μM E-64 followed by 2 h labeling with 2 μM DCG-04 and analyzed with SDS-PAGE. Biotinylated proteins were detected using an α-streptavidin-HRP antibody. Coomassie stain shows the loading control. This experiment was performed in three independent biological replicates showing similar results.

To study the biochemical properties of the newly found SA-activated PLCPs, compared to other apoplastic PLCPs, like the previously described CP1-like PLCPs, substrate specificities of B4FS65, B4FYA3 and Q10716 were tested. These proteases were transiently expressed in *N. benthamiana* (2.16B-C) and apoplastic fluids were isolated followed by substrate cleavage assay as described in 2.6B. Like for the previously described PLCPs a preference for cleavage of the substrate LR was observed (2.17A-C). B4FS65 shows no cleavage of the substrate RR, and minor cleavage activity for FVR with slightly better cleavage for FR (2.17A). B4FYA3 shows about one third of the cleavage activity compared to the LR substrate and not cleavage activity toward the two remaining substrates (2.17B). Q10716 shows moderate cleavage activity for the FR substrate but no activity for FVR. It is the only tested SA-activated PLCPs that shows cleavage activity for RR even if it is scarce (2.17C). The general low cleavage activity only slightly over above the background activity of *N. benthamiana* PLCPs (6.2) of B4FS65 indicates distinct substrate specificities for this protease in comparison to the other tested apoplastic PLCPs or problems in the process of recombinant expression as seen in 2.16. Since B4FS65 is a THI1-like PLCP, which are known for vacuolar localization it might be a problem related to B4FS65 activity at the pH conditions during labeling. The vacuolar pH is close to 7, however during labeling a buffer with pH 6 was used (Shen et al., 2013). For these reasons B4FS65 was excluded from further biochemical assays.

The second approach for chemical characterization of the remaining SA-activated PLCPs B4FYA3 and Q10716 consisted of substrate cleavage assays in the presence of selected PLCP inhibitors to examine the inhibitory profiles of the PLCPs. This was performed as described for 2.7 using the same inhibitors: E-64, CC9 and cMIP. To test their inhibitory efficiency towards the SA-activated PLCPs, an inhibitor concentration range was performed using a substrate cleavage assay with Z-LR-AMC. Equal amounts of active PLCPs were used based on signal quantification from DCG-04 labelled apoplastic fluids (2.16C & 6.10). The cleavage activity of each PLCP in the absence of inhibitors was set to 100% and plotted against Log of inhibitor concentration. CP1A was included as a reference for each measurement. E-64 shows strong inhibition of Q10716 already in the nanomolar-range similar to CP1A. B4FYA3 on the contrary shows significant stronger resistance to E-64 which started inhibition not before 10-times higher concentrations of E-64 were added (2.17D). CC9 also shows PLCP inhibition in the nanomolar-range where CP1A is least- and Q10716 is most susceptible with B4FYA3 showing an intermediate susceptibility (2.17E). cMIP only displays sufficient levels of inhibition in micromolar concentrations where it was observed that B4FYA3 is significantly more resistant to inhibition in comparison to CP1A and Q10716 shows intermediate susceptibility (2.17F).
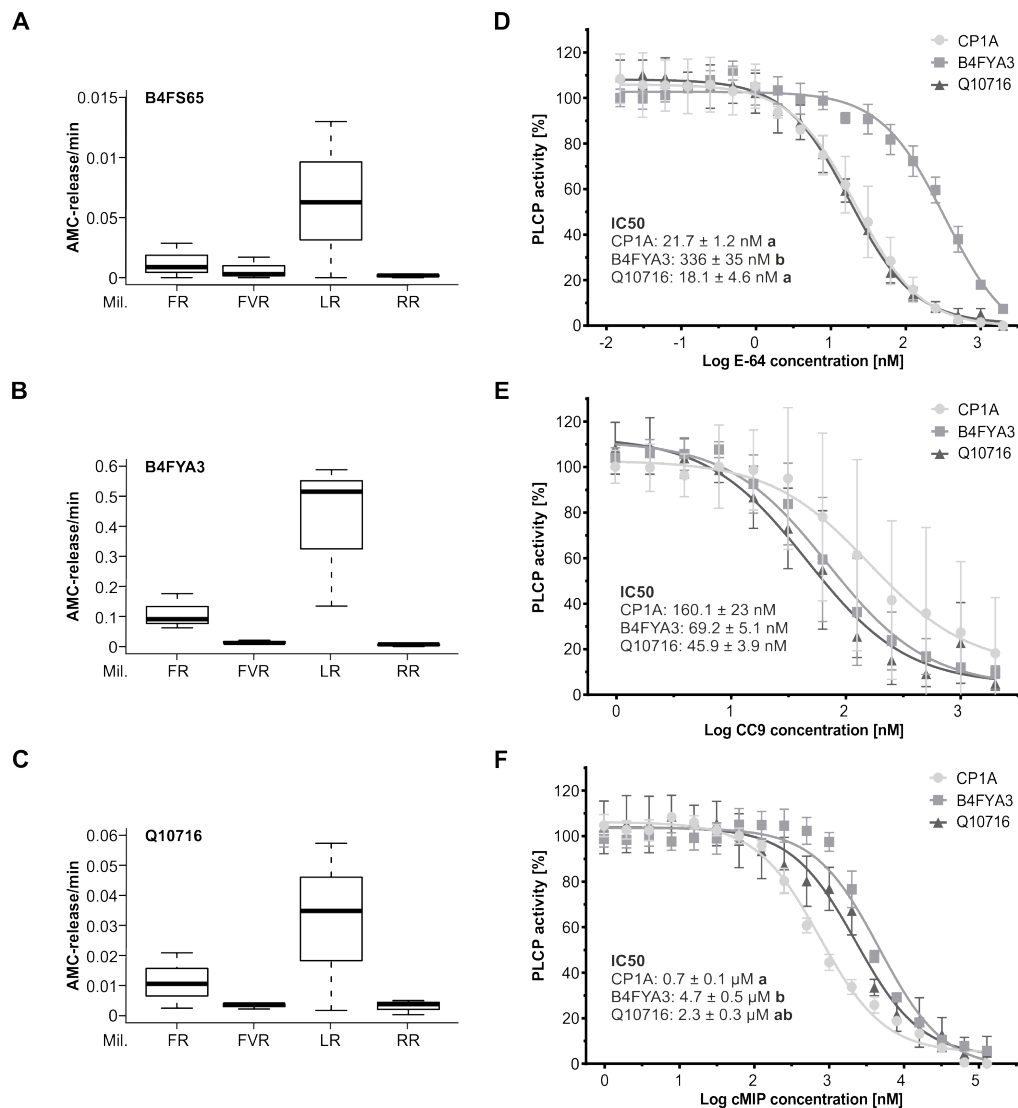
Figure 2.17: **Biochemical characterisation of SA-activated maize root PLCPs in relation to previously described apoplastic PLCPs.**
(A-C) Substrate cleavage assays of B4FS65 **(A)**, B4FYA3 **(B)** and Q10716 **(C)** using synthetic substrates. Recombinant B4FS65, B4FYA3 and Q10716 were tested in substrate cleavage assays using 10 μM of the following substrates: Z-FR-AMC (FR), BZ-FVR-AMC (FVR), Z-LR-AMC (LR) and Z-RR-AMC (RR). The release of AMC (relative fluorescent unit = RFU) per minute was calculated and plotted against each substrate. Activity was normalized to samples treated with E-64. Data was represented in a boxplot as described before. This experiment was performed using three independent biological replicates each with technical duplicates. **(D-F)** SA-activated proteases show distinct inhibitory profiles. Apoplastic fluids of in *N. benthamiana* recombinant produced CP1A, B4FYA3 and Q10716 were evaluated for their activity using 10 μM of the substrate Z-LR-AMC (LR). The inhibitory profiles for E-64 **(D)**, CC9 **(E)** and cMIP **(F)** were tested. Inhibitor concentrations ranging from 15 pM to 128 μM were used. Activity was set to 100% in the absence of inhibitor. Normalized values were plotted against Log of inhibitor concentration. The experiment was performed in three independent biological replicates each with technical duplicates. A nonlinear fit based on a dose response function was performed and LogIC50-values were calculated. Error bars represent the STDEV. Significance was calculated using an unpaired t-test and differing letters behind the IC50-values indicate significant differences (P<0.05).

2.1.10 CC1 a novel, SA-induced root cystatin

Apart from the PLCPs that were identified to be specific to root apoplasts and further characterized, it was noticed that the abundance of cystatin P31726, an endogenous cysteine protease inhibitor, was increased almost fourfold after SA-treatment whereas the abundance of other cysteine protease inhibitors did not change significantly (2.4D, blue). We aimed to compare this novel maize cystatin with the already known defense related leaf apoplastic cystatin CC9. Further on we will refer to the cystatin P31726 as corn cystatin 1 (CC1) according to its uniprot database entry and phylogeny (The UniProt, 2018). 2.18A shows the schematic structure of CC1 and CC9. Both cystatins consist of a signal peptide and a mature cystatin domain with a conserved cystatin motif with CC1 (15 kDA) being smaller than CC9 (19 kDA) (2.18A). They both contain similar secondary structures as one α-helix and β-sheet prior to the cystatin motif and three shorter β-sheets N-terminal of the cystatin motif. CC1 contains an additional short β-sheet C-terminal of the α-helix (2.18A). Comparing whole sequences of CC1 with the already known susceptibility factor to *U. maydis* infection CC9 in maize leaves reveals low sequence similarity (34.9%). On amino acid level CC1 shows gaps in the signal peptide, as well as at the C-terminus of the mature cystatin domain and a short N-terminal extension (6.11A). On the structural level it was noticed that only the cystatin motif and the cystatin secondary structures like α-helix or β-sheet are conserved but differ in orientation. Additionally, unstructured loops display no conservation (6.11B).

Analysis of the whole phylogenic order of CC1 and the previously mentioned leaf cystatin CC9 in context of the remaining maize cystatins together with cystatins of the model plants *A. thaliana* and *Oryza sativa* was performed by Henriette Läßle under supervision of Dr. Japser Depotter. Phylogenetic investigations confirmed the observed sequence variations and showed a distinct phylogenetic heritage of CC1 and CC9. In contrast to CC9, CC1 shows similarity to AtCys1, an Arabidopsis cystatin found to be involved in cell death inhibition (Belenghi et al., 2003). A total of 13 maize cystatin sequences from B73, twelve *O. sativa* cystatins, seven *A. thaliana* cystatins (Massonneau et al., 2005; Martinez et al., 2008; Martinez et al., 2009; van der Linde et al., 2012a) and the EGB cystatins CC1 and CC9 were used to generate a phylogenetic tree with the maximum likelihood method. In line with the low sequence similarity, CC9 is phylogenetically distinct from CC1. CC1 clusters together with the maize cystatins CC-I and CC-II. The rice OC-I as well as AtCYS-1 and OC-II and CC-III are other phylogenic close cystatins to CC1. On the other hand, CC9 is phylogenetically distant to CC1, clustering with CC-IX and CC-XII (2.18B). As CC1 was identified to be SA-responsive so far only in the root apoplast but not in the leaf apoplast, an organ specific role of CC1 associated to SA was hypothesized in roots.

To further understand the biochemical properties of this putative organ specific SA-associated cystatin, CC1 was cloned into the vector pET-15b for heterologous production with a HIS-tag for purification and transformed it into *E. coli* BL21 (6.12). CC1 was successfully produced and purified using Ni^{2+}-NTA. A strong signal for CC1 at the expected size of 15 kDA was observed in elution step 2 and 3 (2.18C). Next, a size-exclusion chromatography using a HiLoad® 16/600 Superdex® 75 pg column in an Äkta system (GE Healthcare, Chicago, Illinois, USA) was performed for further purification. Peak fractions of high protein content of the elution spectrum were analyzed using SDS-PAGE (2.18D, 6.13). Fractions of the void volume still contained protein of various sizes whereas fractions of the two following peaks consisted dominantly of protein with the expected size of 15 kDA for CC1 (2.18D). To confirm the presence of CC1 an α-HIS immunoblot analysis of pooled fractions for both, peak 1 and peak 2 performed. Specific signals at 15 kDA for both peaks corresponding to CC1 were observed, indicating the presence of CC1 in both elution peaks (2.18E). The two distinct peaks for CC1 might be explained either by a change of the hydrodynamic volume through protein-dimerization which is well known for cystatins or changes in protein folding (Batas et al., 1997; Jurczak et al., 2016). To validate CC1 presence in the peaks one could subject fractions to MS analysis, perform analytical ultracentrifugation (AUC) or absolute size exclusion chromatography (ASEC). ASEC combines size exclusion chromatography with a dynamic light scattering (DLS) instrument measuring the interference spectra after Rayleigh scattering of light on small molecules. Based on the measured scattering the molecular weight of the molecule can be calculated (Knobloch et al., 1997). AUC takes advantage of the different sedimentation coefficients between molecules of different shape and size. A high centrifugal force is applied to the samples while their sedimentation over time is optically monitored in real time. Optical systems using absorbance, interference or fluorescence can be used to precisely monitor the sedimentation. The movement of molecules in a high centrifugal field can be interpreted to define the size, shape and interaction of macromolecules (Cole et al., 2008; Ghirlando, 2011).

Figure 2.18: **Comparison of maize apoplastic cystatins CC1 and CC9 and production of CC1.**

(A) Schematic comparison of CC1 and CC9. Secondary structures are indicated for each cystatin as displayed in the figure. Signal peptide (SP, brown) and cystatin domain (CY, red) were predicted. Amino acids forming the cystatin type motif QxVxG (CM) are labelled in yellow.

(B) Phylogeny of plant cystatins. A total of 13 maize cystatin sequences from B73, twelve *O. sativa* cystatins, seven *A. thaliana* cystatins (Massonneau et al., 2005; Martinez et al., 2008; Martinez et al., 2009; van der Linde et al., 2012b) and the EGB cystatins CC1 and CC9 were used to generate a radial phylogenetic tree. We used full length sequences from maize (CC), rice (OC) and Arabidopsis (AtCYS) including the signal peptides. The tree is drawn to scale, with branch lengths measured in the number of substitutions per site. Sequences were aligned using MAFFT (v7.407) (Katoh et al., 2013). RAxML with the GTRGAMMA substitution model (v8.2.0) was used for the construction of a radial tree (Stamatakis, 2014). The robustness was assessed using 100 bootstrap replicates. Bootstrap-supported clusters of related cystatins (cluster I-III) are accentuated by backgrounds in shades of gray. The EGB cystatins CC1 and CC9 were highlighted in red.

(C) Recombinant production of CC1 in E. coli. CC1 was cloned with a N-terminal HIS-tag into the vector pet15b and transformed to *E. coli* Bl21 cells for heterologous protein production followed by Ni^{2+}- Nitrilotriacetic acid (NTA). Samples were taken during the purification process: culture pellet (P), supernatant (SN), column flow through (FT), wash (W) and elutions (E1, E2, E3). Samples were analyzed using coomassie stained SDS-PAGE and HIS-tagged proteins were detected using a primary α-HIS antibody followed by a secondary α-mouse-HRP antibody.

(D) Size-exclusion chromatography (SEC) of heterologous produced CC1. E2 from Ni^{2+}-NTA (C) was subjected to size-exclusion chromatography using a HiLoad® 16/600 Superdex® 75 pg column for protein separation (6.13). Fractions of void volume, peak 1 (P1) and peak 2 (P2) were analyzed coomassie stained SDS-PAGE.

(E) Immunoblot detection of HIS-tagged CC1. Fractions of P1 and P2 (D) were pooled and dilutions were subjected to SDS-PAGE. HIS-tagged proteins were detected using a primary α-HIS antibody followed by a secondary α-mouse-HRP antibody. Coomassie stain shows the western blot loading control. This experiment was performed in three independent biological replicates showing similar results.

Due to higher protein concentration (2.3 mg/ml = 153 mM) purified CC1 from fractions of peak 2 were pooled and tested for inhibitory capacity. Concentrations from 15 pM – 2 µM of CC1 were tested against the CP1-like PLCPs CP1A, CP1B, CP1C and CP1D as well as the SA-associated PLCPs B4FYA3 and Q10716 (2.19A & C). As a reference for inhibition the commercially available chicken cystatin (CC) (Sigma-Aldrich, St. Louis, Missouri, USA) was included (2.19B & D). CC1 and CC both inhibit CP1-like PLCPs efficiently already at nanomolar concentrations whereas CP1D shows a slightly stronger resistance to CC compared especially to CP1C which is most susceptible to CC (2.19A & B). For the inhibition test with B4FYA3 and Q10716 the PLCP CP1A was included in the graph as a reference. Both SA-associated PLCPs show a stronger resistance towards inhibition by CC1 and CC. B4FYA3 is significantly more resistant to CC1 and CC compared to CP1A (2.19C & D) and Q10716 is significantly more resistant only to CC (2.19D).
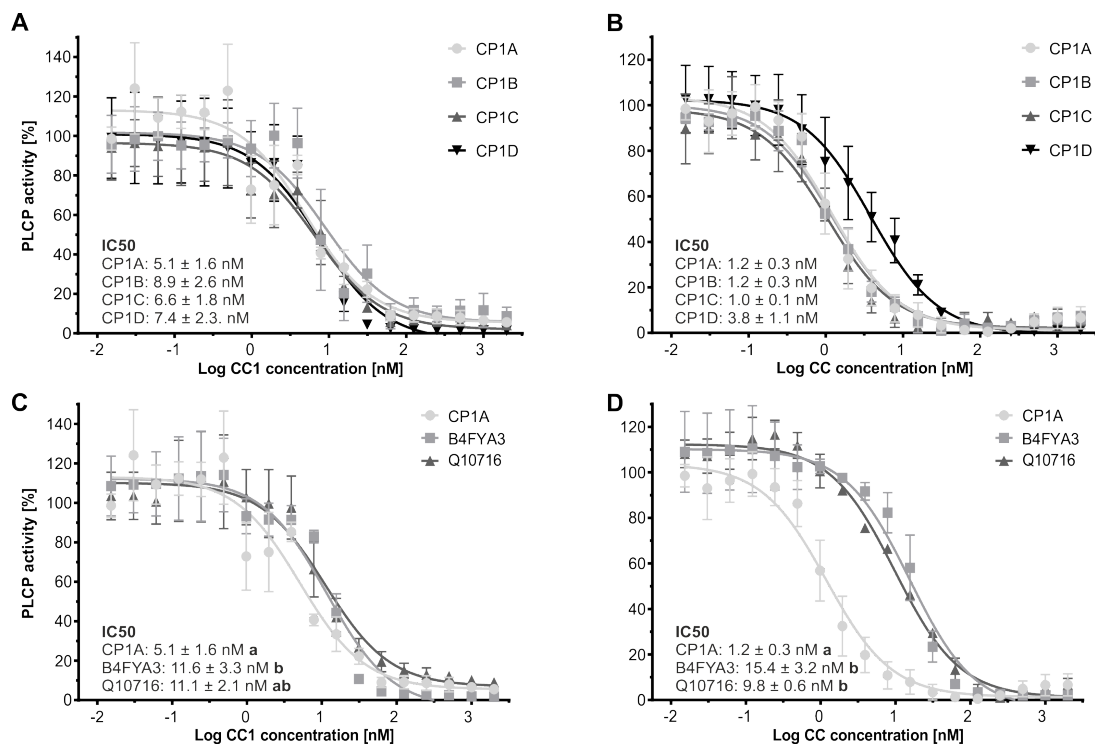
Figure 2.19: **CC1 shows distinct inhibitory efficiency towards maize apoplastic PLCPs.**
Apoplastic fluids of recombinant maize PLCPs CP1A, CP1B, CP1C, CP1D and B4FS65, B4FYA3, Q10716 were tested against heterologous expressed CC1 **(A & C)** and the commercial chicken cystatin (CC) **(B & D)**. Apoplastic fluids were evaluated for their activity using 10 µM of the substrate Z-LR-AMC (LR) in the presence of the inhibitors. Inhibitor concentrations ranged from 15 pM to 2 µM. Activity was set to 100% in the absence of inhibitor. Normalized values were plotted against Log of inhibitor concentration. The experiment was performed in three independent biological replicates each with technical duplicates. A nonlinear fit based on a dose response function was performed and IC50-values were calculated. Error bars represent the STDEV. Significance was calculated using an unpaired t-test and differing letters behind the IC50-values indicate significant differences ($P<0.05$).

2.1.11 Analysis of root PLCP expression and biochemical properties

In previous chapters expression data, substrate specifies, pH-stability and inhibitory susceptibility of root PLCPs was analyzed. The publicly available expression data of roots was collected and normalized to leaf expression levels (2.20A). PLCPs were clustered based on their relative expression pattern in roots versus leaves. As described earlier, most of the PLCPs are higher expressed in roots than in leaves with CP1C showing the highest relative root expression with a 6-fold increase. Interestingly, CP1A and two of the SA-associated PLCPs, B4FYA3 and Q10716 show higher expression levels in leaves than in roots.

Differential affinities towards the tested commercial substrates were observed for CP1-like and other PLCPs, which may be explained by unequal substrate accessibility to their active sites (2.20B). Summarizing PLCPs in three clusters for the substrate specificities confirmed that all tested PLCPs show highest cleavage capacity for the LR-substrate as seen for RAF but differ in their cleavage capacities towards substrates carrying different residues at the P2-position. The RR-substrate was not cleaved by any PLCPs except for CP1A and CP1B. The FVR substrate was also non-favorable for most PLCPs where again CP1A and CP1B show best results of cleavage. As Val is structurally and biochemically similar to Leu, it was surprising to see that the FVR-substrate was cleaved drastically less efficient than the LR-substrate. FVR was the only substrate consisting of three amino acids prior the N-terminal AMC which already made it structurally more difficult for interaction with the enzymes due to its size. The relatively low cleavage of this substrate despite the small Val in the P2-position could be explained by the specific additional amino acid in the P3-position (Richau et al., 2012). The bulky Phe might sterically hinder the interaction and cleavage of the substrate as seen for the FR-substrate. The FR-substrate was second best for CP1A and CP1B, but still unfavorable for most of the PLCPs. Apart from CP1A and CP1B also CP1D and the SA-associated PLCPs B4FYA3 and Q10716 are capable to cleave the FR-substrate to some extend (2.20B). Three-dimensional modelling of all PLCPs revealed an outward orientation of the catalytic His for B4FYA3 and Q10716 as seen for CP1D. Reorientation of the His rest is widening the active site and may facilitate interactions with bulky substrates carrying the Phe in the P2-position. An inward orientation of the catalytic His as seen for CP1A was observed for the remaining PLCPs. The tested PLCPs were clustered after their cleavage specificities in three clusters. Cluster I comprises of CP1A and CP1B, Cluster II contains B4FYA3, Q10716 and CP1D and Cluster III is built of CP1C, CathB, CP2, XCP2 and B4FS65. Cluster I cleaves the substrates FR, FVR, LR and RR. Cluster II cleaves the substrates FR and LR and Cluster III only cleaves the LR substrate. Interestingly, CP1C does not clusters together with other CP1-like PLCPs but with the phylogenetically distant CathB and XCP2 in cluster III which belong to different subfamilies of PLCPs (subfamily 9 and 3, respectively). The observed similarities in substrate specificity may be correlated to similar target preferences for each cluster *in vivo.*

The pH differs in various organelles of the plant providing specific environments influencing the activity of enzymes. Depending on the organelle it ranges from pH 5.2 in the vacuole to 8.4 in peroxisomes in *A. thaliana* (Shen et al., 2013). Based on this, the pH sensitivity for enzyme activity can provide indications for the sub-cellular location of enzyme activity. The optimal pH for PLCP activity is at pH 5 for the CP1-like PLCPs and CathB. It is slightly shifted to pH 6 for B4FYA3, XCP2, Q10716 and CP2. These pH optima fit to an apoplastic location where the pH ranges from pH 5.5 – 6.5 and was measured in this study to be equal to 6 fitting to the reported ph optimum for *A. thaliana* PLCPs (Richau et al., 2012). An even higher pH optimum of pH 7 for B4FS65 points more to a vacuolar localization (Pfanz et al., 1987; Grignon et al., 1991). CP1C and CP1D are most selective for their pH dependent activity which ranges mainly from pH 4 – 6. CP1A, CP1B and B4FYA3 are active starting at a pH of 3 – 7 and XCP2, CathB, Q10716, CP2 and B4FS65 are active from pH 4 up to pH 9 or even 10 (2.20C & 6.14).

These PLCPs were also tested for their susceptibility to various PLCP inhibitors like E-64, cMIP, CC9, CC and CC1. Pit2, the precursor protein of UmcMIP (Mueller et al., 2013; Misas Villamil et al., 2019) were also included (2.20D). Graphs for inhibition of CathB, CP2 and XCP2 and inhibition of Pit2 versus CP1-like and SA-activated PLCPs, which have not been represented in previous figures are shown in 6.15 & 6.16, respectively. In general, it was seen that cMIP and Pit2 were weaker inhibitors towards the tested PLCPs than the other tested inhibitors. CP1A shows to be most resistant to E-64 from all tested CP1-like PLCPs but is highly exceeded in resistance by B4FYA3. Interestingly, CP1C seems to be least resistant towards E-64, an inhibitor produced and first isolated from the soil fungus *Aspergillus japonicas* (Hanada et al., 1978) which might indicate CP1C as a putative favorable target for fungal inhibition through inhibitors similar to E-64. B4FYA3 on the contrary might be induced as a E-64 resistant PLCP to ensure a proper defense reaction. CP1C is most resistant of all tested PLCPs to cMIP. CP1A is the least resistant CP1-like and CathB the overall least resistant PLCP to cMIP tested in this study. In contrast, CP1A is the most resistant CP1-like PLCP to Pit2. CP1B is the least resistant CP1-like PLCP. Q10716 and CP2 are the most and least resistant tested PLCPs to Pit2, respectively. Interestingly we observed Pit2 to be able to inhibit CathB which stands in contrast to previously published results by Mueller et al., (2013) that showed Pit2 to be unable to inhibit CathB. CP1D is the least resistant tested PLCP towards CC9 inhibition. CP1C is the most resistant CP1-like and XCP2 the overall most resistant PLCP. CP2 is most resistant to inhibition of the endogenous root cystatin CC1 and CP1A displays the least resistance. CP1B is the displays the most resistance to CC1 of the tested CP1-like PLCPs. CP1C is the least resistant tested PLCP to the commercial CC. CP1D shows highest resistance among CP1-like PLCPs to CC but the two SA-activated PLCPs B4FYA3 and Q10716 display the highest resistance to CC inhibition of all tested PLCPs. CP1D displayed intermediate susceptibilities to the tested inhibitors compared the other CP1-like PLCPs suggesting that the overall structural changes towards CP1A and CP1B and the specific orientation of His in the catalytic triad do not strongly influence inhibitory interactions. Compared to the clear

correlation between the structural feature of catalytic His orientation and substrate cleavage that we described above there was no clear pattern observable for inhibition susceptibility of PLCPs for the tested inhibitors. We could neither observe a pattern for inhibitor susceptibility based on catalytic His orientation nor based on sequence homology and phylogeny of the PLCPs.

IC50-values [nM]

PLCP \ Inhibitor	CP1A	CP1B	CP1C	CP1D	CathB	CP2	XCP2	B4FYA3	Q10716
E-64	21.66	9.48	2.94	3.35	6.45	36.05	7.74	335.80	18.06
cMIP	749	4443	5583	3115	407	5227	413	4659	2277
Pit2	10558	5078	5152	8077	2142	965	1093	6413	19921
CC9	160.10	83.15	205.00	24.67	251.90	70.33	593.00	69.24	45.93
CC1	5.10	8.93	6.58	7.37	10.69	33.56	20.19	11.63	11.06
CC	1.20	1.21	1.05	3.83	1.50	2.55	1.72	15.43	9.77
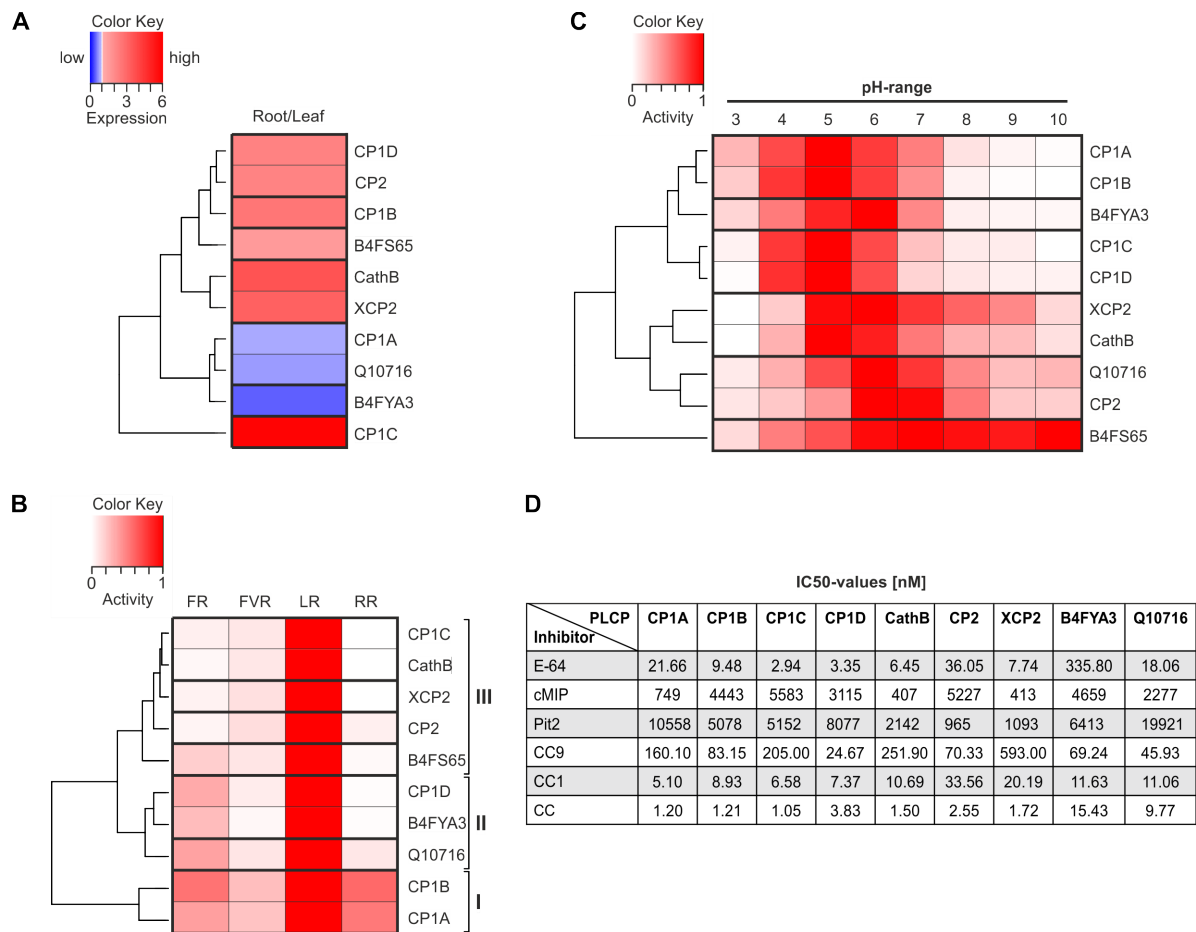
Figure 2.20: **Transcriptional and biochemical analysis of root apoplastic maize PLCPs.**
(A) Expression pattern of root apoplastic maize PLCPs. Relative expression of root apoplastic maize PLCPs in untreated B73 based on publicly available data (Winter et al., 2007; Sekhon et al., 2011; Andorf et al., 2016; Stelpflug et al., 2016). Mean expression of leaves and roots at different developmental stages was calculated and normalized to leaf expression for individual PLCPs. The heat map represents a one – to – one comparison for each PLCP. PLCPs were clustered based on their relative expression pattern to leaves.
(B) Heat-map of relative substrate affinity. Recombinant PLCPs were tested in substrate cleavage assays using 10 µM of the following substrates: Z-FR-AMC (FR), BZ-FVR-AMC (FVR), Z-LR-AMC (LR) and Z-RR-AMC (RR) (Figure 13, 18, 21). PLCP activity was calculated for each PLCP and each substrate relative to the strongest activity. Strongest activity was set to 1 (red) and no activity was set to 0 (white). PLCPs were clustered based on their relative substrate affinity pattern.
(C) pH dependent PLCP activity. Substrate cleavage of heterologous in *N. benthamiana* produced PLCPs was tested at various pH (3 – 10) using the substrate Z-LR-AMC (LR) (6.14). PLCP activity at each pH was calculated relative to the strongest activity. Strongest activity was set to 1 (red) and no activity set to 0 (white). PLCPs were clustered based on their activity pattern at various pH.
(D) Inhibitory profiles of root apoplastic PLCPs. Apoplastic fluids of recombinant in *N. benthamiana* produced PLCPs were evaluated for their activity using 10 µM of the substrate Z-LR-AMC (LR) in the presence of an inhibitor. The inhibitory profile for E-64, cMIP, Pit2, CC9, CC1 and the commercial chicken cystatin (CC) was tested. IC50-values [nM] were calculated for each inhibitor-PLCP combination and displayed in an overview table.

2.2 Conservation of SA-associated root PLCP activation

In an approach to investigate if the observed activation of root PLCPs might be conserved also among other plants, Nick Dunken tested the connection between SA-treatment and PLCP activity in roots of *A. thaliana* Col-0 as part of his bachelor thesis. Under my supervision Nick Dunken could observe an activation of *A. thaliana* root PLCPs upon SA-treatment compared to mock-treated samples (2.21, Dunken, Bachelor thesis, 2017). *A. thaliana* plants grown in liquid culture were treated with SA- and mock-solution followed by an ABPP to monitor changes in total PLCP activity. Due to technical difficulties of apoplastic fluid isolation from Arabidopsis roots total extract (TE) was used for these assays. A general induction of PLCP upon SA-treatment was observed although the loading controls indicate far less total protein content loaded for the SA-treated samples. We saw an induction of PLCP activity at 27 and 37 kDA which might correspond to XCP2, AALP and RD21, from which RD21 was shown to be involved in plant defense (van der Hoorn et al., 2004b; Shindo et al., 2012).
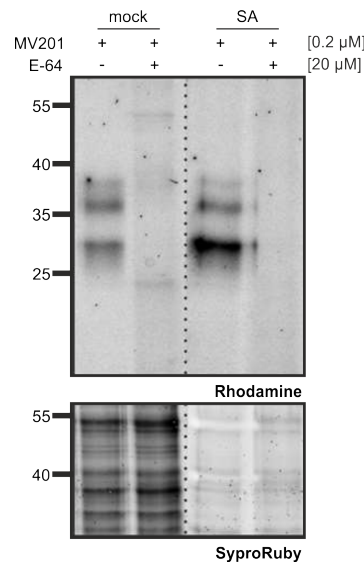
Figure 2.21: **SA-induced PLCP activation in Arabidopsis roots.**
Arabidopsis root total extract (TE) was harvested from Arabidopsis which were mock (-) or SA (+) -treated. TE of both treatments were labelled with the probe MV201 (Richau et al., 2012). Samples were pre-incubated for 30 min with (+) or without (-) 20 µM E-64 followed by 2 h labeling with 0.2 µM MV201. Labeled PLCPs were visualized by fluorescence scanning (Ex. 532 nm, Em. 580 nm). SyproRuby stain (Ex. 450 nm, Em. 610 nm) was performed for visualization of sample loading. This experiment was performed in three independent biological replicates showing similar results.

2.2.1 Summary of organ specific SA-signaling and PLCP activation

In this part of my thesis, it was found that apoplastic PLCP expression and activity differ in leaf and root proteomes and that PLCP activity after SA-treatment is likely a post-translational process. Three different SA-activated, root specific apoplastic PLCPs were identified which may point to a divergent mechanism of SA signaling through distinct PLCPs in different organs. Additionally, CP1C and CP1D, two root specific CP1-like PLCP of the RD21-like subfamily were found. CP1C shows structure and sequence similarities to CP1A but displays different substrate specificity and inhibitor susceptibility. Differences at the surface and in close proximity to the catalytic triad might suggest distinct interaction partners. CP1D, albeit highly similar to CP1C in sequence and structure displays different inhibitor susceptibility and substrate specificity which is closer to CP1A and CP1B. A changed orientation of the catalytic His pointing outward of the catalytic grove compared to the other three CP1-like PLCPs described in this work might be the major driving force of the observed differences for CP1D. Besides, after SA-treatment the root specific corn cystatin 1 (CC1) was identified to be more abundant upon SA-treatment which might hint towards an involvement in organ specific SA signaling.

2.3 Plant PLCP inhibition by endophytic root mircroorganisms

2.3.1 PLCP inhibition by fungal endopyhtes

Changing the perspective of plant root-microbe interactions towards the microbial side one aim of this thesis was to screen for PLCP inhibiting molecules secreted by root endophytic microbes into the apoplastic space. A screen of 102 maize root endophytic fungi (provided by AG Bucher, University of Cologne, Germany) for their PLCP inhibitory capacity was performed (2.22A). Fungal strains were grown for five days in full liquid media (PD), prior to a medium exchange to minimal media (NM) to induce effector production by applied nutrient stress. After one day in NM conditions culture supernatant containing putative PLCP targeting molecules was isolated. Supernatants were used in a substrate cleavage assay as described before. In a first approach 10% of the final reaction volume was culture supernatant. As a control NM was added to RAF and the FR substrate. Possible outcomes of NM substitution with fungal culture supernatant are a reduced (A) or increased substrate cleavage (B). Addition of the PLCP inhibitor E-64 should lead to a total loss of substrate cleavage. To take only PLCP activity into account, measured values of samples containing E-64 were subtracted from control samples consisting of NM with RAF and substrate. Normalization was done to 100% of activity of the control sample. 2.22B shows a representation of nine tested fungi. Fungal screening resulted into mostly non-significant and variable tendencies of increased substrate cleavage. Almost no significant inhibition was observed for the tested fungi. Although, *Bionectria ochroleuca* and *Ceratobasidium sp.* showed a tendency for inhibition (2.22B). The remaining seven fungi show a trend to increase substrate cleavage. Reproducibility of these assays was challenging which is represented by high error bars for most of the fungi. Only the enhanced substrate cleavage effect of *Fusarium Oxysporum* was significant. Since the main focus was on PLCP inhibitors this effect was not followed up in further experiments.
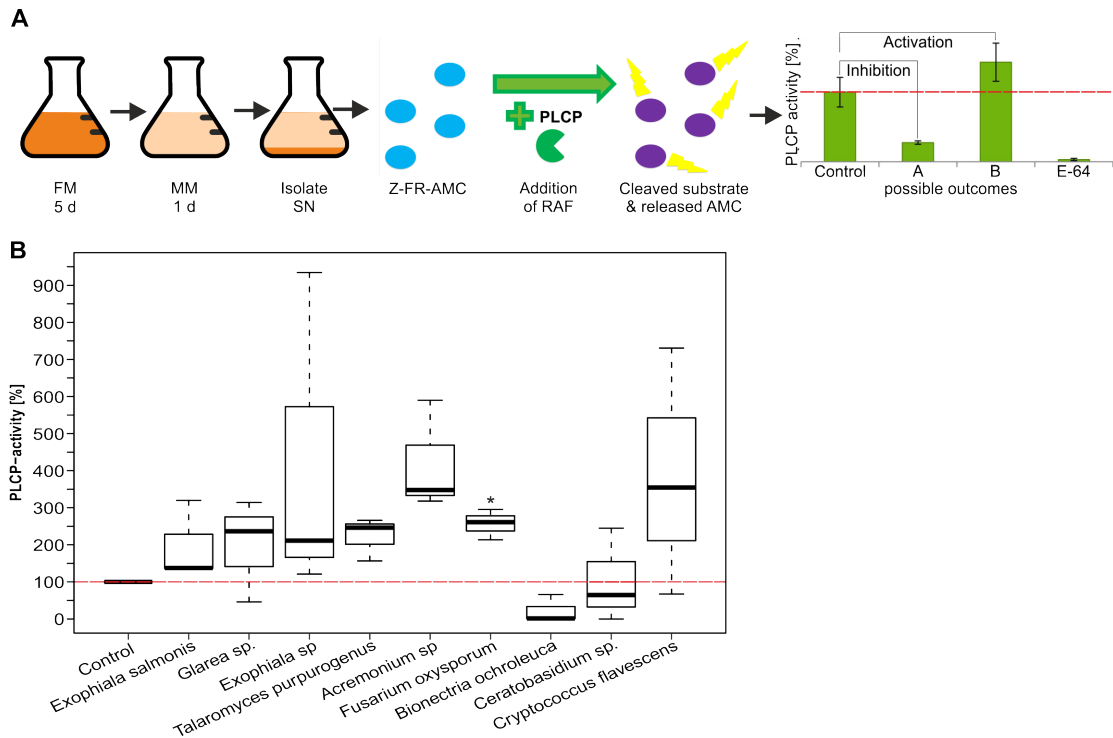
Figure 2.22: **PLCP-inhibitory capacity of root endophytic fungi.**

(A) Workflow to address PLCP-inhibitory capacity of root endophytic fungi. Fungi were grown in an Erlenmeyer flask in 20 ml of full media (FM) for five days (5d) followed by a media-exchange to minimal media (MM) for one day (1d). Culture supernatant (SN) was collected and tested for PLCP-inhibition in a substrate cleavage assay with maize RAF using the fluorogenic substrate Z-FR-AMC. 10 µl culture supernatant was used with 10 µl maize RAF using 10 µM of the substrate. Cleavage of substrate over time was measured via the release of fluorescent AMC. E-64 was added as a negative control of activity. Activity was set to 100% in the absence of bacterial supernatant (dashed red line) and normalized to samples treated with E-64. Putative results compared to the control are inhibition (A) and activation (B).

(B) Fungal secreted molecules affect maize PLCP activity. A representation of nine fungi supernatants from 102 endophytic fungi tested as described before (A) was displayed. Data was represented in a boxplot as described before. This experiment was performed using three independent biological replicates each with technical duplicates. P-values were calculated with an unpaired t-test. *$P<0.05$.

2.3.2 PLCP inhibition by bacterial endophytes

The second approach was to screen a set of maize root endophytic bacteria for their PLCP inhibition capacity. For this purpose, field grown maize plants were collected near to the city of Marburg (Andre Müller in collaboration with Stefanie Glaeser, Hessen, Germany). The roots were separated and surface sterilized. The remaining content of endophytic bacteria was then analyzed using 16S rRNA pyro sequencing and cultivated for further use by Stephanie Glaeser (Justus-Liebig-University, Giessen, Germany). 96 bacteria were successfully cultivated and used for a PLCP inhibition screen. Bacterial strains were grown for one day in full liquid media (DYT), prior to a medium exchange to minimal media (M9) to induce effector production by applied nutrient stress. After one day in M9 conditions, culture supernatant containing putative PLCP targeting molecules was isolated. Supernatants were used in a substrate cleavage assay as described before. In a first approach 10% of the final reaction volume was culture supernatant. As a control M9 was added to RAF and the FR substrate. Possible outcomes of substitution of M9 with bacterial culture supernatant are a reduced (A) or increased substrate cleavage (B). Addition of the PLCP inhibitor E-64 should lead to a total loss of substrate cleavage (2.23A). To take only PLCP activity into account, measured values of samples containing E-64 were subtracted from control samples consisting of NM with RAF and substrate. Normalization was done to 100% activity of the control sample. After 16S rRNA sequencing was performed a comparison to known bacterial genomes was done using a phylogenetic tree (2.23B). On the phyla level the majority of endophytic community consists of proteobacteria (α, β, γ). The second big class are the firmicutes whereas only small numbers of actinobacteria are present (2.23B). 2.23C shows a representative excerpt of the tested bacteria. Bacterial screening showed mostly non-significant modulation of RAF PLCP substrate cleavage. Most bacteria showed enhancement of PLCP substrate cleavage activity like *Curtobacterium albidum*, *Brevibacterium frigoritolerans* or *Brevundimonas nasdae* (2.23C). Interestingly two bacteria, *Flavobacterium oceanosedimentum* and *Mycobacterium aubagnense*, both belonging to the phyla of actinobacteria (2.23B, red) showed significant inhibitory effects on PLCP substrate cleavage activity (2.23C). In total, inhibition was only observed for 2% of the tested bacteria.

While screening the endophyte collection from field grown maize for PLCP inhibition Niu et al. 2017b published the development of a stable maize root synthetic community (SynCom) consisting of only seven members. On the phyla level the SynCom members resemble our field isolated endophyte collection (2.23B). It contains five proteobacteria (α, β, γ), an actinobacterium and one bacteriodite. The SynCom was provided by the group of Roberto Kolter (Harvard Medical School, Boston, USA) and included in our screen. PLCP inhibitory capacity of each single strain was tested (2.23D). Interestingly, three out of seven of the SynCom members, *Stenotrophomonas maltophilia*, *Chryseobacterium indologenes* and *Herbaspirilium frisingense* show a trend for PLCP activation. The other four bacteria *Ochrobactrum pituitosum*, *Curtobacterium pussillum*, *Enterobacter chloacae* and *Pseudomonas putida* show a trend for inhibition of PLCP cleavage activity. Inhibition of *O. pituitosum* and *P. putida* was statistically significant in the first screen (2.23D).
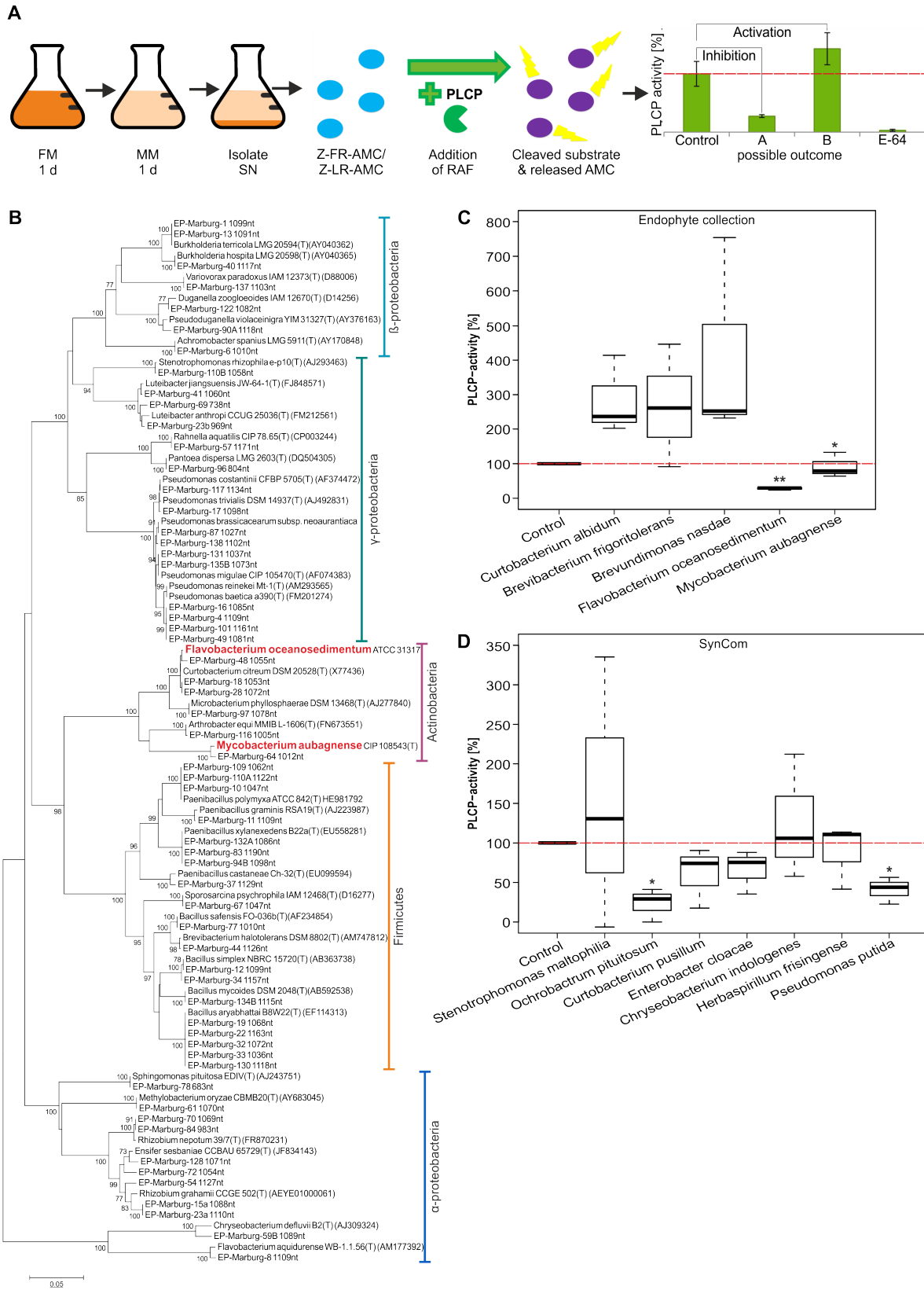
Figure 2.23: **PLCP-inhibitory capacity of root endophytic bacteria.**

(A) Workflow to address PLCP-inhibitory capacity of root endophytic bacteria. Bacteria were grown in a 96-well plate in 100 µl of full media (FM) for one day (1d) followed by a dilution to an Optical density at 600 nM (OD_{600}) of 0.05 and media-exchange to minimal media (MM) for one day (1d). Culture supernatant was collected and tested for PLCP-inhibition in a substrate cleavage assay with maize RAF. Initial screens were performed using the substrate Z-FR-AMC but Z-LR-AMC was used for further analysis displayed in this study due to the higher cleavage activity towards Z-LR-AMC for RAF (2.1A & B). 10 µl culture supernatant was used with 10 µl maize RAF using 10 µM of the respective substrate. Cleavage of substrate over time was measured via the release of fluorescent AMC. E-64 was added as a negative control of activity. Activity was set to 100% in the absence of bacterial supernatant (dashed red line) and normalized to samples treated with E-64. Putative results compared to the control are inhibition (A) and activation (B).
(B) Phylogenetic composition of the bacterial maize root endophytic community. Maize endophytic bacteria were isolated from surface sterilised maize roots and phylogenetic analyses using 16S rRNA sequencing was performed by Stefanie Glaeser (Justus-Liebig-University, Giessen, Germany). Candidates for PLCP inhibition capacity are highlighted in red. 96 of these bacteria could be cultivated and were used for further experiments.
(C-D) Bacterial secreted molecules affect maize PLCP activity. A representation of five bacterial supernatants out of 96 tested bacteria **(C)** and seven members of a synthetic maize root community **(D)** (Niu et al., 2017b) tested in substrate cleavage assays as described before (A) was displayed here. Data was represented in a boxplot as described before. This experiment was performed using three independent biological replicates each with technical duplicates. P-values were calculated with an unpaired t-test. *$P<0.05$; **$P<0.01$.

In the first screen we aimed to induce effector production of the bacteria by applying nutrient stress. Effectors are usually induced upon contact to plants (van der Does et al., 2008). Root exudates consist of a mixture of plant derived compounds released into the rhizospere which can be sensed by microorganisms (Glick, 2012). To investigate if the tested bacteria are able to sense the presence of a plant by these exudates and induce the production of specific plant effectors targeting PLCPs upon their presence, the experimental setup was modified. One day after growth of bacteria in DYT, the media was changed to M9 and supplemented with RE. Additionally, the amount of culture supernatant was risen to 60% of final reaction volume aiming to improve the observed effects seen in 2.23C-D. However, addition of RE did not show a significant increase of inhibition using bacterial supernatant of the endophyte collection (2.24A) or from members of the SynCom. Although, a slight increase in inhibition for *P. putida* was detected (2.24B). In contrast, a reduction in inhibition for *M. aubagnense* after addition of RE was seen. Surprisingly some tendencies of PLCP modulation observed before (2.23C-D) changed after addition of higher volumes of bacterial supernatant independent of the addition of RE. For instance, using higher supernatant volumes of previously inhibiting *C. pusillum* displays an activation of PLCPs (2.24A).

Besides, the previously activating supernatant of *C. indologenes* shows a tendency to inhibit PLCPs when the amount is increased (2.24B). This suggests the secretion of an inhibitor by *C. indologenes* which is either only weakly inhibiting or secreted in low, insufficient concentrations. The inhibition might be only measurable when higher concentrations are used and is otherwise not distinguishable from noise in this assay. To ensure that the measured substrate cleavage activity in our assays was derived by maize root apoplastic PLCPs and not biased by secreted bacterial PLCPs a substrate cleavage assay was performed without RAF but with 60% culture supernatants of the previously tested bacteria together with fluorgenic substrate. As a control, RAF was used together with substrate and M9. Only marginal substrate cleavage activity was measured for all four tested culture supernatants compared to the activity detected for RAF, suggesting that these four bacteria do not secrete PLCPs or other proteases that are able to cleave the substrate and influence the readout of these substrate cleavage assays (6.18A-B).
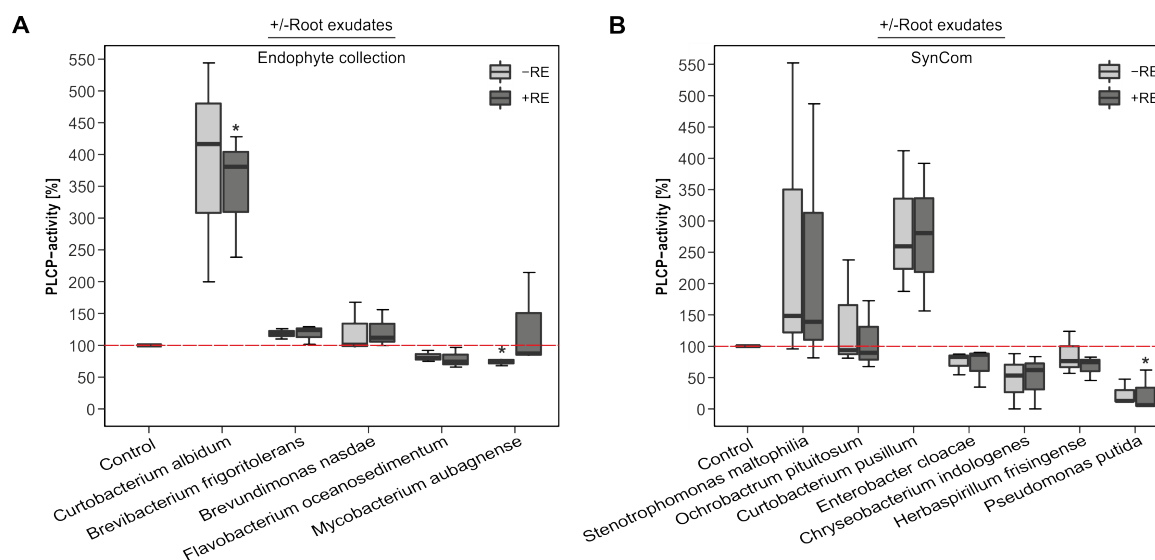
Figure 2.24: **Root exudates do not enhance bacterial PLCP-inhibitory capacity.**
Influence of root exudates (RE) on bacterial PLCP inhibition. 60 µl culture supernatant was used in a substrate cleavage assay as described before (2.23A). After change to MM, bacterial cultures were treated with (+RE) or without (-RE) maize RE. A representation of five bacteria from Figure 2.23B **(A)** and seven members of a synthetic maize root community (SynCom) **(B)** is displayed here. Data was represented in a boxplot as described before. This experiment was performed using three independent biological replicates each with technical duplicates. P-values were calculated with an unpaired t-test. *P<0.05.

Based on the previous results, the focus was set on two candidates from the endophyte collection: *F. oceanosedimentum* and *M. aubagnense*, and two candidates from the SynCom: *E. cloacae* and *P. putida*, that showed PLCP inhibition. The aim was to investigate and identify the molecular compound secreted by each of the candidate bacteria responsible for inhibition of RAF PLCPs. Growth curves for the four candidate bacteria were generated in the different media used in this study (6.19) to ease measurements under reproducible conditions for further experiments.

We aimed to dig deeper and identify the inhibitory compound which could be a peptide, a protein or even a secondary metabolite. First we aimed to evaluate if the observed PLCP inhibition is heat-sensitive, which would point to a protein inhibitor since most proteins degenerate and lose function at a certain temperature. To test this, bacterial culture supernatants were boiled for 15 min at 95°C prior to substrate cleavage assays with RAF. For the candidates *F. oceanosedimentum* as well as for *M. aubagnense* (2.25A) and *E. cloacae* and *P. putida* (2.25B) a loss of PLCP inhibition capacity was reported after heat-treatment at 95°C. Since most proteins but not secondary metabolites are sensitive to heat denaturation these results may suggest that the PLCP inhibition effect is derived from a secreted protein. To further confirm this suggestion and to investigate a size-dependent inhibition, another set of culture supernatants was taken and separated by size using a column with a 3 kDA MWCO (2.25C-D).

For all four tested bacteria it was observed, that the inhibitory effect is derived from the high molecular weight fraction containing molecules higher than 3 kDA (2.25C-D). For the bacteria *F. oceanosedimentum* and *M. aubagnense* a significant reduction of PLCP activity of 40% was detected for HMW fractions compared to 20% reduction in the LWM fractions suggesting that the causative bacterial compound might be a small protein slightly bigger than 3 kDA (2.25C). Similarly, a reduction of activity was observable for the two SynCom members *E. cloacae* and *P. putida* of 70% and nearly 90%, respectively. This inhibitory effect is lost in the LMW fraction of these bacteria. An increase of PLCP activity using those LMW fractions is observed indicating that the inhibitory effect is derived from a secreted bacterial protein significantly bigger than 3 kDA (2.25D) while small compounds in the supernatant favor substrate cleavage of plant PLCPs. Supernatants of the remaining five members of the SynCom were also tested for heat stability and fractionated to analyze size-specific inhibition effects but none of them displayed significant inhibition effects on PLCP activity (6.20A-B).
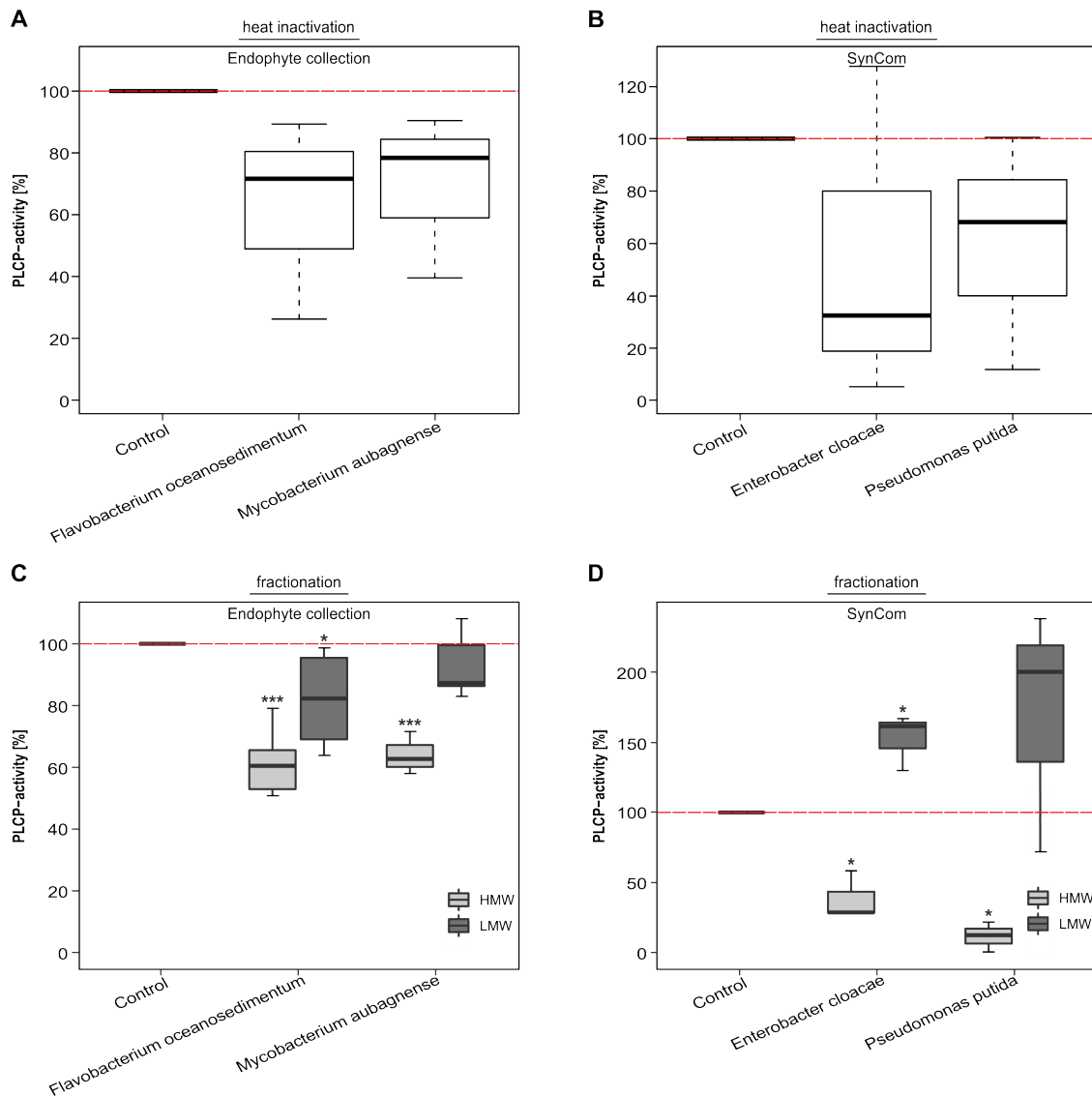
Figure 2.25: **Bacterial PLCP-inhibition is protein-derived.**
(A-B) Boiled bacterial supernatant loses PLCP-inhibitory effect. The bacterial culture supernatants of two candidates of each, the endophyte collection **(A)** and SynCom **(B)**, were boiled at 95°C for 15 min in order to denaturate proteins. 60 µl of the supernatants were tested for maize PLCP inhibition as described before (2.23A). Data was represented in a boxplot as described before. This experiment was performed using three independent biological replicates each with technical duplicates.
(C-D) High molecular weight fractions inhibit PLCPs. Culture supernatants of the bacteria tested in A and B were subjected to size separation using a spin column with a cut-off of 3kDA to fractionate the supernatant into a high molecular weight - (HMW) and low molecular weight (LMW) fractions. Inhibition assays were performed as described in A and B. P-values were calculated with an unpaired t-test. *P<0.05; **P<0.01; ***P<0.001.

The previously described results suggested that the PLCP inhibition observed is protein derived for all four candidate bacteria (2.25). To further investigate the origin of PLCP inhibition *F. oceanosedimentum* and *M. aubagnense* were sequenced. Their genomes as well as the published genomes of *E. cloacae* and *P. putida* (Niu et al., 2017a) were screened for motifs associated to PLCP inhibition (2.26A). Motifs corresponding to the inhibitor family I39 were found in *M. aubagnense*, *E. cloacae* and *P. putida*. These inhibitors are large α-macroglobulins which possess an exposed bait region with recognition sites for several proteases. Once the bait is cleaved by a protease, the conformation of the α-macroglobulin changes and traps the protease inside the large protein (Feldman et al., 1985). In *F. oceanosedimentum* a motif for an I29 inhibitor was found. Inhibitors of this type are found as inhibitory prodomains in several PLCPs, like papain and Cathepsin but also in the PLCP inhibitor salarin. These inhibitors form an α-helix that runs through the protease active site and blocks it (Groves et al., 1996; Olonen et al., 2003). A motif of the I42 family of chagasins was identified in *P. putida*. Chagasins reversible inhibit PLCPs in a similar way as cystatins. They interact in a substrate like manner with the protease but point away from the active site to avoid cleavage which blocks the active site for substrates (Stubbs et al., 1990; Monteiro et al., 2001). In a second attempt, we screened the bacterial genomes for homologs of well-known PLCP inhibitors (2.26B). However, we could not identify a homolog displaying a reasonable E-value for any used PLCP inhibitor in the four PLCP inhibiting bacteria.

A

PFAM-Domain	Family	*F. oceanosedimentum*	*M. aubagnense*	*E. cloacae*	*P. putida*
PF00207	Inhibitor I39	✗	MYCOB_34550	ENTO_39470	PSEU_45970
PF08246	Inhibitor I29	FLAV_37390	✗	✗	✗
PF09394	Inhibitor I42	✗	✗	✗	PSEU_07670

B

Inhibitor	Pathogen	*F. oceanosedimentum*		*M. aubagnense*		*E. cloacae*		*P. putida*	
		Homolog	E-value	Homolog	E-value	Homolog	E-value	Homolog	E-value
Avr2	*C. fulvum*	FLAV_24260	5.1	MYCOB_30490	3.7	ENTO_07880	0.39	PSEU_23140	0.54
		FLAV_36320	8.9	✗		✗		PSEU_35700	1.4
EpiC2B	*P. infestans*	FLAV_05650	6.2	✗		ENTO_18470	1.7	PSEU_21000	1.6
		✗		✗		ENTO_06140	2.6	PSEU_41310	3.1
EpiC1	*P. infestans*	FLAV_03290	0.37	MYCOB_09160	0.19	ENTO_10170	0.23	PSEU_41310	0.38
		FLAV_05650	4.4	MYCOB_27440	6.3	ENTO_11030	1.8	PSEU_32270	1.8
VAP1	*G. rostochiensis*	FLAV_16270	3.3	MYCOB_01420	5.9	ENTO_13510	0.1	PSEU_01550	1.2
		FLAV_16760	5.0	✗		ENTO_07900	9.2	PSEU_54270	4.1
Avrblb2	*P. infestans*	FLAV_10500	0.078	MYCOB_32420	0.097	ENTO_13980	0.96	PSEU_43790	2.7
		FLAV_00720	2.2	MYCOB_25290	0.54	ENTO_34110	1.2	PSEU_06510	9.6
Pit2	*U. maydis*	FLAV_24980	1.1	MYCOB_11170	0.79	ENTO_43560	3.4	PSEU_21360	0.11
		FLAV_32880	1.2	MYCOB_27430	1.2	ENTO_43600	3.6	PSEU_25750	2.8
PopP2	*R. solanacearum*	FLAV_05190	2.6	MYCOB_00580	0.086	ENTO_33390	2.3	PSEU_42520	7.9
		FLAV_34910	6.3	MYCOB_30270	4.3	✗		PSEU_15500	9.6
SDE1	*L. asiaticus*	FLAV_29450	0.80	MYCOB_11540	7.0	ENTO_26150	3.5	PSEU_50390	3.6
		FLAV_04490	1.7	✗		ENTO_08540	4.2	PSEU_47290	5.3
UmcMIP	*U. maydis*	✗		MYCOB_36680	4.2	✗		PSEU_33830	1.7

Figure 2.26: **Identification of PLCP inhibitor candidates in genomes of PLCP inhibiting bacteria.**
(A) Genomes of *F. oceanosedimentum*, *M. aubagnense*, *E. cloacae* and *P. putida* were searched for motifs associated to PLCP inhibition. The following PFAM- and Interpro-identifiers were used in the search: PF09394, PF10467, PF00031, PF08246, PF00197, PF00079, PF12628, SSF141066, SSF56574, PF00207, PF00086, PF13734, PS00287, IPR000010, IPR027214, IPR002160, IPR036331, IPR024321, IPR013201, IPR000215, IPR018990, IPR019508, IPR036186, IPR001599, IPR000716, IPR001713, IPR037296, IPR015112, IPR015113, IPR025896.
(B) Genomes of the bacteria mentioned in (A) were screened for homologues of known PLCP inhibitors. The two best hits for each inhibitor in the bacteria is displayed with the correlating E-value for homologs.

2.3.3 Summary of plant PLCP inhibition by endophytic root mircroorganisms

In this part of the study four bacterial endophytes were identified to secrete molecules into the apoplast that interact with and inhibit maize root PLCP activity. Two of these root bacteria: *F. oceanosedimentum* and *M. aubagnense* belong to the phyla of actinobacteria and were isolated from a maize field close to Marburg in Germany. The SynCom bacteria *E. cloacae* and *P. putida* obtained from the lab of Roberto Kolter (Harvard Medical School, Boston, USA) are members of the proteobacteria. Results of this work indicate that the PLCP inhibition effect of all four bacteria may be protein derived. A genomic approach searching for PLCP inhibitor candidates in the four PLCP inhibiting bacteria could not identify promising homologs of known PLCP inhibitors but revealed PLCP inhibitor motifs which may indicate putative PLCP inhibitors in the genomes of our four candidate bacteria.

3 Discussion

In this study, we aimed to get insight into the role of papain-like cysteine proteases (PLCPs), which have been proposed as hubs during plant immunity and might play a role in plant root-microbe interactions (Misas-Villamil et al., 2016). We found that apoplastic PLCP cleavage activity increases upon treatment of maize roots with SA. The success of our treatment could be confirmed on the transcript level by induction of SA associated PR-genes. However, no transcriptional up-regulation of PLCPs was observed. We aimed to investigate the mechanism behind PLCP activation using a proteomics approach. Comparison of leaf and root apoplastic PLCP abundance and content using shotgun MS revealed several novel root specific PLCPs in addition to previously described leaf PLCPs in maize roots (van der Linde et al., 2012a). For three of these novel PLCPs, we observed a post-translational activation upon SA-treatment. This MS approach also confirmed the successful SA-treatment at the protein level where several described SA related proteins were more prominent in SA- compared to mock-treated samples. In a screening approach of endophytic root microbes, we identified four bacteria to demonstrate inhibitory capacity towards maize root PLCPs. Further experiments suggested the observed inhibition to be derived from secreted proteins and a blast search identified inhibitor candidates in the genomes of the four bacteria.

3.1 Maize displays organ specific SA-signaling via PLCP-activation.

Based on previous studies on maize leaves that reported a SA-induced PLCP activation, we reasoned that PLCPs might also be associated to SA signaling in maize roots. Comparison of the PLCP activity of SA-treated and mock-treated RAFs of plants uncovered an overall increased activity after SA-treatment and a shift to lower molecular weight (MW) for activity signals using ABPP (2.4A). The size shift might be caused by an inactivation of higher MW PLCPs, such as CP1C and an activation of other PLCPs with lower MW. It might also be due to further maturation processes, like cleavage of the granulin domain of CP1-like PLCPs or B4FYA3 (Yamada et al., 2001). The increased PLCP activity could be confirmed using a substrate cleavage assay with the substrates Z-FR-AMC, BZ-FVR-AMC, Z-LR-AMC and Z-RR-AMC, where a five-fold increase of substrate cleavage activity was observed for SA-treated samples (2.1A & B). Besides, we also noticed a 20-fold increased PLCP substrate cleavage activity in RAF compared to LAF using the Z-FR-AMC substrate (2.2A & B). This increased activity may be due to the constantly higher pressure of microbial interactions in the root area compared to aerial plant parts (Andrews et al., 2000; Lindow et al., 2003; Young et al., 2004) and correlates with three distinct peaks visible in RAF compared to leaves where only one peak was observed, suggesting a different set of PLCPs with

distinct biochemical properties active in roots.

The question arose of what may be the cause of the enhanced PLCP activity in SA-treated roots compared to leaves? To address this question, we aimed to identify root PLCPs using two proteomics approaches. In a first approach, we compared PLCP content of RAF and LAF based on IGD-MS of active apoplastic fluid fractionated by IEC. This comparison lead to the identification of the novel root specific CP1-like PLCP CP1C (2.2E). In a second approach we performed MS-analysis of total RAF subjected to OBD were we identified the novel root specific PLCPs: CP1D, B4FS65, B4FYA3, Q10716, A0A1D6KMS8, A0A1D6LPA1, A0A1D6ER43 and A0A1D6GGX8 (2.5 & 2.7). The first approach of MS-analysis of apoplastic PLCP content used IEC followed by substrate cleavage assays using the FR-AMC substrate. Fractionation of RAFs has two major disadvantages that may have resulted in the loss of apoplastic PLCPs in the process. The first disadvantage is the IEC. Proteins that display a pI close to the buffer pH used in chromatography become unpolar and therefore unable to bind to the resin placing them to the void volume. The second disadvantage is the selection of IEC fractions for further steps based on their cleavage activity towards a specific synthetic substrate. As we could show in this study, the cleavage potential of PLCPs largely differs and most tested PLCPs in this study do not show strong cleavage potential to the FR-substrate used for activity tests of IEC fractions. This might lead to overlook of fractions containing PLCPs due to low cleavage activity towards a specific substrate.

A better approach is based on labeling of active PLCPs using the probe DCG-04, followed by a pull down of labelled PLCPs using streptavidin-beads, OBD and MS-analysis. The critical point for our direct DCG-04 labeling is the period of labeling. If the labeling is too short PLCPs less susceptible to E-64 might not be pulled down and if the incubation time is too long, the covalently binding probe might replace endogenous non-covalently binding inhibitors like cystatins (type I25), the PLCP prodomain (type I29) or chagasins (type 42) over time (Groves et al., 1996; Monteiro et al., 2001; Wang et al., 2007; Rawlings et al., 2018). This may alter the experimental outcome of active PLCPs from the real conditions in the plant. However, for the pure purpose of identification of proteases this method might be the most advisable to perform.

In addition to the previously described PLCPs in leaves, we identified several root specific apoplastic PLCPs. We have found significant differences in PLCP repertoire between leaves and roots which might indicate organ specific functions for the root specific PLCPs after SA induction. Remarkably, for all identified PLCPs only peptides from the active C1-protease domain were found in MS-analysis (2.2D). Since only active PLCPs were labelled using ABPP, this confirms that all other protein parts are cleaved of during the maturation process. The signal peptide for apoplastic localization is removed during transportation of the protein from the cytoplasm to the apoplast which is why we have not predicted to find it in the MS (Petersen et al., 2011). The inhibitory prodomain is cleaved during activation of PLCPs (Bryan, 2002; Richau et al., 2012). In this process, also the granulin domain and prolin-rich motif might be auto- or trans-catalytically removed from PLCPs of the RD21

and XBCP3 subfamily, which has been described for RD21 in vacuoles of senescent *A. thaliana* leaves and CYP1 in *Solanum lycopersicum* (Yamada et al., 2001; Gu et al., 2012; Bar-Ziv et al., 2015). The broader repertoire of PLCPs in the root apoplast identified in this study might contribute to a defense associated function since the microbial density in the rhizosphere and surrounding soil is significantly higher than in aerial plant parts (Lindow et al., 2003; Young et al., 2004). A bigger variety of PLCPs associated to distinct interaction partners and substrates might enable the plant to induce specific reactions to individual soil-borne threads such as pathogenic fungi and bacteria.

In the next step, we aimed to investigate if the newly identified root PLCPs might contribute to the observed higher root PLCP activity that has been seen after SA-treatment. For this, we collected publicly available maize leaf and root expression data of our PLCPs. Leaf transcripts were found for PLCPs that were identified to be present in leaves and roots (van der Linde et al., 2012a). Interestingly, leaf transcripts were also found for root specific PLCPs identified in this study such as CP1C. CP1C displays poor expression in leaves and poor cleavage activity for the FR-substrate. It might be that CP1C has not been previously identified in leaf apoplastic fluids because of its low expression which might correlate to low apoplastic protein abundance compared to the previously described leaf CP1-like PLCPs CP1A and CP1B (Winter et al., 2007; Sekhon et al., 2011; Andorf et al., 2015; Stelpflug et al., 2016). In addition, poor substrate cleavage activity is technically challenging to detect in the IEC-IGD-MS approach that was performed on LAF which might also explain why CP1C was not identified in IEC-based approaches in leaves (van der Linde et al., 2012a). Additionally, the significantly higher expression of CP1C in roots might indicate an organ specific function for this PLCP in root tissue.

Observation of the expression of other root specific PLCPs revealed that some display an even higher expression in leaves than in roots (2.20A). Here, it is important to differentiate between protein expression on the one hand and protein abundance on the other hand. Since we identified PLCPs at the level of protein abundance in the apoplastic fluid another explanation might be that CP1C and other RAF specific PLCPs are expressed in aerial plant tissue but not secreted into the apoplast. Activation of PLCPs occurs mainly through auto- or trans-cleavage of the prodomain from the protease domain (Bryan, 2002). PLCPs are reported to be post-translational activated through pH shifts e.g. after translocation into the apoplast (Felle, 1998; Kosegarten et al., 1999; Feliciangeli et al., 2006; Schröder et al., 2010). Based on this it may be possible that the root apoplastic PLCPs serve different functions independent of their protease activity in other plant organelles which might explain the discrepancy between leaf expression levels but absence of proteins in the apoplast. Organ specific post-translational modifications could play a role here, redirecting localization or modifying the activity and specificity of proteases (Yan et al., 1989; Garcia et al., 2008). To further investigate the different PLCP activities in leaves and roots on the level of total protein amount and active protein one could perform an ABPP-pull down assay followed by MS-analysis combined with a shotgun MS approach for leaf- and root apoplastic fluids, as described in this thesis. To be able to

compare the results derived from two fluids of different plant tissues, a normalization to total protein content with the Bradford method could be done (Bradford et al., 1976).

Furthermore, we observed a five-fold increase of overall apoplastic PLCP activity in roots upon SA-treatment using the four fluorogenic substrates mentioned before (2.1A & B). qRT-PCR of several PLCPs was performed on mock- and SA-treated root samples to monitor transcriptional changes between treatments. The success of SA-treatment was confirmed by a transcriptional increase of the SA-marker PR3 and PR5. Nevertheless, we could not see an up-regulation of PLCP expression upon SA-treatment (2.3). Since the increase in RAF PLCP activity upon SA-treatment could not be explained at the transcriptional level, we aimed to further investigate changes on the protein and the activity level.

To proof if a pH shift or a shift in the optimal pH for PLCP activity occurred after SA-treatment that could be associated to PLCP activation we tested the substrate cleavage activity of mock and SA-treated fluids at various ph. No pH shift was detected between mock and SA samples in RAF suggesting that the activation of these PLCPs is independent of the pH (2.1C) and might be explained on the protein abundance level of the identified RAF PLCPs.

Following this up, we investigated if changes in the protein abundance of PLCPs upon SA-treatment could be the cause for higher PLCP activity. Shotgun MS-analysis showed no change in total abundance of PLCPs upon SA-treatment. This includes the five apoplastic PLCPs previously identified in leaves as well as the novel root specific CP1-like PLCPs, CP1C and CP1D (2.4D) (van der Linde et al., 2012a). This result may indicate that the observed higher PLCP activity is not due to changes in their total abundance but might be due to a post-translational modification. Using DCG-04 labeling we could selectively pull down active PLCPs and compare their activity to their total abundance from shotgun analysis after SA-treatment (2.6). Surprisingly, we did not observe any of the five well characterized leaf PLCPs nor the CP1-like PLCPs CP1C and CP1D, being more active after SA-treatment. We initially proposed CP1C and CP1D to play a role in defense in roots as it was reported for CP1A and CP1B in maize leaves but the fact that CP1C an CP1D were not activated after SA suggests a different role in the roots probably not related to SA immunity. Due to the high microbial interaction pressure on roots (Young et al., 2004) compared to aerial parts (Andrews et al., 2000; Lindow et al., 2003) the root specific CP1-like PLCPs, CP1C and CP1D among other non SA-responsive PLCPs might contribute to a basic level of immunity not directly related to SA signaling. Further on, this basic PLCP activity measured for mock-treated plants and unaffected by SA-treatment will be referred to as the basal PLCP activity. CP1C and CP1D may also be involved in processes for instance senescence and apoptosis during the root-development as described for other PLCPs such as SAG12 in *A. thaliana* (Lohman et al., 1994; Noh et al., 1999b; Otegui et al., 2005). Additionally, a role in nitrogen uptake as reported for SAG12 and other root PLCPs might be possible (Godlewski et al., 2007; Rentsch et al., 2007; Paungfoo-Lonhienne et al., 2009).

Remarkably, the PLCP vignain showed a reduction in its total protein abundance but not in abundance of active protein after SA-treatment (2.5 & 2.6). Vignain is proposed to be involved in JA-related herbivory and insect defense like Mir1 (Castano-Duque et al., 2018). This indicates that, although vignain might be degraded upon SA-treatment, its basal activity is conserved by activation of the remaining vignain proteins. The reduction of vignain abundance might be due to a trade-of between JA- and SA-defense responses. Vignain may be degraded for the purpose of resource recycling while the remaining vignain is activated. This "recycling strategy" would free resources for other processes like SA-related defense by degradation of vignain while maintaining its level of activity.

Besides many SA-un-responsive PLCPs we could identify three PLCPs: B4FS65, B4FYA3 and Q10716 to be activated after SA-treatment (2.6). Their activation might be post-translational regulated, since we did not see changes in their total abundance (2.5). B4FS65 belongs to the THI1-like subfamily in which a representative member is the cysteine protease 51 (CP51), an anther-specific cysteine protease, essential for pollen exine formation in *A. thaliana* and potentially involved in programmed cell death (Yang et al., 2014). Q10716 belongs to the Arabidopsis RD19A-like subfamily of which members are known to be involved in *A. thaliana* defense mechanisms such as RD19 that is targeted by the *Ralstonia effector* PopP2 (Bernoux et al., 2008). B4FYA3 shares high sequence similarity with CP14, containing a granulin domain and belonging to the XBCP3-like family. CP14 was described to be involved in programmed cell death during *A. thaliana* development whereas its homolog in *N. benthamiana* NbCP14 was shown to contribute to defense against *Phytophtora infestans* (Kaschani et al., 2010; Bozkurt et al., 2011; Paireder et al., 2016). We propose that these three post-translationally SA-activated PLCPs might contribute to the observed SA-associated enhanced PLCP cleavage activity in maize RAF.

Based on our previous results we aimed to investigate if the activation of specific PLCPs and the shift in ABPP activity signals to lower MW was accompanied with specific changes in PLCP substrate specificity. We further investigated the cleavage specificity of the total root apoplastic PLCP-content. As it was shown in previous studies that the P2 position of a substrate is important for PLCP specificity due to sterical reasons (Greenbaum et al., 2002; Jaishankar et al., 2008) we aimed to characterize the substrate specificities of recombinant expressed PLCPs and raw RAF treated with or without SA for a set of four substrates differing in the amino acid at the P2-position. Although we observed a five-fold increase of total PLCP activity in RAF after SA-treatment we did not see a shift in the substrate preferences for the synthetic substrates compared to mock samples (2.1A & B). This might suggest a need for conserved cleavage affinities for maize roots unaffected by induction of SA-related defense responses through SA-treatment, although single PLCPs were shown to be post-translationally activated.

Biochemical characterization of recombinant root PLCPs revealed a common cleavage preference for the synthetic substrate carrying Leu in the P2-position. This preference was observed for recombinant expressed PLCPs as well as for total RAF and did not change upon SA-treatment (2.20B). A similar preference for Leu in the P2-position was reported for PLCPs of *Trifolium repens* and proposed for *A. thaliana* PLCPs based on a substrate library (Asp et al., 2004; Richau et al., 2012). Strikingly, also the cleavage activity of endogenous *N. benthamiana* PLCPs displays a preference of leucine at the P2-position (Paireder et al., 2016; Paireder et al., 2017) which was confirmed in this study when analyzing the basal activity of *N. benthamiana* control samples expressing inactive CP1A^{mut} or cytosolic GFP proteins (6.2). This Leu substrate preference may indicate a general function or need for PLCP substrate cleavage at sites where Leu at the P2-position is prominent. As cleavage and processing is used in signaling, this preference may also indicate a need of endogenous PLCP substrates where Leu is at the P2 position for efficient processing and transmission of signals through PLCPs. Leu is a small and unpolar amino acid making it easily accessible and fitting in the catalytic cleft of enzymes which might explain the high cleavage preference observed for PLCPs compared to other substrates tested in this study differing in the amino acid at their P2-position.

Apart from the preference for Leu at the P2-position we have identified unique specificities for the other tested substrates. The CP1-like PLCPs we tested in this thesis share high sequence homology, but they display distinct substrate specificities (2.20B). CP1A and CP1B resemble substrate specificity similar to that of the raw maize RAF which might suggest that both proteins greatly contribute to the basal PLCP-activity. CP1C shows a substrate cleavage profile distinct from CP1A and CP1B and is much more restricted to Leu at the P2-position. Surprisingly, this profile is highly similar to the one observed for CathB, which is phylogenetically distinct from CP1C. This observation may suggest that CP1C and CathB target similar substrates *in vivo*. CP1D, which shows overwhelming sequence similarity to CP1C, displays a distinct profile compared to CP1A and CP1B but also to CP1C. Based on our observations, we could not observe a strict link between substrate specificity and sequence homology for example for the four CP1-like PLCPs characterized here.

Surprisingly, the cleavage profile of CP1D resembles the profiles observed for two of the SA-activated PLCPs, B4FYA3 and Q10716. All three PLCPs show a potential for cleavage of the bulky FR-substrate which may be explained by an outward orientation of the imidazole ring of their catalytic His that was discovered in this study (2.12). This orientation might allow access of bulkier substrates to their active sites in contrast to other PLCPs, indicating a major importance for the orientation of the catalytic His for accessibility of the catalytic triad. All other tested PLCPs in this study show an inward orientation of the catalytic His imidazole ring (6.17). Interestingly, the general cleavage activity is reduced in the three PLCPs with an outward oriented imidazole compared to the other tested PLCPs (2.9, 2.14, 2.17).

Here, it might be necessary to differentiate between the single steps of the catalytic reaction: binding-, cleavage- and release of the substrate. During cleavage of substrates the His acts as a base to deprotonate Cys enabling it to perform a nucleophilic attack of its anionic sulfur on the substrate's carbonyl carbon. The outward orientation results in a greater distance to the sulfur of the catalytic Cys. The greater distance may lead to a less efficient proton transfer from Cys sulfur to His imidazole, which is needed for the proteases catalytic activity. An outward oriented imidazole rest from His might facilitate binding of bigger substrates and therefore broaden the substrate range but also lower the general efficiency of binding and cleavage emerging in a generally lower activity to a broader spectrum of substrates.

ABPPs and substrate cleavage assays revealed a discrepancy between high abundance in active protein and low cleavage activity of CP2 for all tested substrates compared to other PLCPs (2.9A & B). This was surprising since CP2 was, as well as CP1A and CP1B, described to be active for RR-substrate cleavage by Ziemann et al. (2018). The observed differences between ABPP- and substrate cleavage assay results might be due to different efficiencies between substrate cleavage or release and substrate binding, since ABPP covalently arrests PLCPs directly at binding whereas the measurable fluorescence of AMC in substrate cleavage assays is only observed after the release of the AMC moiety. Another explanation would be that we so far did not find a suitable synthetic substrate for CP2 and that, based on the presented data in this study, CP2 differs strongly in its substrate specificity from the other tested PLCPs in this study.

Previous studies on recombinant maize PLCPs stated highest cleavage activity for FR- and RR-substrates but did not include FVR- and LR-substrates in their assays (Ziemann et al., 2018). In this thesis we could expand our understanding of maize PLCP cleavage profiles but still only performed a limited approach to identify protease cleavage sites using four synthetic fluorogenic substrates differing in their P2 position. To achieve a more complete characterization of cleavage sites for our desired PLCPs a proteomic identification of protease cleavage sites (PICS) should be performed (Schilling et al., 2011). This technique uses peptide libraries generated from endopeptidase digested proteomes enabling to screen and characterize the protease specificities. After digestion, primary amines and sulfhydryl are chemically capped before a second digestion of the sample by the protease of interest. This is followed by biotinylation of primary amines generated by the protease of interest. These constitute the prime site of cleavage and can be analyzed using LC-MS/MS. Non-prime sides sequences left can be determined using bioinformatics analysis of the extracted N-termini and full-length protein sequences (Schilling et al., 2008; Schilling et al., 2011). A combination of prime- and non-prime sides reveal the cleavage site specificity. To confirm the PICS analysis libraries varying at the P2-position and the P3-position should be included as performed by Richau et al., 2012.

We propose that the general apoplastic PLCP substrate cleavage preference does not change for the plant upon SA-treatment. SA-treatment may lead to a general higher PLCP activity by post-translational activation of PLCPs displaying similar substrate specificities as the basal PLCPs. These SA-induced PLCPs might be favored instead of the basal PLCPs due to distinct surface structures allowing novel interactions for example with novel substrates crucial for defense responses. Based on this hypothesis, there might be other defense-related PLCPs contributing to cleavage of substrates not supported by the SA-activated PLCPs characterized in this study. In light of the arms race between host and microbe, these PLCPs might also be induced for being less prone to effectors of root associated microbes. To test this, one could perform substrate cleavage assays of single recombinant produced basal and SA-activated PLCPs together with supernatants of the four bacteria that were identified in this study to posses PLCP inhibition capacity. For normalisation of this assay the amount of active PLCPs should be normalised using ABPP and equal volumes of culture supernatant from the same culture should be used.

Aside from an increase in PLCP activity and a post-translational activation upon SA-treatment we also observed changes of other SA-related proteins in their total abundance in the shotgun MS approach. Ziemann et al. (2018) investigated the SA-induced changes in maize leaves at the transcriptional level. Since we used a proteomics approach focused on the translational changes only in the apoplast, these two studies should be compared with caution.
Nevertheless, we found several similarities in these datasets between maize root and leaf response to SA such as an increase of PR10, Zeamatin, thioredoxin and other proteins (2.5). In contrast to these described observations that are well in line with the transcriptional SA-effects described by Ziemann et al. (2018), we also observed changes contradictory to the published results.
Chitinases are known to directly attack fungal pathogens through their fungal cell wall degrading activity (Yan et al., 2015). Whereas in Ziemann et al. 2018 an increase for chitinases expression was observed, we saw a reduction of endochitinase abundance in SA samples. This is also in contrast to the enhanced expression of PR3 in our qRT-PCR results, which was shown to possess chitinase activity (Dolezal et al., 2014). These contradictory results might be explained by the different set of data that was analyzed. While an increase in expression of proteins with chitinase activity was observed for total extracts of leaves and roots, a reduced protein abundance was observed only in the RAF. It might be that the expression of chitinases is induced upon SA-treatment in leaves and roots but their localisation in roots becomes non-apoplastic.

Apart from the shikimate pathway plants are also capable to synthesize SA via a phenylalanine-lyase (PAL) dependent pathway located in the plastids. The PAL-pathway is also involved in the production of flavonoids, phenylpropanoids and lignin (Tanaka et al., 1989; D'Maris Amick Dempsey et al., 2011). Differing from the observed induction of the PAL synthesis pathway after SA and Zip1 treatment in maize leaves reported by Ziemann et al. (2018) we observed a reduced abundance of the core enzyme phenylalanine ammonia-lyase catalyzing the first step of this pathway. This may again be explained by the different methods that were used in Ziemann et al., 2018 and this thesis or may point towards an organ specific difference of SA neogenesis upon SA-treatment between maize leaves and roots.

Interestingly, we could not observe SA-activation of CP1A and CP2 which were previously described to be involved in SA-signaling and release of the SA-activating peptide Zip1 from its propetide PROZIP1 (Ziemann et al., 2018). Additionally, neither the Zip1 peptide nor its propeptide PROZIP1 were identified in the apoplast of maize roots. So far, no expression data for PROZIP1 in maize roots is available. Although, absence of Zip1 and its propeptide PROZIP1 in maize roots would suggest an organ specific SA and PLCP related defense mechanism, it might be that a PROZIP1-like protein is present in the root apoplast to fulfill a function similar to PROZIP1.
To confirm that PLCP activation occurs post-translational and to enhance our understanding of maize root SA-induced processes and signaling, it would be reasonable to study the gene expression levels in maize roots after mock- and SA-treatment via qRT-PCR or by sequencing of the total RNA as it was done for maize leaves (Ziemann et al., 2018). RNA sequencing would also allow us to dig deeper in organ specific gene expression as we already observed organ specificity at the protein level. If the propeptide PROZIP1 or a PROZIP1-like propeptide might be confirmed to be in roots, a first hint for identification of interacting PLCPs would be to test propeptide-cleavage by root specific PLCPs *in vitro*. Presence of usually cellular localized SA-associated proteins in our dataset could point towards an additional apoplastic localization of these proteins. It could also be explained with SA-induced cell death leakage or cellular damage occurring during sample preparation.

Strikingly, an increase of CC1 at the protein abundance level was observed upon SA-treatment suggesting a role in closer PLCP regulation after SA-treatment (2.5) (Turk et al., 1991). CC1 belongs to the cystatin family, which are known PLCP inhibitors. In a first thought, the finding that this cystatin is more abundant after SA-treatment seems to be counter-intuitive since we also observed an increase in PLCP activity. We propose that CC1 may acts as a negative feedback regulator for increased PLCP activity. PLCPs them self cleave based on their substrate specificity and the substrate availability without distinguishing between self and non-self-proteins. Therefore, a high PLCP activity also brings the risk of self-damage and growth defects to the plant (Berdowska et al., 2000). Following this idea, an increase of an endogenous PLCP inhibitor, such as CC1, may serve as a regulator for simultaneously increased PLCP activation and putative PLCP-associated SA-neogenesis even at elevated levels of total activity (Shah, 2003; Ziemann et al., 2018). According to this, one would assume CC1 to be specific to SA-activated PLCPs. In contrast to this hypothesis, we saw only intermediate inhibitory capacity toward the SA-activated PLCPs B4FYA3 and Q10716 but strongest efficiency towards the CP1-like PLCPs of CC1 (2.20). Although the results described in this thesis suggest a root specificity for CC1, transcripts and protein of CC1 were also found in leaf total extracts and Misas Villamil et al., (unpublished data) showed the presence of CC1 in the apoplast of SA-treated maize leaves (Sekhon et al., 2011; Stelpflug et al., 2016; Walley et al., 2016). A correlation of CC1 to SA-signaling in maize leaves remains to be proven. Van der Linde et al. (2012a) showed that CC9 blocks SA-signaling and PLCP activation in maize leaves. These experiments by van der Linde et al. (2012a) could be repeated with CC1 instead of CC9. If CC1 is root specifically involved in SA-signaling but not in leaves, no effect on SA-signaling and PLCP activation should occur in leaves overexpressing CC1.

To confirm if SA-induction of PLCP activity is a common plant root mechanism, one could test the model system *A. thaliana*. Although new tools such as CRISPR-Cas9 genome editing and *barley-stripe-mosaic-virus* (BSMV)-induced gene silencing/expression facilitate work on maize, *A. thaliana* offers a far easier accessible model system, providing already numerous knock out-mutants (Alonso et al., 2003; Char et al., 2017; Cheuk et al., 2017). In an approach to study the connection between SA and PLCP activity in *A. thaliana* Col-0 roots, Nick Dunken could show under my supervision an activation of *A. thaliana* root PLCPs upon SA-treatment compared to mock samples (2.21 , Dunken, Bachelor thesis, 2017). Interestingly, no activation of PLCPs in *A. thaliana* leaves could be seen upon SA-treatment (Gu et al., 2010). Additional studies in the roots of *S. lycopersicum* demonstrated an activation of PLCPs upon SA-treatment whereas no activation in leaves was reported (Kovács et al., 2016). Interestingly, SA-treatment of *N. benthamiana* leaves in this study also did not prompt an increased PLCP cleavage activity of basal *N. benthamiana* PLCPs while expressing GFP or CP1A^{mut} proteins, albeit successful treatment was monitored via occurring cell death (6.8 & 6.9). Altogether, the SA-induced PLCP activation in roots of monocotyledons and dicotyledons might suggest a conserved correlation between SA and PLCP activity for roots of various plants. Further experiments focusing on this hypothesis might include qRT-PCR or even RNA sequencing also in additional systems like *A. thaliana*, *S. lycopersicum* or *N. benthamiana* mock- and SA-treated roots for identification of conserved PR-gene induction in roots and observation of transcriptional changes for root PLCPs. MS shotgun analysis together with a DCG-04-labeling MS approach could be used to monitor the changes in total protein abundance and post-translational changes focusing on PLCPs. Prediction programs such as signalP and secretomeP (Bendtsen et al., 2005; Almagro Armenteros et al., 2019) could be used to focus the data analysis on putative secreted apoplastic proteins. Since SA-induced PLCP activation was so far only reported in maize leaves but not in Arabidopsis-, *S. lycopersicum*-, or *N. benthamiana* leaves, it remains to be evaluated if it is a conserved mechanism in leaf tissue as seen in roots.

Based on the data presented in this study we hypothesize that the general mechanisms underlying SA-signaling, including an increased PLCP activity and SA neo-genesis as well as PCD-associated activation of the proteasome might be conserved between maize leaves and roots and may also be conserved in other plant species for root tissues, such as *A. thaliana*, *N. bentamiana* and *S. lycopersicum*. The detailed immune response, such as the involvement of specific PLCPs might be organ specific and adapted to the needs of defense provided by microbial interactors and the surrounding environment.

3.2 Plant PLCP inhibition as a decisive trait for bacterial endophytes.

Plants are colonized by a pleiotropy of microbial endophytes and epiphytes and serve them as a source of nutrients. They engage close interactions ranging from beneficial to pathogenic for the plant. To investigate microbial capacity to inhibit maize root PLCPs, a first screen of endophytic fungi and bacteria was conducted where no fungal candidate was found to secrete PLCP-inhibitory compounds. However, we identified four bacterial candidates that secreted PLCP-inhibiting proteins. An additional genomic approach to identify putative effectors in the genomes of these bacteria was performed but did not lead to the identification of promising PLCP-inhibitor homologs. Nevertheless, we found candidate proteins in the searched bacteria that carry PLCP-inhibitory motifs. We hypothesize that the inhibition of plant PLCPs is decisive for endophytic microbes and microbe communities for their first interaction with host plants and to develop a stable interaction with their host.

As it was proposed that PLCPs are hubs in plant immunity (Misas Villamil et al., 2019) we were keen to investigate endophytic microbes for their ability to inhibit PLCPs which may not only facilitate their interaction with plants but also shape the microbial community and facilitate the interactions of other microbes with the host plant.

In a first approach to identify fungi capable of inhibiting plant PLCPs we found that a striking majority of fungi did not reduce but increase activity of plant derived root apoplastic PLCPs in our assays. This was surprising since fungi were shown to secrete effectors and toxins inhibiting PLCPs as seen for *Clitocybe nebularis* and *Cladosporium fulvum* (Shabab et al., 2008; Šmid et al., 2015). Generally it was noticed that the results were hardly conclusive due to strong variation between biological replicates.

High variation is due to poor reproducibility of this assay especially for high sample numbers as in this first screen. The growth conditions for the fungi were unknown which might have resulted in drastic differences of culture density between biological replicates. Additionally, a standardized inoculation of culture was difficult as well as the measurement of culture density. Spore counting might help to enable inoculation with fixed amounts of fungus, but it will be difficult to apply in a bigger screen like displayed here. Culture density was difficult to assess since for most fungal candidates a measurement of optical density was not applicable due to the unknown correlation between fungal culture density and optical density or due to ball- or sphere-like fungal growth in liquid media for some samples. One possibility to improve monitoring of culture density would be to filter the fungal culture, collect the fungal biomass and take a defined portion to measure the dry weight. However, it will be challenging to keep these cultures under sterile conditions during the whole process. The described experimental challenges might have led to missing of putatively interesting fungal plant PLCP interactions and should be addressed in further screens.

Albeit the methological challenges we could measure interesting effects on PLCP acitivty for some fungal endophytes. *Fusarium oxysporum* culture supernatant showed significant activation of maize root PLCPs (2.22B). These results could be explained by secreted fungal proteases that were capable to cleave the synthetic substrate used in this assay. Although *F. oxysporum* was reported to live endophytically and nonpathogenic in some banana cultivars, it is mostly known for the lifestyle of a necrotrophic root pathogen (Athman et al., 2006). As a necrotrophic soil inhabiting fungus *F. oxysporum* needs to secrete enzymes and toxins to actively kill plant cells and gain access to nutrients, which would fit to a secretion of putative PLCPs known to be PCD associated (Kistler, 1997; Michielse et al., 2009). To confirm this hypothesis, further substrate cleavage assays of only fungal supernatant without RAF could be performed like it was done for the bacterial candidates in this study. This could confirm if *F. oxysporum* itself secretes proteases cleaving the synthetic substrate used in this assays.

In this first screen, we could observe a non-significant tendency for PLCP inhibition only for *Bionectra ochroleuca*. Further tests with increased amount of culture supernatant in substrate cleavage assays as well as size separation of culture supernatant prior to the assays as was performed for candidate bacteria in this study should be considered as next steps for investigation of *B. ochroleuca* derived PLCP inhibition capacity. *B. ochroleuca* was previously described as an endophytic fungus of *Nothapodytes foetida* and was reported to produce antifungal as well as antibacterial compounds. It was supposed to act as a biocontrol and be used as a bio fumigant in agronomy (Samaga et al., 2014; Wang et al., 2014; Rodrigues et al., 2019). Based on these reports *B. ochroleuca* may be a good candidate as a hub in microbiome composition and should be considered for further studies on fungal inhibition capacity on maize root PLCPs.

Additionally, to the endophytic fungi we also tested a set of endophytic bacteria isolated from field-grown maize. Bacteria conduct a biotrophic lifestyle while interacting with plants and are therefore targeted most efficient by SA-associated plant defense responses.

16S-rRNA analysis of our root endophytic bacteria from field grown maize revealed that the phyla Actinobacteria and Proteobacteria make up a big part of the whole endophytic community. The majority of identified bacteria belong to the phyla of Proteobacteria, consisting of α-, β- and γ-Proteobacteria. The second most represented group are the Firmicutes followed by a group of Actinobacteria (2.23B). These observed microbiome composition is in line with the composition of previously reported endophytic communities for *A. thaliana* roots (Bulgarelli et al., 2012; Lundberg et al., 2012) and *S. lycopersicum* leaves (Romero et al., 2014). Also the SynCom used in this study provided by Niu et al. (2017b) resembles a comparable composition on the phyla level suggesting that the taxonomic composition of bacterial endophytic microbiomes is conserved on the phyla level. For future approaches for identification of PLCP inhibition, Actinobacteria and Proteobacteria may present promising candidates.

Both candidate bacteria, *Flavobacterium oceanosedimentum* and *Mycobacterium aubagnense*, from our endophyte collection belong to the Actinobacteria which are known for their use as bio remediates, putative biocontrol agents and plant growth promoting bacteria (2.23B) (Arunachalam Palaniyandi et al., 2013; Palaniyandi et al., 2013; Alvarez et al., 2017). Interestingly the two bacteria from the SynCom, *Enterobacter cloacae* and *Pseudomonas putida*, belong to the phyla of Proteobacteria which are known for plant beneficial effects including nutrient fixation and uptake and production of antimicrobial compounds (Liu et al., 1992; Haas et al., 2003; Miller et al., 2010; Bruto et al., 2014).

Members of the *Flavobacterium* genus are well known for their capacity to degrade complex organic compounds and the potential to enhance plant growth (Kolton et al., 2016). Several studies have shown an increase of the *Flavobacterium* genus along soil, rhizosphere and rhizoplane (Kolton et al., 2016). These findings suggest a central role of *Flavobacteria* not only for the plant but also for other microbiome members.

One member of the *Mycobacteria*, *Mycobacterium immunogenum* was reported to be beneficial for plant growth by enhancing plant height and shoot growth in *S. lycopersicum* (Cetintas et al., 2018). Bacteria of the genera *Pseudomonas* and *Enterobacter* were shown to facilitate plant uptake of insoluble phosphate compounds, enhance salt stress tolerance and increase resistance towards necrotrophic pathogens in maize roots (Vives-Peris et al., 2018).

All these perceptions suggest that our four bacterial candidates *F. oceanosedimentum*, *M. aubagnense*, *E. cloacae* and *P. putida* might be as well exhibit beneficial effects for the host plant or its microbiome. Our study observed their capacity to inhibit plant root PLCPs which may suggest that one important trait of the four candidate bacteria leading to beneficial effects is their capacity for plant PLCP inhibition (2.23 & 2.25). Inhibition of plant PLCPs might facilitate the development of a close interaction between microbe and plant but also facilitate colonization of other bacteria.

So far, several effector proteins from plant pathogens were reported to inhibit plant PLCPs. Rcr3 from tomato is targeted by the effector proteins Avr2 from *C. fulvum*, EpiC1 and EpiC2B from *P. infestans* as well as by Gr-VAP1 from *G. rostociensis* to just name some examples (Luderer et al., 2002; Song et al., 2009; Lozano- Torres et al., 2012). Since endophytic bacteria are generally not considered to be pathogenic, is is unlikely that they need PLCP inhibitors to induce negative effect on the plant, like disease symptoms (Turner et al., 2013). However, also mutualistic microbes need to overcome the first lines of plant defense to develop a successful colonisation of the host (Oldroyd, 2013). For this it might be useful for the individual microbe but also the whole microbe community, if SA-signaling and especially PLCP activity is reduced. It could be shown in the *A. thaliana*, that an induction of the SA-associated defense response had a negative effect on diversity of endophytes (Kniskern et al., 2007). This might indicate that PLCP activity can be used by the plant for selection of associated endophytes.

Based on our results the compounds responsible for the PLCP inhibition from the four candidate bacteria may be a protein with a molecular weight above 3 kDA. To confirm the proteinaceous nature of the inhibitor additional tests with samples preincubated with proteinase K to degrade the protein should be performed. If the compound is a secreted protein the inhibition effect should vanish after this treatment.

Effectors targeting the host plant are usually not induced in axenic culture but only after a certain trigger (Bolton et al., 2008). In the first bacterial and fungal screens, we managed to induce production of PLCP inhibitors in our four candidate bacteria by applying nutrient stress. Root exudates may also function as such a trigger for effector production. They consist of a mixture of plant derived compounds released into the rhizosphere. Their composition is highly variable depending on the developmental stage of the plant, the soil conditions and biotic and abiotic stresses (Bais et al., 2006; Badri et al., 2009). They may consist of sugars, amino acids, organic acids, enzymes and growth factors which provide a rich nutrient source (Koo et al., 2005). Root exudates reportedly also induced gene expression in rhizobic microbes (Peters et al., 1988; Bauer et al., 1990). Based on this we modified our bacterial screen by addition of RE to putatively induce plant related gene expression of PLCP inhibitors. Surprisingly we observed that none of the tested bacteria do react to addition of RE with an increased inhibitory capacity (2.24). This might indicate that production of PLCP inhibition is independent of the presence of a putative host plant but depends on nutrient stress. It may be that these PLCP inhibitors do not primarily target plant PLCPs but serve a different function for the bacteria, like positive or negative effects on other microbes in the community to ensure a proper nutrient supply.

In an attempt to identify putative PLCP inhibitor candidates we screened the genomes of the four bacterial candidates. A search for known motifs associated to PLCP inhibition and homologues of known pathogen derived PLCP inhibitors was conducted (2.26). Unfortunately, we could not identify homologs of the used known inhibitors with significant confidence in any of the bacterial candidates. Effectors are under a high selective pressure for diversification due to the arms race between host and microbe. The conservation of effectors across microbes is therefore generally low which might explain the poor outcome of our screen (Plissonneau et al., 2017).
While looking for known motifs we could identify a protein containing a chagasin motif in *E. cloacae*. Chagasins belong to the I42 inhibitor family and are known, reversible PLCP inhibitors indicating this protein to be a putative candidate involved in the observed PLCP inhibition (Monteiro et al., 2001). Additionally, we found motifs of the inhibitor family I39 in *M. aubagnense*, *E. cloacae* and *P. putida*. These inhibitors are large α-macroglobulins found in human blood, which trap proteases inside to prevent them access to substrates and therefore might also be valuable targets as the cause of the observed PLCP inhibition (Feldman et al., 1985). In *F. oceanosedimentum* a motif for an I29 inhibitor was found. Inhibitors of this type are found as part of inhibitory prodomains in several PLCPs like Cathepsins but also in the PLCP inhibitor salarin (Groves et al., 1996; Olonen et

al., 2003). Therefore the I29 motif might not only suggest for the presence of a PLCP inhibitor but could also point to the presence of a bacterial PLCP.

For the identification of the inhibitory compounds another approach should be performed. Bacterial supernatants could be fractionated by size exclusion chromatography (SEC) followed by a test for each fraction's inhibitory capacity in PLCP substrate cleavage assays as described before. Fractions displaying strong inhibitory capacity could then be analyzed by MS on the bases of the sequenced bacterial genomes to identify candidate proteins for PLCP inhibition. Inhibitor candidates could be recombinant produced in *E. coli* for in vitro characterization including test for inhibition of PLCPs in substrate cleavage assays.

Interestingly *E. cloacae*, which is a hub for stability of the SynCom shows PLCP inhibition as well as the SynCom member *P. putida* (2.23 & 2.25). Remarkably, this rate of PLCP inhibiting bacteria is higher than our observation while screening endophytic maize root bacteria where only 2% of bacteria inhibited PLCPs. This might suggest that for a stable root community, bacteria showing PLCP inhibition are recruited by the plant.

The observation that the hub bacterium *E. cloacae* is able to inhibit PLCPs may point to an important role for PLCP inhibition not only for plant-microbe but also for microbe-microbe interactions and shaping of the microbiome. Since also *P. putida* shows PLCP inhibitory capacity without being essential for stability of the SynCom, it might be that PLCP inhibition is a necessary but not sufficient trait for microbiome stability. Altogether, these results strengthen the hypothesis that PLCP inhibition is important for plant-microbe interactions in the root area and may also play a role for the bacterial community hosting the endorhiza. We propose that PLCP activity and bacterial PLCP inhibition might not only affect the first steps of plant-microbe interactions but also affect other microbes in a community background.

To prove this hypothesis, one could perform colonization assays as described by Niu et al., 2017 under sterile conditions. As a control, the SynCom could be inoculated on maize seedling growing in sterile soil. To test the importance of PLCP inhibition for plant-microbe and microbe-microbe interactions members of the SynCom could be substituted by endophytic bacteria tested to inhibit PLCPs or not. To rule out secondary effects apart from PLCP inhibition induced by an exchange of bacteria one could knock out or overexpress the identified PLCP inhibitors in the respective bacterium.

Another possibility would be to use two *P. fuorescence strains*, where one is expressing Pit2 while the other is not. If our hypothesis is true Pit2 production would benefit host colonization and may eventually even lead a pathogenic lifestyle of *P. fluorescence*. Since this Pit2 is HA-tagged, additional western blots of apoplastic fluid and root tissue could be performed to monitor the localization of Pit2.

A time course could be performed for several days to monitor the formation of a stable bacterial community via MySeq analysis. As a readout of PLCP-inhibition ABPPs of RAF could be performed. The importance for first interactions between plant and microbe of specific PLCPs could be addressed by performing colonization assays on CRISPR-Cas9 knock out lines. Knock out-plants for the CP1-like PLCPs: CP1A, CP1B and CP1C were generated as part of this thesis in cooperation with Jochen Kumlehn (IPK Gatersleben, Saxony-Anhalt, Germany). Generation of additional knock out-plants especially for the SA-activated root specific PLCPs identified in this study and application in colonization assays may provide further understanding of the crosstalk between plant PLCPs and bacterial inhibitors as well as their impact on plant-microbe and microbe-microbe interactions.

3.3 Model of SA-induced plant microbe interactions

In this study we found that SA leads to a post-translational activation of some SA-activated PLCPs and an increase of CC1 abundance in the apoplast. Additionally, we found that endophytic bacteria are able to secrete proteins putatively targeting and inhibiting PLCP activity in the root apoplast . However, in the process of this thesis more questions arose that were summarised in a model in 3.1. Although we observed an increase in CC1 and confirmed its potential *in vitro* to inhibit all tested PLCPs required as a negative feedback to SA, it is not sure if this might be the real function of CC1. The presence of a cystatin acting as a susceptibility factor as described for CC9 in maize leaves might also be possible and accessible for endophytic bacteria (van der Linde et al., 2012a). The presence of signaling peptides involved in root SA-signaling and their PLCP-activity dependence as seen for PROZIP1 in leaves might be interesting to be addressed (Ziemann et al., 2018).

It also remains unclear how and if endophytic bacteria are recognized hence inducing SA defense signaling or not. Although we propose that endophytic bacteria are capable of inhibiting plant PLCPs, so far it remains elusive if this inhibition is generally targeting all RAF PLCPs or only specific ones. It might also be that some plant PLCPs avoid inhibition and execute negative effects on bacteria through cleavage of bacterial compounds. Finally, also the proposed hub role of PLCP inhibiting bacteria pointing to an effect of distinct members of the microbial community remains to be investigated since the bacteria might influence other community members not only with PLCP inhibition but also through production of diverse proteins and secondary metabolites.

Both, the further biochemical and biological characterization of root apoplastic PLCPs and their organ specific SA-signaling, as well as the impact of PLCP inhibition on microbial communities will provide us with a deeper understanding of the diverse roles of PLCPs in the root apoplast.

This work provides advances in understanding of the root specific SA-responses and the role of PLCPs in plant-microbe and microbe-microbe interactions for future work. Besides new insights in organ specific SA-induced PLCP activation my work provides rise into new research challenges that need to be addressed in future studies.
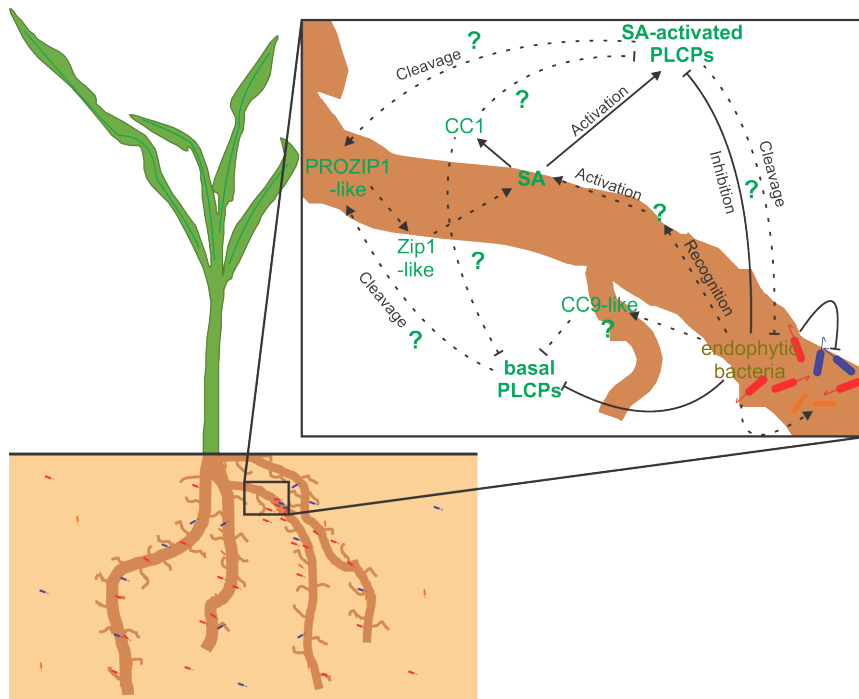
Figure 3.1: **SA-mediated interaction between endophytic bacteria and maize roots.**
Induction of SA defense signaling leads to post-translational activation of SA-activated PLCPs and an increased production of CC1. SA-activated and basal PLCPs might be inhibited by CC1 in a negative feedback loop of SA induction. We defined basal PLCPs as constitutively and SA-independent PLCPs contributing to the PLCP activity observed for mock-treated plants. Endophytic bacteria secrete effector proteins inhibiting plant PLCPs and might influence additional microbes in the community. Endophytic bacteria might also be targeted by SA-activated PLCPs and recognized leading to an activation of SA defense responses. As seen for maize leaves CC9-like susceptibility factors might also be present in roots used by endophytic bacteria to reduce PLCP-activity. PLCP activity might also be needed for release of Zip1-like signaling peptides from their propeptide inducing a positive feedback for SA-activation as seen in maize plants.

4 Material and Methods

4.1 Material

4.1.1 Chemicals

The chemicals used in this study were ordered from Biozym (Hessisch Oldendorf, Germany), Expedeon (San Diego, California, USA), Difco/Becton, Dickinson and Company (Franklin Lakes, USA), GE Healthcare (Chicago, Illinois, USA), Invitrogen (Carlsbad, California, USA), Merck (Darmstadt, Germany), Roche (Basel, Switzerland), Roth (Karlsruhe, Germany) and Sigma-Aldrich (St. louis, Mississippi, USA) unless stated otherwise.

4.1.2 Kits

Plasmid DNA extraction was done using the QIAprep® Mini Plasmid Kit (Qiagen, Hilden,Germany). PCR-clean up and gel-extraction of nucleic acids was performed using the NucleoSpin gel and PCR Clean-up kit (Macherey-Nagel, Düren, Germany). Isolation of genomic DNA from maize plants was performed using the MasterPure™ Complete DNA and RNA Purification Kit from Epicentre (Epicentre, Chicago, USA). The enzymatic degradation of RNA was done with RNaseA (Serva, Heidelberg, Germany) and enzymatic degradation of DNA was done with the TURBO DNA-free™ Kit (Ambion®/ Thermo Fischer scientific, Waltham, Massachusetts, USA). Synthesis of cDNA was performed using RevertAid H Minus First Strand cDNA Synthesis Kit (Thermo Fischer scientific, Waltham, Massachusetts, USA). For ligation of a DNA-fragment in the pGEM®-T vector the pGEM®-T easy kit was used (Promega, Madison, Wisconsin, USA). For Gibson assembly cloning reactions the 2x Hifi DNA assembly mix (NEB, Massachusetts, USA) was used. To remove existing recognition sites single silent mutations were induced with the Quickchange (Multi) Kit (Agilent Technologies, Santa Clara, USA).

4.1.3 Enzymes, Antibodies and additional materials

The restriction enzymes used in this study were purchased from New England Biolabs (NEB, Massachusetts, USA). DNA polymerases used in this study were KOD Xtreme™ Hot Start DNA Polymerase (Novagen®/Merck Millipore, Darmstadt, Germany), or GoTaq® Green Master Mix (Promega, Madison, Wisconsin, USA). Ligation of DNA molecules was done with T4 DNA ligase (Thermo Fischer scientific, Waltham, Massachusetts, USA). Additionally used enzymes are indicated in the respective method sections. Antibodies, antibiotica and marker used in this study are listed in 4.1, 4.2 and 4.1, respectively.

Table 4.1: **Antibodies used in this study**

Antibody	Organism	Working dilution	Supplier
RuBisCo	chicken	1/10000	Sigma (St. louis; Mississippi; USA)
Histone H3	rabbit	1/5000	Agisera (Vannas; Sweden)
HA	mouse	1/30000	Sigma (St. louis; Mississippi; USA)
His	mouse	1/10000	Sigma (St. louis; Mississippi; USA)
Strep-HRP		1/1000	Sigma (St. louis; Mississippi; USA)
mCherry	mouse	1/1000	ChromoTek (Martinsried; Germany)
rabbit IgG	goat	1/3000	Cell Signaling technology (Massachusetts; United States)
mouse IgG	goat	1/3000	Thermo Fischer scientific (Waltham; Massachusetts; USA)
Chicken IgY	rabbit	1/20000	Sigma (St. louis; Mississippi; USA)

Table 4.2: **Antibiotics and working solutions used in this study**

Antibiotic	Final concentration [µg/ml]
Carbenicillin (Carb)	100
Chloramphenicol (Clm)	34
Gentamycin (Gent)	50
Rifampicin (Rif)	40
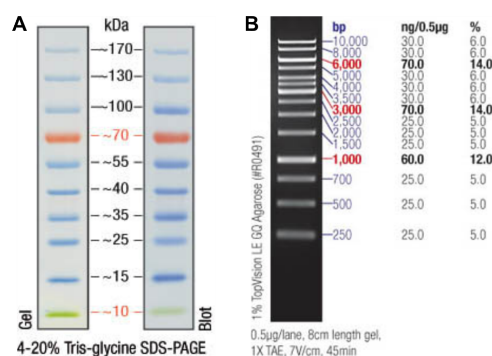
Figure 4.1: **Standard marker used in this study.**
(**A**) Pageruler prestained protein ladder used for size determination on a SDS gel and PVDF membrane.
(**B**) 1 kb generuler DNA ladder used for size determination on an agarose gel of DNA fragments.

4.1.4 Buffer & solutions

All buffers, media and solutions were autoclaved for 5 min at 121°C. Heat-sensitive solutions were filter-sterilized (0.2 µm pore size, GE Healthcare, Chicago, Illinois, USA). The exact composition of all buffers, media and solutions are listed in the following chapters.

4.1.5 Plant material and growth conditions

4.1.5.1 *Zea mays*

The *Zea mays* variety Early Golden Bantam (EGB) was grown in phyto-chambers at 28°C on a long day period (16 h light) with 80% humidity. Temperature was decreased to 22°C for 8 h during the night.

4.1.5.2 *Nicotiana benthamiana*

N. benthamiana plants were grown in a greenhouse at 23°C on a long day period (16 h light) and at 20°C for 8 h dark period with 30 – 40% humidity.

4.1.5.3 *Arabidopsis thaliana*

A. thaliana Col-0 plants were grown in sterile conditions on solid $\frac{1}{2}$ MS media (4.1.6.1) in phyto-chambers at 22°C on a short day period (8 h light) with 80% humidity. Temperature was decreased to 18°C for 16 h during the night (dark period).

4.1.6 Media and microbial cultivation conditions

4.1.6.1 Media

Table 4.3: **Media used in this study.**

Media name	Ingredient	Final concentration	Remarks
dYT liquid (Sambrook 1989)	Trypton	1.6% (w/v)	prepared in $H_2O_{bid.}$
	Yeast-extract	1.0% (w/v)	
	NaCL	0.5% (w/v)	
YT solid	Trypton	0.8% (w/v)	prepared in $H_2O_{bid.}$
	Yeast-extract	0.5% (w/v)	
	NaCL	0.5% (w/v)	
	Agar	1.3% (w/v)	
$\frac{1}{2} \times$ **TSB** liquid	TSB	1.5% (w/v)	prepared in $H_2O_{bid.}$
$\frac{1}{2} \times$ **TSB** solid	TSB	1.5% (w/v)	prepared in $H_2O_{bid.}$
	Agar	1.5% (w/v)	
$5 \times$ **M9** salts	Na_2HPO_4*$2H_2O$	256 mM	prepared in $H_2O_{bid.}$
	KH_2PO_4	110 mM	
	NaCl	43 mM	
	NH_4Cl	93.5 mM	
M9 liquid	$5 \times$ M9 salts	20% (v/v)	prepared in $H_2O_{bid.}$
	$MgSO_4$*$7H_2$	2 mM	
	$CaCl_2$*$2H_2$	0.1 mM	
	50% (w/v) Glucose	0.4%	
PD liquid	PD-broth	2.4% (w/v)	prepared in $H_2O_{bid.}$
PD solid	PD-agar	3.9% (w/v)	prepared in $H_2O_{bid.}$
	Tris-HCl pH 8	0.01 M	
Tracelements (Holliday 1974)	H_3BO_3	0.006% (w/v)	prepared in $H_2O_{bid.}$
	MnCl*$4H_2O$	0.014% (w/v)	
	$ZnCl_2$	0.04% (w/v)	
	Na_2MoO_4*H_2O	0.04% (w/v)	
	$FeCl_3$*$6H_2O$	0.01% (w/v)	

Table 4.3: **Media used in this study.**

Media name	Ingredient	Final concentration	Remarks
	$CuSO_4$	0.003% (w/v)	
Salt solution	KH_2PO_4	1.6% (w/v)	prepared in $H_2O_{bid.}$
(Holliday 1974)	Na_2SO_4	0.4% (w/v)	
	KCl	0.8% (w/v)	
	$MgSO_4*7H_2$	0.4% (w/v)	
	$CaCl_2*2H_2$	0.13% (w/v)	
	Traceelements	0.8% (v/v)	
NM liquid	KNO_3	0.3% (w/v)	prepared in $H_2O_{bid.}$
	Salt solution	6.25% (v/v)	
	50% (w/v) Glucose	2% (v/v)	sterile filtrated and added after autoclaving
$\frac{1}{2}$ **MS** liquid (Murashige and Skoog 1962)	MS-medium	0.4% (w/v)	prepared in $H_2O_{bid.}$
	MES-hydrate	0.045% (w/v)	adjust to pH 5.7
$\frac{1}{2}$ **MS** solid (Murashige and Skoog 1962)	MS-medium	0.4% (w/v)	prepared in $H_2O_{bid.}$
	MES-hydrate	0.045% (w/v)	
	Agar	0.8% (w/v)	adjust to pH 5.7

4.1.6.2 Cultivation of endophytic fungi

Endopyhtic fungi were cultivated at 22°C on PD agar media, in liquid PD or NM media (4.1.6.1) with 200 rpm orbital shaking. No antibiotics were added. Glycerolstocks for long term-storage of cultures were done by adding 25% Final concentration (f.c.) (v/v) dYT glycerol to a thickly grown overnight culture in a total volume of 1.5 mL and stored in a screw cap vial at -80°C. For reuse of the long term cultures, strains were streaked out on PD agar medium.

4.1.6.3 Cultivation of enodphytic bacteria and synthetic community

Bacteria of our endophyte collection or from the synthetic community were cultivated at 28°C on dYT or TSB agar media. Bacteria were grown in liquid dYT, TSB or M9 media (4.1.6.1) with 200 rpm orbital shaking. No antibiotics were added. Glycerolstocks for long term storage of cultures were

done by adding 25% f.c. (v/v) dYT glycerol to a thickly grown overnight culture in a total volume of 1.5 mL and stored in a screw cap vial at -80°C. For reuse of the long term cultures, strains were streaked out on dYT or TSB agar medium.

4.1.6.4 Cultivation of *E. coli*

E. coli was cultivated at 37°C either on dYT agar or in liquid dYT with 200 rpm orbital shaking. Both, solid and liquid media, were supplied with the appropriate antibiotics for selection of the respective strains. Glycerolstocks for long term storage of cultures were done by adding 25% f.c. (v/v) dYT glycerol to a thickly grown overnight culture in a total volume of 1.5 mL and stored in a screw cap vial at -80°C. For reuse of the long term cultures, strains were streaked out on dYT agar medium.

4.1.6.5 Cultivation of *A. tumefaciens*

A. tumefaciens liquid cultures were grown in liquid dYT medium under orbital shaking with 200 rpm or grown on dYT agar incubated at 28°C. The respective antibiotics for selection of each strain were added during cultivation. Glycerolstocks for long term storage of cultures were done by adding 25% f.c. (v/v) dYT glycerol to a thickly grown overnight culture in a total volume of 1.5 mL and stored in a screw cap vial at -80°C. For reuse of the long term cultures, strains were streaked out on dYT agar medium.

4.1.7 Microbial strains

4.1.7.1 *A. tumefaciens* strains

The strain used in this study for *A. tumefaciens*-mediated transformation of *N. benthamiana* was GV3101 (Koncz and Schell, 1986). This strain contains a chromosomal rifampicin resistance, the Ti-plasmid pMP90 with vir-genes and a gentamycin resistance as well as a Ti-helperplasmid bearing a tetracycline resistance. All plasmids generated for transformation of this strain are listed in 4.12. All strains used for expression in *N. benthamiana* are listed in 4.4.

Table 4.4: *A. tumefaciens* **strains used for recombinant protein production in** *N. benthamiana*

Name	Background	Resistence	Purpose of use
pL1M-F3-2x35S-p19-pterm	GV3101	Carb; Rif; Gent; (Tet)	for *N. benthamiana* expression
pL1M-F2-2x35S-eGFP	GV3101	Carb; Rif; Gent; (Tet)	for *N. benthamiana* expression
pL1M-F1-XCP2-Streptwin::2x35S	GV3101	Carb; Rif; Gent; (Tet)	for *N. benthamiana* expression
pL1M-F1-CatB-Streptwin::2x35S	GV3101	Carb; Rif; Gent; (Tet)	for *N. benthamiana* expression
pL1M-F1-CP1A-nogran-Streptwin::2x35S	GV3101	Carb; Rif; Gent; (Tet)	for *N. benthamiana* expression
pL1M-F1-CCP2-Streptwin::2x35S	GV3101	Carb; Rif; Gent; (Tet)	for *N. benthamiana* expression
pL1M-F1-CP1B-nogran-Streptwin::2x35S	GV3101	Carb; Rif; Gent; (Tet)	for *N. benthamiana* expression
pL1M-F1-CP1C-nongran-HA::2x35S	GV3101	Carb; Rif; Gent; (Tet)	for *N. benthamiana* expression
pL1M-F1-CP1A-nogran-mut2-Streptwin::2x35S	GV3101	Carb; Rif; Gent; (Tet)	mutation C151S and C154S. For *N. benthamiana* expression
pL1M-CP1D-HA::2x35S	GV3101	Carb; Rif; Gent; (Tet)	for *N. benthamiana* expression
pL1M-F1-B4FS65-HA::2x35S	GV3101	Carb; Rif; Gent; (Tet)	for *N. benthamiana* expression
pL1M-F1-B4FYA3-HA::2x35S	GV3101	Carb; Rif; Gent; (Tet)	for *N. benthamiana* expression
pL1M-F1-Q10716-HA::2x35S	GV3101	Carb; Rif; Gent; (Tet)	for *N. benthamiana* expression
pL1M-F1-CP1A-nogran-mCherry-2x35S	GV3101	Carb; Rif; Gent; (Tet)	for *N. benthamiana* expression
pL1M-F1-CP1Amut-nogran-mCherry-2x35S	GV3101	Carb; Rif; Gent; (Tet)	for *N. benthamiana* expression
pL1M-F1-B4FS65-mCherry-2x35S	GV3101	Carb; Rif; Gent; (Tet)	for *N. benthamiana* expression
pL1M-F1-B4FYA3-mCherry-2x35S	GV3101	Carb; Rif; Gent; (Tet)	for *N. benthamiana* expression
pL1M-F1-Q10716-mCherry-2x35S	GV3101	Carb; Rif; Gent; (Tet)	for *N. benthamiana* expression
pL1M-F1-CP1D-mCherry-2x35S	GV3101	Carb; Rif; Gent; (Tet)	for *N. benthamiana* expression

4.1.7.2 *E. coli* **strains**

For plasmid amplification during normal cloning procedures, *E. coli* K-12 DH5α [F- Φ80d lacZ ΔM15 Δ (lacZYA-argF) U169 deoR recA1 endA1 hsdR17 (rK-, mK+) phoA supE44 λ- thi-lgyr A96 relA1] was used (Hanahan, 1983; GibcoBRL, Eggenstein, Germany). For heterologous protein expression *E. coli* BL21 (DE3) pLys [F- ompT gal dcm lon hsdSB(rB -mB -) A (DE3) pLysS (cmR)] (Novagen/Merck, Darmstadt, Germany) was used. All plasmids generated for transformation of BL21 (DE3) pLys are listed in chapter 4.1.9.2. Strains used for protein production are listed in 4.5.

Table 4.5: *E. coli* **strains used for protein production in this study**

Name	Background	Resistence	Purpose of use
pET15b-CC1-no-signalP-HIS	BL21	Carb; Clm	protein production
pET15b CC9 ohne SignalP	BL21	Carb; Clm	protein production

4.1.7.3 Maize root endophytic bacteria

Table 4.6: **Maize root endophytic bacteria.**

Number	Name
1	*Burkholderia terricola*
2	*Burkholderia terricola*
3	*Curtobacterium albidum*
4	*Curtobacterium citreum*
5	*Burkholderia hospita*
6	*Burkholderia terricola*
7	*Flavobacterium oceanosedimentum*
8	*Mycobacterium aubagnense*
9	*Microbacterium oleivorans*
10	*Microbacterium hominis*
11	*Mycobacterium aubagnense*
12	*Microbacterium phyllosphaerae*
13	*Arthrobacter equi*
14	*Microbacterium oleivorans*
15	*Streptomyces rishiriensis*
16	*Arthrobacter oryzae*
17	*Clavibacter michiganensis subsp. tessellarius*
18	*Microbacterium thalassium*
19	*Microbacterium aerolatum*

Table 4.6: **Maize root endophytic bacteria.**

Number	Name
20	*Microbacterium immunditiarum*
21	*Streptomyces omiyaensis*
22	*Curtobacterium herbarum*
23	*Arthrobacter parietis*
24	*Arthrobacter parietis*
25	*Terrabacter tumescens*
26	*Curtobacterium flaccumfaciens*
27	*Frigoribacterium faeni*
28	*Microbacterium lacticum*
29	*Arthrobacter nitroguajacolicus*
30	*Ensifer adhaerens*
31	*Ensifer adhaerens*
32	*Brevibacterium halotolerans*
33	*Brevibacterium frigoritolerans*
34	*Ensifer adhaerens*
35	*Ensifer adhaerens*
36	*Ensifer sesbaniae*
37	*Rhizobium grahamii*
38	*Ensifer adhaerens*
39	*Ensifer adhaerens*
40	*Sphingomonas pituitosa*
41	*Rhizobium grahamii*
42	*Rhizobium mesosinicum*
43	*Rhizobium nepotum*
44	*Rhizobium nepotum*
45	*Rhizobium nepotum*
46	*Rhizobium skierniewicense*
47	*Rhizobium nepotum*
48	*Sphingomonas echinoides*
49	*Sphingobium quisquiliarum*
50	*Sphingopyxis panaciterrae*
51	*Rhizobium nepotum*
52	*Paenibacillus xylanexedens*
53	*Psychrobacillus psychrodurans*
54	*Rhizobium lusitanum*

Table 4.6: **Maize root endophytic bacteria.**

Number	Name
55	*Rhizobium jaguaris*
56	*Sporosarcina globispora*
57	*Sporosarcina psychrophila*
58	*Methylobacterium mesophilicum*
59	*Brevundimonas nasdae*
60	*Phyllobacterium trifolii*
61	*Phyllobacterium brassicacearum*
62	*Rhizobium alamii*
63	*Methylobacterium oryzae*
64	*Paenibacillus graminis*
65	*Paenibacillus graminis*
66	*Paenibacillus peoriae*
67	*Paenibacillus polymyxa*
68	*Paenibacillus peoriae*
69	*Paenibacillus polymyxa*
70	*Paenibacillus polymyxa*
71	*Paenibacillus xylanexedens*
72	*Paenibacillus xylanexedens*
73	*Mucilaginibacter polysacchareus*
74	*Bacillus simplex*
75	*Bacillus simplex*
76	*Pedobacter terrae*
77	*Pedobacter sandarakinus*
78	*Chitinophaga ginsengisegetis*
79	*Flavobacterium frigidimaris*
80	*Flavobacterium aquidurense*
81	*Chryseobacterium defluvii*
82	*Bacillus aryabhattai*
83	*Bacillus aryabhattai*
84	*Bacillus acidiceler*
85	*Bacillus aryabhattai*
86	*Pedobacter terrae*
87	*Pedobacter terrae*
88	*Bacillus licheniformis*
89	*Bacillus aryabhattai*

Table 4.6: **Maize root endophytic bacteria.**

Number	Name
90	*Bacillus aryabhattai*
91	*Bacillus aryabhattai*
92	*Bacillus aryabhattai*
93	*Pseudomonas brassicacearum subsp. neoaurantiaca*
94	*Bacillus safensis*
95	*Bacillus simplex*
96	*Bacillus pumilus*
97	*Bacillus safensis*
98	*Bacillus mycoides*
99	*Bacillus mycoides*

4.1.7.4 Maize root endophytic fungi

Table 4.7: **Maize root endophytic fungi.**

Storage number	Fungus number	Name
1	1.6	*Phoma glomerata*
2	1.7	*Dendryphion nanum*
3	1.8	*Pyrenochaeta inflorescentiae*
4	2.1	*Hypoxylon rubiginosum*
5	2.5	*Coniochaeta sp.*
6	2.9	*Gibberella avenacea*
7	2.11	*Gibberella avenacea*
8	2.18	*Gibberella avenacea*
9	2.19	*Gibberella avenacea*
10	2.22	*Gibberella avenacea*
11	2P8	*Gibberella avenacea*
12	2P15	*Gibberella avenacea*
13	2P16	*Absidia glauca*
14	3.1	*Neonectria-ramulariae*
15	3.2 b	*Ilyonectria-rufa*
16	3.2 w	*Penicillium dalea*
17	3.3	*Ilyonectria-robusta*
18	3.4	*Dendryphion-nanum*
19	3.5	*Cryptosporiopsis ericae*
20	3.8	*Diatrype flavovirens*

Table 4.7: **Maize root endophytic fungi.**

Storage number	Fungus number	Name
21	3.11	*Gibberella avenacea*
22	3.12	*Gibberella avenacea*
23	3.13	*Gibberella avenacea*
24	4.3	*Paraphoma-chrysanthemicola*
25	4.5	*Lecythophora sp*
26	4.8	*Gibberella avenacea*
27	4.9	*Gibberella avenacea*
28	4.1	*Gibberella avenacea*
29	4.11	*Gibberella avenacea*
30	4.12	*Alternaria sp.*
31	4P1	*Fusarium acuminatum*
32	4P3	*Fusarium culmorum*
33	4P11	*Cryptosporiopsis sp.*
34	4PI	*Gibberella avenacea*
35	4A-1	*Cryptosporiopsis sp.*
36	4A-2	*Mycocentrospora acerina*
37	4B-2	*Neosetophoma samarorum*
38	4B-6	*Leptodontidium orchidicola*
39	5B-6	*Cadophora luteo olivacea*
40	H16	*Paecilomyces marquandii*
41	H17	*Bionectria ochroleuca*
42	H18	*Mucor circinelloides*
43	H19	*Mucor racemosus*
44	H20	*Fusarium redolens*
45	H21	*Ilyonectria torresensis*
46	H22	*Fusarium redolens*
47	H23	*Fusarium redolens*
48	H24	*Fusarium redolens*
49	H25	*Fusarium redolens*
50	H26	*Fusarium redolens*
51	H28	*Trichoderma (Hypocrea rufa)*
52	H29	*Fusarium redolens*
53	H30	*Fusarium redolens*
54	H31	*Fusarium redolens*
55	H32	*Ceratobasidium sp.*

Table 4.7: **Maize root endophytic fungi.**

Storage number	Fungus number	Name
56	H33	*Fusarium redolens*
57	H34	*Fusarium redolens*
58	H37	*Acremonium sp G4*
59	H38	*Fusarium redolens*
60	H39	*Acremonium strictum*
61	H40	*Exophiala salmonis*
62	H46	*Glarea sp.*
63	H47	*Acremonium sp. (Sarocladium sp.)*
64	H48	*Acremonium sp G4*
65	H51	*Exophiala sp KL 2011f*
66	H52	*Exophiala salmonis*
67	H53	*Microdochium bolleyi*
68	H54	*Microdochium sp 5/97 48*
69	H55	*Periconia macrospinosa*
70	H56	*Acremonium zeae*
71	H58	*Ilyonectria torresensis*
72	H60	*Cryptococcus flavescens*
73	M1	*Ilyonectria torresensis*
74	M2	*Pleosporales sp 28e*
75	M3	*Pleosporales sp 28e*
76	M4	*Talaromyces purpurogenus*
77	M5	*Acremonium sp R8 9*
78	M6	*Ilyonectria torresensis*
79	M7	*Acremonium sp R8 9*
80	M8	*Acremonium sp R8 9*
81	M9	*Acremonium sp R8 9*
82	M10	*Exophiala sp KL 2011f*
83	M11	*Acremonium sp R8 9*
84	M12	*Talaromyces sp.*
85	M13	*Microdochium bolleyi*
86	M14	*Periconia macrospinosa*
87	M15	*Fusarium oxysporum*
88	M16	*Ilyonectria torresensis*
89	M17	*Ilyonectria torresensis*
90	M18	*Microdochium bolleyi*

Table 4.7: **Maize root endophytic fungi.**

Storage number	Fungus number	Name
91	M19	*Blastobotrys sp*
92	M20	*Periconia macrospinosa*
93	M21	*Periconia macrospinosa*
94	M22	*Pleosporales sp XS52s1*
95	M29	*Trichoderma hamatum*
96	M30	*Hypocrea pachybasioides*
97	M31	*Trichoderma hamatum*
98	M32	*Trichoderma hamatum*
99	M33	*Fusarium redolens*
100	M34	*Fusarium redolens*
101	M35	*Fusarium redolens*
102	M36	*Fusarium redolens*
103	M37	*Fusarium redolens*
104	M38	*Fusarium redolens*
105	M39	*Fusarium redolens*
106	M40	*Fusarium redolens*
107	M41	*Fusarium redolens*
108	M42	*Fusarium redolens*
109	M43	*Fusarium redolens*
110	M44	*Fusarium redolens*
111	M45	*Fusarium redolens*
112	M46	*Trichoderma hamatum*
113	M47	*Trichoderma hamatum*
114	M48	*Trichoderma viride*
115	M50	*Trichoderma hamatum*
116	M51	*Trichoderma viride*
117	M52	*Trichoderma hamatum*
118	M53	*Trichoderma asperellum*
119	M54	*Acremonium sp R8 9*
120	M56	*Periconia macrospinosa*
121	M57	*Periconia macrospinosa*
122	M58	*Periconia macrospinosa*
123	M59	*Arthopyreniaceae sp.*
124	M60	*Cladosporium sp.*

4.1.7.5 Maize root synthetic community

Table 4.8: **Maize root synthetic community bacteria.**

Number	Name
1	*Stenotrophomonas maltophilia*
2	*Ochrobactrum pituitosum*
3	*Curtobacterium pusillum*
4	*Enterobacter cloacae*
5	*Chryseobacterium indologenes*
6	*Herbaspirillum frisingense*
7	*Pseudomonas putida*

4.1.8 Oligonucleotides

All oligonucleotides used in this study were purchased from Sigma-Aldrich (St. louis, Mississippi, USA) and are listed in the following tables.

Table 4.9: **General primer used in this study.**

Description	Sequence (5'-3')	Purpose of use
CP1A-F-BsaI-overhang	GGTCTCAAATGGCTGCCTCCACCACG	For direct cloning into pL1VB-F binary for transient expresion
CP1A-nogranulin-R-BsaI overhang	GGTCTCACGAACCGTTAGCGCCCTCCTTCAA	For direct cloning into pL1VB-F binary for transient expresion
CP1B-F-BsaI over-hang	GGTCTCAAATGGGCGCCTCCACCACG	For direct cloning into pL1VB-F binary for transient expresion
CP1B-R-BsaI over-hang	GGTCTCACGAACCGTTGGCGCCCTTCTTCAG	For direct cloning into pL1VB-F binary for transient expresion
CP1Csp-BsaI-F	TTGGTCTCAAATGGCTGCTCTGGG	For direct cloning into pL1VB-F binary for transient expresion
CP1Csp-BsaI-R	TTGGTCTCACGAACCGTTCGCCCTTCT	For direct cloning into pL1VB-F binary for transient expresion
CCP2-F-BsaI-overhang-new	GGTCTCAAATGGCCCCACGCCGCCTG	For direct cloning into pL1VB-F for transient expresion. CCP2 contains BpiI internal site
CCP2-R-BsaI-overhang-new	GGTCTCACGAACCTGCGACAATAGGGTAGGA	For direct cloning into pL1VB-F for transient expresion. CCP2 contains BpiI internal site

Table 4.9: **General primer used in this study.**

Description	Sequence (5'-3')	Purpose of use
XCP2-F-BsaI over-hang	GGTCTCAAATGGCTTGGT CTTGTGCT	For direct cloning into pL1VB-F binary for transient expresion
XCP2-R-BsaI over-hang	GGTCTCACGAACCATGGT CCTTGGTCGGGTA	For direct cloning into pL1VB-F binary for transient expresion
CatB-F-BsaI over-hang	GGTCTCAAATGGGCGGC GAACTGCTG	For direct cloning into pL1VB-F binary for transient expresion
CatB-R-BsaI over-hang	GGTCTCACGAACCAACTA TAGCTCTTCCAACGG	For direct cloning into pL1VB-F binary for transient expresion
CP1A CcatC-ScatS	AGGACCAGGGCAGCAGC GGGAGCAGTTGGGCTTT CTCAAC	mutation primer CP1A CatCys-Ser
CP1Cnsp-BsaI-R	TTGGTCTCACGAACCGTT TGCGCCCTTCTTG	MoCloL1 primer for putative root PLCP: CP1Cnsp later CP1D
CP1D F without N-term and gran	TTGGTCTCAAATGGCTGC CCTGG	MoClo L1 for transformation and transient expression
JSH-B4FS65-BsaI-Primer-F	TTGGTCTCAAATGGCGTC CTCCTCCAAAG	MoClo primer for root PLCP
JSH-B4FS65-BsaI-Primer-R	TTGGTCTCACGAACCCAT TAGTGGATAGGACGGG CGGATG	MoClo primer for root PLCP
JSH-B4FYA3-BsaI-Primer-F	TTGGTCTCAAATGCCCTC CGTCCAC	MoClo primer for root PLCP
JSH-B4FYA3-BsaI-Primer-R	TTGGTCTCACGAACCGGT AGGAAATGATGCCATCAT GT	MoClo primer for root PLCP
JSH-Q10716-BsaI-Primer-F	TTGGTCTCAAATGGCTCA TCGCGTTCTCC	MoClo primer for root PLCP
JSH-Q10716-BsaI-Primer-R	TTGGTCTCACGAACCCTC CTTCGAGGCGTGGACTG	MoClo primer for root PLCP
JSH-B4FS65-BsaI-SDM-Primer	GGCGGCATCACCACGGA AACCGACTACC	Primer for BsaI domestication
JSH-Q10716-BsaI-SDM-Primer-1	CGTGCTCCCCACCGATG GTTTACCCGACGATT	Primer for BsaI domestication
JSH-Q10716-BsaI-SDM-Primer-2	CGTCGATTCCATGGTCAG TACCGTGTCCGCAGTC	Primer for BsaI domestication

Table 4.9: **General primer used in this study.**

Description	Sequence (5'-3')	Purpose of use
CC1-F	GCCGCGCGGCAGCCATA TGCTCGAGGCTACGCGC AGCGCACAAAAGGAG	CC1 expression in *E. coli* with N-term HIS-Tag
CC1-R	GCTTTGTTAGCAGCCGGA TCCTTAGGCGCTAGCAC CCTCTTC	CC1 expression in *E. coli* with N-term HIS-Tag

Table 4.10: **qRT-PCR primer used in this study.**

Description	Sequence (5'-3')
CP1AqRT-PCR-R2	ATCCTCACGTACCCGGACTC
CP1BqRT-PCR-F2	GGACGGTGTGATGTCAACAG
CP1BqRT-PCR-R2	ATGTTGCGCTCCATCCTG
CP1CqRT-PCR-F1	GCAATGCGGAAGTTGCTG
CP1CqRT-PCR-R1	CACTCTACGAGCTCCTGTTC
CP1DqRT-PCR-F1	GAAGTTGCTGGGCTTTCTC
CP1DqRT-PCR-R1	CCATAAGCCCACCATTGC
CatBqRT-PCR-F2	GCATGGCGCTACTTTGTTC
CatBqRT-PCR-R2	GGTTCTGCTCCTTGCATTTC
CP2qRT-PCR-F1	CTGTGAGGTACGGCAAGAG
CP2qRT-PCR-R1	ACTCCTCCCAGCTCATGTC
XCP2qRT-PCR-F1	GAGGTGCTCGTCACTATATCC
XCP2qRT-PCR-R1	CCCGCTGTAGAACTGGAAG
ZmGAPDH-RT-Fw	CTTCGGCATTGTTGAGGGTTTG
ZmGAPDH-RT-Rv	TCCTTGGCTGAGGGTCCGTC
PR3-Zm1085-fw	GAACAACTACAGCAGCCAGGTG
PR3-Zm1085-rv	GAGACAATAGCTGACATGCGTC
PR5-fw	TATCGGCCGGAATAGGCTCTG
PR5-rv	CGCGTACATACAAATGCGTGC
CC9-qRT-Fw	TATGGGTCCTTGACGTTCTC
CC9-qRT-Rv	GGATCATCCGTAGCCATCTG

Table 4.11: **List of primers used to verify single guide RNA targets in HillA and HillB maize lines.**

Description	Sequence (5'-3')	Purpose of use
CP1A gR1 and 3 f	GAGGGATCACGGAATCTGAG	Sequencing of Hi2-lines to check if gRNA-targets are correct for CP1A
CP1A gR1 and 3 r	GGCGGAGATTGGTATGGAAG	Sequencing of Hi2-lines to check if gRNA-targets are correct for CP1A
CP1A gR2 f	TATAGCGGCGTGAGCTATCC	Sequencing of Hi2-lines to check if gRNA-targets are correct for CP1A
CP1A gR2 r	GGCAGCAGCTGTAGTGATCG	Sequencing of Hi2-lines to check if gRNA-targets are correct for CP1A
CP1B gR1 and 3 f	CCTCCATCTCAACTCTCATC	Sequencing of Hi2-lines to check if gRNA-targets are correct for CP1B
CP1B gR1 and 3 r	CCGCAAGTTGTGGATGAG	Sequencing of Hi2-lines to check if gRNA-targets are correct for CP1B
CP1B gR2 f	GGTGTGAGCTATCATCCACTTC	Sequencing of Hi2-lines to check if gRNA-targets are correct for CP1B
CP1B gR2 r	CAGCAGCTGTAGTGGTCGTC	Sequencing of Hi2-lines to check if gRNA-targets are correct for CP1B
CP1C gR1 - 4 f	CAGACGGTACAAAGAAAGG	Sequencing of Hi2-lines to check if gRNA-targets are correct for CP1C
CP1C gR1 - 4 r	AGTTTAAGCACCGATCAG	Sequencing of Hi2-lines to check if gRNA-targets are correct for CP1C
Zip1 gR1 and 3 f	AAACTGAGCGGTCTCACAGC	Sequencing of Hi2-lines to check if gRNA-targets are correct for Zip1
Zip1 gR1 and 3 r	CTGCTGCTGCTGGAGAACAC	Sequencing of Hi2-lines to check if gRNA-targets are correct for Zip1
Zip1 gR2 f	AGACGCATGCCCATTGGTTG	Sequencing of Hi2-lines to check if gRNA-targets are correct for Zip1
Zip1 gR2 r	AGGACCACATAGCTTGGGATTC	Sequencing of Hi2-lines to check if gRNA-targets are correct for Zip1
CP1C gDNA Crispr-targets F2	GGCACAAACAGACGGTACAAAG	Sequencing of Hi2-lines to check if gRNA-targets are correct for CP1C
CP1C gDNA Crispr-targets R2	CTTGCTGTCGAACAGAACCGGA	Sequencing of Hi2-lines to check if gRNA-targets are correct for CP1C
CP1C-CrisprF1	GAGAGGAAAGGCACAAACAGAC	Sequencing of Hi2-lines to check if gRNA-targets are correct for CP1C

Table 4.11: **List of primers used to verify single guide RNA targets in HillA and HillB maize lines.**

Description	Sequence (5'-3')	Purpose of use
CP1C-CrisprF2	AAGAAAGGGACGCTCGTCTC	Sequencing of Hi2-lines to check if gRNA-targets are correct for CP1C
CP1C-CrisprF3	CGGCATGTCCATCATCACCTAC	Sequencing of Hi2-lines to check if gRNA-targets are correct for CP1C
CP1C-CrisprF4	TCCTCCTCCTCGCCGTATC	Sequencing of Hi2-lines to check if gRNA-targets are correct for CP1C
CP1C-CrisprF5	GCCCGGCGGCATGTCCATCATC	Sequencing of Hi2-lines to check if gRNA-targets are correct for CP1C
CP1C-CrisprR1	CGAACAGAACCGGACGTGGT	Sequencing of Hi2-lines to check if gRNA-targets are correct for CP1C
CP1C-CrisprR2	GTTCCTCGGTTGGTTGACGC	Sequencing of Hi2-lines to check if gRNA-targets are correct for CP1C
CP1C-CrisprR3	GGTTGACGCTAACTTCGGAT	Sequencing of Hi2-lines to check if gRNA-targets are correct for CP1C
CP1C-CrisprR4	CCTATCATAACAGTTAGTGG	Sequencing of Hi2-lines to check if gRNA-targets are correct for CP1C
CP1C-CrisprR5	GAGATTTAATCAGCACATCAA	Sequencing of Hi2-lines to check if gRNA-targets are correct for CP1C

4.1.9 Plasmids

All plasmids in this study were tested via restriction enzyme digest. In case of insertion of plasmid parts that were generated via PCR, the newly generated sequences were verified via sequencing (Eurofins formerly GATC, Cologne, Germany).

4.1.9.1 Plasmids for first amplification of PCR product

pGEM®-T (Promega, Madison, Wisconsin, USA) plasmid was used for the intermediate cloning of primary PCR prodcuts of maize PLCPs and generation of maize PLCP expression constructs. T7 and SP6 RNA polymerase promoters flank a multiple cloning site within the α-peptide coding region for β-galactosidase. Insertional inactivation of the α-peptide allows recombinant clones to be directly identified by Blue/White Screening on indicator plates (4.2.2.5). This plasmid contains a carbenicillin resistance.

4.1.9.2 Plasmids for expression of recombinant proteins in *E. coli*

pET-15b (Novagen/Merck, Darmstadt, Germany) plasmid contains a N-terminal His-Tag sequence followed by a thrombin site and three cloning sites. It was used for expression of the maize cystatins CC1 an CC9 amplified with the respective primers listed in 4.1.8. This plasmid contains a carbenicillin resistance.

4.1.9.3 Plasmids for multiple gene constructs using the modular cloning (MoClo) system in *E. coli*

pICH47732 (Weber et al., 2011)
This plasmid contains a carbenicilin resistance and was used as level 1 (L1) acceptor plasmid for assembly of L0 parts into transcriptional units.

pICH44022 (Weber et al., 2011)
This plasmid contains a CDS, P19 suppressor of gene silencing (*Tomato Bushy Stunt Virus*) and was used for assembly of level 1 (L1) transcriptional units.

pICH51288 (Weber et al., 2011)
This plasmid contains a 2x35s promotor (*Cauliflower Mosaic Virus*) + 5'UTR, omega (*Tobacco Mosaic Virus*) and was used for assembly of level 1 (L1) transcriptional units.

pICH41414 (Weber et al., 2011)
This plasmid contains a 3'UTR, polyadenylation signal/terminator, 35s (*Cauliflower Mosaic Virus*) and was used for assembly of level 1 (L1) transcriptional units.

pICSL50009 (Weber et al., 2011)
This plasmid contains a HA tag (6x Human influenza hemagglutinin) and was used for assembly of level 1 (L1) transcriptional units.

pICSL50004 (Weber et al., 2011)
This plasmid contains a CDS, mCherry variant of RFP (*Discosoma sp.*) in PAGM1301 BB and was used for assembly of level 1 (L1) transcriptional units.

pICSL50008 (Weber et al., 2011)
This plasmid contains a CDS, GFP (*A. victoria*) in pAGM1301 BB and was used for assembly of level 1 (L1) transcriptional units.

4.1.9.4 Plasmids for transient protein expression in *N. benthamiana*

Plasmids used for the transient expression of proteins in *N. benthamiana* were generated by using the MoClo cloning system and the MoClo Plant tool kit that are listed in 4.1.9.3. L1 constructs generated and used in this work are listed in 4.12. The assembly of fragments was done as described in 4.2.3.13 and afterwards transformed into *E. coli* DH5α cells as described in 4.2.2.3.

Table 4.12: **Constructs for recombinant protein expression in *N. benthamiana***

Backbone	Expression construct	Reference
pICH47732	2x35S-p19-pterm	Schulze Huynck et al. 2019
pICH47732	2x35S-eGFP	Schulze Huynck et al. 2019
pICH47732	XCP2-Streptwin::2x35S	Schulze Huynck et al. 2019
pICH47732	CatB-Streptwin::2x35S	Schulze Huynck et al. 2019
pICH47732	CP1A-nogran-Streptwin::2x35S	Schulze Huynck et al. 2019
pICH47732	CCP2-Streptwin::2x35S	Schulze Huynck et al. 2019
pICH47732	CP1B-nogran-Streptwin::2x35S	Schulze Huynck et al. 2019
pICH47732	CP1C-nongran-HA::2x35S	Schulze Huynck et al. 2019
pICH47732	CP1A-nogran-mut2-Streptwin::2x35S	Schulze Huynck et al. 2019
pICH47732	CP1D-HA::2x35S	This study
pICH47732	B4FS65-HA::2x35S	This study
pICH47732	B4FYA3-HA::2x35S	This study
pICH47732	Q10716-HA::2x35S	This study
pICH47732	CP1A-nogran-mCherry-2x35S	This study
pICH47732	CP1Amut-nogran-mCherry-2x35S	This study
pICH47732	B4FS65-mCherry-2x35S	This study
pICH47732	B4FYA3-mCherry-2x35S	This study
pICH47732	Q10716-mCherry-2x35S	This study
pICH47732	CP1D-mCherry-2x35S	This study

4.2 Methods

4.2.1 Plant methods

4.2.1.1 Seed sterilisation: *Zea mays*

Maize seeds were filled in 50 ml falcon tubes and mixed with 25 ml of 70% Ethanol (EtOH). All further steps were carried out under sterile conditions. EtOH was discarded and 1.2% sodium hypochlorite was added. Seeds were incubated for 20 - 30 min at Room temperature (RT) on a tube roller. Afterwards, sodium hypochlorite was discarded and seeds were washed at least 5 times with $H_2O_{bid.}$ with 5 min incubation on a tube roller in between washing steps. Finally, seeds were transferred to sterile wet Whatman paper and vernalized at RT for 3 days.

4.2.1.2 Seed sterilisation: *A. thaliana*

Arabidopsis seeds were collected in a 15 ml falcon tube and mixed with 10 ml 70% EtOH. All further steps were carried out under sterile condictions. Seeds were incubated for 5 min at RT on a tube roller and spun down to decant the EtOH. 1.2% of sodium hypochlorite was added to the seeds which were incubated for 10 min on a tube roller before they were spun down to decant the sodium hypochlorite. Samples were washed at least 3 times with with $H_2O_{bid.}$ and spun down to decant

$H_2O_{bid.}$ between washing steps. Seeds were dissolved in 300 µl 0.15% agar and vernalized at 4°C for 3 days in darkness.

4.2.1.3 Extraction of maize root exudates

All following steps were carried out under sterile conditions until harvest of the root exudates. Sterilised maize seeds were transferred to magenta vessels (Sigma-Aldrich, St. louis, Mississippi, USA) filled with sterilised Vermiculit (2 - 3 cm depth). Per vessel 50 ml sterile $H_2O_{bid.}$ and up to 15 seeds were added. Vermiculit should cover the seeds from light and the bottom of the vessel should be covered with aluminium foil. Vessels were incubated for 5 days at conditions described above (4.1.5.1). 20 ml of sterile $H_2O_{bid.}$ were added and samples were incubated for another 2 days. Then 40 ml of sterile $H_2O_{bid.}$ were added and samples were incubated for another day. Fluid surrounding the roots was collected and sterile filtrated to remove dirt. Samples were lyophilized and remaining root exudates were resuspendet in $H_2O_{bid.}$ with a f.c. of 5 mg/ml. Root exudates were stored at -20°C until further use.

4.2.1.4 SA treatment of maize roots and leaves

Maize plants were sowed in Seramis clay granulate (Sermanis GmbH, Mogendorf, Germany) for root treatment and in soil for leaf treatment and grown for 7-10 days until the three leaf stage. Afterwards, 2 mM SA was dissolved in 0.1% EtOH and poured to the maize roots every twelve hours for two days. As a control, mock treated plants were poured with a solution consisting of 0.1% EtOH. Plants were harvested 12 h after last treatment. For leaf treatment same solution were infiltrated into the third leaf using a 1 ml tuberculin-syringe without a hypodermic needle and harvested after 48 h.

4.2.1.5 SA treatment of *N. benthamiana* leaves

N. benthamiana plants were grown under conditions described above (4.1.5.2) for 5 to 6 weeks. With *A. tumefaciens* infiltrated leaves (4.2.1.7) were sprayed with 5 mM SA dissolved in 0.1% EtOH two days post infiltration. As a control mock treated plants were sprayed with a solution consisting of 0.1% EtOH. Samples were harvested 24 h post treatment.

4.2.1.6 SA treatment of *A. thaliana* roots

All steps were carried out under sterile conditions. Sterilised *A. thaliana* seeds were vernalized for 3 days in darkness at 4°C and spread on solid $\frac{1}{2}$ MS media. *A. thaliana* were incubated for 18 days in a growth chamber under conditions as describe above (4.1.5.3). Plants were then transferred to sterile 6-well plates containing 5 ml per well of liquid $\frac{1}{2}$ MS media. Plants were incubated for 1 day before the media was exchanged with 5 ml per well of 2 mM SA dissolved in $\frac{1}{2}$ MS media. After another 12 h this media exchange was repeated. For control conditions fresh media without SA was

used instead. 12 h post the last SA-treatment roots were separated from the plant and frozen in liquid nitrogen. Harvested roots were ground and stored at -80°C until further use.

4.2.1.7 Recombinant expression of PLCPs in *N. benthamiana* leaves

Agrobacterium tumefaciens containing the desired constructs were grown in 10 ml liquid dYT media with appropriate antibiotics over night (O/N) until an OD_{600} between 0.4 and 2.0. Cultures were centrifuged for 8 min at 4000 × Gravitational acceleration on earth ($9.81\frac{m}{s^2}$) (× g) and resuspended in freshly prepared 10 mM Magnesium chloride ($MgCl_2$) to an OD_{600} = 1 with 200 µM acetosyringone (Sigma-Aldrich, Taufkirchen, Germany). After 1 h incubation in the dark cultures were infiltrated into 5 - 6 week old *N. benthamiana* leaves using a tuberculin-syringe without needle. Three days post infiltration leaves were harvested and the apoplastic fluid was isolated.

4.2.1.8 Apoplastic fluid isolation

For root apoplastic fluids maize plants grown in Seramis were carefully removed from the pots and Seramis clay granulate was removed from the roots using forceps and washes with $H_2O_{bid.}$. Roots were separated from the aerial plant parts and put into a beaker filled with $H_2O_{bid.}$. A metal-sieve was added on top to prevent roots from swimming out of the $H_2O_{bid.}$. Roots were then vacuum infiltrated 3 times for 15 min at 60 mbar with an interval of 2 min atmospheric pressure. Roots were transferred to syringes hanging in 50 ml falcon tubes and centrifuged at 4°C for 20 min at 3000 × g to isolate the apoplastic fluid. Prior to storage at -20°C or direct use in experiments the fluid was passed through a 45 µM syringe filter. Fractionation of apoplastic fluid was performed according to van der Linde et al., 2012a. Apoplastic fluid from maize leaves was prepared as described above except that the leaves were centrifuged at 4°C for 20 min at 2000 × g. Apoplastic fluid from *N. benthamiana* leaves was prepared as described for maize leaves except that the leaves were vacuum infiltrated 3 times for 10 min at 60 mbar.

4.2.2 Microbiological methods

4.2.2.1 Chemocompetent *E. coli*

All used buffers and equipment need to be pre-chilled and each step was carried out on ice in a cold room. *E. coli* cells of a single colony were grown in dYT-media at 37 Degree Celsius (°C) and 200 rpm until they reached an OD_{600} of approximately 0.6. Cells were then cooled on ice for 30 Minute(s) (min) and afterwards centrifuged for 8 min at 4°C and 1250 × g. The supernatant was decanted an cells in $\frac{1}{3}$ of their initial culture volume of cold RF1-solution re-suspended. The cells were then incubated for 30 min at 4°C followed by centrifugation for 8 min at 4°C and 1250 × g. The supernatant was decanted again and the cells were re-suspended in $\frac{1}{20}$ of their initial culture volume of cold RF2-solution. The solution was transferred in pre-chilled tubes and incubated for a minimum

of 30 min at 0°C. Cell-aliquots of 50 Microliter (µl) were transferred to pre-chilled reaction tubes and shock-frozen with liquid nitrogen. The aliquots were stored at -80°C until further use.

Table 4.13: **RF1 solution, pH = 5.8.**

Components	Final concentration
RbCl	100 mM
MnCl2 x 4H2O	50 mM
Kaliumacetat	30 mM
CaCl2 x 2H2O	10 mM
Glycerol (w/v)	15%

Table 4.14: **RF2 solution, pH = 5.8.**

Components	Final concentration
MOPS	10 mM
RbCl	10 mM
CaCl2 x 2H2O	75 mM
Glycerol (w/v)	15%

4.2.2.2 Chemocompetent *A. tumefaciens*

The preparation of chemocompetent *A. tumefaciens* cells as well as the transformation of those cells was done as described in (Hofgen and Willmitzer, 1988). Instead of YEB media, dYT liquid and YT agar medium were used, containing the respective antibiotics for selection.

4.2.2.3 Transformation of *E. coli*

50 µl of previously at -80°C stored competent *E. coli* cells were thawed on ice. 5-10 µl plasmid DNA was added and gently mixed with the bacteria. The mix was then incubated for 15 - 45 min on ice before they were heat-shocked for 45 seconds at 42°C. Cells were cooled down on ice for 1 - 2 min after the heat-shock and 300 µl of dYT was added. For recovery the cells were incubated shaking at 200 rpm for 30 min at 37°C before they were plated on YT-agar plates containing the appropriate antibiotics. The YT-agar plates were then incubated shaking at 200 rpm and 37°C over night and single colonies were picked afterwards. Single colony transformants were grown in YT-media over night at 200 rpm and 37°C and verified by colony-PCR or plasmid extraction followed by a restriction digest.

4.2.2.4 Transformation of *A. tumefaciens*

electro-competent

2 ng of plasmid DNA was added to 50 µl of electro-competent *A. tumefaciens* cells. The mix was homogenized by gently pipetting up and down several times. The mix was then transferred to a pre-chilled cuvette. Moisture was wiped from the cuvette, which was put in an eporator (Eppendorf, Hamburg, Germany) . Electro-poration was carried out at 1440 V for 5 ms. 400 µl of dYT media was added immediately after Electro-poration and the sample was transferred to a new tube for incubation at RT for 1 h. The sample was then spread on dYT-agar plates containing appropriate antibiotics and incubated for 48 h at 28°C before single colony transformants were picked for over night cultivation and confirmation of the transformation by colony-PCR or plasmid extraction followed by a restriction digest.

chemical-competent

10 µl of plasmid DNA was added to 50 µl of chemocompetent *A. tumefaciens* cells. The mix was homogenized by gently pipetting up and down several times and frozen in liquid nitrogen. The frozen sample was thawed in a 37°C water bath for 5 min. 500 µl of dYT media containing appropriate antibiotics was added and samples were incubated shaking at 200 Rounds per minute (rpm) and 28°C for 2 - 3 h. Samples were spread on dYT-agar plates containing appropriate antibiotics and incubated for 48 h at 28°C before single colony transformants were picked for over night cultivation and confirmation of the transformation by colony-PCR or plasmid extraction followed by a restriction digest.

4.2.2.5 Blue-white screen of *E. coli* transformants

For cloning of maize PLCPs together with other building blocks in the Modular cloning (MoClo) vector, we used a Blue-white selection approach. By insertion of a cloned PCR product and other building blocks of the MoClo tool kit in the vector (4.2.3.13) the lacZ gene inside the plasmid gets disrupted, which leads to a lack of β-galactosidase expression. As a result, the colonies that contain the desired fragment at this site appear white on 5-bromo-4-chloro-3-indolyl-β-D-galactopyranoside (X-Gal) containing media plates. These colonies are therefore easily distinguishable from the blue colonies, which still express β-galactosidase. 50 µl of X-Gal solution (2% (w/v) X-Gal, dissolved in Dimethylformamid (DMF)) was spread on selective Yeast extract tryptone (YT)-agar plates for this screening.

4.2.2.6 Isolation of bacterial supernatant

For a first screen bacteria were grown in 200 µl dYT minimal media in sterile deep-well-plates (Axygen/Corning, Kaiserslautern, Germany) O/N at 28°C, 200 rpm orbital shaking. Culture OD_{600} was measured and bacteria were diluted to OD_{600} = 0.05 in 200 µl M9 minimal media. To test effector triggering effects of Root exudates (RE), 0.25 mg/ml f.c. sterile RE were added to one sample while a control sample was not treated with RE. Sam-

ples were grown O/N as described before followed by centrifugation for 5 min at 1500 $\times g$ to isolate culture supernatant for further use in substrate cleavage assays (4.2.4.9). After the first screen bacteria were grown in media volumes of 20 ml. Additionally, OD_{600} of cultures was measured prior to substrate cleavage assays, adjusted to an OD_{600} = 0.8 in fresh media and incubated for 30 min before the supernatant was collected.

4.2.2.7 Isolation of fungal supernatant

All steps were carried out under sterile conditions if not stated differently. To start liquid culture 4 ml of liquid PD media were added to fungi grown previously on solid PD media. Mycelia and spores were scratched from the plate and dissolved in liquid PD media. 500 µl of the suspension were transfered to 20 ml of fresh liquid PD media in an Erlenmeyer flask and incubated for 5 days at 22°C and 200 rpm orbital shaking. Cultures were filtered using Miracloth (Millipore/Merck, Darmstadt, Germany) and collected cell material was washed 2 times with 10 ml $H_2O_{bid.}$. Collected material was transfered to fresh NM minimal media and incubated for 1 day as described before. To test effector triggering effects of RE, 0.25 mg/ml f.c. sterile RE were added to one sample while a control sample was not treated with RE. For isolation of culture supernatant, samples were filtered through Miracloth and the flow through was collected for further use in substrate cleavage assays (4.2.4.9).

4.2.2.8 Growth curve of endophytic bacteria

Bacteria were grown in the appropriate media (M9, dYT, TSB 4.1.6.1) at 28°C and set to an OD_{600} of 0.05. The OD_{600} of bacterial cultures was measured every two hours for 18 hours. This was repeated three times for every bacterium in each media.

4.2.2.9 Optical determination of cell density

The cell density was determined by measuring the Optical density at 600 nM (OD_{600}) in a GENESYS^{TM} 10S UV/VIS-Spectral-photometer (Thermo Fischer scientific, Waltham, Massachusetts, USA) while using the corresponding culture media as a reference. To ensure measurement in the linear correlation between absorption and cell density, cultures were diluted to absorption values lower than 0.8. For bacteria an absorption of 1.0 at OD_{600} accounts for 8×10^8 cells/ml.

4.2.3 Molecular biological methods

4.2.3.1 Isolation of genomic DNA from maize plants

Isolation of genomic DNA from maize plants was performed using the MasterPure™ Complete DNA and RNA Purification Kit from Epicentre (Epicentre, Chicago, USA) according to manufacturers instruction.

4.2.3.2 Isolation of plasmid DNA from *E. coli*

For isolation of plasmid DNA the QIAprep Mini Plasmid Prep Kit (Quiagen, Hilden, Germany), which uses the principle of alkaline lysis, was used. All centrifugation steps were carried out at RT if not indicated differently. A thickly grown *E. coli* overnight culture was centrifuged at 17000 $\times$ *g* for 5 min in a reaction tube. The supernatant was discarded and the cell pellet resuspended in 250 µl P1 buffer. For lysis 250 µl of P2 buffer were added and mixed several times by inverting the tube. After incubation for up to 5 min at RT 300 µl of P3 buffer were added to neutralize the lysed cell extract and precipitation of protein. Precipitated protein and cell debris was pelleted by centrifugation at 17000 $\times$ *g* for 10 min. The supernatant was transferred to a new reaction tube filled with 600 µl 2-propanol, mixed by inversion and Deoxyribonucleic acid (DNA) was precipitated at -20°C. After precipitation of DNA the sample was centrifuged at 17000 $\times$ *g* for 10 min and the supernatant was decanted. To wash of remaining 2-propanol 800 µl of EtOH was added. The sample was centrifuged at 17000 $\times$ *g* for 10 min and the supernatant was decanted. The pellet was dried and and re-suspended in in 30 - 50 µl of TE-RNAse buffer.

Table 4.15: **TE buffer, pH = 8.0.**

Components	Final concentration
Tris-base	10 mM
Na2-EDTA	1 mM

4.2.3.3 Isolation of RNA from maize plants

Since RNA is prone to degradation by RNAses also present on the human skin RNA samples have to be handled with extreme caution. Therefore filter tips, nuclease free tubes and water and EtOH-washed nitrile gloves were used throughout the isolation of RNA from plant material. All centrifugation steps were carried out at RT if not indicated differently. Plant material was ground on liquid nitrogen and a 500 ml aliquot was taken. The tube with the aliquot was removed from liquid nitrogen and 1 ml of TRIzol-reagent (Ambion, life technologies^{TM}, Carlsbad, California, USA) was added and directly mixed firmly to avoid freezing of the TRIzol-reagent. Samples were transferred to an ice cooled rack and kept cool throughout the RNA isolation process. After the homogenisation of the plant sample with the TRIzol-reagent the mix was centrifuged for 10 min at 12000 $\times$ *g*. The supernatant was separated from the pellet containing cell debris and transferred to a new tube. 200 µl of chloroform was added to the supernatant and tubes inverted to homogenise the sample. After 15 min centrifugation at 12000 $\times$ *g* the water phase containing nucleic acids was transferred to a new tube. 500 µl 2-propanol was added to the sample which was then incubated for 10 min at RT followed by a centrifugation step for 10 min at 12000 $\times$ *g*. The supernatant was decanted and the pellet washed and mixed with 1 ml 75% EtOH. After homogenisation the sample was centrifuged for 5 min at 7500 $\times$ *g* and the supernatant was removed. The pellet was left on the bench for evaporation

of remaining EtOH. 20-50 µl (depending on the desired final RNA concentration) of nuclease-free $H_2O_{bid.}$ was added to the RNA-pellet which was then resolved for 10 min at 55 - 60°C. The quality of the isolated RNA was controlled by gel-electrophoresis and RNA was stored at -80°C until further use.

4.2.3.4 DNAse digest after RNA isolation

Digest of DNA after RNA isolation was performed using the Turbo DNA-Free^{TM} Kit from Ambion (Ambion, life technologies^{TM}, Carlsbad, California, USA). To prevent RNA degradation filter tips, nuclease free tubes and water and EtOH-washed nitrile gloves were used. All centrifugation steps were carried out at RT if not indicated differently. 0.1 volumes of 10 $\times$ TURBO DNAse buffer of total sample volume and 1 µl TURBO DNAse were added to the template RNA and incubated for 30 min at 37°C. To inactivate the DNAse 0.1 volumes of DNAse inactivation reagent was added, mixed with the sample and incubated for 2-5 min at RT. Samples were mixed during incubation to prevent sedimentation of DNAse inactivation reagent. Samples were centrifuged for 1.5 min at 10000 $\times$ g after incubation. The supernatant containing DNA-free RNA was transferred to a new nuclease-free reaction tube and stored at -80°C. The quality of the isolated RNA was controlled by gel-electrophoresis.

4.2.3.5 Synthesis of cDNA

Synthesis of cDNA was performed using Thermo Scientific RevertAid H Minus First Strand cDNA Synthesis Kit by Thermo (Thermo Fischer scientific, Waltham, Massachusetts, USA). RNA-samples and components of the kit were thawed, briefly mixed and kept on ice. Template RNA (1 - 5 Microgram (µg)), oligo(dT)$_{18}$ primer (15 - 20 pmol) was added to a nuclease-free reaction tube and filled up with nuclease-free water to 12 µl. Due to high GC-content in the maize genome samples were incubated at 65°C for 5 min, afterwards chilled on ice and spun down before placed back on ice. 5x Reaction buffer (4 µl), RiboLock RNase Inhibitor (1 µl, 20 Unit of enzyme activity (U)/µl), 10 mM dNTP Mix (2 µl), RevertAid H Minus M-MulV Reverse Transcriptase (1 µl, 200 U/µl) was added to the sample which was then incubated at 25 °C for 5 min followed by incubation at 45°C for 60 min to synthesize cDNA. To stop the reaction samples were heated up to 70°C for 5 min. cDNA was stored at -20°C until further use.

4.2.3.6 Quantification of nucleic acids

Quantification of nucleic acids was performed using a Nanodrop 2000c spectrophotometer (Thermo Fischer scientific, Waltham, Massachusetts, USA) according to manufacturers instructions using 1 µl of sample after using 1 µl of the appropriate buffer as a blank control.

4.2.3.7 Purification of nucleic acids

Nucleic acids were purified using the NucleoSpin gel and PCR Clean-up kit (Macherey-Nagel, Düren, Germany) according to the manufacturers manual. Depending on the starting material 200 µl NTI-reagent were added per 100 µl PCR-product or 100 mg gel. In case that the starting material was a gel, the samples were incubated for 5-10 min at 50°C until the gel was dissolved. The DNA was bound by addition of the samples to the columns, which were placed in reaction tubes and centrifuged for 30 s at 11000 $\times g$. The flow through was discarded and 700 µl NT3-reagent was added to wash the silica membrane. Samples were centrifuged again for 30 s at 11000 $\times g$. The flow through was discarded again and the membrane was dried by an additional centrifugation step for 1 min at 11000 $\times g$. The DNA was eluted in 20 µl NE-buffer or $H_2O_{bid.}$ and incubated for 1 min at RT followed by a final centrifugation for 1 min at 11000 $\times g$.

4.2.3.8 Sequencing of nucleic acids

Sequencing reactions were done externally by the company Eurofins (formerly GATC, Cologne, Germany). Prior to sequencing of plasmids or PCR fragments, DNA was purified using Nucleospin® Gel and PCR Clean-up kit (Macherey-Nagel, Düren, Germany) as described in 4.2.3.7. DNA sequencing results were analysed and validated using the program Clone Manager 9 (Sci-Ed, Denver, USA).

4.2.3.9 Restriction digest of nucleic acids

Site-specific restriction of DNA was performed via *type II* restriction endonucleases (New England Biolabs, Massachusetts, USA). The amount of DNA used for digestion ranged from 0.5 - 2 µg. The restriction reaction was set up following manufacturers instructions as seen in 4.16. Reaction samples were incubated for 1 Hour (h) at the appropriate temperature indicated for the used restriction enzyme or O/N at 4°C.

Table 4.16: **Restriction digest: Reaction mix example.**

Components	Amount
DNA (plasmid DNA or cleaned PCR-product)	0.5 - 2 μg
10x NEB-buffer	5 μl
Restriction enzyme	1 μl or 10 U
Nuclease-free water	ad 50 μl

4.2.3.10 poly-A tailing

For ligation of DNA-fragments in the pGEM®-T vector system A-tails were added to blunt end fragments. For A-tailing we added 0.2 volume of the GoTaq® Green Master Mix (Promega, Madison,

Wisconsin, USA) to 20 µl of DNA-fragment and incubated samples either for 20 min at 72°C or O/N at 4°C.

4.2.3.11 Fragment assembly using pGEM®-T vector system

For ligation of a DNA-fragment in the pGEM®-T vector system manufacturer's instructions were followed. Reagents were briefly mixed, spun down an pipetted together as seen in 4.17. Reactions were mixed by pipetting up and down and incubate the reaction O/N at 4°C. For the ligation of a desired insert DNA-fragment in a corresponding vector backbone, a molar ratio of 2:1 - 3:1 was used.

Table 4.17: **pGEM-T ligation pipetting scheme.**

Components	Amount
2x Rapid Ligation & T4 DNA Ligase Buffer	5 μl
pGEM®-T Vector (50 ng)	1 μl
PCR product	X μl
T4 DNA Ligase (3 U/μl)	1 μl
Nuclease-free water	ad 10 μl

4.2.3.12 Fragment assembly after Gibson system

Gibson assembly cloning makes use of homologous recombination of DNA fragments. DNA fragments need to have around 20 Base pairs (bp) overlap with the adjacent DNA fragment for the homologous recombination. The reaction mix (New England Biolabs, Massachusetts, USA) was put together as shown in 4.18, mixed and shortly centrifuged. Afterwards the reaction mix was incubated for 30 min at 50°C followed by incubation for 2 min on ice.

Table 4.18: **Gibson assembly pipetting scheme.**

Components	Amount
Acceptor plasmid	50 - 100 ng
Insert	2:1 molar ratio of insert:acceptor
2x Hifi DNA assembly mix	5 μl
$H_2O_{bid.}$	ad 10 μl

4.2.3.13 Strain and plasmid construction

Golden gate modular cloning system was applied to generate plasmids (Engler et al., 2014). Oligonucleotides that were used for PCR are listed in 4.1.8. To obtain XCP2, CathB, CP2, B4FS65 and Q10716 the respective transcripts were amplified by PCR from maize cDNA. To obtain CP1A,

CP1B, CP1C, CP1D and B4FYA3 the respective transcripts were amplified by PCR from maize cDNA leaving out the DNA sequence coding for the granulin-domains. PLCP transcript IDs are listed in 4.19 while the primers used for amplification are listed in 4.1.8. The amplified sequences were then ligated according to (Weber et al., 2011; Engler et al., 2014), sub-transformed to *E. coli* DH5α competent cells (Thermo scientific, Rockfort, USA) and then transformed to *A. tumefaciens* GV3101 competent cells for recombinant expression in *N. benthamiana*. To obtain CP1A^{mut} site directed mutagenesis was performed on CP1A according to the instructions of the QuikChange Multi Site-Directed Mutagenesis Kit (Agilent Technologies, Santa Clara, USA) with primers targeting nucleotides of the active site of CP1A. Strains used in this study are listed in 4.4.

Table 4.19: **Maizegdb transcript IDs of PLCPs used in this study.**

PLCP	Transcript ID
CP1A	GRMZM2G166281_T01
CP1B	GRMZM2G073465_T03
CP2	Zm00001d020636_T001
XCP2	GRMZM2G066326_T01
Cathepsin B	GRMZM2G108849_T04
CP1C	GRMZM2G340065_T01
CP1D	GRMZM2G010435_T01
B4FS65	Zm00001d005391_T001
B4FYA3	GRMZM2G006377_T01
Q10716	GRMZM2G098298_T01

4.2.3.14 Fragment assembly after MoClo system

For ligation of DNA-fragments in L1 acceptors of the MoClo kit, the enzyme *BsaI* (New England Biolabs, Massachusetts, USA) was used in a digestion-ligation reaction. The *type II* restriction endonuclease *BsaI* cuts DNA outside of its recognition site which is used to assemble multiple DNA fragments with matching overhangs correctly. Reactions were set up as described in 4.20.

Table 4.20: **MoClo L1 ligation pipetting scheme.**

Components	Amount
Acceptor plasmid	50 - 100 ng
Insert	2:1 molar ratio of insert:acceptor
BsaI	10 U
CutSmart buffer	1 μl
T4 DNA Ligase	200 U
ATP (10 mM)	1 μl
$H_2O_{bid.}$	ad 20 μl

Reactions were incubated as mentioned in 4.21.

Table 4.21: **MoClo L1 incubation protocol.**

Steps	Temperature [°C]	Time [min]
1	40	10
2	16	10
3	Repeat 1. & 2.	5×
4	50	10
5	80	20
6	4	∞

4.2.3.15 *in vitro* mutagenesis of nucleic acids

To be able to use the MoClo (see 4.2.3.14) system the target sequence must not contain any recognition site for the restriction enzymes *BsaI* and *BpiI* (New England Biolabs, Massachusetts, USA). To remove existing recognition sites single silent mutations were induced with the Quickchange (Multi) Kit (Agilent Technologies, Santa Clara, USA) following manufacturer instructions.

4.2.3.16 Polymerase chain reaction (PCR)

For amplification of DNA fragments Polymerase chain reaction (PCR) was used. Different polymerases were used depending on the experimental purpose. For amplification of DNA fragments from *Zea mays* the KOD Xtreme^{TM} Hot Start polymerase (Novagen/Merck, Darmstadt, Germany) or the Taq-Polymerase containing GoTaq® Green Master Mix (Promega, Madison, Wisconsin, USA) was used. For analytical purposes the Taq-Polymerase containing GoTaq® Green Master Mix was used. PCR reactions were set up in a reaction volume of 25 µl or 50 µl depending on its purpose of use. PCR reactions were set up according to the manufacturers instructions as shown in 4.22 and 4.23. In case of a colony-PCR cell material of the desired colony was used as a template. The reactions using Taq- or KOD-polymerase were incubated as stated in 4.24 and 4.25, respectively adjusted to the used primer annealing temperatures and fragment sizes for each experiment. PCR product size was verified by subsequent separation on agarose gel via gel electrophoresis (4.2.3.18).

Table 4.22: **Taq-PCR pipetting scheme.**

Components	Amount
2x GoTaq® Green Master Mix	12.5 μl
Template	100 - 500 ng
Forward Primer	1.0 μM
Reverse Primer	1.0 μM
H$_2$O$_{bid.}$	ad 25 μl

Table 4.23: **KOD-PCR pipetting scheme.**

Components	Amount
2x Xtreme buffer	25 μl
dNTPs	0.4 mM
Template	100 - 500 ng
Forward Primer	0.3 μM
Reverse Primer	0.3 μM
$H_2O_{bid.}$	ad 50 μl

Table 4.24: **PCR program with Taq polymerase.**

Steps	Temperature [°C]	Time [min]	Description
1	94	5	initial denaturation
2	94	0.5	denaturation
3	50 - 65	0.5 - 1	annealing (temperature is primer-dependent)
4	72	1 min/kb	elongation
5	Repeat 2. - 4.	35$\times$	
6	72	5	final elongation
7	4	∞	

Table 4.25: **PCR program with KOD polymerase.**

Steps	Temperature [°C]	Time [min]	Description
1	94	2	initial denaturation
2	98	0.25	denaturation
3	50 - 65	0.5 - 1	annealing (temperature is primer-dependent)
4	68	1 min/kb	elongation
5	Repeat 2. - 4.	40$\times$	
6	68	5	final elongation
7	4	∞	

4.2.3.17 Quantitative real-time PCR

cDNA (4.2.3.5) synthesised from freshly prepared RNA (4.2.3.3) was used as a template for Quantitative real-time polymerase chain reaction (qRT-PCR). Reactions were set up using the SYBR® Green Supermix (Promega, Madison, Wisconsin, USA) according to manufacturers instruction of a total volume of 25 μl with 1 μl of cDNA per reaction. qRT-PCR analysis were performed with

an CFX Connect^{TM} Real-Time System (Bio-Rad, Munich, Germany) with the program CFX Manager 3.1 (Bio-Rad, Munich, Germany) as stated in 4.26. Relative expression values between target genes normalised to house-keeping genes were calculated manually (Pfaffl et al., 2002). Primer efficiency was tested using a cDNA dilution series prior to usage in quantitative real-time PCR.

Table 4.26: **qRT-PCR program.**

Steps	Temperature [°C]	Time [min]
1	95	2
2	95	0.5
3	62	0.5
4	72	0.5
5	Repeat 2. - 4.	45$\times$

4.2.3.18 Agarose gel electrophoresis

Agarose gel electrophoresis was used for size separation and estimation of nucleic acids. Agarose gels of 1% agarose concentration were prepared in 1$\times$ TAE buffer by boiling in the microwave. After boiling the buffer was mixed and cooled until it reached a temperature of approximately 60°C and ethidium bromide (f.c. 0.2 μg/ml) was added. The gel was poured in a mould with a comb for solidification. Afterwards the gel was transferred into a chamber containing 1$\times$ TAE buffer (4.27) and loaded with samples, which contained 1$\times$ DNA-loading dye (4.28). Size separation and estimation of the DNA was achieved by application of a constant voltage of 100 - 120 Volt (V) depending on the size of the gel in parallel with the GeneRuler 1 kb DNA Ladder (Thermo Fischer scientific, Waltham, Massachusetts, USA). DNA bands were visualised by UV radiation at 365 nm using the gel documentation unit (Peqlab/VWR, Langenfeld, Germany).

Table 4.27: **50x TAE-Buffer in H$_2$O$_{bid.}$.**

Components	Final concentration [M]
Tris-base	2
Acetic acid	2
EDTA pH 8.0	0.05

Table 4.28: **6x DNA loading dye in H$_2$O$_{bid.}$.**

Components	Final concentration
Sucrose	50% (w/v)
Bromophenol blue	0.13% (w/v)

4.2.4 Biochemical methods

4.2.4.1 Recombinant protein production of CC1 and CC9

E. coli BL21 cells expressing the protein of interest were grown in 5 ml liquid dYT media supplemented with the appropriate antibiotics O/N at 37°C and 200 rpm orbital shaking. OD_{600} of O/N was measured and cultures were diluted in 1 L of fresh media. Cultures were incubated as described before until an OD_{600} of 0.5 was reached. Protein production was induced by addition of 2 mM Isopropyl-B-D-thiogalactopyranoside (IPTG) f.c.. Induced cultures were incubated for 2 h as described before. Cells were harvested by centrifugation at $8000 \times g$ and 4°C for 15 min. The supernatant was decanted and pellets were frozen at -20°C for cell lysis. Pellets were resuspendet in 5 ml binding buffer (4.29) and incubated for 15 min at RT followed by sonification 4 x 60s using Bandelin sonoplus (Bandelin, Berlin, Germany). Samples were centrifuged for 20 min at $40000 \times g$ and 4°C. Test samples of supernatant and pellet were taken to evaluate protein production. Supernatants were collected and sterile filtrated prior to subjection to Ni^{2+}-NTA (4.2.4.2).

Table 4.29: **Binding buffer in $H_2O_{bid.}$ pH 7.4.**

Components	Final concentration
Sodium phosphate	20 mM
NaCl	500 mM
Triton X-100	0.1% (v/v)
Imidazol	80 mM
cOmplete^{TM} tablets	1/10 ml
Lysozyme	100 μg/ml

4.2.4.2 Ni^{2+}-NTA

Columns were loaded with 1.5 ml chelating sepharose fast flow (Sigma-Aldrich, St. louis, Mississippi, USA) and 5 Column volume (CV) of 0.1 M nickel sulphate followed by 2 CV $H_2O_{bid.}$. For column equilibration 2 CV $H_2O_{bid.}$ were added followed by 5 CV of binding buffer (4.29). Samples from recombinant protein production (4.2.4.1) were added to closed columns and incubated for 30 - 90 min at 4°C. Control samples were taken from flow through, wash step and each elution step. The flow through was collected and the column was washed with >3 CV of binding buffer, which was also collected. For elution, three times 5 ml of elution buffer based on binding buffer (without cOmplete™ and lysozyme) with various imidazol concentrations (E1: 200 mM, E2: 300 mM, E3: 500 mM imidazole) was added to the column. Samples were incubated for 10 - 15 min at RT with each elution buffer prior to sample collection and addition of the following elution buffer. Elutions were incubated for 1 h at RT with 50 mM Dithiotreitol (DTT) f.c. to avoid formation of dimers. Control samples were analysed via SDS-Polyacrylamide gel electrophoresis (PAGE) and elution samples containing the protein of interest were subjected to SEC (4.2.4.3).

4.2.4.3 Size-exclusion chromatography SEC

SEC was performed using a HiLoad® 16/600 Superdex® 75 pg column in an Äkta system (GE Healthcare, Chicago, Illinois, USA) using a buffer consisting of 50 mM Tris-HCl pH 7.5 and 150 mM NaCl. 2 ml fractions were collected and analysed for protein content using SDS-PAGE.

4.2.4.4 Activity based protein profiling (ABPP)

Root apoplastic fluid or plant total extract powder was incubated for 2 h in 50 mM sodium acetate pH 6, 10 mM DTT and 0.2 - 2 µM of the probe MV201 or DCG-04, respectively (Greenbaum et al., 2000; Richau et al., 2012). As a negative control, one set of samples was pre-incubated for 30 min with 20 µM E-64 (Sigma-Aldrich, St. louis, Mississippi, USA) prior to labelling. MV201 labelling was performed in darkness. Labelling was stopped by addition of $1 \times$ SDS-loading dye f.c. (Laemmli, 1970). Samples were heated to 95°C for 5 min and proteins were separated on 12% SDS-gels. For MV201 labelled samples SDS-PAGE was performed in darkness and visualized on gel fluorescent scanning using a Chemi-Doc MP System (Bio-Rad, California, USA) with Rhodamine settings (excitation: 532 nm, emission: 580 nm). The loading control gel was stained with SyproRuby (Invitrogen, Carlsbad, California, USA) according to the protocol provided by the manufacturer. Detection of DCG-04 labelled samples was performed using a streptavidin-HRP antibody (Sigma-Aldrich, St. louis, Mississippi, USA).

4.2.4.5 PLCP pulldown using streptavidin-beads

Root apoplastic fluid was incubated for 4 h at room temperature in 50 mM sodium acetate pH 6, 10 mM DTT and 2 µM DCG-04 (Greenbaum et al., 2000) in a total volume of 2.5 ml. As a negative control, one set of samples was pre-incubated for 30 min with 20 µM E-64 (Sigma-Aldrich, St. louis, Mississippi, USA) prior to labelling. After labelling, samples were transferred and eluted using NaP25 columns (GE healthcare, Chicago, Illinois, USA) equilibrated with 50 mM Tris-HCl pH 8. 100 µl streptavidin sepharose high performance (Sigma-Aldrich, St. louis, Mississippi, USA), equilibrated with 50 mM Tris-HCl pH 8 and 1 tablet inhibitor cocktail mix (cOmplete™, EDTA-free Protease Inhibitor Cocktail ,Roche, Basel, Switzerland) was mixed with the sample and incubated for 1h at room temperature rotating. Samples were centrifuged for 3 min at $1400 \times g$ and the supernatant was discarded. Sepharose beads were gently re-suspended in 1 ml 50 mM Tris-HCl pH 8 in a new tube. The sepharose beads were washed two times with 1% SDS and two times with 6 M Urea. Beads were once washed with 1ml 50 mM Tris-HCl pH 8 containing 0.1% Tween20 and once with $H_2O_{bid.}$. Beads were stored at -20°C until further analysis. Control samples were taken after each step. To confirm the pulldown assay an immunoblot with control samples was performed using streptavidin-HRP antibody (1 µg/ml) (Sigma-Aldrich, St. louis, Mississippi, USA). The immunoblot was developed using SuperSignal™ West Pico Chemiluminescent Substrate (Thermo Fischer scientific, Waltham, Massachusetts, USA).

4.2.4.6 Sample preparation for LC/MS/MS

Samples for LC-MS from proteins labelled with DCG-04 and enriched on streptavidin beads were either prepared by gel electrophoresis and subsequent in-gel digestion (IGD) or the captured proteins were directly digested on the beads (OBD). To identify and cut out gel regions containing DCG-04 targets we employed the "blind-cut"-method (van der Linde et al., 2012a). In-gel digestion (IGD) with trypsin was performed by following a published protocol (Kaschani et al., 2009). Affinity enriched protein samples that were not eluted from the capture resin were on-bead digested (OBD). Briefly, streptavidin beads were washed twice with water to remove SDS. Then bound proteins were reduced with DTT (5 mM) in 50 mM ammonium bicarbonate (ABC) for 30 min at room temperature. Protein reduction was followed by alkylation with iodoacetamide (IAM, 10 mM also in 50 mM ABC, 30 min, room temperature) and quenching of excess IAM with DTT (final concentration DTT 10 mM). Reduction and alkylation was followed by a sequential digestion of proteins with first LysC for 3 h at 37°C followed by a 16 h digestion with trypsin (37°C). The digestion was stopped by adding formic acid (FA) to a final concentration of 0.5%. The supernatant containing the digestion products was passed through home-made glass microfibre StageTips (GE Healthcare; pore-size: 1.2 µM; thickness: 0.26 mm). Cleared tryptic digests were desalted on home-made C18 StageTips as described (Rappsilber et al., 2007). Peptides were passed over a 2 disc StageTip. After elution from the StageTips, samples were dried using a vacuum concentrator (Eppendorf, Hamburg, Germany) and the peptides were taken up in 0.1% formic acid solution (10 µL).

4.2.4.7 LC/MS/MS

Experiments were performed on an Orbitrap Elite instrument (Thermo Fischer scientific, Waltham, Massachusetts, USA, (Michalski et al., 2012)) that was coupled to an EASY-nLC 1000 liquid chromatography (LC) system (Thermo Fischer scientific, Waltham, Massachusetts, USA). The LC was operated in the one-column mode. The analytical column was a fused silica capillary (inner diameter 75 µm × 35 cm) with an integrated PicoFrit emitter (New Objective, Woburn, USA) packed in-house with Reprosil-Pur 120 C18-AQ 1.9 µm. The analytical column was encased by a column oven (Sonation, Biberach an der Riß, Germany) and attached to a nanospray flex ion source (Thermo Fischer scientific, Waltham, Massachusetts, USA). The column oven temperature was adjusted to 45°C during data acquisition. The LC was equipped with two mobile phases: solvent A (0.1% formic acid, FA, in water) and solvent B (0.1% FA in acetonitrile, ACN). All solvents were of UHPLC (ultra-high performance liquid chromatography) grade (Sigma-Aldrich, St. louis, Mississippi, USA). Peptides were directly loaded onto the analytical column with a maximum flow rate that would not exceed the set pressure limit of 980 bar (usually around 0.5 – 0.8 µL/min). Peptides were subsequently separated on the analytical column by running a 40 min (ISD) or 140 min (OBD) gradient of solvent A and solvent B (start with 7% B; gradient 7% to 35% B for 30 min (ISD) or 120 min (OBD); gradient 35% to 100% B for 5 min (ISD) or 10 min (OBD) and 100% B for 5 min (ISD) or 10 min (OBD)) at

a flow rate of 300 nl/min. The mass spectrometer was operated using Xcalibur software (version 2.2 SP1.48). The mass spectrometer was set in the positive ion mode. Precursor ion scanning was performed in the Orbitrap analyzer (FTMS; Fourier Transform Mass Spectrometry) in the scan range of m/z 300-1800 and at a resolution of 60000 with the internal lock mass option turned on (lock mass was 445.120025 m/z, polysiloxane) (Olsen et al., 2005). Product ion spectra were recorded in a data dependent fashion in the ion trap (ITMS; Ion Trap Mass Spectrometry) in a variable scan range and at a rapid scan rate. The ionization potential (spray voltage) was set to 1.8 kV. Peptides were analyzed using a repeating cycle consisting of a full precursor ion scan (1.0×10^6 ions or 200 ms (IGD) and 3.0×10^6 ions or 50 ms) followed by 10 product ion scans (3.0×10^4 ions or 150 ms (IGD) and 1.0×10^4 ions or 50 ms (OBD)) where peptides are isolated based on their intensity in the full survey scan (threshold of 500 counts) for tandem mass spectrum (MS2) generation that permits peptide sequencing and identification. CID (collision-induced dissociation) collision energy was set to 35% for the generation of MS2 spectra. During MS2 data acquisition dynamic ion exclusion was set to 120 seconds with a maximum list of excluded ions consisting of 500 members and a repeat count of one. Ion injection time prediction, preview mode for the FTMS, monoisotopic precursor selection and charge state screening were enabled. Only charge states higher than 1 were considered for fragmentation.

4.2.4.8 Peptide and Protein Identification using MaxQuant

RAW spectra were submitted to an Andromeda (Cox et al., 2011) search in MaxQuant (version 1.5.3.30) using the default settings (Cox and Mann, 2008). Label-free quantification and match-between-runs was activated (Cox et al., 2014). MS/MS spectra data were searched against the Uniprot *Zea mays* cv B73 database UP000007305_ 4577.fasta (99369 entries, downloaded 6/4/2018) and the in-house ACE_ 0229_ EGB apoplastic PLCPs AS.fasta database containing Sequences of interest from *Zea mays* cv Early Golden Bantam (7 entries). All searches included a contaminants database (as implemented in MaxQuant, 245 sequences). The contaminants database contains known MS contaminants and was included to estimate the level of contamination. Enzyme specificity was set to "Trypsin/P". The instrument type in Andromeda searches was set to Orbitrap and the precursor mass tolerance was set to ±20 ppm (first search) and ±4.5 ppm (main search). The MS/MS match tolerance was set to ±0.5 Da. The peptide spectrum matches FDR and the protein FDR were set to 0.01 (based on target-decoy approach and decoy mode "revert"). Minimum peptide length was 7 amino acids. Label-free protein quantification was switched on, and unique and razor peptides were considered for quantification with a minimum ratio count of 2. Retention times were recalibrated based on the built-in nonlinear time-rescaling algorithm. MS/MS identifications were transferred between LC-MS/MS runs with the "Match between runs" option in which the maximal match time window was set to 0.7 min and the alignment time window set to 20 min. The quantification is based on the "value at maximum" of the extracted ion current. Modified peptides were allowed for quantification. The minimum score for modified peptides was 40. Further analysis

and filtering of the results was done in Perseus v1.5.5.3. (Tyanova et al., 2016). The mass spectrometry proteomics data have been deposited to the ProteomeXchange Consortium via the PRIDE (Vizcaino et al., 2016) partner repository (https://www.ebi.ac.uk/pride/archive/) with the dataset identifier PXD013124.

4.2.4.9 Substrate cleavage assay using fluorogenic substrates

Root apoplastic fluids as well as apoplstic fluids containing overexpressed PLCPs were tested for its activity using the following substrates: Z-FR-AMC, BZ-FVR-AMC, Z-LR-AMC, Z-RR-AMC (Sigma-Aldrich, St. louis, Mississippi, USA). For sample measurement 10 µl of apoplastic fluids were mixed with reaction buffer (10 mM sodium phosphate pH 6, 150 mM sodium chloride, 1 mM EDTA and 0.5 mM DTT) and 10 µM substrate. Samples were incubated for 5 min at RT prior to start of the measurement. AMC-release was measured over time for 20 min (Excitation: 350 nm, Emission: 460 nm) using a Tecan Infinite 200 Pro plate reader (Tecan Group Ltd., Männendorf, Switzerland). As a control for PLCP activity 2 µM E-64 (Sigma-Aldrich, St. louis, Mississippi, USA) was added to normalize values. cMIP was obtained as synthetic peptide from GenScript (New Jersey, USA) and diluted in $H_2O_{bid.}$ to the needed concentration. Inhibitors and microbial culture supernatants were used as described in the results section and added to the indicated concentrations in the experiments ranging from 15 pM to 128 µM. Relative PLCP activity was calculated to the measured activity without addition of inhibitors. For tests of pH-dependent cleavage activity the substrate Z-LR-AMC was used in various buffers described in 4.30.

Table 4.30: **Various buffers for substrate cleavage assays in $H_2O_{bid.}$ (50 ml final volume).**

pH	Components [M]	Volume [ml]
3	0.1 Glycine	25
	0.1 HCl	5.7
4	0.1 AcOH	20.5
	0.1 NaOAC	4.5
5	0.1 ACOH	7.4
	0.1 NaOAC	17.6
6	0.1 Na_2HPO_4	50
7	0.1 NaH_2PO_4	9.75
	0.1 Na_2HPO_4	15.25
8	0.1 Tris-HCl	50

Table 4.30: **Various buffers for substrate cleavage assays in H$_2$O$_{bid.}$ (50 ml final volume).**

pH	Components [M]	Volume [ml]
9	0.1 Glycine	12.5
	0.1 NaOH	2.2
10	0.1 Glycine	12.5
	0.1 NaOH	8

4.2.4.10 SDS-PAGE for protein separation

Sodium dodecyl sulfate polyacrylamide gel electrophoresis (SDS-PAGE) was used for separation of denatured and negatively charged proteins based on their molecular weight. SDS gels consist of two parts. The upper part stacking gel (4.31) and the lower resolving gel (4.32). Due to the discontinuous gel composition the proteins accumulate size-independent at the end of the stacking gel. Due to the higher pH and higher polyacrylamide concentration the proteins can be separated by their size where smaller proteins are less retarded in the polyacrylamide matrix than bigger proteins. Prior to loading, the samples were boiled at 96°C for 5 min in 1 × SDS gel loading dye containing 100 mM DTT (4.33) and spun down afterwards. The gel was placed in the chamber (Invitrogen, Carlsbad, California, USA), which was then filled with SDS running buffer (4.34). The protein samples as well as 5 μl of protein ladder (Thermo Fischer scientific, Waltham, Massachusetts, USA) were loaded into the SDS gel wells. Proteins were separated based on their molecular weight by application of a constant electric field of 200 V for approximately 60 min. The SDS gel was further used for protein staining (4.2.4.11) or immunoblot (4.2.4.15).

Table 4.31: **SDS stacking gel composition.**

Components	Amount
Polyacrylamide	6% (v/v)
Tris-HCl pH 6.8	125 mM
SDS	0.1% (w/v)
$Ammonium per sulfate$(APS)	0.1% (w/v)
$Tetramethylethylenediamine$(TEMED)	0.1% (v/v)

Table 4.32: **SDS resolving gel composition.**

Components	Amount
Polyacrylamide	12 - 15% (v/v)
Tris-HCl pH 6.8	375 mM
SDS	0.1% (w/v)
APS	0.1% (w/v)
TEMED	0.04% (v/v)

Table 4.33: **Protein gel loading dye.**

Components	Amount
Tris-HCl pH 6.8	4 M
SDS	6% (w/v)
Bromophenol blue	0.15% (w/v)
Glycerol	60% (v/v)

Table 4.34: **SDS gel running buffer.**

Components	Amount
Tris-HCl ph 8.3	25 mM
Glycine	192 mM
SDS	4 mM

4.2.4.11 Coomassie brilliant blue staining

Gel or membrane containing sample proteins was stained with coomassie brilliant blue staining solution (4.35) for 3 to 4 h at RT. Destain was performed with coomassie brilliant blue destain solution (4.36) until the desired stain is reached. The destain solution should be changed several times during washing.

Table 4.35: **Coomassie brilliant blue staining solution in H$_2$O$_{bid.}$.**

Components	Final concentration
H$_2$O$_{bid.}$	40% (v/v)
$Methanol$(MeOH)	45% (v/v)
Acetic acid	10% (v/v)
Coomassie blue R350	0.1% (w/v)

Table 4.36: **Coomassie brilliant blue destaining solution in H$_2$O$_{bid.}$.**

Components	Final concentration
H$_2$O$_{bid.}$	40% (v/v)
MeOH	45% (v/v)
Acetic acid	10% (v/v)

4.2.4.12 Instant-blue staining

Instant blue reagent™(Expedeon, San Diego, California, USA) was added to the membrane or gel for staining. Proteins should be stained after 15 min. Samples can be destained with H$_2$O$_{bid.}$ to remove background signals until desired stain is reached. H$_2$O$_{bid.}$ should be changed several times during washing.

4.2.4.13 SyproRuby staining

The protein gel was placed in fix solution (4.37) for 30 min. Fix solution was discarded and SYPRO®Ruby solution was added. Samples were incubated shaking O/N. SYPRO®Ruby solution was discarded and the gel washed by addition of wash solution (4.38) for 15 min while shaking. The wash step was repeated one additional time. Prior to imaging, the gel was rinsed with H$_2$O$_{bid.}$ to prevent corrosive damage to the imager. Imaging was performed at Ex. 450 nM and Em. 610 nM.

Table 4.37: **SyproRuby fix solution in H$_2$O$_{bid.}$.**

Components	Final concentration
MeOH	50% (v/v)
Acetic acid	7% (v/v)

Table 4.38: **SyproRuby wash solution in H$_2$O$_{bid.}$.**

Components	Final concentration
MeOH	10% (v/v)
Acetic acid	7% (v/v)

4.2.4.14 Ponceau S

The membrane containing the protein of interest was covered with Ponseau S stain (4.39) and kept on an orbital shaker for 5 min. Samples can be destained with H$_2$O$_{bid.}$ to remove background signals until desired stain is reached. H$_2$O$_{bid.}$ should be changed several times during washing.

Table 4.39: **Ponceau S staining solution in H$_2$O$_{bid.}$.**

Components	Final concentration
Ponceau S	0.1% (w/v)
Acetic acid	20% (v/v)

4.2.4.15 Immunoblot and detection of proteins via chemiluminescence

SDS-PAGE separated protein gels were blotted to a PVDF and desired tagged proteins were detected by immunostaining using specific antibodies. Prior to blotting, the PVDF membrane (Amersham Hybond P 0.45 PVDF blotting membrane, GE Healthcare, Chicago, USA) was activated by addition of pure MeOH and Whatman paper (Whatman, Maidstone, United Kingdom) were soaked in transfer buffer (4.40). The SDS protein gel was taken from the running chamber and washed with H$_2$O$_{bid.}$ and transfer buffer to remove remaining SDS-running buffer (4.34). The blot was build from bottom to top as follows: Whatman paper, activated PVDF-membrane, SDS-gel, Whatman paper. To guarantee a good quality protein transfer, air bubbles between the layers were removed. The blot was transferred to a Trans-Blot Turbo Transfer system (Bio-rad, Hercules, California, USA) and proteins were transferred by adding a constant voltage of 25 V and 1 Ampere (A) for 25 - 30 min depending on the size of the desired protein. After blotting the membrane was slewed in methanol to fix the transferred protein. Thereafter the membrane was incubated with blocking solution (4% Bovine serum albumin in 4.41) for 1 h at RT or O/N at 4°C. Antibodies were diluted in blocking solution according to manufacturer instructions. The primary antibody which is specific for the tag of the desired protein was added either for 1 h at RT or O/N at 4°C. Excessive and unspecific bound primary antibody were removed by three wash steps including 5 min incubation with TBS-Tween buffer (4.41). Afterwards the membrane was incubated for 1 h at RT with the secondary antibody which is specific to the primary antibody. To remove excessive and unspecific bound secondary antibody the membrane was washed again for three times with 4.41 as described before. Desired tagged proteins were visualised by addition of the ECL reagent (SuperSignal® Pico Chemilumines-

cent Substrate, Thermo Fischer scientific, Waltham, Massachusetts, USA) to the membrane, which was placed in a hermetic plastic bag. The ECL substrate is processed by the HRP bound to the secondary antibody, releasing a chemiluminescent signal (475 nm) which was documented using a ChemiDoc™MP (Bio-Rad, Hercules, California, USA).

Table 4.40: **Transfer buffer in $H_2O_{bid.}$.**

Components	Final concentration
Glycin	39 mM
Tris-base	48 mM
SDS	0.0375%
MeOH	20%

Table 4.41: **TBS-T in $H_2O_{bid.}$, pH 7.5.**

Components	Final concentration [M]
Tris-base	0.5
NaCl	1.5
Tween-20	0.1% (v/v)

4.2.4.16 Protein quantification after Bradford

Quantification of protein amount was performed according to Bradford (1976) using Roti®-Quant solution (Carl Roth GmbH & Co. KG, Karlsruhe, Germany) performing the protein assay in 96-well culture plates as indicated by the manufacturer.

4.2.4.17 Heat-denaturation of protein content

Protein content in culture supernatants from 4.2.2.6 was denatured by incubation for 15 min at 95°C prior to use in substrate cleavage assays (4.2.4.9).

4.2.4.18 Supernatant fractionation

Culture supernatant obtained from 4.2.2.6 were separated into high molecular weight (HMW) and low molecular weight (LMW) fractions using vivaspin-500 (Sartorius, Göttingen, Germany) according to the manufacturers instructions.

4.2.5 Computational methods and statistical analysis

Heat-maps were performed using the heatmap.2 function of the package gplots (version 3.0.1) in r-studio (R version 3.5.1). Venn diagram was created using the draw.pairwise.venn function of the

package Venn diagram (version 1.6.0) in r-studio (R version 3.5.1.). For generation of a phylogenetic tree 52 maize PLCP sequences of the line B73 retrieved from the MEROPS database (Rawlings et al., 2018) and our six identified PLCPs from Early golden Bantam (EGB) were used. Additionally, we included one type member of each PLCP subfamily of A. thaliana and two serine proteases DEGP2 and DGP11 from *A. thaliana* as outgroup (Beers et al., 2004; Richau et al., 2012). For generation of a phylogenetic tree of cystatins sequences were obtained for 13 maize cystatins from B73, twelve *O. sativa* cystatins and seven *A. thaliana* cystatins (Massonneau et al., 2005; M. Martinez et al., 2008; Manuel Martinez et al., 2009; van der Linde et al., 2012b). Following methods were applied for both phylogenetic trees. MAFFT (v7.407) (Katoh and Standley, 2013). RAxML with the GTRGAMMA substitution model (v8.2.0) was used for the construction of the tree (Stamatakis, 2014). The tree is drawn to scale, with branch lengths measured in the number of substitutions per site. The robustness was assessed using 100 bootstrap replicates. Inhibitor motif and homolog search in genomes of candidate bacteria was performed using Blast2go (BioBam, Valencia, Spain). Quantification of PLCP-signals after ABPP using rhodamine fluorescence signal strength was performed using ImageLabTM software (Bio-Rad, Hercules, California, USA). Phyre2 (Kelley et al., 2015) was used for modelling of PLCPs based on caricain PDB: 1pciA (Groves et al., 1996). For the inhibitor concentration range plots a non-linear fit based on the dose response function and calculation of IC50 was performed in Origin 2018 (OriginLab, Northampton, MA) and GraphPad Prism 6 (GraphPad Software, San Diego, USA).

5 Bibliography

Abad, **L. R.**, **D'Urzo**, **M. P.**, **Liu**, **D.**, **Narasimhan**, **M. L.**, **Reuveni**, **M.**, **Zhu**, **J. K.**, **Niu**, **X.**, **Singh**, **N. K.**, **Hasegawa**, **P. M.**, & **Bressan**, **R. A.** (1996). Antifungal activity of tobacco osmotin has specificity and involves plasma membrane permeabilization. *Plant Science*, *118*(1), 11–23. doi:https://doi.org/10.1016/0168-9452(96)04420-2

Adamczyk, **B.**, **Smolander**, **A.**, **Kitunen**, **V.**, & **Godlewski**, **M.** (2010). Proteins as nitrogen source for plants: A short story about exudation of proteases by plant roots. *Plant signaling & behavior*, *5*(7), 817–819.

Albrecht, **C.**, **Boutrot**, **F.**, **Segonzac**, **C.**, **Schwessinger**, **B.**, **Gimenez-Ibanez**, **S.**, **Chinchilla**, **D.**, **Rathjen**, **J. P.**, **de Vries**, **S. C.**, & **Zipfel**, **C.** (2012). Brassinosteroids inhibit pathogen-associated molecular pattern–triggered immune signaling independent of the receptor kinase bak1. *Proceedings of the National Academy of Sciences*, *109*(1), 303–308.

Aleklett, **K.**, **Hart**, **M.**, & **Shade**, **A.** (2014). The microbial ecology of flowers: An emerging frontier in phyllosphere research. *Botany*, *92*(4), 253–266.

Ali, **A.**, **Shah**, **L.**, **Rahman**, **S.**, **Riaz**, **M. W.**, **Yahya**, **M.**, **Xu**, **Y. J.**, **Liu**, **F.**, **Si**, **W.**, **Jiang**, **H.**, & **Cheng**, **B.** (2018). Plant defense mechanism and current understanding of salicylic acid and nprs in activating sar. *Physiological and Molecular Plant Pathology*, *104*, 15–22. doi:https://doi.org/10.1016/j.pmpp.2018.08.001

Ali, **M. R. M.**, **Uemura**, **T.**, **Ramadan**, **A.**, **Adachi**, **K.**, **Nemoto**, **K.**, **Nozawa**, **A.**, **Hoshino**, **R.**, **Abe**, **H.**, **Sawasaki**, **T.**, & **Arimura**, **G.-i.** (2019). The ring-type e3 ubiquitin ligase jul1 targets the vq-motif protein jav1 to coordinate jasmonate signaling. *Plant Physiology*, *179*(4), 1273. doi:10.1104/pp.18.00715

Almagro Armenteros, **J. J.**, **Tsirigos**, **K. D.**, **Sønderby**, **C. K.**, **Petersen**, **T. N.**, **Winther**, **O.**, **Brunak**, **S.**, **von Heijne**, **G.**, & **Nielsen**, **H.** (2019). Signalp 5.0 improves signal peptide predictions using deep neural networks. *Nature Biotechnology*, *37*(4), 420–423. doi:10.1038/s41587-019-0036-z

Alonso, **J. M.**, **Stepanova**, **A. N.**, **Leisse**, **T. J.**, **Kim**, **C. J.**, **Chen**, **H.**, **Shinn**, **P.**, **Stevenson**, **D. K.**, **Zimmerman**, **J.**, **Barajas**, **P.**, **Cheuk**, **R.**, **Gadrinab**, **C.**, **Heller**, **C.**, **Jeske**, **A.**, **Koesema**, **E.**, **Meyers**, **C. C.**, **Parker**, **H.**, **Prednis**, **L.**, **Ansari**, **Y.**, **Choy**, **N.**, **Deen**, **H.**, **Geralt**, **M.**, **Hazari**, **N.**, **Hom**, **E.**, **Karnes**, **M.**, **Mulholland**, **C.**, **Ndubaku**, **R.**, **Schmidt**, **I.**, **Guzman**, **P.**, **Aguilar-Henonin**, **L.**, **Schmid**, **M.**, **Weigel**, **D.**, **Carter**, **D. E.**, **Marchand**, **T.**, **Risseeuw**, **E.**, **Brogden**, **D.**, **Zeko**, **A.**, **Crosby**, **W. L.**, **Berry**, **C. C.**, & **Ecker**, **J. R.** (2003). Genome-wide insertional mutagenesis of arabidopsis thaliana. *Science*, *301*(5633), 653–657. doi:10.1126/science.1086391. eprint: https://science.sciencemag.org/content/301/5633/653.full.pdf

Alvarez, **A.**, **Saez**, **J. M.**, **Davila Costa**, **J. S.**, **Colin**, **V. L.**, **Fuentes**, **M. S.**, **Cuozzo**, **S. A.**, **Benimeli**, **C. S.**, **Polti**, **M. A.**, & **Amoroso**, **M. J.** (2017). Actinobacteria: Current research and perspectives for bioremediation of pesticides and heavy metals. *Chemosphere*, *166*, 41–62. doi:https://doi.org/10.1016/j.chemosphere.2016.09.070

Andorf, **C. M.** [Carson M.], **Cannon**, **E. K.**, **Portwood**, **2.**, **John L.**, **Gardiner**, **J. M.**, **Harper**, **L. C.**, **Schaeffer**, **M. L.**, **Braun**, **B. L.**, **Campbell**, **D. A.**, **Vinnakota**, **A. G.**, **Sribalusu**, **V. V.**, **Huerta**, **M.**, **Cho**, **K. T.**, **Wimalanathan**, **K.**, **Richter**, **J. D.**, **Mauch**, **E. D.**, **Rao**, **B. S.**, **Birkett**, **S. M.**, **Sen**, **T. Z.**, & **Lawrence-Dill**, **C. J.** (2016). Maizegdb update: New tools, data and interface for the maize model organism database. *Nucleic acids research*, *44*(D1), D1195–D1201. doi:10.1093/nar/gkv1007

Andorf, **C. M.** [Carson M], **Cannon**, **E. K.**, **Portwood**, **J. L.**, **Gardiner**, **J. M.**, **Harper**, **L. C.**, **Schaeffer**, **M. L.**, **Braun**, **B. L.**, **Campbell**, **D. A.**, **Vinnakota**, **A. G.**, & **Sribalusu**, **V. V.** (2015). Maizegdb update: New tools, data and interface for the maize model organism database. *Nucleic acids research*, *44*(D1), D1195–D1201.

Andrews, **J. H.**, & **Harris**, **R. F.** (2000). The ecology and biogeography of microorganisms on plant surfaces. *Annual review of phytopathology*, *38*(1), 145–180.

Arunachalam Palaniyandi, **S.**, **Yang**, **S. H.**, **Damodharan**, **K.**, & **Suh**, **J.-W.** (2013). Genetic and functional characterization of culturable plant-beneficial actinobacteria associated with yam rhizosphere. *Journal of Basic Microbiology*, *53*(12), 985–995. doi:10.1002/jobm.201200531

Asp, **T.**, **Bowra**, **S.**, **Borg**, **S.**, & **Holm**, **P. B.** (2004). Molecular cloning, functional expression in escherichia coli and enzymatic characterisation of a cysteine protease from white clover (trifolium repens). *Biochimica et Biophysica Acta (BBA) - Proteins and Proteomics*, *1699*(1), 111–122. doi:https://doi.org/10.1016/j.bbapap.2004.02.002

Athman, **S. Y.**, **Dubois**, **T.**, **Coyne**, **D.**, **Gold**, **C. S.**, **Labuschagne**, **N.**, & **Viljoen**, **A.** (2006). Effect of endophytic fusarium oxysporum on host preference of radopholus similis to tissue culture banana plants. *Journal of nematology*, *38*(4), 455.

Azarkan, **M.**, **Dibiani**, **R.**, **Baulard**, **C.**, & **Baeyens-Volant**, **D.** (2006). Effects of mechanical wounding on carica papaya cysteine endopeptidases accumulation and activity. *Int J Biol Macromol*, *38*(3-5), 216–24. doi:10.1016/j.ijbiomac.2006.02.021

Badri, **D. V.**, & **Vivanco**, **J. M.** (2009). Regulation and function of root exudates. *Plant, Cell & Environment*, *32*(6), 666–681. doi:10.1111/j.1365-3040.2009.01926.x

Bai, **Y.**, **Müller**, **D. B.**, **Srinivas**, **G.**, **Garrido-Oter**, **R.**, **Potthoff**, **E.**, **Rott**, **M.**, **Dombrowski**, **N.**, **Münch**, **P. C.**, **Spaepen**, **S.**, **Remus-Emsermann**, **M.**, **Hüttel**, **B.**, **McHardy**, **A. C.**, **Vorholt**, **J. A.**, & **Schulze-Lefert**, **P.** (2015). Functional overlap of the arabidopsis leaf and root microbiota. *Nature*, *528*, 364. doi:10.1038/nature16192

Bais, **H. P.**, **Weir**, **T. L.**, **Perry**, **L. G.**, **Gilroy**, **S.**, & **Vivanco**, **J. M.** (2006). The role of root exudates in rhizosphere interactions with plants and other organisms. *Annual Review of Plant Biology*, *57*(1), 233–266. doi:10.1146/annurev.arplant.57.032905.105159

Bar-Ziv, **A.**, **Levy**, **Y.**, **Citovsky**, **V.**, & **Gafni**, **Y.** (2015). The tomato yellow leaf curl virus (tylcv) v2 protein inhibits enzymatic activity of the host papain-like cysteine protease cyp1. *Biochemical and Biophysical Research Communications*, *460*(3), 525–529. doi:https://doi.org/10.1016/j.bbrc.2015.03.063

Barret, **M.**, **Briand**, **M.**, **Bonneau**, **S.**, **Préveaux**, **A.**, **Valière**, **S.**, **Bouchez**, **O.**, **Hunault**, **G.**, **Simoneau**, **P.**, & **Jacques**, **M.-A.** (2015). Emergence shapes the structure of the seed microbiota. *Appl. Environ. Microbiol.*, *81*(4), 1257–1266.

Barrett, **A. J.**, **Kembhavi**, **A. A.**, **Brown**, **M. A.**, **Kirschke**, **H.**, **Knight**, **C. G.**, **Tamai**, **M.**, & **Hanada**, **K.** (1982). L-trans-epoxysuccinyl-leucylamido(4-guanidino)butane (e-64) and its analogues as inhibitors of cysteine proteinases including cathepsins b, h and l. *Biochem J*, *201*(1), 189–198. Retrieved from http://www.ncbi.nlm.nih.gov/entrez/query.fcgi?cmd=Retrieve&db=PubMed&dopt=Citation&list_uids=7044372

Barrett, **A. J.**, **Kembhavi**, **A. A.**, & **Hanada**, **K.** (1981). E-64 [l-trans-epoxysuccinyl-leucyl-amido(4-guanidino)butane] and related epoxides as inhibitors of cysteine proteinases. *Acta Biol Med Ger*, *40*(10-11), 1513–1517. Retrieved from http://www.ncbi.nlm.nih.gov/entrez/query.fcgi?cmd=Retrieve&db=PubMed&dopt=Citation&list_uids=7044005

Bárzana, **G.**, **Aroca**, **R.**, **Bienert**, **G. P.**, **Chaumont**, **F.**, & **Ruiz-Lozano**, **J. M.** (2014). New insights into the regulation of aquaporins by the arbuscular mycorrhizal symbiosis in maize plants under drought stress and possible implications for plant performance. *Molecular Plant-Microbe Interactions*, *27*(4), 349–363.

Batas, **B.**, **Jones**, **H. R.**, & **Chaudhuri**, **J. B.** (1997). Studies of the hydrodynamic volume changes that occur during refolding of lysozyme using size-exclusion chromatography. *Journal of Chromatography A*, *766*(1), 109–119. doi:https://doi.org/10.1016/S0021-9673(96)01020-5

Bateman, **A.** [A.], & **Bennett**, **H. P.** [H. P.]. (1998). Granulins: The structure and function of an emerging family of growth factors. *Journal of endocrinology*, *158*(2), 145–151. Retrieved from http://www.ncbi.nlm.nih.gov/entrez/query.fcgi?cmd=Retrieve&db=PubMed&dopt=Citation&list_uids=9771457%20http://joe.endocrinology-journals.org/content/158/2/145.full.pdf

Bateman, **A.** [Andrew], & **Bennett**, **H. P.** [Hugh PJ]. (2009). The granulin gene family: From cancer to dementia. *Bioessays*, *31*(11), 1245–1254.

Bauer, **W. D.**, & **Caetano-Anollés**, **G.** (1990). Chemotaxis, induced gene expression and competitiveness in the rhizosphere. *Plant and Soil*, *129*(1), 45–52. doi:10.1007/BF00011690

Beers, **E. P.**, **Jones**, **A. M.**, & **Dickerman**, **A. W.** (2004). The s8 serine, c1a cysteine and a1 aspartic protease families in arabidopsis. *Phytochemistry*, *65*(1), 43–58.

Belenghi, **B.**, **Acconcia**, **F.**, **Trovato**, **M.**, **Perazzolli**, **M.**, **Bocedi**, **A.**, **Polticelli**, **F.**, **Ascenzi**, **P.**, & **Delledonne**, **M.** (2003). Atcys1, a cystatin from arabidopsis thaliana, suppresses hypersensitive cell death. *Eur J Biochem*, *270*(12), 2593–2604. doi:10.1046/j.1432-1033.2003.03630.x

Bendtsen, **J. D.**, **Kiemer**, **L.**, **Fausbøll**, **A.**, & **Brunak**, **S.** (2005). Non-classical protein secretion in bacteria. *BMC Microbiology*, *5*(1), 58. doi:10.1186/1471-2180-5-58

Berdowska, **I.**, & **Siewiński**, **M.** (2000). Rola katepsyn cysteinowych oraz ich inhibitorow w procesach fizjologicznych i nowotworowych. *Postępy Biochemii*, *46*(1), 73–84.

Berendsen, **R. L.**, **Pieterse**, **C. M. J.**, & **Bakker**, **P. A. H. M.** (2012). The rhizosphere microbiome and plant health. *Trends in Plant Science*, *17*(8), 478–486. doi:https://doi.org/10.1016/j.tplants.2012.04.001

Berg, **G.**, **Grube**, **M.**, **Schloter**, **M.**, & **Smalla**, **K.** (2014). Unraveling the plant microbiome: Looking back and future perspectives. *Frontiers in microbiology*, *5*, 148.

Berg, **M.**, & **Koskella**, **B.** (2018). Nutrient-and dose-dependent microbiome-mediated protection against a plant pathogen. *Current Biology*, *28*(15), 2487–2492. e3.

Bernoux, **M.**, **Moncuquet**, **P.**, **Kroj**, **T.**, & **Dodds**, **P. N.** (2014). A novel conserved mechanism for plant nlr protein pairs: The 'integrated decoy'hypothesis. *Frontiers in plant science*, *5*, 606.

Bernoux, **M.**, **Timmers**, **T.**, **Jauneau**, **A.**, **Brière**, **C.**, **de Wit**, **P. J.**, **Marco**, **Y.**, & **Deslandes**, **L.** (2008). Rd19, an arabidopsis cysteine protease required for rrs1-r-mediated resistance, is re-localized to the nucleus by the ralstonia solanacearum popp2 effector. *Plant Cell*, *20*(8), 2252–2264. doi:10.1105/tpc.108.058685

Bode, **W.** [Wolfram], & **Huber**, **R.** (2000). Structural basis of the endoproteinase–protein inhibitor interaction11dedicated to prof. dr. hans neurath on the occasion of his 90th birthday. *Biochimica et Biophysica Acta (BBA) - Protein Structure and Molecular Enzymology*, *1477*(1), 241–252. doi:https://doi.org/10.1016/S0167-4838(99)00276-9

Boller, **T.** [Thomas], & **Felix**, **G.** (2009). A renaissance of elicitors: Perception of microbe-associated molecular patterns and danger signals by pattern-recognition receptors. *Annual Rev Plant Biol*, *60*(1), 379–406. doi:10.1146/annurev.arplant.57.032905.105346

Boller, **T.** [Thomas], & **He**, **S. Y.** (2009). Innate immunity in plants: An arms race between pattern recognition receptors in plants and effectors in microbial pathogens. *Science*, *324*(5928), 742–744.

Bolton, **M. D.**, & **Thomma**, **B. P.** (2008). The complexity of nitrogen metabolism and nitrogen-regulated gene expression in plant pathogenic fungi. *Physiological and Molecular Plant Pathology*, *72*(4-6), 104–110.

Bonito, **G.**, **Reynolds**, **H.**, **Robeson Ii**, **M. S.**, **Nelson**, **J.**, **Hodkinson**, **B. P.**, **Tuskan**, **G.**, **Schadt**, **C. W.**, & **Vilgalys**, **R.** (2014). Plant host and soil origin influence fungal and bacterial assemblages in the roots of woody plants. *Molecular Ecology*, *23*(13), 3356–3370. doi:10.1111/mec.12821

Bordenstein, **S. R.**, & **Theis**, **K. R.** (2015). Host biology in light of the microbiome: Ten principles of holobionts and hologenomes. *PLoS biology*, *13*(8), e1002226.

Bozkurt, **T. O.**, **Schornack**, **S.**, **Win**, **J.**, **Shindo**, **T.**, **Ilyas**, **M.**, **Oliva**, **R.**, **Cano**, **L. M.**, **Jones**, **A. M. E.**, **Huitema**, **E.**, **van der Hoorn**, **R. A. L.**, & **Kamoun**, **S.** (2011). Phytophthora infestans effector avrblb2 prevents secretion of a plant immune protease at the haustorial interface. *Proceedings of the National Academy of Sciences of the United States of America*, *108*(51), 20832–20837. doi:10.1073/pnas.1112708109

Brader, **G.**, **Compant**, **S.**, **Vescio**, **K.**, **Mitter**, **B.**, **Trognitz**, **F.**, **Ma**, **L.-J.**, & **Sessitsch**, **A.** (2017). Ecology and genomic insights into plant-pathogenic and plant-nonpathogenic endophytes. *Annual Review of Phytopathology*, *55*, 61–83.

Bradford, **M. M.** (1976). A rapid and sensitive method for the quantitation of microgram quantities of protein utilizing the principle of protein-dye binding. *Anal Biochem*, *72*, 248–254. doi:S0003269776699996

Brefort, **T.**, **Doehlemann**, **G.**, **Mendoza-Mendoza**, **A.**, **Reissmann**, **S.**, **Djamei**, **A.**, & **Kahmann**, **R.** (2009). Ustilago maydis as a pathogen. *Annu Rev Phytopathol*, *47*, 423–445. doi:10.1146/annurev-phyto-080508-081923

Bruto, **M.**, **Prigent-Combaret**, **C.**, **Muller**, **D.**, & **Moënne-Loccoz**, **Y.** (2014). Analysis of genes contributing to plant-beneficial functions in plant growth-promoting rhizobacteria and related proteobacteria. *Scientific Reports*, *4*, 6261. doi:10.1038/srep06261

Brutus, **A.**, **Sicilia**, **F.**, **Macone**, **A.**, **Cervone**, **F.**, & **De Lorenzo**, **G.** (2010). A domain swap approach reveals a role of the plant wall-associated kinase 1 (wak1) as a receptor of oligogalacturonides. *Proceedings of the National Academy of Sciences*, *107*(20), 9452–9457.

Bryan, **P. N.** (2002). Prodomains and protein folding catalysis. *Chemical reviews*, *102*(12), 4805–4816.

Bulgarelli, **D.**, **Rott**, **M.**, **Schlaeppi**, **K.**, **Ver Loren van Themaat**, **E.**, **Ahmadinejad**, **N.**, **Assenza**, **F.**, **Rauf**, **P.**, **Huettel**, **B.**, **Reinhardt**, **R.**, **Schmelzer**, **E.**, **Peplies**, **J.**, **Gloeckner**, **F. O.**, **Amann**, **R.**, **Eickhorst**, **T.**, & **Schulze-Lefert**, **P.** (2012). Revealing structure and assembly cues for arabidopsis root-inhabiting bacterial microbiota. *Nature*, *488*, 91. doi:10.1038/nature11336

Burns, **K. N.**, **Kluepfel**, **D. A.**, **Strauss**, **S. L.**, **Bokulich**, **N. A.**, **Cantu**, **D.**, & **Steenwerth**, **K. L.** (2015). Vineyard soil bacterial diversity and composition revealed by 16s rrna genes: Differentiation by geographic features. *Soil Biology and Biochemistry*, *91*, 232–247. doi:https://doi.org/10.1016/j.soilbio.2015.09.002

Cai, **Y. M.**, **Yu**, **J.**, **Ge**, **Y.**, **Mironov**, **A.**, & **Gallois**, **P.** (2018). Two proteases with caspase-3-like activity, cathepsin b and proteasome, antagonistically control er-stress-induced programmed cell death in arabidopsis. *New Phytol*, *218*(3), 1143–1155. doi:10.1111/nph.14676

Campisano, **A.**, **Antonielli**, **L.**, **Pancher**, **M.**, **Yousaf**, **S.**, **Pindo**, **M.**, & **Pertot**, **I.** (2014). Bacterial endophytic communities in the grapevine depend on pest management. *PLoS One*, *9*(11), e112763.

Cao, **H.**, **Glazebrook**, **J.**, **Clarke**, **J. D.**, **Volko**, **S.**, & **Dong**, **X.** (1997). The arabidopsis npr1 gene that controls systemic acquired resistance encodes a novel protein containing ankyrin repeats. *Cell*, *88*(1), 57–63.

Castano-Duque, **L.**, & **Luthe**, **D. S.** (2018). Protein networks reveal organ-specific defense strategies in maize in response to an aboveground herbivore. *Arthropod-Plant Interactions*, *12*(1), 147–175. doi:10.1007/s11829-017-9562-0

Cetintas, **R.**, **Kusek**, **M.**, & **Fateh**, **S. A.** (2018). Effect of some plant growth-promoting rhizobacteria strains on root-knot nematode, meloidogyne incognita, on tomatoes. *Egyptian Journal of Biological Pest Control*, *28*(1), 7. doi:10.1186/s41938-017-0008-x

Char, **S. N.**, **Neelakandan**, **A. K.**, **Nahampun**, **H.**, **Frame**, **B.**, **Main**, **M.**, **Spalding**, **M. H.**, **Becraft**, **P. W.**, **Meyers**, **B. C.**, **Walbot**, **V.**, & **Wang**, **K.** (2017). An agrobacterium-delivered crispr/cas9 system for high-frequency targeted mutagenesis in maize. *Plant biotechnology journal*, *15*(2), 257–268.

Chen, **Z.** [Zhi-Yuan], **Brown**, **R. L.**, **Damann**, **K. E.**, & **Cleveland**, **T. E.** (2010). Pr10 expression in maize and its effect on host resistance against aspergillus flavus infection and aflatoxin production. *Molecular plant pathology*, *11*(1), 69–81.

Chen, **Z.** [Zhixiang], **Silva**, **H.**, & **Klessig**, **D. F.** (1993). Active oxygen species in the induction of plant systemic acquired resistance by salicylic acid. *Science*, *262*(5141), 1883–1886.

Cheong, **Y. H.**, **Chang**, **H.-S.**, **Gupta**, **R.**, **Wang**, **X.**, **Zhu**, **T.**, & **Luan**, **S.** (2002). Transcriptional profiling reveals novel interactions between wounding, pathogen, abiotic stress, and hormonal responses in arabidopsis. *Plant physiology*, *129*(2), 661–677.

Cheuk, **A.**, & **Houde**, **M.** (2017). A rapid and efficient method for uniform gene expression using the barley stripe mosaic virus. *Plant methods*, *13*, 24–24. doi:10.1186/s13007-017-0175-5

Cheval, **C.**, **Aldon**, **D.**, **Galaud**, **J.-P.**, & **Ranty**, **B.** (2013). Calcium/calmodulin-mediated regulation of plant immunity. *Biochimica et Biophysica Acta (BBA)-Molecular Cell Research*, *1833*(7), 1766–1771.

Chisholm, **S. T.**, **Coaker**, **G.**, **Day**, **B.**, & **Staskawicz**, **B. J.** (2006). Host-microbe interactions: Shaping the evolution of the plant immune response. *Cell*, *124*(4), 803–14. doi:10.1016/j.cell.2006.02.008

Christensen, **J.** (1963). Corn smut caused by ustilago maydis. *Am Phytopathol Soc Monogr*, *2*, 1–41.

Clark, **K.**, **Franco**, **J. Y.**, **Schwizer**, **S.**, **Pang**, **Z.**, **Hawara**, **E.**, **Liebrand**, **T. W. H.**, **Pagliaccia**, **D.**, **Zeng**, **L.**, **Gurung**, **F. B.**, **Wang**, **P.**, **Shi**, **J.**, **Wang**, **Y.**, **Ancona**, **V.**, **van der Hoorn**, **R. A. L.**, **Wang**, **N.**, **Coaker**, **G.**, & **Ma**, **W.** (2018). An effector from the huanglongbing-associated pathogen targets citrus proteases. *Nature communications*, *9*(1), 1718–1718. doi:10.1038/s41467-018-04140-9

Cole, **J. L.**, **Lary**, **J. W.**, **P. Moody**, **T.**, & **Laue**, **T. M.** (2008). Analytical ultracentrifugation: Sedimentation velocity and sedimentation equilibrium. In *Methods in cell biology* (Vol. 84, pp. 143–179). doi:https://doi.org/10.1016/S0091-679X(07)84006-4

Coll, **N. S.**, **Epple**, **P.**, & **Dangl**, **J. L.** (2011). Programmed cell death in the plant immune system. *Cell Death Differ*, *18*(8), 1247–1256. doi:10.1038/cdd.2011.37

Compant, **S.**, **Clément**, **C.**, & **Sessitsch**, **A.** (2010). Plant growth-promoting bacteria in the rhizo- and endosphere of plants: Their role, colonization, mechanisms involved and prospects for utilization. *Soil Biology and Biochemistry*, *42*(5), 669–678.

Compant, **S.**, **Mitter**, **B.**, **Colli-Mull**, **J. G.**, **Gangl**, **H.**, & **Sessitsch**, **A.** (2011). Endophytes of grapevine flowers, berries, and seeds: Identification of cultivable bacteria, comparison with other plant parts, and visualization of niches of colonization. *Microbial ecology*, *62*(1), 188–197.

Compant, **S.**, **Reiter**, **B.**, **Sessitsch**, **A.**, **Nowak**, **J.**, **Clément**, **C.**, & **Ait Barka**, **E.** (2005). Endophytic colonization of vitis vinifera l. by plant growth-promoting bacterium burkholderia sp. strain psjn. *Applied and Environmental Microbiology*, *71*(4), 1685. doi:10.1128/AEM.71.4.1685-1693.2005

Compant, **S.**, **Samad**, **A.**, **Faist**, **H.**, & **Sessitsch**, **A.** (2019). A review on the plant microbiome: Ecology, functions, and emerging trends in microbial application. *Journal of Advanced Research*, *19*, 29–37. doi:https://doi.org/10.1016/j.jare.2019.03.004

Conrath, **U.**, **Beckers**, **G. J.**, **Langenbach**, **C. J.**, & **Jaskiewicz**, **M. R.** (2015). Priming for enhanced defense. *Annual review of phytopathology*, *53*.

Correa-Galeote, **D.**, **Bedmar**, **E. J.**, & **Arone**, **G. J.** (2018). Maize endophytic bacterial diversity as affected by soil cultivation history. *Frontiers in Microbiology*, *9*(484). doi:10.3389/fmicb.2018.00484

Coulombe, **R.**, **Grochulski**, **P.**, **Sivaraman**, **J.**, **Ménard**, **R.**, **Mort**, **J. S.**, & **Cygler**, **M.** (1996). Structure of human procathepsin l reveals the molecular basis of inhibition by the prosegment. *The EMBO Journal*, *15*(20), 5492–5503. doi:10.1002/j.1460-2075.1996.tb00934.x

Couto, **D.**, & **Zipfel**, **C.** [Cyril]. (2016). Regulation of pattern recognition receptor signalling in plants. *Nature Reviews Immunology*, *16*, 537. doi:10.1038/nri.2016.77

Cox, **J.**, **Hein**, **M. Y.**, **Luber**, **C. A.**, **Paron**, **I.**, **Nagaraj**, **N.**, & **Mann**, **M.** (2014). Accurate proteome-wide label-free quantification by delayed normalization and maximal peptide ratio extraction, termed maxlfq. *Molecular & Cellular Proteomics*, *13*(9), 2513. doi:10.1074/mcp.M113.031591

Cox, **J.**, & **Mann**, **M.** (2008). Maxquant enables high peptide identification rates, individualized p.p.b.-range mass accuracies and proteome-wide protein quantification. *Nature Biotechnology*, *26*(12), 1367–1372. doi:10.1038/nbt.1511

Cox, **J.**, **Neuhauser**, **N.**, **Michalski**, **A.**, **Scheltema**, **R. A.**, **Olsen**, **J. V.**, & **Mann**, **M.** (2011). Andromeda: A peptide search engine integrated into the maxquant environment. *Journal of Proteome Research*, *10*(4), 1794–1805. doi:10.1021/pr101065j

Cui, **H.**, **Tsuda**, **K.**, & **Parker**, **J. E.** (2015). Effector-triggered immunity: From pathogen perception to robust defense. *Annual review of plant biology*, *66*, 487–511.

D'Maris Amick Dempsey, **A. C.**, **Vlot**, **M. C. W.**, & **Daniel**, **F. K.** (2011). Salicylic acid biosynthesis and metabolism. *The Arabidopsis book/American Society of Plant Biologists*, *9*.

Dangl, **J. L.**, & **Jones**, **J. D.** (2001). Plant pathogens and integrated defence responses to infection. *Nature*, *411*(6839), 826–33. doi:10.1038/35081161

De Vrieze, **M.**, **Germanier**, **F.**, **Vuille**, **N.**, & **Weisskopf**, **L.** (2018). Combining different potato-associated pseudomonas strains for improved biocontrol of phytophthora infestans. *Frontiers in microbiology*, *9*, 2573.

de Wit, **P. J.** [Pierre JGM]. (2007). How plants recognize pathogens and defend themselves. *Cellular and Molecular Life Sciences*, *64*(21), 2726–2732.

Di, **X.**, **Gomila**, **J.**, **Ma**, **L.**, **van den Burg**, **H. A.**, & **Takken**, **F. L. W.** (2016). Uptake of the fusarium effector avr2 by tomato is not a cell autonomous event. *Frontiers in Plant Science*, *7*(1915). doi:10.3389/fpls.2016.01915

Ding, **Y.**, **Sun**, **T.**, **Ao**, **K.**, **Peng**, **Y.**, **Zhang**, **Y.**, **Li**, **X.**, & **Zhang**, **Y.** (2018). Opposite roles of salicylic acid receptors npr1 and npr3/npr4 in transcriptional regulation of plant immunity. *Cell*, *173*(6), 1454–1467. e15.

Dixon, **M. S.**, **Golstein**, **C.**, **Thomas**, **C. M.**, **Van der Biezen**, **E. A.**, & **Jones**, **J. D.** (2000). Genetic complexity of pathogen perception by plants: The example of rcr3, a tomato gene required specifically by cf-2. *Proceedings of the National Academy of Sciences*, *97*(16), 8807–8814.

Dodds, **P. N.** [Peter N], & **Rathjen**, **J. P.** (2010). Plant immunity: Towards an integrated view of plant–pathogen interactions. *Nature Reviews Genetics*, *11*(8), 539.

Doehlemann, **G.**, **Wahl**, **R.**, **Vranes**, **M.**, **de Vries**, **R. P.**, **Kamper**, **J.**, & **Kahmann**, **R.** (2008). Establishment of compatibility in the ustilago maydis/maize pathosystem. *J Plant Physiol*, *165*(1), 29–40. doi:10.1016/j.jplph.2007.05.016

Dolezal, **A. L.**, **Shu**, **X.**, **OBrian**, **G. R.**, **Nielsen**, **D. M.**, **Woloshuk**, **C. P.**, **Boston**, **R. S.**, & **Payne**, **G. A.** (2014). Aspergillus flavus infection induces transcriptional and physical changes in developing maize kernels. *Frontiers in microbiology*, *5*, 384.

Dong, **X.** (2004). Npr1, all things considered. *Current opinion in plant biology*, *7*(5), 547–552.

Donn, **S.**, **Kirkegaard**, **J. A.**, **Perera**, **G.**, **Richardson**, **A. E.**, & **Watt**, **M.** (2015). Evolution of bacterial communities in the wheat crop rhizosphere. *Environmental microbiology*, *17*(3), 610–621.

Draeger, **C.**, **Ndinyanka Fabrice**, **T.**, **Gineau**, **E.**, **Mouille**, **G.**, **Kuhn**, **B. M.**, **Moller**, **I.**, **Abdou**, **M.-T.**, **Frey**, **B.**, **Pauly**, **M.**, **Bacic**, **A.**, & **Ringli**, **C.** (2015). Arabidopsis leucine-rich repeat extensin (lrx) proteins modify cell wall composition and influence plant growth. *BMC Plant Biology*, *15*(1), 155. doi:10.1186/s12870-015-0548-8

Drag, **M.**, & **Salvesen**, **G. S.** (2010). Emerging principles in protease-based drug discovery. *Nature Reviews Drug Discovery*, *9*, 690. doi:10.1038/nrd3053

Du, **L.**, **Ali**, **G. S.**, **Simons**, **K. A.**, **Hou**, **J.**, **Yang**, **T.**, **Reddy**, **A.**, & **Poovaiah**, **B.** (2009). Ca 2+/calmodulin regulates salicylic-acid-mediated plant immunity. *Nature*, *457*(7233), 1154.

Duncan, **K. E.**, & **Howard**, **R. J.** (2010). Biology of maize kernel infection by fusarium verticillioides. *Molecular plant-microbe interactions*, *23*(1), 6–16.

Duxbury, **Z.**, **Ma**, **Y.**, **Furzer**, **O. J.**, **Huh**, **S. U.**, **Cevik**, **V.**, **Jones**, **J. D.**, & **Sarris**, **P. F.** (2016). Pathogen perception by nlrs in plants and animals: Parallel worlds. *BioEssays*, *38*(8), 769–781.

Edwards, **J.**, **Johnson**, **C.**, **Santos-Medellín**, **C.**, **Lurie**, **E.**, **Podishetty**, **N. K.**, **Bhatnagar**, **S.**, **Eisen**, **J. A.**, & **Sundaresan**, **V.** (2015). Structure, variation, and assembly of the root-associated microbiomes of rice. *Proceedings of the National Academy of Sciences*, *112*(8), E911–E920.

Eitzen, **K.**, **Schulze Hüynck**, **J.**, **Schurack**, **S.**, & **Döhlemann**, **G.** (2019). Krieg und frieden: Molekulares ping-pong zwischen pilzen und pflanzen. *BIOspektrum*, *25*(4), 378–381. doi:10.1007/s12268-019-1064-4

Engler, **C.**, **Youles**, **M.**, **Gruetzner**, **R.**, **Ehnert**, **T. M.**, **Werner**, **S.**, **Jones**, **J. D.**, **Patron**, **N. J.**, & **Marillonnet**, **S.** (2014). A golden gate modular cloning toolbox for plants. *ACS Synth Biol*, *3*(11), 839–43. doi:10.1021/sb4001504

Faist, **H.**, **Keller**, **A.**, **Hentschel**, **U.**, & **Deeken**, **R.** (2016). Grapevine (vitis vinifera) crown galls host distinct microbiota. *Applied and Environmental Microbiology*, *82*(18), 5542. doi:10.1128/AEM.01131-16

FAO, **P.** (2012). Disponível em:< http://faostat. fao. org/site/567/default. aspx>. *Acesso em*, *1*.

Feldman, **S. R.**, **Gonias**, **S. L.**, & **Pizzo**, **S. V.** (1985). Model of alpha 2-macroglobulin structure and function. *Proceedings of the National Academy of Sciences*, *82*(17), 5700–5704.

Feliciangeli, **S. F.**, **Thomas**, **L.**, **Scott**, **G. K.**, **Subbian**, **E.**, **Hung**, **C.-H.**, **Molloy**, **S. S.**, **Jean**, **F.**, **Shinde**, **U.**, & **Thomas**, **G.** (2006). Identification of a ph sensor in the furin propeptide that regulates enzyme activation. *Journal of Biological Chemistry*, *281*(23), 16108–16116.

Felle, **H. H.** (1998). The apoplastic ph of the zea mays root cortex as measured with ph-sensitive microelectrodes: Aspects of regulation. *Journal of Experimental Botany*, *49*(323), 987–995.

Fierer, **N.** (2017). Embracing the unknown: Disentangling the complexities of the soil microbiome. *Nature Reviews Microbiology*, *15*(10), 579.

Flor, **H. H.** (1971). Current status of the gene-for-gene concept. *Annual Review of Phytopathology*, *9*(1), 275–296. doi:doi:10.1146/annurev.py.09.090171.001423

Fomina, **M.**, **Alexander**, **I. J.**, **Colpaert**, **J.**, & **Gadd**, **G.** (2005). Solubilization of toxic metal minerals and metal tolerance of mycorrhizal fungi. *Soil Biology and Biochemistry*, *37*(5), 851–866.

Fox, **T.**, **De Miguel**, **E.**, **Mort**, **J. S.**, & **Storer**, **A. C.** (1992). Potent slow-binding inhibition of cathepsin b by its propeptide. *Biochemistry*, *31*(50), 12571–12576. doi:10.1021/bi00165a005

Frank, **S.**, **Hollmann**, **J.**, **Mulisch**, **M.**, **Matros**, **A.**, **Carrión**, **C. C.**, **Mock**, **H.-P.**, **Hensel**, **G.**, & **Krupinska**, **K.** (2019). The hordeum vulgare cysteine protease hvpap14 plays a role in degradation of chloroplast proteins. *Journal of Experimental Botany*. doi:10.1093/jxb/erz356

Franklin-Tong, **V. E.**, & **Gourlay**, **C. W.** (2008). A role for actin in regulating apoptosis/programmed cell death: Evidence spanning yeast, plants and animals. *Biochemical Journal*, *413*(3), 389. doi:10.1042/BJ20080320

Fu, **Z. Q.**, **Yan**, **S.**, **Saleh**, **A.**, **Wang**, **W.**, **Ruble**, **J.**, **Oka**, **N.**, **Mohan**, **R.**, **Spoel**, **S. H.**, **Tada**, **Y.**, & **Zheng**, **N.** (2012). Npr3 and npr4 are receptors for the immune signal salicylic acid in plants. *Nature*, *486*(7402), 228.

Fujioka, **S.**, & **Yokota**, **T.** (2003). Biosynthesis and metabolism of brassinosteroids. *Annual Review of Plant Biology*, *54*(1), 137–164. doi:10.1146/annurev.arplant.54.031902.134921

Garcia, **B. A.**, **Thomas**, **C. E.**, **Kelleher**, **N. L.**, & **Mizzen**, **C. A.** (2008). Tissue-specific expression and post-translational modification of histone h3 variants. *Journal of Proteome Research*, *7*(10), 4225–4236. doi:10.1021/pr800044q

Garcion, **C.**, **Lohmann**, **A.**, **Lamodière**, **E.**, **Catinot**, **J.**, **Buchala**, **A.**, **Doermann**, **P.**, & **Métraux**, **J.-P.** (2008). Characterization and biological function of the isochorismate synthase2 gene of arabidopsis. *Plant Physiology*, *147*(3), 1279–1287. doi:10.1104/pp.108.119420

Garrett, **W. S.** (2017). Gut microbiota in 2016: A banner year for gut microbiota research. *Nature Reviews Gastroenterology & Hepatology*, *14*(2), 78.

Gay, **N. J.**, & **Gangloff**, **M.** (2007). Structure and function of toll receptors and their ligands. *Annu. Rev. Biochem.*, *76*, 141–165.

Gfeller, **A.**, **Liechti**, **R.**, & **Farmer**, **E. E.** (2010). Arabidopsis jasmonate signaling pathway. *Sci. Signal.*, *3*(109), cm4–cm4.

Ghirlando, **R.** (2011). The analysis of macromolecular interactions by sedimentation equilibrium. *Methods*, *54*(1), 145–156. doi:https://doi.org/10.1016/j.ymeth.2010.12.005

Gill, **T. A.**, **Sandoya**, **G.**, **Williams**, **P.**, & **Luthe**, **D. S.** (2011). Belowground resistance to western corn rootworm in lepidopteran-resistant maize genotypes. *Journal of Economic Entomology*, *104*(1), 299–307. doi:10.1603/EC10117

Gilroy, **E. M.**, **Hein**, **I.**, **van der Hoorn**, **R.**, **Boevink**, **P. C.**, **Venter**, **E.**, **McLellan**, **H.**, **Kaffarnik**, **F.**, **Hrubikova**, **K.**, **Shaw**, **J.**, **Holeva**, **M.**, **López**, **E. C.**, **Borras-Hidalgo**, **O.**, **Pritchard**, **L.**, **Loake**, **G. J.**, **Lacomme**, **C.**, & **Birch**, **P. R. J.** (2007). Involvement of cathepsin b in the plant disease resistance hypersensitive response. *Plant J*, *52*(1), 1–13. doi:10.1111/j.1365-313X.2007.03226.x

Glassner, **H.**, **Zchori-Fein**, **E.**, **Yaron**, **S.**, **Sessitsch**, **A.**, **Sauer**, **U.**, & **Compant**, **S.** (2018). Bacterial niches inside seeds of cucumis melo l. *Plant and soil*, *422*(1-2), 101–113.

Glazebrook, **J.** (2005). Contrasting mechanisms of defense against biotrophic and necrotrophic pathogens. *Annu Rev Phytopathol*, *43*, 205–227. Retrieved from %3CGo%20to%20ISI%3E: //000232286700010%20http://www.annualreviews.org/doi/pdf/10.1146/annurev.phyto. 43.040204.135923

Glick, **B. R.** (2012). Plant growth-promoting bacteria: Mechanisms and applications. *Scientifica*, *2012*, 15. doi:10.6064/2012/963401

Glick, **B. R.**, **Penrose**, **D. M.**, & **Li**, **J.** (1998). A model for the lowering of plant ethylene concentrations by plant growth-promoting bacteria. *Journal of Theoretical Biology*, *190*(1), 63–68. doi:https://doi.org/10.1006/jtbi.1997.0532

Godlewski, **M.**, & **Adamczyk**, **B.** (2007). The ability of plants to secrete proteases by roots. *Plant Physiology and Biochemistry*, *45*(9), 657–664.

Gómez Expósito, **R.**, **de Bruijn**, **I.**, **Postma**, **J.**, & **Raaijmakers**, **J. M.** (2017). Current insights into the role of rhizosphere bacteria in disease suppressive soils. *Frontiers in Microbiology*, *8*, 2529.

Gomez-Gomez, **L.**, & **Boller**, **T.** [T.]. (2000). Fls2: An lrr receptor-like kinase involved in the perception of the bacterial elicitor flagellin in arabidopsis. *Mol Cell*, *5*(6), 1003–11. Retrieved from http://ac.els-cdn.com/S1097276500802658/1-s2.0-S1097276500802658-main.pdf?_tid=03b35a6e-915b-11e2-9f4e-00000aab0f02&acdnat=1363783266_fb69605db2326ee9a63940641990f8f4

Gómez-Gómez, **L.**, **Felix**, **G.**, & **Boller**, **T.** (1999). A single locus determines sensitivity to bacterial flagellin in arabidopsis thaliana. *The Plant Journal*, *18*(3), 277–284. doi:10.1046/j.1365-313X.1999.00451.x

Greenbaum, **D.**, **Medzihradszky**, **K. F.**, & **Burlingame**, **M.**, **A. & Bogyo**. (2000). Epoxide electrophiles as activity-dependent cysteine protease profiling and discovery tools. *Chem Biol*, *7*, 569–581. doi:10.1016/S1074-5521(00)00014-4

Greenbaum, **D. C.**, **Arnold**, **W. D.**, **Lu**, **F.**, **Hayrapetian**, **L.**, **Baruch**, **A.**, **Krumrine**, **J.**, **Toba**, **S.**, **Chehade**, **K.**, **Brömme**, **D.**, & **Kuntz**, **I. D.** (2002). Small molecule affinity fingerprinting: A tool for enzyme family subclassification, target identification, and inhibitor design. *Chemistry & biology*, *9*(10), 1085–1094.

Grignon, **C.**, & **Sentenac**, **A.** (1991). Ph and ionic conditions in the apoplast. *Annual review of plant biology*, *42*(1), 103–128.

Groeme, **R.**, **Airouche**, **S.**, **Kopecny**, **D.**, **Jaekel**, **J.**, **Savko**, **M.**, **Berjont**, **N.**, **Bussieres**, **L.**, **Le Mignon**, **M.**, **Jagic**, **F.**, **Zieglmayer**, **P.**, **Baron-Bodo**, **V.**, **Bordas-Le Floch**, **V.**, **Mascarell**, **L.**, **Briozzo**, **P.**, & **Moingeon**, **P.** (2016). Structural and functional characterization of the major allergen amb a 11 from short ragweed pollen. *J Biol Chem*, *291*(25), 13076–87. doi:10.1074/jbc.M115.702001

Grosse-Holz, **F. M.**, & **van der Hoorn**, **R. A. L.** (2016). Juggling jobs: Roles and mechanisms of multifunctional protease inhibitors in plants. *New Phytologist*, *210*(3), 794–807. doi:10.1111/nph.13839

Groves, **M. R.**, **Taylor**, **M. A.**, **Scott**, **M.**, **Cummings**, **N. J.**, **Pickersgill**, **R. W.**, & **Jenkins**, **J. A.** (1996). The prosequence of procaricain forms an alpha-helical domain that prevents access to the substrate-binding cleft. *Structure*, *4*(10), 1193–203. doi:10.1016/S0969-2126(96)00127-X

Grzonka, **Z.**, **Jankowska**, **E.**, **Kasprzykowski**, **F.**, **Kasprzykowska**, **R.**, **Lankiewicz**, **L.**, **Wiczk**, **W.**, **Wieczerzak**, **E.**, **Ciarkowski**, **J.**, **Drabik**, **P.**, **Janowski**, **R.**, **Kozak**, **M.**, **Jaskólski**, **M.**, & **Grubb**, **A.** (2001). Structural studies of cysteine proteases and their inhibitors. *Acta biochimica Polonica*, *48*(1), 1–20. Retrieved from http://europepmc.org/abstract/MED/11440158

Gu, **C.**, **Kolodziejek**, **I.**, **Misas-Villamil**, **J.**, **Shindo**, **T.**, **Colby**, **T.**, **Verdoes**, **M.**, **Richau**, **K. H.**, **Schmidt**, **J.**, **Overkleeft**, **H. S.**, & **van der Hoorn**, **R. A. L.** (2010). Proteasome activity profiling: A simple, robust and versatile method revealing subunit-selective inhibitors and cytoplasmic, defense-induced proteasome activities. *The Plant Journal*, *62*(1), 160–170. doi:10.1111/j.1365-313X.2009.04122.x

Gu, **C.**, **Shabab**, **M.**, **Strasser**, **R.**, **Wolters**, **P. J.**, **Shindo**, **T.**, **Niemer**, **M.**, **Kaschani**, **F.**, **Mach**, **L.**, & **van der Hoorn**, **R. A. L.** (2012). Post-translational regulation and trafficking of the granulin-containing protease rd21 of arabidopsis thaliana. *PLOS ONE*, *7*(3), e32422. doi:10.1371/journal.pone.0032422

Haas, **D.**, & **Keel**, **C.** (2003). Regulation of antibiotic production in root-colonizing pseudomonas spp. and relevance for biological control of plant disease. *Annual Review of Phytopathology*, *41*(1), 117–153. doi:10.1146/annurev.phyto.41.052002.095656

Hallmann, **J.**, **Quadt-Hallmann**, **A.**, **Mahaffee**, **W. F.**, & **Kloepper**, **J. W.** (1997). Bacterial endophytes in agricultural crops. *Canadian Journal of Microbiology*, *43*(10), 895–914. doi:10.1139/m97-131

Hanada, **K.**, **Tamai**, **M.**, **Yamagishi**, **M.**, **Ohmura**, **S.**, **Sawada**, **J.**, & **Tanaka**, **I.** (1978). Isolation and characterization of e–64, a new thiol protease inhibitor. *Agricultural and Biological Chemistry*, *42*(3), 523–528.

Hanahan, **D.** (1983). Studies on transformation of escherichia coli with plasmids. *J Mol Biol*, *166*(4), 557–80. Retrieved from http://ac.els-cdn.com/S0022283683802848/1-s2.0-S0022283683802848-main.pdf?_tid=319cff98-915b-11e2-88d0-00000aacb35d&acdnat=1363783343_8a7aba7fc69521c5c66dcf4ce14253b4

Hancock, **J.**, & **Huisman**, **O.** (1981). Nutrient movement in host-pathogen systems. *Annual review of phytopathology*, *19*(1), 309–331.

Hardoim, **P. R.**, **Van Overbeek**, **L. S.**, **Berg**, **G.**, **Pirttilä**, **A. M.**, **Compant**, **S.**, **Campisano**, **A.**, **Döring**, **M.**, & **Sessitsch**, **A.** (2015). The hidden world within plants: Ecological and evolutionary considerations for defining functioning of microbial endophytes. *Microbiol. Mol. Biol. Rev.*, *79*(3), 293–320.

Helm, **M.**, **Schmid**, **M.**, **Hierl**, **G.**, **Terneus**, **K.**, **Tan**, **L.**, **Lottspeich**, **F.**, **Kieliszewski**, **M. J.**, & **Gietl**, **C.** (2008). Kdel-tailed cysteine endopeptidases involved in programmed cell death, intercalation of new cells, and dismantling of extensin scaffolds. *American Journal of Botany*, *95*(9), 1049–1062. doi:10.3732/ajb.2007404

Hiltner, **L.** (1994). Über neuere erfahrungen und probleme auf dem gebiete der bodenbakteriologie und unter besonderer berucksichtigung der grund und brache. *Zbl. Bakteriol*, *2*, 14–25.

Höfgen, **R.**, & **Willmitzer**, **L.** (1988). Storage of competent cells for agrobacterium transformation. *Nucleic acids research*, *16*(20), 9877.

Honma, **M.**, & **Shimomura**, **T.** (1978). Metabolism of 1-aminocyclopropane-1-carboxylic acid. *Agricultural and Biological Chemistry*, *42*(10), 1825–1831. doi:10.1080/00021369.1978.10863261

Hopkins, **S. R.**, **Wojdak**, **J. M.**, & **Belden**, **L. K.** (2017). Defensive symbionts mediate host–parasite interactions at multiple scales. *Trends in parasitology*, *33*(1), 53–64.

Howing, **T.**, **Dann**, **M.**, **Hoefle**, **C.**, **Huckelhoven**, **R.**, & **Gietl**, **C.** (2017). Involvement of arabidopsis thaliana endoplasmic reticulum kdel-tailed cysteine endopeptidase 1 (atcep1) in powdery mildew-induced and atcpr5-controlled cell death. *PLoS One*, *12*(8), e0183870. doi:10.1371/journal.pone.0183870

Howing, **T.**, **Huesmann**, **C.**, **Hoefle**, **C.**, **Nagel**, **M. K.**, **Isono**, **E.**, **Huckelhoven**, **R.**, & **Gietl**, **C.** (2014). Endoplasmic reticulum kdel-tailed cysteine endopeptidase 1 of arabidopsis (atcep1) is involved in pathogen defense. *Front Plant Sci*, *5*, 58. doi:10.3389/fpls.2014.00058

Hu, **L.**, **Robert**, **C. A. M.**, **Cadot**, **S.**, **Zhang**, **X.**, **Ye**, **M.**, **Li**, **B.**, **Manzo**, **D.**, **Chervet**, **N.**, **Steinger**, **T.**, **van der Heijden**, **M. G. A.**, **Schlaeppi**, **K.**, & **Erb**, **M.** (2018). Root exudate metabolites drive plant-soil feedbacks on growth and defense by shaping the rhizosphere microbiota. *Nature Communications*, *9*(1), 2738. doi:10.1038/s41467-018-05122-7

Hückelhoven, **R.** (2007). Cell wall-associated mechanisms of disease resistance and susceptibility. *Annu Rev Phytopathol*, *45*, 101–27. doi:10.1146/annurev.phyto.45.062806.094325

Huffaker, **A.**, **Dafoe**, **N. J.**, & **Schmelz**, **E. A.** (2011). Zmpep1, an ortholog of arabidopsis elicitor petide 1, regulates maize innate immunity and enhances disease resistance. *Plant Physiol*, *155*(3), 1325–1338. doi:10.1104/pp.110.166710

Huntington, **J. A.**, **Read**, **R. J.**, & **Carrell**, **R. W.** (2000). Structure of a serpin–protease complex shows inhibition by deformation. *Nature*, *407*(6806), 923–926. doi:10.1038/35038119

Il, **P. J.**, **MR**, **W.**, **EK**, **C.**, **JM**, **G.**, **LC**, **H.**, **ML**, **S.**, **JR**, **W.**, **TZ**, **S.**, **KT**, **C.**, **DA**, **S.**, **BL**, **B.**, **M**, **D.**, **B**, **D.**, **CG**, **E.**, **N**, **M.**, **E**, **C.**, **M**, **S.**, **P**, **S.**, **J**, **T.**, **S**, **Z.**, & **CM.**, **A.** (2018). Maizegdb 2018: The maize multi-genome genetics and genomics database. *Nucleic Acids Res.* doi:10.1093/nar/gky1046

Irene, **D.**, **Chen**, **B.-J.**, **Lo**, **S.-H.**, **Liu**, **T.-H.**, **Tzen**, **J. T.-C.**, & **Chyan**, **C.-L.** (2012). Resonance assignments and secondary structure of a phytocystatin from ananas comosus. *Biomolecular NMR Assignments*, *6*(1), 99–101. doi:10.1007/s12104-011-9334-1

Jacob, **F.**, **Vernaldi**, **S.**, & **Maekawa**, **T.** (2013). Evolution and conservation of plant nlr functions. *Frontiers in immunology*, *4*, 297.

Jaishankar, **P.**, **Hansell**, **E.**, **Zhao**, **D.-M.**, **Doyle**, **P. S.**, **McKerrow**, **J. H.**, & **Renslo**, **A. R.** (2008). Potency and selectivity of p2/p3-modified inhibitors of cysteine proteases from trypanosomes. *Bioorganic & Medicinal Chemistry Letters*, *18*(2), 624–628. doi:https://doi.org/10.1016/j.bmcl.2007.11.070

Jakobsen, **I.**, **Abbott**, **L.**, & **Robson**, **A.** (1992). External hyphae of vesicular-arbuscular mycorrhizal fungi associated with trifolium subterraneum l. 1. spread of hyphae and phosphorus inflow into roots. *New Phytologist*, *120*(3), 371–380.

James, **A. M.**, **Haywood**, **J.**, & **Mylne**, **J. S.** (2018). Macrocyclization by asparaginyl endopeptidases. *New Phytologist*, *218*(3), 923–928. doi:10.1111/nph.14511

Jashni, **M. K.**, **Dols**, **I. H. M.**, **Iida**, **Y.**, **Boeren**, **S.**, **Beenen**, **H. G.**, **Mehrabi**, **R.**, **Collemare**, **J.**, & **de Wit**, **P. J. G. M.** (2015). Synergistic action of a metalloprotease and a serine protease from fusarium oxysporum f. sp. lycopersici cleaves chitin-binding tomato chitinases, reduces their antifungal activity, and enhances fungal virulence. *Molecular Plant-Microbe Interactions*, *28*(9), 996–1008. doi:10.1094/MPMI-04-15-0074-R

Jia, **Y.**, **McAdams**, **S. A.**, **Bryan**, **G. T.**, **Hershey**, **H. P.**, & **Valent**, **B.** (2000). Direct interaction of resistance gene and avirulence gene products confers rice blast resistance. *EMBO J*, *19*(15), 4004–14. doi:10.1093/emboj/19.15.4004

Johnston-Monje, **D.**, & **Raizada**, **M. N.** (2011). Conservation and diversity of seed associated endophytes in zea across boundaries of evolution, ethnography and ecology. *PLoS One*, *6*(6), e20396.

Jones, **J. D.**, & **Dangl**, **J. L.** (2006). The plant immune system. *Nature*, *444*(7117), 323–9. doi:10.1038/nature05286

Jones, **P. G.**, & **Thornton**, **P. K.** (2003). The potential impacts of climate change on maize production in africa and latin america in 2055. *Global environmental change*, *13*(1), 51–59.

Jurczak, **P.**, **Groves**, **P.**, **Szymanska**, **A.**, & **Rodziewicz-Motowidlo**, **S.** (2016). Human cystatin c monomer, dimer, oligomer, and amyloid structures are related to health and disease. *FEBS Letters*, *590*(23), 4192–4201. doi:10.1002/1873-3468.12463

Kadota, **Y.**, **Liebrand**, **T. W. H.**, **Goto**, **Y.**, **Sklenar**, **J.**, **Derbyshire**, **P.**, **Menke**, **F. L. H.**, **Torres**, **M.-A.**, **Molina**, **A.**, **Zipfel**, **C.**, **Coaker**, **G.**, & **Shirasu**, **K.** (2019). Quantitative phosphoproteomic analysis reveals common regulatory mechanisms between effector- and pamp-triggered immunity in plants. *New Phytologist*, *221*(4), 2160–2175. doi:10.1111/nph.15523

Karrer, **K. M.**, **Peiffer**, **S. L.**, & **DiTomas**, **M. E.** (1993). Two distinct gene subfamilies within the family of cysteine protease genes. *Proceedings of the National Academy of Sciences*, *90*(7), 3063–3067.

Kaschani, **F.**, **Shabab**, **M.**, **Bozkurt**, **T.**, **Shindo**, **T.**, **Schornack**, **S.**, **Gu**, **C.**, **Ilyas**, **M.**, **Win**, **J.**, **Kamoun**, **S.**, & **van der Hoorn**, **R. A.** (2010). An effector-targeted protease contributes to defense against phytophthora infestans and is under diversifying selection in natural hosts. *Plant Physiol*, *154*(4), 1794–1804. doi:10.1104/pp.110.158030

Katoh, **K.**, & **Standley**, **D. M.** (2013). Mafft multiple sequence alignment software version 7: Improvements in performance and usability. *Molecular Biology and Evolution*, *30*(4), 772–80. doi:10.1093/molbev/mst010

Kelley, **L. A.**, **Mezulis**, **S.**, **Yates**, **C. M.**, **Wass**, **M. N.**, & **Sternberg**, **M. J. E.** (2015). The phyre2 web portal for protein modeling, prediction and analysis. *Nature Protocols*, *10*, 845. doi:10.1038/nprot.2015.053

Kinkema, **M.**, **Fan**, **W.**, & **Dong**, **X.** (2000). Nuclear localization of npr1 is required for activation of pr gene expression. *The Plant Cell*, *12*(12), 2339–2350.

Kistler, **H. C.** (1997). Genetic diversity in the plant-pathogenic fungus fusarium oxysporum. *Phytopathology*, *87*(4), 474–479. doi:10.1094/PHYTO.1997.87.4.474

Klessig, **D. F.**, **Choi**, **H. W.**, & **Dempsey**, **D. A.** (2018). Systemic acquired resistance and salicylic acid: Past, present, and future. *Mol Plant Microbe Interact*, *31*(9), 871–888. doi:10.1094/mpmi-03-18-0067-cr

Kniskern, **J. M.**, **Traw**, **M. B.**, & **Bergelson**, **J.** (2007). Salicylic acid and jasmonic acid signaling defense pathways reduce natural bacterial diversity on arabidopsis thaliana. *Molecular plant-microbe interactions*, *20*(12), 1512–1522.

Knobloch, **J. E.**, & **Shaklee**, **P. N.** (1997). Absolute molecular weight distribution of low-molecular-weight heparins by size-exclusion chromatography with multiangle laser light scattering detection. *Analytical Biochemistry*, *245*(2), 231–241. doi:https://doi.org/10.1006/abio.1996.9984

Koeck, **M.**, **Hardham**, **A. R.**, & **Dodds**, **P. N.** (2011). The role of effectors of biotrophic and hemibiotrophic fungi in infection. *Cell Microbiol*, *[in press]*. doi:10.1111/j.1462-5822.2011.01665.x

Kolton, **M.**, **Erlacher**, **A.**, **Berg**, **G.**, & **Cytryn**, **E.** (2016). The flavobacterium genus in the plant holobiont: Ecological, physiological, and applicative insights. In **S. Castro-Sowinski** (Ed.), *Microbial models: From environmental to industrial sustainability* (pp. 189–207). doi:10.1007/978-981-10-2555-6_9

Koncz, **C.**, & **Schell**, **J.** (1986). The promoter of tl-dna gene 5 controls the tissue-specific expression of chimaeric genes carried by a novel type of agrobacterium binary vector. *Molecular and General Genetics MGG*, *204*(3), 383–396. doi:10.1007/BF00331014

Konno, **K.**, **Hirayama**, **C.**, **Nakamura**, **M.**, **Tateishi**, **K.**, **Tamura**, **Y.**, **Hattori**, **M.**, & **Kohno**, **K.** (2004). Papain protects papaya trees from herbivorous insects: Role of cysteine proteases in latex. *Plant J*, *37*(3), 370–8.

Koo, **B. J.**, **Adriano**, **D. C.**, **Bolan**, **N. S.**, & **Barton**, **C. D.** (2005). Root exudates and microorganisms. In **D. Hillel** (Ed.), *Encyclopedia of soils in the environment* (pp. 421–428). doi:https://doi.org/10.1016/B0-12-348530-4/00461-6

Kosegarten, **H.**, **Grolig**, **F.**, **Esch**, **A.**, **Glüsenkamp**, **K.-H.**, & **Mengel**, **K.** (1999). Effects of nh 4+, no 3- and hco 3- on apoplast ph in the outer cortex of root zones of maize, as measured by the fluorescence ratio of fluorescein boronic acid. *Planta*, *209*(4), 444–452.

Kovács, **J.**, **Poór**, **P.**, **Szepesi**, **Á.**, & **Tari**, **I.** (2016). Salicylic acid induced cysteine protease activity during programmed cell death in tomato plants. *Acta Biologica Hungarica*, *67*(2), 148–158.

Krylov, **D. M.**, **Wolf**, **Y. I.**, **Rogozin**, **I. B.**, & **Koonin**, **E. V.** (2003). Gene loss, protein sequence divergence, gene dispensability, expression level, and interactivity are correlated in eukaryotic evolution. *Genome research*, *13*(10), 2229–2235.

Kunkel, **B. N.**, & **Brooks**, **D. M.** (2002). Cross talk between signaling pathways in pathogen defense. *Curr Opin Plant Biol*, *5*(4), 325–31. Retrieved from http://ac.els-cdn.com/S1369526602002753/1-s2.0-S1369526602002753-main.pdf?_tid=0f0a9610-915c-11e2-9c01-00000aab0f02&acdnat=1363783715_1d42fc775e02e467d9aca244ce177a7b

Laemmli, **U. K.** (1970). Cleavage of structural proteins during the assembly of the head of bacteriophage t4. *Nature*, *227*(5259), 680–5. Retrieved from http://www.ncbi.nlm.nih.gov/entrez/query.fcgi?cmd=Retrieve&db=PubMed&dopt=Citation&list_uids=5432063

Lampl, **N.**, **Alkan**, **N.**, **Davydov**, **O.**, & **Fluhr**, **R.** (2013). Set-point control of rd 21 protease activity by atserpin1 controls cell death in a rabidopsis. *The Plant Journal*, *74*(3), 498–510.

Lange, **B. M.**, **Lapierre**, **C.**, & **Sandermann Jr**, **H.** (1995). Elicitor-induced spruce stress lignin (structural similarity to early developmental lignins). *Plant Physiology*, *108*(3), 1277–1287.

Lee, **J.**, **Eschen-Lippold**, **L.**, **Lassowskat**, **I.**, **Böttcher**, **C.**, & **Scheel**, **D.** (2015). Cellular reprogramming through mitogen-activated protein kinases. *Frontiers in plant science*, *6*, 940.

Li, **S.-B.**, **Xie**, **Z.-Z.**, **Hu**, **C.-G.**, & **Zhang**, **J.-Z.** (2016). A review of auxin response factors (arfs) in plants. *Frontiers in Plant Science*, *7*(47). doi:10.3389/fpls.2016.00047

Lindow, **S. E.**, & **Brandl**, **M. T.** (2003). Microbiology of the phyllosphere. *Appl. Environ. Microbiol.*, *69*(4), 1875–1883.

Liu, **D.**, **Raghothama**, **K. G.**, **Hasegawa**, **P. M.**, & **Bressan**, **R. A.** (1994). Osmotin overexpression in potato delays development of disease symptoms. *Proceedings of the National Academy of Sciences*, *91*(5), 1888–1892.

Liu, **S. T.**, **Lee**, **L. Y.**, **Tai**, **C. Y.**, **Hung**, **C. H.**, **Chang**, **Y. S.**, **Wolfram**, **J. H.**, **Rogers**, **R.**, & **Goldstein**, **A. H.** (1992). Cloning of an erwinia herbicola gene necessary for gluconic acid production and enhanced mineral phosphate solubilization in escherichia coli hb101: Nucleotide sequence and probable involvement in biosynthesis of the coenzyme pyrroloquinoline quinone. *Journal of Bacteriology*, *174*(18), 5814. doi:10.1128/jb.174.18.5814-5819.1992

Liu, **Y.**, **Zuo**, **S.**, **Xu**, **L.**, **Zou**, **Y.**, & **Song**, **W.** (2012). Study on diversity of endophytic bacterial communities in seeds of hybrid maize and their parental lines. *Archives of microbiology*, *194*(12), 1001–1012.

Lohman, **K. N.**, **Gan**, **S.**, **John**, **M. C.**, & **Amasino**, **R. M.** (1994). Molecular analysis of natural leaf senescence in arabidopsis thaliana. *Physiologia Plantarum*, *92*(2), 322–328.

Lopez, **L.**, **Camas**, **A.**, **Shivaji**, **R.**, **Ankala**, **A.**, **Williams**, **P.**, & **Luthe**, **D.** (2007). Mir1-cp, a novel defense cysteine protease accumulates in maize vascular tissues in response to herbivory. *Planta*, *226*(2), 517–527.

Lorenzo, **O.**, **Piqueras**, **R.**, **Sánchez-Serrano**, **J. J.**, & **Solano**, **R.** (2003). Ethylene response factor 1 integrates signals from ethylene and jasmonate pathways in plant defense. *Plant Cell*, *15*(1), 165–78. Retrieved from http://www.ncbi.nlm.nih.gov/entrez/query.fcgi?cmd=Retrieve&db=PubMed&dopt=Citation&list_uids=12509529%20http://www.plantcell.org/content/15/1/165.full.pdf

Louis, **J.**, **Basu**, **S.**, **Varsani**, **S.**, **Castano-Duque**, **L.**, **Jiang**, **V.**, **Williams**, **W. P.**, **Felton**, **G. W.**, & **Luthe**, **D. S.** (2015). Ethylene contributes to maize insect resistance1-mediated maize defense against the phloem sap-sucking corn leaf aphid. *Plant Physiology*, *169*(1), 313. doi:10.1104/pp.15.00958

Lozano-Durán, **R.**, **Macho**, **A. P.**, **Boutrot**, **F.**, **Segonzac**, **C.**, **Somssich**, **I. E.**, & **Zipfel**, **C.** (2013). The transcriptional regulator bzr1 mediates trade-off between plant innate immunity and growth. *elife*, *2*, e00983.

Lozano-Durán, **R.**, & **Zipfel**, **C.** [Cyril]. (2015). Trade-off between growth and immunity: Role of brassinosteroids. *Trends in plant science*, *20*(1), 12–19.

Lozano-Torres, **J. L.**, **Wilbers**, **R. H.**, **Gawronski**, **P.**, **Boshoven**, **J. C.**, **Finkers-Tomczak**, **A.**, **Cordewener**, **J. H.**, **America**, **A. H.**, **Overmars**, **H. A.**, **Van 't Klooster**, **J. W.**, **Baranowski**, **L.**, **Sobczak**, **M.**, **Ilyas**, **M.**, **van der Hoorn**, **R. A.**, **Schots**, **A.**, **de Wit**, **P. J.**, **Bakker**, **J.**, **Goverse**, **A.**, & **Smant**, **G.** (2012). Dual disease resistance mediated by the immune receptor cf-2 in tomato requires a common virulence target of a fungus and a nematode. *Proc Natl Acad Sci U S A*, *109*(25), 10119–24. doi:10.1073/pnas.1202867109

Lu, **H.**, **Chandrasekar**, **B.**, **Oeljeklaus**, **J.**, **Misas-Villamil**, **J. C.**, **Wang**, **Z.**, **Shindo**, **T.**, **Bogyo**, **M.**, **Kaiser**, **M.**, & **van der Hoorn**, **R. A.** (2015). Subfamily-specific fluorescent probes for cysteine proteases display dynamic protease activities during seed germination. *Plant Physiol*, *168*(4), 1462–75. doi:10.1104/pp.114.254466

Luderer, **R.**, **Takken**, **F. L.**, **de Wit**, **P. J.**, & **Joosten**, **M. H.** (2002). Cladosporium fulvum overcomes cf-2-mediated resistance by producing truncated avr2 elicitor proteins. *Mol Microbiol*, *45*(3), 875–84.

Lundberg, **D. S.**, **Lebeis**, **S. L.**, **Paredes**, **S. H.**, **Yourstone**, **S.**, **Gehring**, **J.**, **Malfatti**, **S.**, **Tremblay**, **J.**, **Engelbrektson**, **A.**, **Kunin**, **V.**, **Rio**, **T. G. d.**, **Edgar**, **R. C.**, **Eickhorst**, **T.**, **Ley**, **R. E.**, **Hugenholtz**, **P.**, **Tringe**, **S. G.**, & **Dangl**, **J. L.** (2012). Defining the core arabidopsis thaliana root microbiome. *Nature*, *488*, 86. doi:10.1038/nature11237

Maeda, **H.**, & **Dudareva**, **N.** (2012). The shikimate pathway and aromatic amino acid biosynthesis in plants. *Annual review of plant biology*, *63*, 73–105.

Mansfield, **J.**, **Genin**, **S.**, **Magori**, **S.**, **Citovsky**, **V.**, **Sriariyanum**, **M.**, **Ronald**, **P.**, **Dow**, **M.**, **Verdier**, **V.**, **Beer**, **S. V.**, & **Machado**, **M. A.** (2012). Top 10 plant pathogenic bacteria in molecular plant pathology. *Molecular plant pathology*, *13*(6), 614–629.

Margulis, **L.**, & **Fester**, **R.** (1991). *Symbiosis as a source of evolutionary innovation: Speciation and morphogenesis*. Mit Press.

Marquez-Santacruz, **H. A.**, **Hernandez-Leon**, **R.**, **Orozco-Mosqueda**, **M. C.**, **Velazquez-Sepulveda**, **I.**, & **Santoyo**, **G.** (2010). Diversity of bacterial endophytes in roots of mexican husk tomato plants (physalis ixocarpa) and their detection in the rhizosphere. *Genet Mol Res*, *9*(4), 2372–80. doi:10.4238/vol9-4gmr921

Martinez, **M.** [M.], & **Diaz**, **I.** (2008). The origin and evolution of plant cystatins and their target cysteine proteinases indicate a complex functional relationship. *BMC Evol Biol*, *8*, 198. doi:10.1186/1471-2148-8-198

Martinez, **M.** [Manuel], **Cambra**, **I.**, **Carrillo**, **L.**, **Diaz-Mendoza**, **M.**, & **Diaz**, **I.** (2009). Characterization of the entire cystatin gene family in barley and their target cathepsin l-like cysteine-proteases, partners in the hordein mobilization during seed germination. *Plant Physiol*, *151*(3), 1531–1545. doi:10.1104/pp.109.146019

Martínez, **M.**, **Cambra**, **I.**, **González-Melendi**, **P.**, **Santamaría**, **M. E.**, & **Díaz**, **I.** (2012). C1a cysteine-proteases and their inhibitors in plants. *Physiologia Plantarum*, *145*(1), 85–94.

Massonneau, **A.**, **Condamine**, **P.**, **Wisniewski**, **J. P.**, **Zivy**, **M.**, & **Rogowsky**, **P. M.** (2005). Maize cystatins respond to developmental cues, cold stress and drought. *Biochim Biophys Acta*, *1729*(3), 186–199. doi:10.1016/j.bbaexp.2005.05.004

Mavrodi, **D. V.**, **Peever**, **T. L.**, **Mavrodi**, **O. V.**, **Parejko**, **J. A.**, **Raaijmakers**, **J. M.**, **Lemanceau**, **P.**, **Mazurier**, **S.**, **Heide**, **L.**, **Blankenfeldt**, **W.**, **Weller**, **D. M.**, & **Thomashow**, **L. S.** (2010).

Diversity and evolution of the phenazine biosynthesis pathway. *Applied and Environmental Microbiology*, *76*(3), 866. doi:10.1128/AEM.02009-09

McLellan, H., Gilroy, E. M., Yun, B. W., Birch, P. R., & Loake, G. J. (2009). Functional redundancy in the arabidopsis cathepsin b gene family contributes to basal defence, the hypersensitive response and senescence. *New Phytol*, *183*(2), 408–418. doi:10.1111/j.1469-8137.2009.02865.x

Ménard, R., Plouffe, C., Laflamme, P., Vernet, T., Tessier, D. C., Thomas, D. Y., & Storer, A. C. (1995). Modification of the electrostatic environment is tolerated in the oxyanion hole of the cysteine protease papain. *Biochemistry*, *34*(2), 464–471. doi:10.1021/bi00002a010

Menard, R., Carriere, J., Laflamme, P., Plouffe, C., Khouri, H. E., Vernet, T., Tessier, D. C., Thomas, D. Y., & Storer, A. C. (1991). Contribution of the glutamine 19 side chain to transition-state stabilization in the oxyanion hole of papain. *Biochemistry*, *30*(37), 8924–8928. doi:10.1021/bi00101a002

Mendes, R., Garbeva, P., & Raaijmakers, J. M. (2013). The rhizosphere microbiome: Significance of plant beneficial, plant pathogenic, and human pathogenic microorganisms. *FEMS Microbiology Reviews*, *37*(5), 634–663. doi:10.1111/1574-6976.12028

Michaelis, L., & Menten, M. L. (1913). Kinetics of invertase action. *Biochemische Zeitschrift*, *49*, 333–369.

Michalski, A., Damoc, E., Lange, O., Denisov, E., Nolting, D., Müller, M., Viner, R., Schwartz, J., Remes, P., Belford, M., Dunyach, J.-J., Cox, J., Horning, S., Mann, M., & Makarov, A. (2012). Ultra high resolution linear ion trap orbitrap mass spectrometer (orbitrap elite) facilitates top down lc ms/ms and versatile peptide fragmentation modes. *Molecular & Cellular Proteomics*, *11*(3), O111.013698. doi:10.1074/mcp.O111.013698

Michielse, C. B., & Rep, M. (2009). Pathogen profile update: Fusarium oxysporum. *Molecular Plant Pathology*, *10*(3), 311–324. doi:10.1111/j.1364-3703.2009.00538.x

Miller, S. H., Browne, P., Prigent-Combaret, C., Combes-Meynet, E., Morrissey, J. P., & O'Gara, F. (2010). Biochemical and genomic comparison of inorganic phosphate solubilization in pseudomonas species. *Environmental Microbiology Reports*, *2*(3), 403–411. doi:10.1111/j.1758-2229.2009.00105.x

Misas Villamil, J. C., Mueller, A. N., Demir, F., Meyer, U., Okmen, B., Schulze Huynck, J., Breuer, M., Dauben, H., Win, J., Huesgen, P. F., & Doehlemann, G. (2019). A fungal substrate mimicking molecule suppresses plant immunity via an inter-kingdom conserved motif. *Nat Commun*, *10*(1), 1576. doi:10.1038/s41467-019-09472-8

Misas-Villamil, J. C., & van der Hoorn, R. A. (2008). Enzyme-inhibitor interactions at the plant-pathogen interface. *Curr Opin Plant Biol*, *11*(4), 380–8. doi:10.1016/j.pbi.2008.04.007

Misas-Villamil, J. C., van der Hoorn, R. A., & Doehlemann, G. (2016). Papain-like cysteine proteases as hubs in plant immunity. *New Phytol*, *212*(4), 902–907. doi:10.1111/nph.14117

Mitter, B., Pfaffenbichler, N., Flavell, R., Compant, S., Antonielli, L., Petric, A., Berninger, T., Naveed, M., Sheibani-Tezerji, R., & von Maltzahn, G. (2017). A new approach to modify plant microbiomes and traits by introducing beneficial bacteria at flowering into progeny seeds. *Frontiers in microbiology*, *8*, 11.

Mok, **D. W. S.**, & **Mok**, **M. C.** (2001). Cytokinin metabolism and action. *Annual Review of Plant Physiology and Plant Molecular Biology*, *52*(1), 89–118. doi:10.1146/annurev.arplant.52.1.89

Monteiro, **A. C.**, **Abrahamson**, **M.**, **Lima**, **A. P.**, **Vannier-Santos**, **M. A.**, & **Scharfstein**, **J.** (2001). Identification, characterization and localization of chagasin, a tight-binding cysteine protease inhibitor in trypanosoma cruzi. *J Cell Sci*, *114*(Pt 21), 3933–42.

Moore, **J. W.**, **Loake**, **G. J.**, & **Spoel**, **S. H.** (2011). Transcription dynamics in plant immunity. *The Plant Cell*, *23*(8), 2809–2820.

Mueller, **A. N.**, **Ziemann**, **S.**, **Treitschke**, **S.**, **Assmann**, **D.**, & **Doehlemann**, **G.** (2013). Compatibility in the ustilago maydis-maize interaction requires inhibition of host cysteine proteases by the fungal effector pit2. *PLoS Pathog*, *9*(2), e1003177. doi:10.1371/journal.ppat.1003177

Nagata, **K.**, **Kudo**, **N.**, **Abe**, **K.**, **Arai**, **S.**, & **Tanokura**, **M.** (2000). Three-dimensional solution structure of oryzacystatin-i, a cysteine proteinase inhibitor of the rice, oryza sativa l. japonica. *Biochemistry*, *39*(48), 14753–60. doi:bi0006971

Nayaka, **S. C.**, **Shankar**, **A. C.**, **Reddy**, **M. S.**, **Niranjana**, **S. R.**, **Prakash**, **H. S.**, **Shetty**, **H. S.**, & **Mortensen**, **C. N.** (2009). Control of fusarium verticillioides, cause of ear rot of maize, by pseudomonas fluorescens. *Pest Manag Sci*, *65*(7), 769–75. doi:10.1002/ps.1751

Niemer, **M.**, **Mehofer**, **U.**, **Verdianz**, **M.**, **Porodko**, **A.**, **Schähs**, **P.**, **Kracher**, **D.**, **Lenarcic**, **B.**, **Novinec**, **M.**, & **Mach**, **L.** (2016). Nicotiana benthamiana cathepsin b displays distinct enzymatic features which differ from its human relative and aleurain-like protease. *Biochimie*, *122*, 119–125.

Niu, **B.**, & **Kolter**, **R.** (2017). Complete genome sequences of seven strains composing a model bacterial community of maize roots. *Genome Announc*, *5*(36). doi:10.1128/genomeA.00997-17

Niu, **B.**, **Paulson**, **J. N.**, **Zheng**, **X.**, & **Kolter**, **R.** (2017). Simplified and representative bacterial community of maize roots. *Proc Natl Acad Sci U S A*, *114*(12), E2450–E2459. doi:10.1073/pnas.1616148114

Noh, **Y.-S.**, & **Amasino**, **R. M.** (1999a). Identification of a promoter region responsible for the senescence-specific expression of sag12. *Plant molecular biology*, *41*(2), 181–194.

Noh, **Y.-S.**, & **Amasino**, **R. M.** (1999b). Regulation of developmental senescence is conserved between arabidopsis and brassica napus. *Plant Molecular Biology*, *41*(2), 195–206.

Ochieng, **J.**, & **Chaudhuri**, **G.** (2010). Cystatin superfamily. *Journal of health care for the poor and underserved*, *21*(1 Suppl), 51.

Okmen, **B.**, & **Doehlemann**, **G.** (2016). Clash between the borders: Spotlight on apoplastic processes in plant-microbe interactions. *New Phytol*, *212*(4), 799–801. doi:10.1111/nph.14311

Oldroyd, **G. E.** (2013). Speak, friend, and enter: Signalling systems that promote beneficial symbiotic associations in plants. *Nature Reviews Microbiology*, *11*(4), 252.

Olonen, **A.**, **Kalkkinen**, **N.**, & **Paulin**, **L.** (2003). A new type of cysteine proteinase inhibitor–the salarin gene from atlantic salmon (salmo salar l.) and arctic charr (salvelinus alpinus). *Biochimie*, *85*(7), 677–81. doi:10.1016/s0300-9084(03)00128-7

Olsen, **J. V.**, **de Godoy**, **L. M. F.**, **Li**, **G.**, **Macek**, **B.**, **Mortensen**, **P.**, **Pesch**, **R.**, **Makarov**, **A.**, **Lange**, **O.**, **Horning**, **S.**, & **Mann**, **M.** (2005). Parts per million mass accuracy on an orbitrap

mass spectrometer via lock mass injection into a c-trap. *Molecular & Cellular Proteomics*, *4*(12), 2010. doi:10.1074/mcp.T500030-MCP200

Ormancey, **M.**, **Thuleau**, **P.**, **van der Hoorn**, **R. A. L.**, **Grat**, **S.**, **Testard**, **A.**, **Kamal**, **K. Y.**, **Boudsocq**, **M.**, **Cotelle**, **V.**, & **Mazars**, **C.** (2019). Sphingolipid-induced cell death in arabidopsis is negatively regulated by the papain-like cysteine protease rd21. *Plant Science*, *280*, 12–17. doi:https://doi.org/10.1016/j.plantsci.2018.10.028

Osbourn, **A. E.** (1996). Preformed antimicrobial compounds and plant defense against fungal attack. *The plant cell*, *8*(10), 1821.

Osonubi, **O.**, **Mulongoy**, **K.**, **Awotoye**, **O.**, **Atayese**, **M.**, & **Okali**, **D.** (1991). Effects of ectomycorrhizal and vesicular-arbuscular mycorrhizal fungi on drought tolerance of four leguminous woody seedlings. *Plant and soil*, *136*(1), 131–143.

Otegui, **M. S.**, **Noh**, **Y.**, **Martínez**, **D. E.**, **Vila Petroff**, **M. G.**, **Andrew Staehelin**, **L.**, **Amasino**, **R. M.**, & **Guiamet**, **J. J.** (2005). Senescence-associated vacuoles with intense proteolytic activity develop in leaves of arabidopsis and soybean. *The Plant Journal*, *41*(6), 831–844.

Otto, **H.-H.**, & **Schirmeister**, **T.** (1997). Cysteine proteases and their inhibitors. *Chemical Reviews*, *97*(1), 133–172. doi:10.1021/cr950025u

Paireder, **M.** [M.], **Tholen**, **S.**, **Porodko**, **A.**, **Biniossek**, **M. L.**, **Mayer**, **B.**, **Novinec**, **M.**, **Schilling**, **O.**, & **Mach**, **L.** (2017). The papain-like cysteine proteinases nbcysp6 and nbcysp7 are highly processive enzymes with substrate specificities complementary to nicotiana benthamiana cathepsin b. *Biochim Biophys Acta Proteins Proteom*, *1865*(4), 444–452. doi:10.1016/j.bbapap.2017.02.007

Paireder, **M.** [Melanie], **Mehofer**, **U.**, **Tholen**, **S.**, **Porodko**, **A.**, **Schähs**, **P.**, **Maresch**, **D.**, **Biniossek**, **M. L.**, **van der Hoorn**, **R. A. L.**, **Lenarcic**, **B.**, **Novinec**, **M.**, **Schilling**, **O.**, & **Mach**, **L.** (2016). The death enzyme cp14 is a unique papain-like cysteine proteinase with a pronounced s2 subsite selectivity. *Archives of Biochemistry and Biophysics*, *603*, 110–117. doi:https://doi.org/10.1016/j.abb.2016.05.017

Palaniyandi, **S. A.**, **Yang**, **S. H.**, **Zhang**, **L.**, & **Suh**, **J.-W.** (2013). Effects of actinobacteria on plant disease suppression and growth promotion. *Applied Microbiology and Biotechnology*, *97*(22), 9621–9636. doi:10.1007/s00253-013-5206-1

Panstruga, **R.**, & **Dodds**, **P. N.** [P. N.]. (2009). Terrific protein traffic: The mystery of effector protein delivery by filamentous plant pathogens. *Science*, *324*(5928), 748–50. doi:10.1126/science.1171652

Paungfoo-Lonhienne, **C.**, **Schenk**, **P. M.**, **Lonhienne**, **T. G.**, **Brackin**, **R.**, **Meier**, **S.**, **Rentsch**, **D.**, & **Schmidt**, **S.** (2009). Nitrogen affects cluster root formation and expression of putative peptide transporters. *Journal of Experimental Botany*, *60*(9), 2665–2676.

Pechan, **T.**, **Cohen**, **A.**, **Williams**, **W. P.**, & **Luthe**, **D. S.** (2002). Insect feeding mobilizes a unique plant defense protease that disrupts the peritrophic matrix of caterpillars. *Proceedings of the National Academy of Sciences of the United States of America*, *99*(20), 13319–13323. Retrieved from http://www.jstor.org/stable/3073394

Peiffer, **J. A.**, **Spor**, **A.**, **Koren**, **O.**, **Jin**, **Z.**, **Tringe**, **S. G.**, **Dangl**, **J. L.**, **Buckler**, **E. S.**, & **Ley**, **R. E.** (2013). Diversity and heritability of the maize rhizosphere microbiome under field conditions. *Proceedings of the National Academy of Sciences*, *110*(16), 6548–6553.

Penninckx, **I.**, **Eggermont**, **K.**, **Terras**, **F.**, **Thomma**, **B.**, **De Samblanx**, **G. W.**, **Buchala**, **A.**, **Métraux**, **J.-P.**, **Manners**, **J. M.**, & **Broekaert**, **W. F.** (1996). Pathogen-induced systemic activation of a plant defensin gene in arabidopsis follows a salicylic acid-independent pathway. *The Plant Cell*, *8*(12), 2309–2323.

Peters, **N. K.**, & **Long**, **S. R.** (1988). Alfalfa root exudates and compounds which promote or inhibit induction of rhizobium meliloti nodulation genes. *Plant Physiology*, *88*(2), 396. doi:10.1104/pp.88.2.396

Petersen, **T. N.**, **Brunak**, **S.**, **Von Heijne**, **G.**, & **Nielsen**, **H.** (2011). Signalp 4.0: Discriminating signal peptides from transmembrane regions. *Nature methods*, *8*(10), 785.

Pfaffl, **M. W.**, **Horgan**, **G. W.**, & **Dempfle**, **L.** (2002). Relative expression software tool (rest©) for group-wise comparison and statistical analysis of relative expression results in real-time pcr. *Nucleic Acids Research*, *30*(9), e36–e36. doi:10.1093/nar/30.9.e36

Pfanz, **H.**, & **Dietz**, **K.-J.** (1987). A fluorescence method for the determination of the apoplastic proton concentration in intact leaf tissues. *Journal of Plant Physiology*, *129*(1), 41–48. doi:https://doi.org/10.1016/S0176-1617(87)80100-1

Picot, **A.**, **Barreau**, **C.**, **Pinson-Gadais**, **L.**, **Caron**, **D.**, **Lannou**, **C.**, & **Richard-Forget**, **F.** (2010). Factors of the fusarium verticillioides-maize environment modulating fumonisin production. *Critical reviews in microbiology*, *36*(3), 221–231.

Pieterse, **C. M.**, **Van der Does**, **D.**, **Zamioudis**, **C.**, **Leon-Reyes**, **A.**, & **Van Wees**, **S. C.** (2012). Hormonal modulation of plant immunity. *Annual review of cell and developmental biology*, *28*, 489–521.

Plissonneau, **C.**, **Benevenuto**, **J.**, **Mohd-Assaad**, **N.**, **Fouché**, **S.**, **Hartmann**, **F. E.**, & **Croll**, **D.** (2017). Using population and comparative genomics to understand the genetic basis of effector-driven fungal pathogen evolution. *Frontiers in plant science*, *8*, 119.

Podobnik, **M.**, **Kuhelj**, **R.**, **Turk**, **V.**, & **Turk**, **D.** (1997). Crystal structure of the wild-type human procathepsin b at 2.5 a resolution reveals the native active site of a papain-like cysteine protease zymogen. *J Mol Biol*, *271*(5), 774–88. doi:10.1006/jmbi.1997.1218

Rai, **M. K.**, **Shekhawat**, **N. S.**, **Harish**, **Gupta**, **A. K.**, **Phulwaria**, **M.**, **Ram**, **K.**, & **Jaiswal**, **U.** (2011). The role of abscisic acid in plant tissue culture: A review of recent progress. *Plant Cell, Tissue and Organ Culture (PCTOC)*, *106*(2), 179–190. doi:10.1007/s11240-011-9923-9

Rajaraman, **J.**, **Douchkov**, **D.**, **Lück**, **S.**, **Hensel**, **G.**, **Nowara**, **D.**, **Pogoda**, **M.**, **Rutten**, **T.**, **Meitzel**, **T.**, **Brassac**, **J.**, **Höfle**, **C.**, **Hückelhoven**, **R.**, **Klinkenberg**, **J.**, **Trujillo**, **M.**, **Bauer**, **E.**, **Schmutzer**, **T.**, **Himmelbach**, **A.**, **Mascher**, **M.**, **Lazzari**, **B.**, **Stein**, **N.**, **Kumlehn**, **J.**, & **Schweizer**, **P.** (2018). Evolutionarily conserved partial gene duplication in the triticeae tribe of grasses confers pathogen resistance. *Genome Biology*, *19*(1), 116. doi:10.1186/s13059-018-1472-7

Ranum, **P.**, **Peña-Rosas**, **J. P.**, & **Garcia-Casal**, **M. N.** (2014). Global maize production, utilization, and consumption. *Annals of the New York Academy of Sciences*, *1312*(1), 105–112.

Rappsilber, **J.**, **Mann**, **M.**, & **Ishihama**, **Y.** (2007). Protocol for micro-purification, enrichment, prefractionation and storage of peptides for proteomics using stagetips. *Nature Protocols*, *2*(8), 1896–1906. doi:10.1038/nprot.2007.261

Rascovan, **N.**, **Carbonetto**, **B.**, **Perrig**, **D.**, **Díaz**, **M.**, **Canciani**, **W.**, **Abalo**, **M.**, **Alloati**, **J.**, **González-Anta**, **G.**, & **Vazquez**, **M. P.** (2016). Integrated analysis of root microbiomes of soybean and wheat from agricultural fields. *Scientific reports*, *6*, 28084.

Rawlings, **N. D.**, **Barrett**, **A. J.**, **Thomas**, **P. D.**, **Huang**, **X.**, **Bateman**, **A.**, & **Finn**, **R. D.** (2018). The merops database of proteolytic enzymes, their substrates and inhibitors in 2017 and a comparison with peptidases in the panther database. *Nucleic acids research*, *46*(D1), D624–D632. doi:10.1093/nar/gkx1134

Ray, **S.**, **Alves**, **P. C. M. S.**, **Ahmad**, **I.**, **Gaffoor**, **I.**, **Acevedo**, **F. E.**, **Peiffer**, **M.**, **Jin**, **S.**, **Han**, **Y.**, **Shakeel**, **S.**, **Felton**, **G. W.**, & **Luthe**, **D. S.** (2016). Turnabout is fair play: Herbivory-induced plant chitinases excreted in fall armyworm frass suppress herbivore defenses in maize. *Plant Physiology*, *171*(1), 694. doi:10.1104/pp.15.01854

Rekhter, **D.**, **Lüdke**, **D.**, **Ding**, **Y.**, **Feussner**, **K.**, **Zienkiewicz**, **K.**, **Lipka**, **V.**, **Wiermer**, **M.**, **Zhang**, **Y.**, & **Feussner**, **I.** (2019). Isochorismate-derived biosynthesis of the plant stress hormone salicylic acid. *Science*, *365*(6452), 498. doi:10.1126/science.aaw1720

Rentsch, **D.**, **Schmidt**, **S.**, & **Tegeder**, **M.** (2007). Transporters for uptake and allocation of organic nitrogen compounds in plants. *FEBS letters*, *581*(12), 2281–2289.

Richau, **K. H.**, **Kaschani**, **F.**, **Verdoes**, **M.**, **Pansuriya**, **T. C.**, **Niessen**, **S.**, **Stüber**, **K.**, **Colby**, **T.**, **Overkleeft**, **H. S.**, **Bogyo**, **M.**, & **Van der Hoorn**, **R. A.** (2012). Subclassification and biochemical analysis of plant papain-like cysteine proteases displays subfamily-specific characteristics. *Plant Physiol*, *158*(4), 1583–99. doi:10.1104/pp.112.194001

Ringli, **C.** (2005). The role of extracellular lrr-extensin (lrx) proteins in cell wall formation. *Plant Biosystems - An International Journal Dealing with all Aspects of Plant Biology*, *139*(1), 32–35. doi:10.1080/11263500500059892

Robert-Seilaniantz, **A.**, **Grant**, **M.**, & **Jones**, **J. D. G.** (2011). Hormone crosstalk in plant disease and defense: More than just jasmonate-salicylate antagonism. *Annu Rev Phytopathol*, *49*, 317–343. Retrieved from %3CGo%20to%20ISI%3E://000294828400016

Roberts, **W. K.**, & **Selitrennikoff**, **C. P.** (1990). Zeamatin, an antifungal protein from maize with membrane-permeabilizing activity. *Microbiology*, *136*(9), 1771–1778. doi:https://doi.org/10.1099/00221287-136-9-1771

Rodrigues, **A. G.**, **Romano de Oliveira Gonçalves**, **P. J.**, **Ottoni**, **C. A.**, **de Cássia Ruiz**, **R.**, **Morgano**, **M. A.**, **de Araújo**, **W. L.**, **de Melo**, **I. S.**, & **De Souza**, **A. O.** (2019). Functional textiles impregnated with biogenic silver nanoparticles from bionectria ochroleuca and its antimicrobial activity. *Biomedical Microdevices*, *21*(3), 56. doi:10.1007/s10544-019-0410-0

Rodrigues, **C.**, **Vandenberghe**, **L. P. d. S.**, **de Oliveira**, **J.**, & **Soccol**, **C. R.** (2012). New perspectives of gibberellic acid production: A review. *Critical Reviews in Biotechnology*, *32*(3), 263–273. doi:10.3109/07388551.2011.615297

Romero, **F. M.**, **Marina**, **M.**, & **Pieckenstain**, **F. L.** (2014). The communities of tomato (solanum lycopersicum l.) leaf endophytic bacteria, analyzed by 16s-ribosomal rna gene pyrosequencing. *FEMS Microbiology Letters*, *351*(2), 187–194. doi:10.1111/1574-6968.12377

Rooney, **H. C.**, **van't Klooster**, **J. W.**, **van der Hoorn**, **R. A.**, **Joosten**, **M. H.**, **Jones**, **J. D.**, & **de Wit**, **P. J.** (2005). Cladosporium avr2 inhibits tomato rcr3 protease required for cf-2-dependent disease resistance. *Science*, *308*(5729), 1783–6. doi:10.1126/science.1111404

Rosenberg, **E.**, **Koren**, **O.**, **Reshef**, **L.**, **Efrony**, **R.**, & **Zilber-Rosenberg**, **I.** (2007). The role of microorganisms in coral health, disease and evolution. *Nature Reviews Microbiology*, *5*(5), 355.

Rosenberg, **E.**, & **Zilber-Rosenberg**, **I.** (2016). Microbes drive evolution of animals and plants: The hologenome concept. *MBio*, *7*(2), e01395–15.

Rudrappa, **T.**, **Czymmek**, **K. J.**, **Paré**, **P. W.**, & **Bais**, **H. P.** (2008). Root-secreted malic acid recruits beneficial soil bacteria. *Plant physiology*, *148*(3), 1547–1556.

Ryals, **J.**, **Lawton**, **K. A.**, **Delaney**, **T. P.**, **Friedrich**, **L.**, **Kessmann**, **H.**, **Neuenschwander**, **U.**, **Uknes**, **S.**, **Vernooij**, **B.**, & **Weymann**, **K.** (1995). Signal transduction in systemic acquired resistance. *Proceedings of the National Academy of Sciences*, *92*(10), 4202–4205.

Rzychon, **M.**, **Chmiel**, **D.**, & **Stec-Niemczyk**, **J.** (2004). Modes of inhibition of cysteine proteases. *Acta Biochim. Pol*, *51*(4), 861–873.

Samad, **A.**, **Trognitz**, **F.**, **Compant**, **S.**, **Antonielli**, **L.**, & **Sessitsch**, **A.** (2017). Shared and host-specific microbiome diversity and functioning of grapevine and accompanying weed plants. *Environmental Microbiology*, *19*(4), 1407–1424. doi:10.1111/1462-2920.13618

Samaga, **P. V.**, **Rai**, **V. R.**, & **Rai**, **K. M. L.** (2014). Bionectria ochroleuca notl33—an endophytic fungus from nothapodytes foetida producing antimicrobial and free radical scavenging metabolites. *Annals of Microbiology*, *64*(1), 275–285. doi:10.1007/s13213-013-0661-6

Schechter, **I.**, & **Berger**, **A.** (1967). On the size of the active site in proteases. i. *Biochem. Biophys. Res. Commun*, *27*(2), 157–162.

Schilling, **O.** [O.], **auf dem Keller**, **U.**, & **Overall**, **C. M.** (2011). Protease specificity profiling by tandem mass spectrometry using proteome-derived peptide libraries. *Methods Mol Biol*, *753*, 257–72. doi:10.1007/978-1-61779-148-2_17

Schilling, **O.** [Oliver], & **Overall**, **C. M.** (2008). Proteome-derived, database-searchable peptide libraries for identifying protease cleavage sites. *Nature biotechnology*, *26*(6), 685.

Schimoler-O'Rourke, **R.**, **Richardson**, **M.**, & **Selitrennikoff**, **C. P.** (2001). Zeamatin inhibits trypsin and alpha-amylase activities. *Appl. Environ. Microbiol.*, *67*(5), 2365–2366.

Schlaeppi, **K.**, **Dombrowski**, **N.**, **Oter**, **R. G.**, **Ver Loren van Themaat**, **E.**, & **Schulze-Lefert**, **P.** (2014). Quantitative divergence of the bacterial root microbiota in arabidopsis thaliana relatives. *Proceedings of the National Academy of Sciences*, *111*(2), 585. doi:10.1073/pnas.1321597111

Schlatter, **D.**, **Kinkel**, **L.**, **Thomashow**, **L.**, **Weller**, **D.**, & **Paulitz**, **T.** (2017). Disease suppressive soils: New insights from the soil microbiome. *Phytopathology*, *107*(11), 1284–1297.

Schröder, **B. A.**, **Wrocklage**, **C.**, **Hasilik**, **A.**, & **Saftig**, **P.** (2010). The proteome of lysosomes. *Proteomics*, *10*(22), 4053–4076.

Schulze Hüynck, **J.**, **Kaschani**, **F.**, **van der Linde**, **K.**, **Ziemann**, **S.**, **Muller**, **A. N.**, **Colby**, **T.**, **Kaiser**, **M.**, **Misas Villamil**, **J. C.**, & **Doehlemann**, **G.** (2019). Proteases underground: Analysis of the maize root apoplast identifies organ specific papain-like cysteine protease activity. *Front Plant Sci*, *10*, 473. doi:10.3389/fpls.2019.00473

Sekhon, **R. S.** [R. S.], **Lin**, **H.**, **Childs**, **K. L.**, **Hansey**, **C. N.**, **Buell**, **C. R.**, **de Leon**, **N.**, & **Kaeppler**, **S. M.** (2011). Genome-wide atlas of transcription during maize development. *The Plant Journal*, *66*(4), 553–63. doi:10.1111/j.1365-313X.2011.04527.x

Sekhon, **R. S.** [Rajandeep S.], **Saski**, **C.**, **Kumar**, **R.**, **Flinn**, **B.**, **Luo**, **F.**, **Beissinger**, **T. M.**, **Ackerman**, **A. J.**, **Breitzman**, **M. W.**, **Bridges**, **W. C.**, **de Leon**, **N.**, & **Kaeppler**, **S. M.** (2019). Integrated genome-scale analysis identifies novel genes and networks underlying senescence in maize. *The Plant Cell*, tpc.00930.2018. doi:10.1105/tpc.18.00930

Seybold, **H.**, **Trempel**, **F.**, **Ranf**, **S.**, **Scheel**, **D.**, **Romeis**, **T.**, & **Lee**, **J.** (2014). Ca2+ signalling in plant immune response: From pattern recognition receptors to ca2+ decoding mechanisms. *New Phytologist*, *204*(4), 782–790.

Shabab, **M.**, **Shindo**, **T.**, **Gu**, **C.**, **Kaschani**, **F.**, **Pansuriya**, **T.**, **Chintha**, **R.**, **Harzen**, **A.**, **Colby**, **T.**, **Kamoun**, **S.**, & **van der Hoorn**, **R. A.** (2008). Fungal effector protein avr2 targets diversifying defense-related cys proteases of tomato. *Plant Cell*, *20*(4), 1169–1183. doi:10.1105/tpc.107.056325

Shade, **A.**, **Jacques**, **M.-A.**, & **Barret**, **M.** (2017). Ecological patterns of seed microbiome diversity, transmission, and assembly. *Current opinion in microbiology*, *37*, 15–22.

Shah, **J.** (2003). The salicylic acid loop in plant defense. *Current Opinion in Plant Biology*, *6*(4), 365–371. doi:https://doi.org/10.1016/S1369-5266(03)00058-X

Sheard, **L. B.**, **Tan**, **X.**, **Mao**, **H.**, **Withers**, **J.**, **Ben-Nissan**, **G.**, **Hinds**, **T. R.**, **Kobayashi**, **Y.**, **Hsu**, **F.-F.**, **Sharon**, **M.**, & **Browse**, **J.** (2010). Jasmonate perception by inositol-phosphate-potentiated coi1–jaz co-receptor. *Nature*, *468*(7322), 400.

Shen, **J.**, **Zeng**, **Y.**, **Zhuang**, **X.**, **Sun**, **L.**, **Yao**, **X.**, **Pimpl**, **P.**, & **Jiang**, **L.** (2013). Organelle ph in the arabidopsis endomembrane system. *Molecular Plant*, *6*(5), 1419–1437. doi:https://doi.org/10.1093/mp/sst079

Shi, **Y.**, **Yang**, **H.**, **Zhang**, **T.**, **Sun**, **J.**, & **Lou**, **K.** (2014). Illumina-based analysis of endophytic bacterial diversity and space-time dynamics in sugar beet on the north slope of tianshan mountain. *Applied Microbiology and Biotechnology*, *98*(14), 6375–6385. doi:10.1007/s00253-014-5720-9

Shindo, **T.** [T.], & **van der Hoorn**, **R. A.** (2008). Papain-like cysteine proteases: Key players at molecular battlefields employed by both plants and their invaders. *Mol Plant Pathol*, *9*(1), 119–25. doi:10.1111/j.1364-3703.2007.00439.x

Shindo, **T.** [Takayuki], **Misas-Villamil**, **J. C.**, **Hörger**, **A. C.**, **Song**, **J.**, & **van der Hoorn**, **R. A. L.** (2012). A role in immunity for arabidopsis cysteine protease rd21, the ortholog of the tomato immune protease c14. *PLOS ONE*, *7*(1), e29317. doi:10.1371/journal.pone.0029317

Sivaraman, **J.**, **Lalumiere**, **M.**, **Menard**, **R.**, & **Cygler**, **M.** (1999). Crystal structure of wild-type human procathepsin k. *Protein Sci*, *8*(2), 283–90. doi:10.1110/ps.8.2.283

Smertenko, **A. P.**, **Bozhkov**, **P. V.**, **Filonova**, **L. H.**, **von Arnold**, **S.**, & **Hussey**, **P. J.** (2003). Reorganisation of the cytoskeleton during developmental programmed cell death in picea abies embryos. *The Plant Journal*, *33*(5), 813–824. doi:10.1046/j.1365-313X.2003.01670.x

Šmid, **I.**, **Rotter**, **A.**, **Gruden**, **K.**, **Brzin**, **J.**, **Buh Gašparič**, **M.**, **Kos**, **J.**, **Žel**, **J.**, & **Sabotič**, **J.** (2015). Clitocypin, a fungal cysteine protease inhibitor, exerts its insecticidal effect on colorado

potato beetle larvae by inhibiting their digestive cysteine proteases. *Pesticide Biochemistry and Physiology*, *122*, 59–66. doi:https://doi.org/10.1016/j.pestbp.2014.12.022

Song, **J.**, **Win**, **J.**, **Tian**, **M.**, **Schornack**, **S.**, **Kaschani**, **F.**, **Ilyas**, **M.**, **van der Hoorn**, **R. A.**, & **Kamoun**, **S.** (2009). Apoplastic effectors secreted by two unrelated eukaryotic plant pathogens target the tomato defense protease rcr3. *Proc Natl Acad Sci U S A*, *106*(5), 1654–9. doi:10.1073/pnas.0809201106

Sørensen, **J.**, & **Sessitsch**, **A.** (2007). Plant-associated bacteria - lifestyle and molecular interactions. *Modern Soil Microbiology*, 211–236.

Stamatakis, **A.** (2014). Raxml version 8: A tool for phylogenetic analysis and post-analysis of large phylogenies. *Bioinformatics*, *30*(9), 1312–3. doi:10.1093/bioinformatics/btu033

Stelpflug, **S. C.**, **Sekhon**, **R. S.**, **Vaillancourt**, **B.**, **Hirsch**, **C. N.**, **Buell**, **C. R.**, **de Leon**, **N.**, & **Kaeppler**, **S. M.** (2016). An expanded maize gene expression atlas based on rna sequencing and its use to explore root development. *The plant genome*, *9*(1).

Stennicke, **H. R.**, **Ryan**, **C. A.**, & **Salvesen**, **G. S.** (2002). Reprieval from execution: The molecular basis of caspase inhibition. *Trends in Biochemical Sciences*, *27*(2), 94–101. doi:https://doi.org/10.1016/S0968-0004(01)02045-X

Stergiopoulos, **I.**, & **de Wit**, **P. J.** [P. J.]. (2009). Fungal effector proteins. *Annu Rev Phytopathol*, *47*, 233–63. doi:10.1146/annurev.phyto.112408.132637

Steven, **B.**, **Huntley**, **R. B.**, & **Zeng**, **Q.** (2018). The influence of flower anatomy and apple cultivar on the apple flower phytobiome. *Phytobiomes*, *2*(3), 171–179.

Stubbs, **M. T.**, **Laber**, **B.**, **Bode**, **W.**, **Huber**, **R.**, **Jerala**, **R.**, **Lenarčič**, **B.**, & **Turk**, **V.** (1990). The refined 2.4 å x-ray crystal structure of recombinant human stefin b in complex with the cysteine proteinase papain: A novel type of proteinase inhibitor interaction. *EMBO J*, *9*(6), 1939–47. Retrieved from http://www.ncbi.nlm.nih.gov/entrez/query.fcgi?cmd=Retrieve&db=PubMed&dopt=Citation&list_uids=2347312%20http://www.ncbi.nlm.nih.gov/pmc/articles/PMC551902/pdf/emboj00233-0254.pdf?tool=pmcentrez

Subramanian, **K.**, **Balakrishnan**, **N.**, & **Senthil**, **N.** (2013). Mycorrhizal symbiosis to increase the grain micronutrient content in maize. *Australian Journal of Crop Science*, *7*(7), 900.

Tada, **Y.**, **Spoel**, **S. H.**, **Pajerowska-Mukhtar**, **K.**, **Mou**, **Z.**, **Song**, **J.**, **Wang**, **C.**, **Zuo**, **J.**, & **Dong**, **X.** (2008). Plant immunity requires conformational charges of npr1 via s-nitrosylation and thioredoxins. *Science*, *321*(5891), 952–956.

Tanaka, **Y.**, **Matsuoka**, **M.**, **Yamanoto**, **N.**, **Ohashi**, **Y.**, **Kano-Murakami**, **Y.**, & **Ozeki**, **Y.** (1989). Structure and characterization of a cdna clone for phenylalanine ammonia-lyase from cut-injured roots of sweet potato. *Plant Physiology*, *90*(4), 1403. doi:10.1104/pp.90.4.1403

The UniProt, **C.** (2018). Uniprot: A worldwide hub of protein knowledge. *Nucleic Acids Research*, *47*(D1), D506–D515. doi:10.1093/nar/gky1049

Thomas, **S. G.**, **Huang**, **S.**, **Li**, **S.**, **Staiger**, **C. J.**, & **Franklin-Tong**, **V. E.** (2006). Actin depolymerization is sufficient to induce programmed cell death in self-incompatible pollen. *J Cell Biol*, *174*(2), 221–229.

Thomashow, **L. S.**, & **Weller**, **D. M.** (1988). Role of a phenazine antibiotic from pseudomonas fluorescens in biological control of gaeumannomyces graminis var. tritici. *Journal of Bacteriology*, *170*(8), 3499. doi:10.1128/jb.170.8.3499-3508.1988

Tian, **M.**, **Win**, **J.**, **Song**, **J.**, **van der Hoorn**, **R.**, **van der Knaap**, **E.**, & **Kamoun**, **S.** (2007). A phytophthora infestans cystatin-like protein targets a novel tomato papain-like apoplastic protease. *Plant Physiol*, *143*(1), 364–77. doi:10.1104/pp.106.090050

Trivedi, **P.**, **Delgado-Baquerizo**, **M.**, **Trivedi**, **C.**, **Hamonts**, **K.**, **Anderson**, **I. C.**, & **Singh**, **B. K.** (2017). Keystone microbial taxa regulate the invasion of a fungal pathogen in agroecosystems. *Soil Biology and Biochemistry*, *111*, 10–14.

Tronchet, **M.**, **BalaguÉ**, **C.**, **Kroj**, **T.**, **Jouanin**, **L.**, & **Roby**, **D.** (2010). Cinnamyl alcohol dehydrogenases-c and d, key enzymes in lignin biosynthesis, play an essential role in disease resistance in arabidopsis. *Molecular Plant Pathology*, *11*(1), 83–92. doi:10.1111/j.1364-3703.2009.00578.x

Turk, **D.**, **Podobnik**, **M.**, **Popovic**, **T.**, **Katunuma**, **N.**, **Bode**, **W.**, **Huber**, **R.**, & **Turk**, **V.** (1995). Crystal structure of cathepsin b inhibited with ca030 at 2.0-. ang. resolution: A basis for the design of specific epoxysuccinyl inhibitors. *Biochemistry*, *34*(14), 4791–4797.

Turk, **V.**, & **Bode**, **W.** [W.]. (1991). The cystatins: Protein inhibitors of cysteine proteinases. *FEBS Lett*, *285*(2), 213–9. doi:0014-5793(91)80804-C

Turner, **T. R.**, **James**, **E. K.**, & **Poole**, **P. S.** (2013). The plant microbiome. *Genome biology*, *14*(6), 209.

Tyanova, **S.**, **Temu**, **T.**, **Sinitcyn**, **P.**, **Carlson**, **A.**, **Hein**, **M. Y.**, **Geiger**, **T.**, **Mann**, **M.**, & **Cox**, **J.** (2016). The perseus computational platform for comprehensive analysis of (prote)omics data. *Nature Methods*, *13*, 731. doi:10.1038/nmeth.3901

van der Does, **H. C.**, **Duyvesteijn**, **R. G.**, **Goltstein**, **P. M.**, **van Schie**, **C. C.**, **Manders**, **E. M.**, **Cornelissen**, **B. J.**, & **Rep**, **M.** (2008). Expression of effector gene six1 of fusarium oxysporum requires living plant cells. *Fungal Genetics and Biology*, *45*(9), 1257–1264.

van der Heijden, **M. G.**, & **Schlaeppi**, **K.** (2015). Root surface as a frontier for plant microbiome research. *Proceedings of the National Academy of Sciences*, *112*(8), 2299–2300.

van der Hoorn, **R. A.**, & **Jones**, **J. D.** (2004). The plant proteolytic machinery and its role in defence. *Curr Opin Plant Biol*, *7*(4), 400–7. doi:10.1016/j.pbi.2004.04.003

van der Hoorn, **R. A. L.** (2008). Plant proteases: From phenotypes to molecular mechanisms. *Annu Rev Plant Biol*, *59*(1), 191–223. doi:10.1146/annurev.arplant.59.032607.092835

van der Hoorn, **R. A. L.**, & **Kamoun**, **S.** (2008). From guard to decoy: A new model for perception of plant pathogen effectors. *The Plant Cell*, *20*(8), 2009–2017.

van der Hoorn, **R. A. L.**, **Leeuwenburgh**, **M. A.**, **Bogyo**, **M.**, **Joosten**, **M. H. A. J.**, & **Peck**, **S. C.** (2004). Activity profiling of papain-like cysteine proteases in plants. *Plant Physiol*, *135*(3), 1170–1178. doi:10.1104/pp.104.041467

van der Linde, **K.**, **Hemetsberger**, **C.**, **Kastner**, **C.**, **Kaschani**, **F.**, **van der Hoorn**, **R. A.**, **Kumlehn**, **J.**, & **Doehlemann**, **G.** (2012). A maize cystatin suppresses host immunity by inhibiting apoplastic cysteine proteases. *Plant Cell*, *24*(3), 1285–300. doi:10.1105/tpc.111.093732

van der Linde, **K.**, **Mueller**, **A. N.**, **Hemetsberger**, **C.**, **Kashani**, **F.**, **van der Hoorn**, **R. A.**, & **Doehlemann**, **G.** (2012). The maize cystatin cc9 interacts with apoplastic cysteine proteases. *Plant Signal Behav*, *7*(11), 1397–401. doi:10.4161/psb.21902

van der Wel, **H.**, & **Loeve**, **K.** (1972). Isolation and characterization of thaumatin i and ii, the sweet-tasting proteins from thaumatococcus daniellii benth. *European Journal of Biochemistry*, *31*(2), 221–225.

van Loon, **L.**, **Rep**, **M.**, & **Pieterse**, **C.** (2006). Significance of inducible defense-related proteins in infected plants. *Annu Rev Phytopathol*, *44*(1), 135–162. doi:10.1146/annurev.phyto.44.070505.143425

Vandenkoornhuyse, **P.**, **Quaiser**, **A.**, **Duhamel**, **M.**, **Le Van**, **A.**, & **Dufresne**, **A.** (2015). The importance of the microbiome of the plant holobiont. *New Phytologist*, *206*(4), 1196–1206. doi:10.1111/nph.13312

Vernooij, **B.**, **Friedrich**, **L.**, **Morse**, **A.**, **Reist**, **R.**, **Kolditz-Jawhar**, **R.**, **Ward**, **E.**, **Uknes**, **S.**, **Kessmann**, **H.**, & **Ryals**, **J.** (1994). Salicylic acid is not the translocated signal responsible for inducing systemic acquired resistance but is required in signal transduction. *The Plant Cell*, *6*(7), 959–965.

Vives-Peris, **V.**, **Gómez-Cadenas**, **A.**, & **Pérez-Clemente**, **R. M.** (2018). Salt stress alleviation in citrus plants by plant growth-promoting rhizobacteria pseudomonas putida and novosphingobium sp. *Plant Cell Reports*, *37*(11), 1557–1569. doi:10.1007/s00299-018-2328-z

Vizcaíno, **J. A.**, **Csordas**, **A.**, **del-Toro**, **N.**, **Dianes**, **J. A.**, **Griss**, **J.**, **Lavidas**, **I.**, **Mayer**, **G.**, **Perez-Riverol**, **Y.**, **Reisinger**, **F.**, **Ternent**, **T.**, **Xu**, **Q.-W.**, **Wang**, **R.**, & **Hermjakob**, **H.** (2015). 2016 update of the pride database and its related tools. *Nucleic Acids Research*, *44*(D1), D447–D456. doi:10.1093/nar/gkv1145

Vorholt, **J. A.** (2012). Microbial life in the phyllosphere. *Nature Reviews Microbiology*, *10*(12), 828.

Wallace, **J. G.**, **Kremling**, **K. A.**, **Kovar**, **L. L.**, & **Buckler**, **E. S.** (2018). Quantitative genetics of the maize leaf microbiome. *Phytobiomes Journal*, *2*(4), 208–224.

Walley, **J. W.**, **Sartor**, **R. C.**, **Shen**, **Z.**, **Schmitz**, **R. J.**, **Wu**, **K. J.**, **Urich**, **M. A.**, **Nery**, **J. R.**, **Smith**, **L. G.**, **Schnable**, **J. C.**, **Ecker**, **J. R.**, & **Briggs**, **S. P.** (2016). Integration of omic networks in a developmental atlas of maize. *Science*, *353*(6301), 814. doi:10.1126/science.aag1125

Wang, **B.**, **You**, **J.**, **King**, **J. B.**, **Cai**, **S.**, **Park**, **E.**, **Powell**, **D. R.**, & **Cichewicz**, **R. H.** (2014). Polyketide glycosides from bionectria ochroleuca inhibit candida albicans biofilm formation. *Journal of Natural Products*, *77*(10), 2273–2279. doi:10.1021/np500531j

Wang, **J.** [Jizong], **Hu**, **M.**, **Wang**, **J.**, **Qi**, **J.**, **Han**, **Z.**, **Wang**, **G.**, **Qi**, **Y.**, **Wang**, **H.-W.**, **Zhou**, **J.-M.**, & **Chai**, **J.** (2019). Reconstitution and structure of a plant nlr resistosome conferring immunity. *Science*, *364*(6435), eaav5870.

Wang, **J.** [Jizong], **Wang**, **J.** [Jia], **Hu**, **M.**, **Wu**, **S.**, **Qi**, **J.**, **Wang**, **G.**, **Han**, **Z.**, **Qi**, **Y.**, **Gao**, **N.**, & **Wang**, **H.-W.** (2019). Ligand-triggered allosteric adp release primes a plant nlr complex. *Science*, *364*(6435), eaav5868.

Wang, **S. X.**, **Pandey**, **K. C.**, **Scharfstein**, **J.**, **Whisstock**, **J.**, **Huang**, **R. K.**, **Jacobelli**, **J.**, **Fletterick**, **R. J.**, **Rosenthal**, **P. J.**, **Abrahamson**, **M.**, **Brinen**, **L. S.**, **Rossi**, **A.**, **Sali**, **A.**, & **McKerrow**, **J. H.** (2007). The structure of chagasin in complex with a cysteine protease clarifies the binding

mode and evolution of an inhibitor family. *Structure*, *15*(5), 535–543. doi:https://doi.org/10.1016/j.str.2007.03.012

Weber, **E.**, **Engler**, **C.**, **Gruetzner**, **R.**, **Werner**, **S.**, & **Marillonnet**, **S.** (2011). A modular cloning system for standardized assembly of multigene constructs. *PLoS One*, *6*(2), e16765. doi:10.1371/journal.pone.0016765

Wiederanders, **B.**, **Kaulmann**, **G.**, & **Schilling**, **K.** (2003). Functions of propeptide parts in cysteine proteases. *Current Protein and Peptide Science*, *4*(5), 309–326. doi:10.2174/1389203033487081

Wildermuth, **M. C.**, **Dewdney**, **J.**, **Wu**, **G.**, & **Ausubel**, **F. M.** (2001). Isochorismate synthase is required to synthesize salicylic acid for plant defence. *Nature*, *414*(6863), 562–5. doi:10.1038/35107108

Winter, **D.**, **Vinegar**, **B.**, **Nahal**, **H.**, **Ammar**, **R.**, **Wilson**, **G. V.**, & **Provart**, **N. J.** (2007). An "electronic fluorescent pictograph" browser for exploring and analyzing large-scale biological data sets. *PLOS ONE*, *2*(8), e718. doi:10.1371/journal.pone.0000718

Wu, **C.-H.**, **Krasileva**, **K. V.**, **Banfield**, **M. J.**, **Terauchi**, **R.**, & **Kamoun**, **S.** (2015). The "sensor domains" of plant nlr proteins: More than decoys? *Frontiers in plant science*, *6*, 134.

Yamada, **K.**, **Matsushima**, **R.**, **Nishimura**, **M.**, & **Hara-Nishimura**, **I.** (2001). A slow maturation of a cysteine protease with a granulin domain in the vacuoles of senescing arabidopsis leaves. *Plant Physiology*, *127*(4), 1626. doi:10.1104/pp.010551

Yan, **J.**, **Yuan**, **S.-s.**, **Jiang**, **L.-l.**, **Ye**, **X.-j.**, **Ng**, **T. B.**, & **Wu**, **Z.-j.** (2015). Plant antifungal proteins and their applications in agriculture. *Applied microbiology and biotechnology*, *99*(12), 4961–4981.

Yan, **S. C. B.**, **Grinnell**, **B. W.**, & **Wold**, **F.** (1989). Post-translational modifications of proteins: Some problems left to solve. *Trends in Biochemical Sciences*, *14*(7), 264–268. doi:https://doi.org/10.1016/0968-0004(89)90060-1

Yang, **J.**, **Kloepper**, **J. W.**, & **Ryu**, **C.-M.** (2009). Rhizosphere bacteria help plants tolerate abiotic stress. *Trends in plant science*, *14*(1), 1–4.

Yang, **Y.**, **Dong**, **C.**, **Yu**, **J.**, **Shi**, **L.**, **Tong**, **C.**, **Li**, **Z.**, **Huang**, **J.**, & **Liu**, **S.** (2014). Cysteine protease 51 (cp51), an anther-specific cysteine protease gene, is essential for pollen exine formation in arabidopsis. *Plant Cell, Tissue and Organ Culture (PCTOC)*, *119*(2), 383–397.

Yang, **Y.-X.**, **J. Ahammed**, **G.**, **Wu**, **C.**, **Fan**, **S.-y.**, & **Zhou**, **Y.-H.** (2015). Crosstalk among jasmonate, salicylate and ethylene signaling pathways in plant disease and immune responses. *Current Protein and Peptide Science*, *16*(5), 450–461. Retrieved from https://www.ingentaconnect.com/content/ben/cpps/2015/00000016/00000005/art00010

Young, **I. M.**, & **Crawford**, **J. W.** (2004). Interactions and self-organization in the soil-microbe complex. *Science*, *304*(5677), 1634–1637.

Zarraonaindia, **I.**, **Owens**, **S. M.**, **Weisenhorn**, **P.**, **West**, **K.**, **Hampton-Marcell**, **J.**, **Lax**, **S.**, **Bokulich**, **N. A.**, **Mills**, **D. A.**, **Martin**, **G.**, & **Taghavi**, **S.** (2015). The soil microbiome influences grapevine-associated microbiota. *MBio*, *6*(2), e02527–14.

Zhalnina, **K.**, **Louie**, **K. B.**, **Hao**, **Z.**, **Mansoori**, **N.**, **da Rocha**, **U. N.**, **Shi**, **S.**, **Cho**, **H.**, **Karaoz**, **U.**, **Loqué**, **D.**, **Bowen**, **B. P.**, **Firestone**, **M. K.**, **Northen**, **T. R.**, & **Brodie**, **E. L.** (2018). Dynamic root exudate chemistry and microbial substrate preferences drive patterns in rhizosphere mi-

crobial community assembly. *Nature Microbiology*, *3*(4), 470–480. doi:$10.1038/s41564\text{-}018\text{-}0129\text{-}3$

Zhao, **P.**, **Zhou**, **X.-m.**, **Zhang**, **L.-y.**, **Wang**, **W.**, **Ma**, **L.-g.**, **Yang**, **L.-b.**, **Peng**, **X.-b.**, **Bozhkov**, **P. V.**, & **Sun**, **M.-x.** (2013). A bipartite molecular module controls cell death activation in the basal cell lineage of plant embryos. *PLoS biology*, *11*(9), e1001655.

Ziemann, **S.**, **van der Linde**, **K.**, **Lahrmann**, **U.**, **Acar**, **B.**, **Kaschani**, **F.**, **Colby**, **T.**, **Kaiser**, **M.**, **Ding**, **Y.**, **Schmelz**, **E.**, **Huffaker**, **A.**, **Holton**, **N.**, **Zipfel**, **C.**, & **Doehlemann**, **G.** (2018). An apoplastic peptide activates salicylic acid signalling in maize. *Nat Plants*, *4*(3), 172–180. doi:$10.1038/s41477\text{-}018\text{-}0116\text{-}y$

Zipfel, **C.** [C.], **Kunze**, **G.**, **Chinchilla**, **D.**, **Caniard**, **A.**, **Jones**, **J. D.**, **Boller**, **T.**, & **Felix**, **G.** (2006). Perception of the bacterial pamp ef-tu by the receptor efr restricts agrobacterium-mediated transformation. *Cell*, *125*(4), 749–60. doi:$10.1016/j.cell.2006.03.037$

Zipfel, **C.** [Cyril]. (2014). Plant pattern-recognition receptors. *Trends in immunology*, *35*(7), 345–351.

6 Appendix
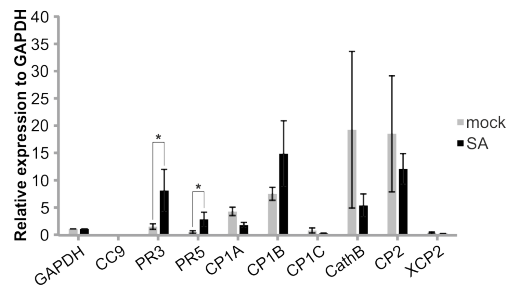
Figure 6.1: **Expression pattern of root apoplastic maize PLCPs upon SA-treatment.**
qPCR analysis of maize roots treated with – or without SA. Expression for the SA-marker genes PR3 and PR5 and the maize PLCPs: CP1A, CP1B, CP1C, CathB, CP2 and XCP2 is displayed. Expression was normalised to expression levels of the housekeeping gene GAPDH. CC9 was included as a control for maize JA marker genes. Error bars represent the SEM. P-values were calculated with an unpaired t-test. *P<0.05. The experiment was performed in three independent biological replicates using technical triplicates.
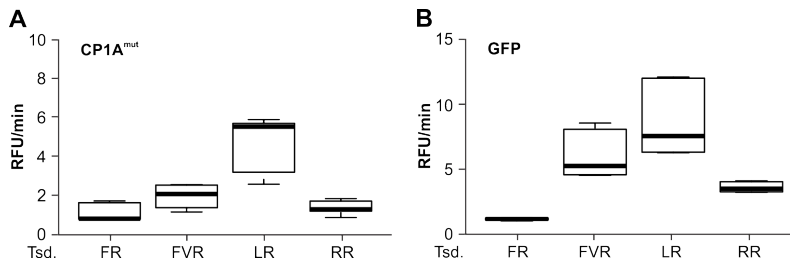
Figure 6.2: **Substrate cleavage assay of the catalytic inactive PLCP CP1A^{mut} and GFP.**
Apoplastic fluids of *N. benthamiana* overexpressed CP1A^{mut} **(A)** and GFP **(B)** were tested for their activity using 10 µM of the following substrates: Z-FR-AMC (FR), BZ-FVR-AMC (FVR), Z-LR-AMC (LR) and Z-RR-AMC (RR). The release of AMC (relative fluorescent unit = RFU) per minute was measured and plotted for each substrate. Activity was normalized to E-64 treated samples. Data was represented in a boxplot as described before. This experiment was performed using three independent biological replicates each with technical duplicates.
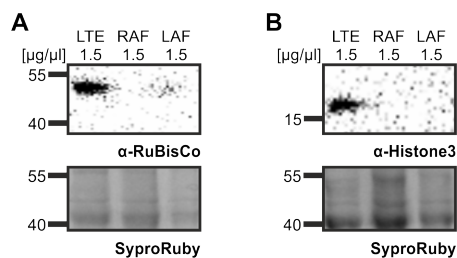
Figure 6.3: **Maize root and leaf apoplastic fluid is clean from cellular contaminants.**
Maize leaf total extract (LTE), root apoplastic fluid (RAF) and leaf apoplastic fluid (LAF) were separated using SDS-PAGE and RuBisCo **(A)** and Histone3 **(B)** were detected using α-RuBisCo and α-Histone3 antibodies, respectively. SyproRuby-staining (Ex. 450 nm, Em. 610 nm) was performed as loading control.
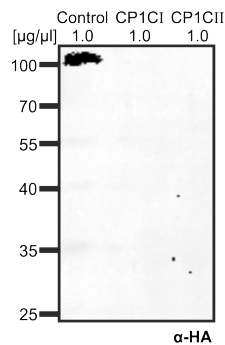
Figure 6.4: **Recombinant CP1C, heterologous expressed in *N. benthamiana* loses the HA-tag.**
Immunoblot of maize root PLCP. CP1C was fused with a C-terminal HA-tag and recombinant expressed in *N. benthamiana*. Leaf apoplastic fluids of two biological replicates (I, II) were isolated and samples were analyzed with SDS-PAGE. HA-tagged proteins were detected using an α-HA antibody followed by an α-mouse-HRP antibody.
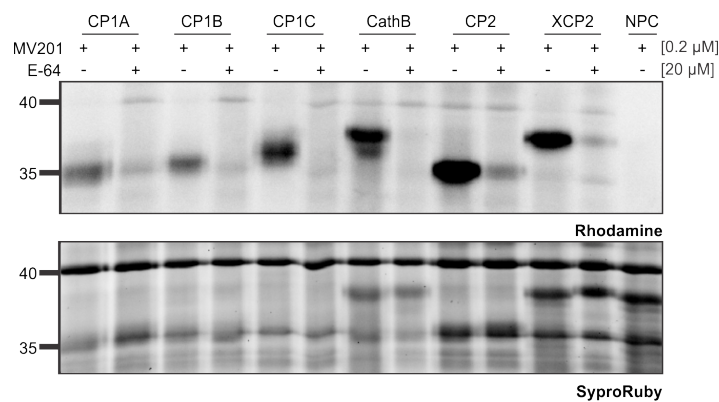
Figure 6.5: **MV201 labeling of recombinant PLCPs.**
Samples were pre-treated for 30 min with (+) or without (-) 20 μM E-64 followed by labeling with 0.2 μM MV201 for 2 h at room temperature. Samples were separated by SDS-PAGE and labeled PLCPs were visualized by fluorescence scanning (Ex. 532 nm, Em. 580 nm). A No-Probe-Control (NPC) was included containing an equal mix of apoplastic fluid, neither treated with E-64, nor with MV201. SyproRuby-staining (Ex. 450 nm, Em. 610 nm) was performed as loading control. Fluorescent quantification was performed to calculate signal intensities of PLCPs. Based on this, samples were normalized to equal amounts of active PLCPs for subsequent assays. This experiment was performed in three independent biological replicates showing similar results.
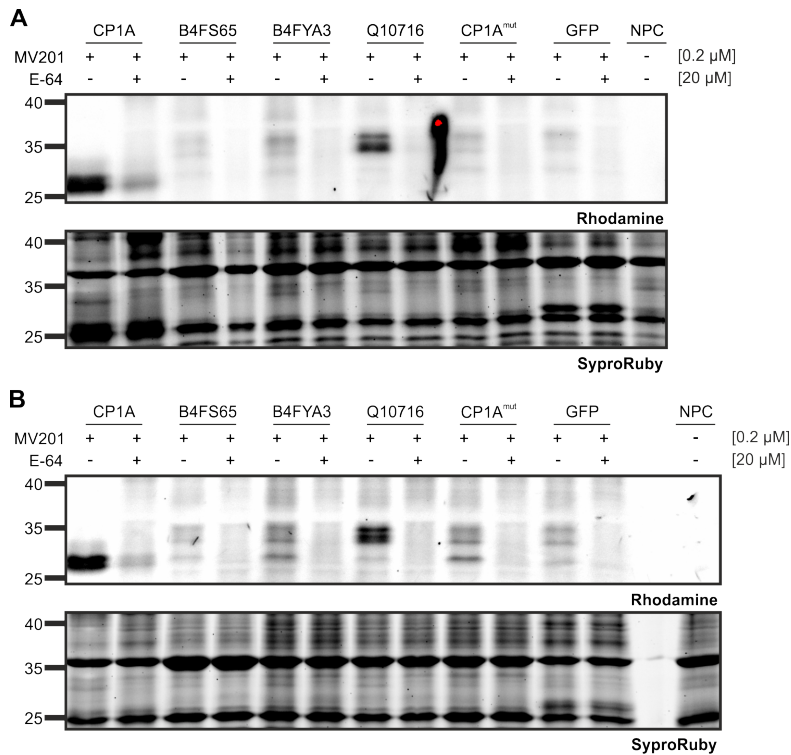
Figure 6.6: **MV201 labeling of recombinant PLCPs treated with mock or SA.**
Activity of recombinant expressed SA-activated maize root PLCPs with mock- **(A)** and with 5 mM SA-treatment **(B)**. Leaves were treated with mock or SA 48 h post infiltration. Leaf apoplastic fluids of *N. benthamiana* overexpressed PLCPs: CP1A, B4FS65, B4FYA3, Q10716, CP1A^{mut} as well as GFP were pre-treated for 30 min with (+) or without (-) 20 µM E-64 followed by labeling with 0.2 µM MV201 (Richau et al., 2012) for 2 h at room temperature. Samples were separated by SDS-PAGE and labeled PLCPs were visualized by fluorescent scanning (Ex. 532 nm, Em. 580 nm). A no-probe-control (NPC) was included containing an equal mix of apoplstic fluid, neither treated with E-64, nor with MV201. SyproRuby-staining (Ex. 450 nm, Em. 610 nm) was performed as loading control. This experiment was performed in three independent biological replicates showing similar results.
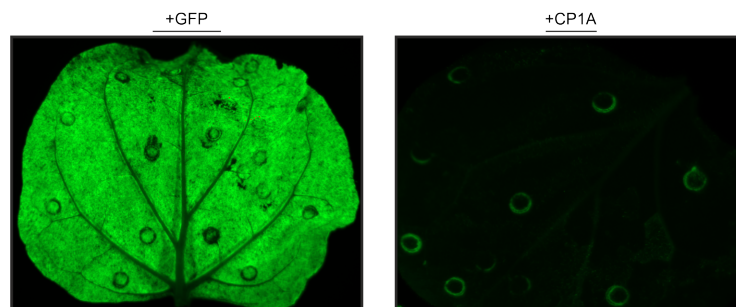
Figure 6.7: **Visual confirmation of successful GFP expression.**
N. benthamiana leaves infiltrated with *A. tumefaciens* for recombinant expression of GFP or CP1A. GFP signal was observed for infiltrated leaves (Ex. 488 nm, Em. 510 nm). Signals in the "+CP1A" sample are due to cell death at infiltration sites. Pictures were taken before AF isolation.
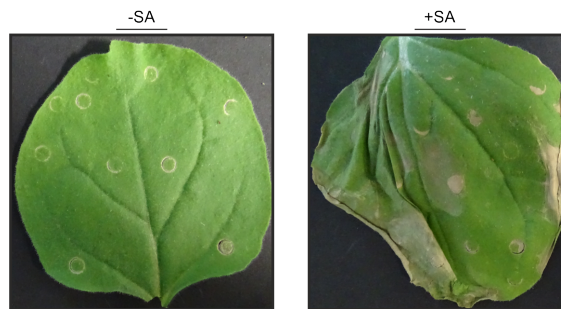
Figure 6.8: **Visual confirmation of successful SA-treatment.**
N. benthamiana leaves infiltrated with *A. tumefaciens* for recombinant expression of maize PLCPs were sprayed with mock or 5 mM SA one day before AF isolation. Pictures were taken at the day of AF isolation.
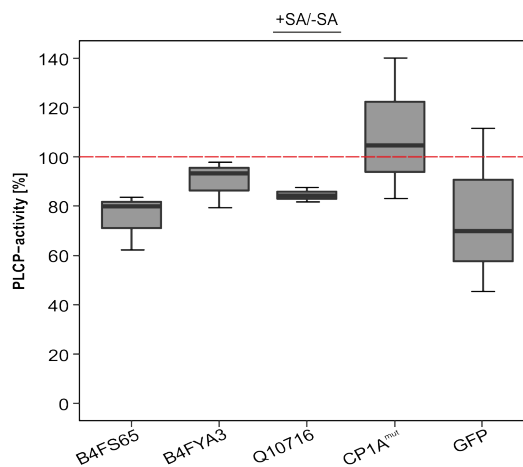
Figure 6.9: **Substrate cleavage assay of recombinant PLCPs treated with - or without SA.**
Maize apoplastic PLCPs: CP1A, B4FS65, B4FYA3, Q10716, CP1A^{mut} as well as GFP were recombinant expressed in *N. benthamiana*. Leaves were treated with mock or SA 48 h post infiltration. Leaf apoplastic fluids were isolated and tested in substrate cleavage assays using 10 μM of the substrate Z-LR-AMC. Mock activity was set to 100% and normalized to E-64 treated samples. Activity of SA-treated samples is displayed relative to activity of mock samples. Data was presented in a boxplot as described before. This experiment was performed using three independent biological replicates each with technical duplicates.
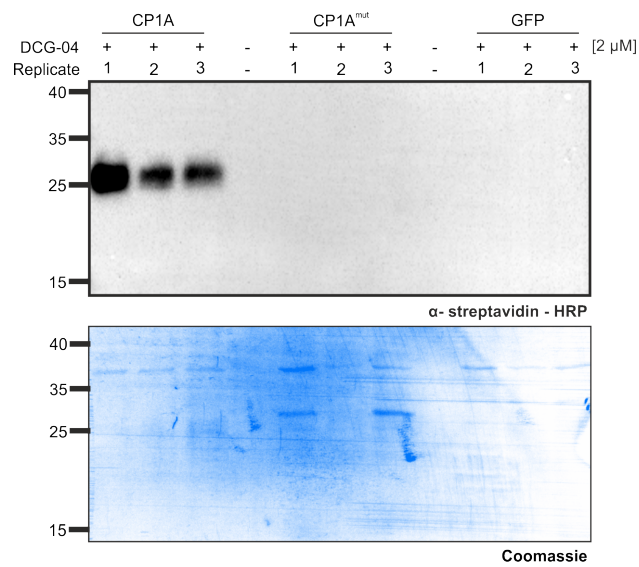
Figure 6.10: **DCG-04 labeling of recombinant expressed proteins in *N. benthamiana.***
Leaf apoplastic fluids of three replicates of recombinant *N. benthamiana* expressed CP1A, CP1A^{mut} and GFP were labelled with the probe DCG-04 to normalize active PLCP content between biological replicates for further assays. Samples were labelled for 2 h with 2 μM DCG-04 and analyzed via SDS-PAGE. Biotinylated proteins were detected using an α-streptavidin-HRP antibody. Coomassie stain shows the loading control.

A

```
          SP
CC1     1 MRKHRIVSLVAA------------LLVLLALAAVSSTRSTQKE--SVADNAG---------
CC9     1 MAFLSTNALMSVPITAAAAPRHRRSLVVVRAAAVKSNEHLQEEQASVADGARGRRRAMVLL
consensus 1 MaflstnaLmsvpitaaaaprhrrsLVvvraAAVkSnehlQeEqaSVADgArgrrramvll
          SP

CC1    39 ----------------------MLAGGIKDVPANENDLQLQELARFAVNEHNQKANALLG
CC9    62 AATAAVTGSSVAICRSARAAGVTTLSGQYVKI-ENVKDPYVQGVGEWAVKEHNRQTGESLQ
consensus 62 aataavtgssvaicrsaraagvttLsGqyvki-eNvkDpyvQgvgewAVkEHNrqtgesLq

                                                              CY
CC1    77 FEKLVKAKTQVVAGTMYYLTIEVKDGEVKKLYEAKVWEKPW--ENFKQLQEFKPVEEGASA
CC9   122 FAEVVSGMEQVVAGTNYKLNLATKDPT--SSYQAVVFDPLPNSSKNRQLMSFKSI------
consensus 122 FaevVsgmeQVVAGTnYkLnlatKDpt--ssYqAvVfdplpnssknrQLmsFKsi------
                                                              CY
```

B

Figure 6.11: **Sequence and structural comparison of CC9 and CC1.**
(A) Sequence homology between CC1 and CC9. Amino acid sequences of CC1 and CC9 were aligned to evaluate their sequence conservation. Black background indicates conserved amino acids among both PLCPs, light grey background indicates similar amino acids among the two PLCPs and white background indicates different amino acids or gaps. Signal peptide (SP, brown), cystatin domain (CY, red) were predicted. Amino acids forming the cystatin type motif QxVxG are labelled in yellow.
(B) A 3D-model of superimposed mature CC9 and CC1 without signal peptide was generated. CC9 (grey) and CC1 (red) were modelled without signal peptide using Phyre2 (Kelley et al., 2015) based on the crystal structure of AcCYS: 2l4v (Irene et al., 2012) and oryzacystatin-I: 1eqk (Nagata et al., 2000), respectively. Amino acids forming the cystatin type motif QxVxG are labelled in yellow.

Figure 6.12: **Plasmid map of the vector pET-15b with CC1-HIS.**
The sequence of CC1 with a N-terminal HIS-tag was integrated in the multiple cloning site of the vector pET-15b (Novagen, Merck, Darmstadt, Germany). The resulting plasmid map is displayed here.
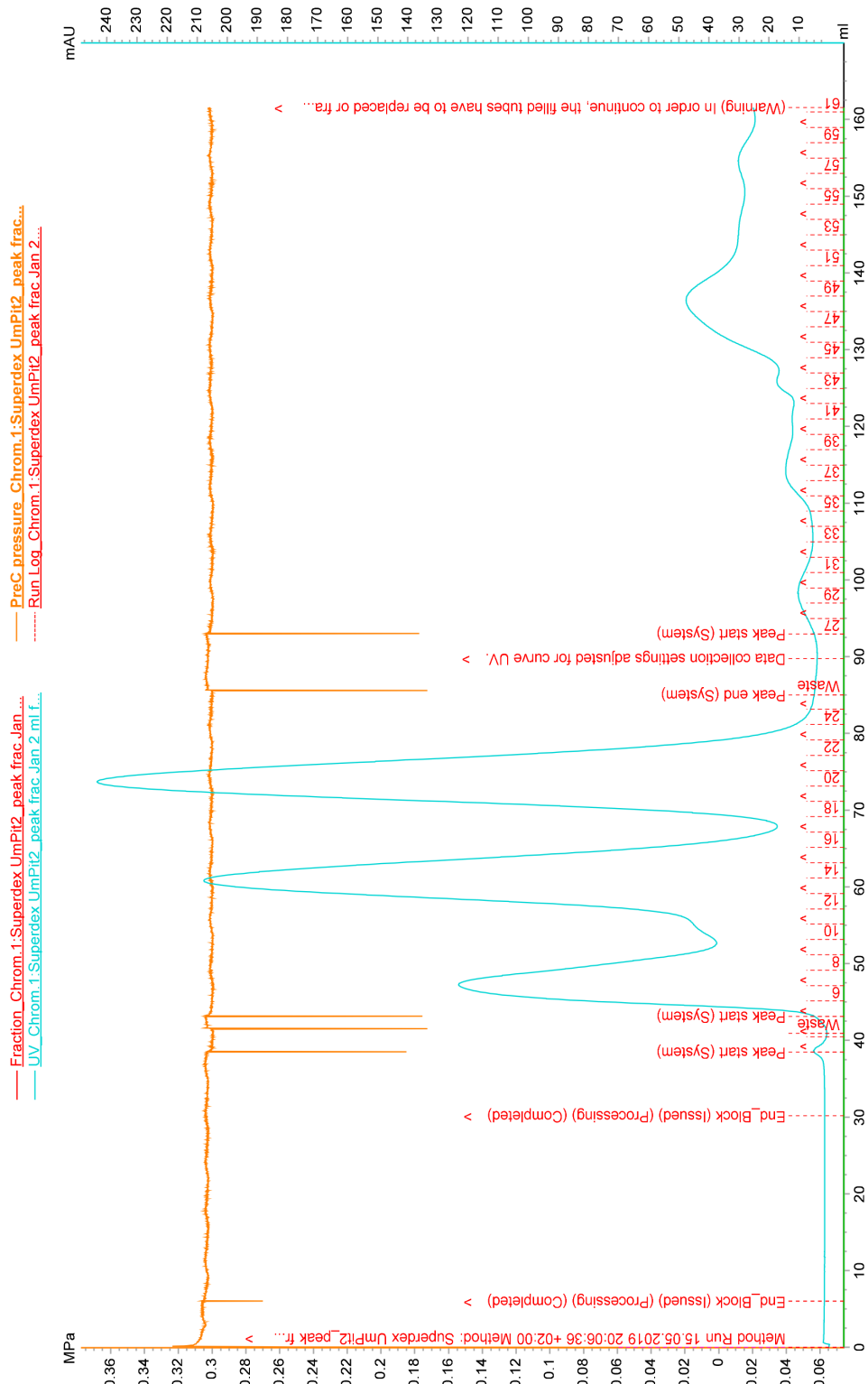
Figure 6.13: **Gel-filtration chromatogram of the purification of recombinant CC1.**
Heterologous produced CC1 was subjected to Ni^{2+}-NTA followed by size exclusion chromatography of Elution 2 and 3 (Figure 22C) using HiLoad® 16/600 Superdex® 75 pg. The left y-axis indicates the pressure in MPa whereas the right y-axis indicates the protein concentration in mAU. Buffer volume is indicated on the x-axis in ml and collected fraction number is noted in red.
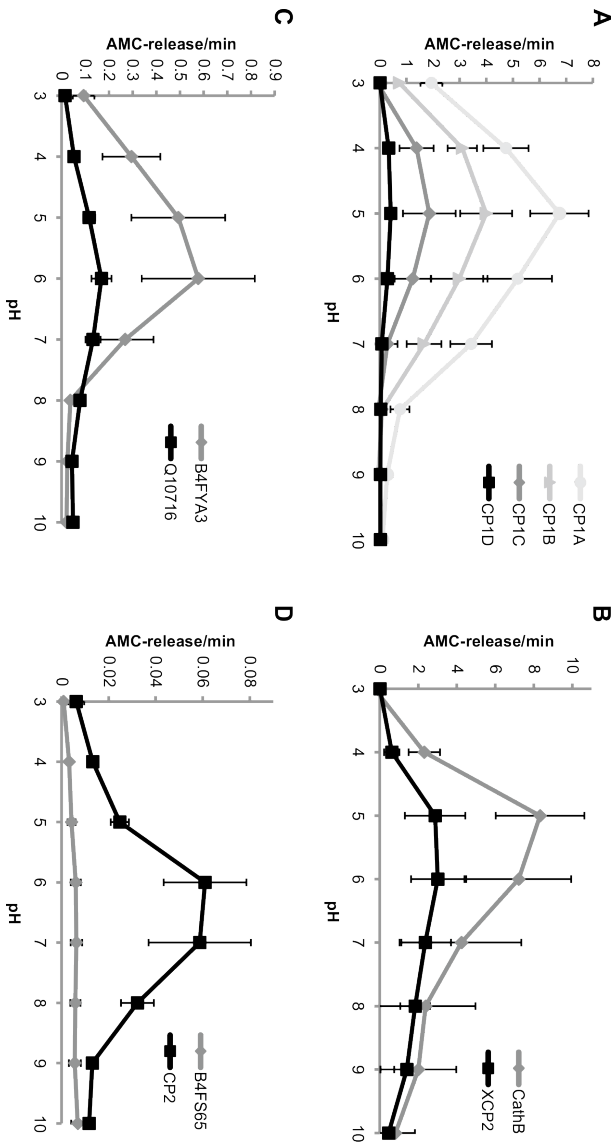
Figure 6.14: **pH dependency of maize root apoplastic PLCPs.**
Apoplastic fluids of recombinant PLCPs produced in *N. benthamiana*: CP1A, CP1B, CP1C and CP1D (**A**), Cathepsin B, XCP2 (**B**), B4FYA3, Q10716 (**C**) B4FS65 and CP2 (**D**) were tested for their activity at different pH (3 to 10) using 10 µM of the substrate Z-LR-AMC as described before. The release of AMC per minute was measured and plotted against pH. Error bars represent the SEM. Activity was normalized to samples treated with E-64. The experiment was performed in three independent biological replicates using technical duplicates.
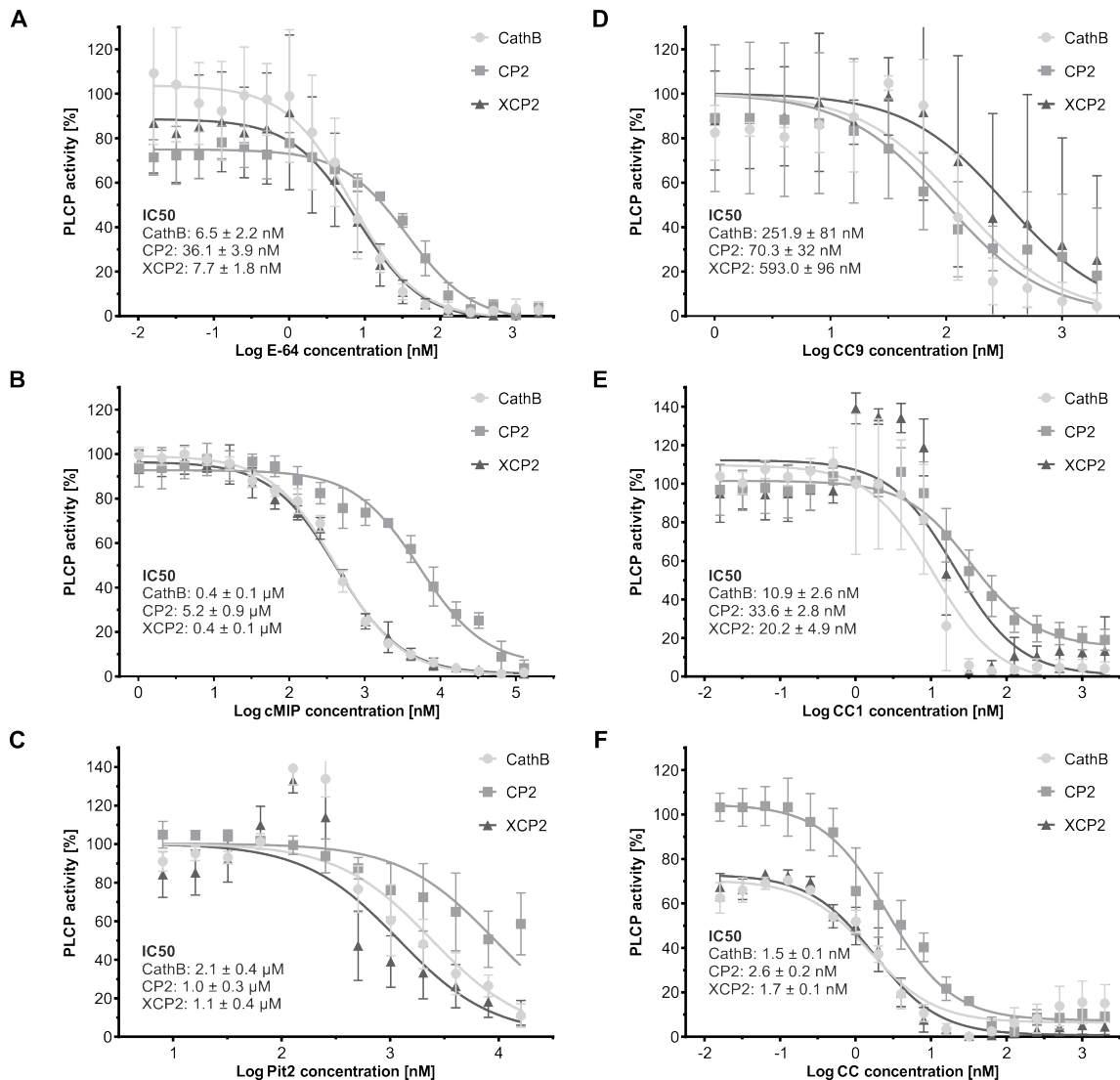
Figure 6.15: **Inhibitory efficiencies of various inhibitors towards the apoplastic PLCPs CathB, CP2 and XCP2.**
Apoplastic fluids of recombinant maize PLCPs CathB, CP2 and XCP2 were tested against E-64 **(A)**, cMIP **(B)**, Pit2 **(C)**, CC9 **(D)**, CC1 **(E)** and CC **(F)**. Apoplastic fluids were evaluated for their activity using 10 µM of the substrate Z-LR-AMC (LR) in the presence of the inhibitors in concentrations as used before. Activity was set to 100% in the absence of inhibitor. Normalized values were plotted against Log of inhibitor concentration. The experiment was performed in three independent biological replicates each with technical duplicates. A nonlinear fit based on a dose response function was performed and IC50-values were calculated. Error bars represent the SEM.
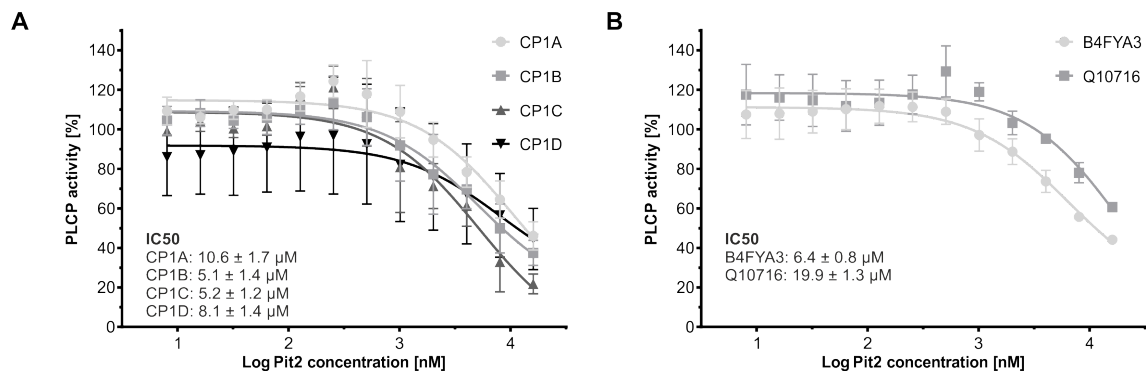
Figure 6.16: **Pit2 inhibitory efficiency towards CP1-like and SA-activated root apoplastic PLCPs.**
Apoplastic fluids of recombinant maize PLCPs CP1A, CP1B, CP1C, CP1D **(A)** and B4FYA3, Q10716 **(B)**
were tested against heterologous expressed Pit2. Apoplastic fluids were evaluated for their activity using 10
µM of the substrate Z-LR-AMC (LR) in the presence of Pit2 as described before. Concentrations ranged from
8 nM to 16 µM. Activity was set to 100% in the absence of inhibitor. Normalized values were plotted against
Log of inhibitor concentration. The experiment was performed in three independent biological replicates each
with technical duplicates. A nonlinear fit based on a dose response function was performed and IC50-values
were calculated. Error bars represent the SEM.
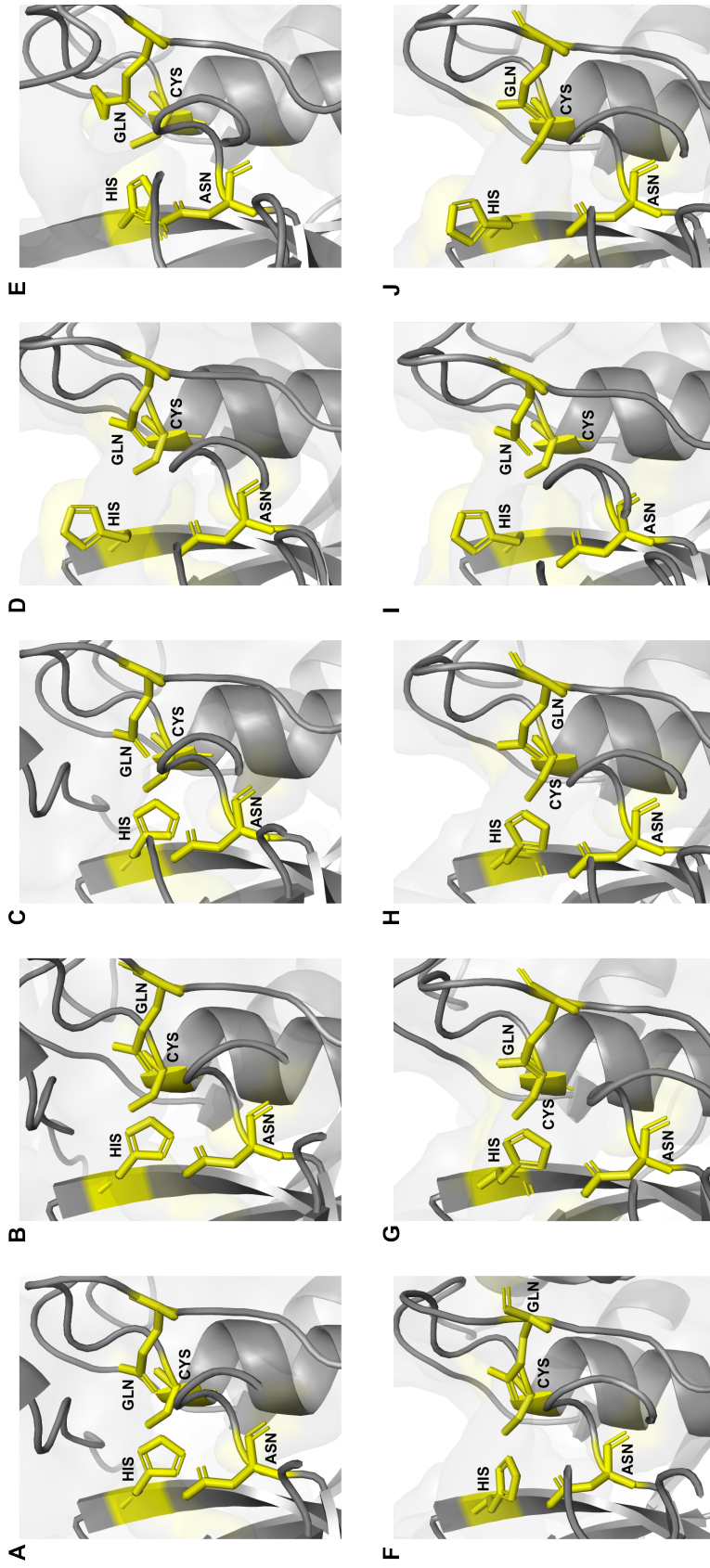
Figure 6.17: **Maize root apoplastic PLCPs differ in the orientation of the imidazole ring of their catalytic HIS.**
Close-up of the active site in 3D-models of the mature root apoplstic PLCPs: CP1A (**A**), CP1B (**B**), CP1C (**C**), CP1D (**D**), CathB (**E**), CP2 (**F**), XCP2 (**G**), B4FS65 (**H**), B4FYA3 (**I**) and Q10716 (**J**) were modelled using Phyre2 based on the crystal structure of caricain PDB: 1pciA for CP1A, CP1B, CP1C, CP1D and B4FYA3, human procathepsin B PDB: d3pbha for CathB, human procathepsin K PDB: d7pcka for CP2 and Amb a 11 cysteine protease PDB: c5egwA for XCP2, B4FS65 and Q10716 (Groves et al., 1996; Podobnik et al., 1997; Sivaraman et al., 1999; Kelley et al., 2015; Groeme et al., 2016). The catalytic Cys, His, Asn and Gln are indicated in yellow.

189
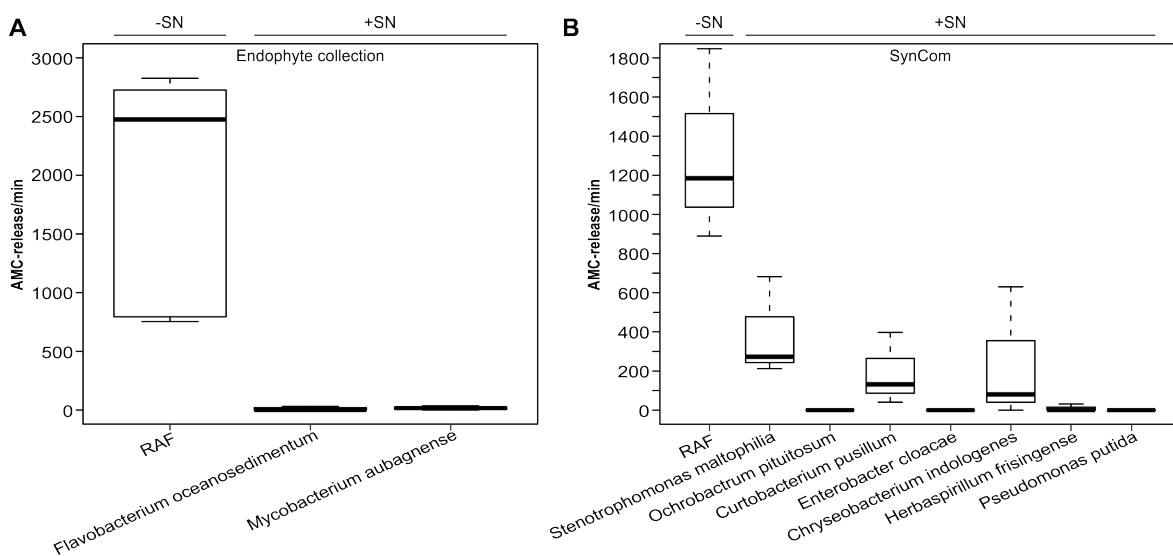
Figure 6.18: **Substrate cleavage activity of bacterial supernatant without RAF.**
60 µl of bacterial culture supernatant of two candidates of endophyte collection **(A)** and the bacterial SynCom **(B)** was isolated and then tested for substrate cleavage activity as described before (2.23A). As a control RAF was used with 60 µl of bacterial growth media instead of bacterial culture supernatant. Data was presented in a boxplot as described before. These experiments were performed using three independent biological replicates each with technical duplicates.
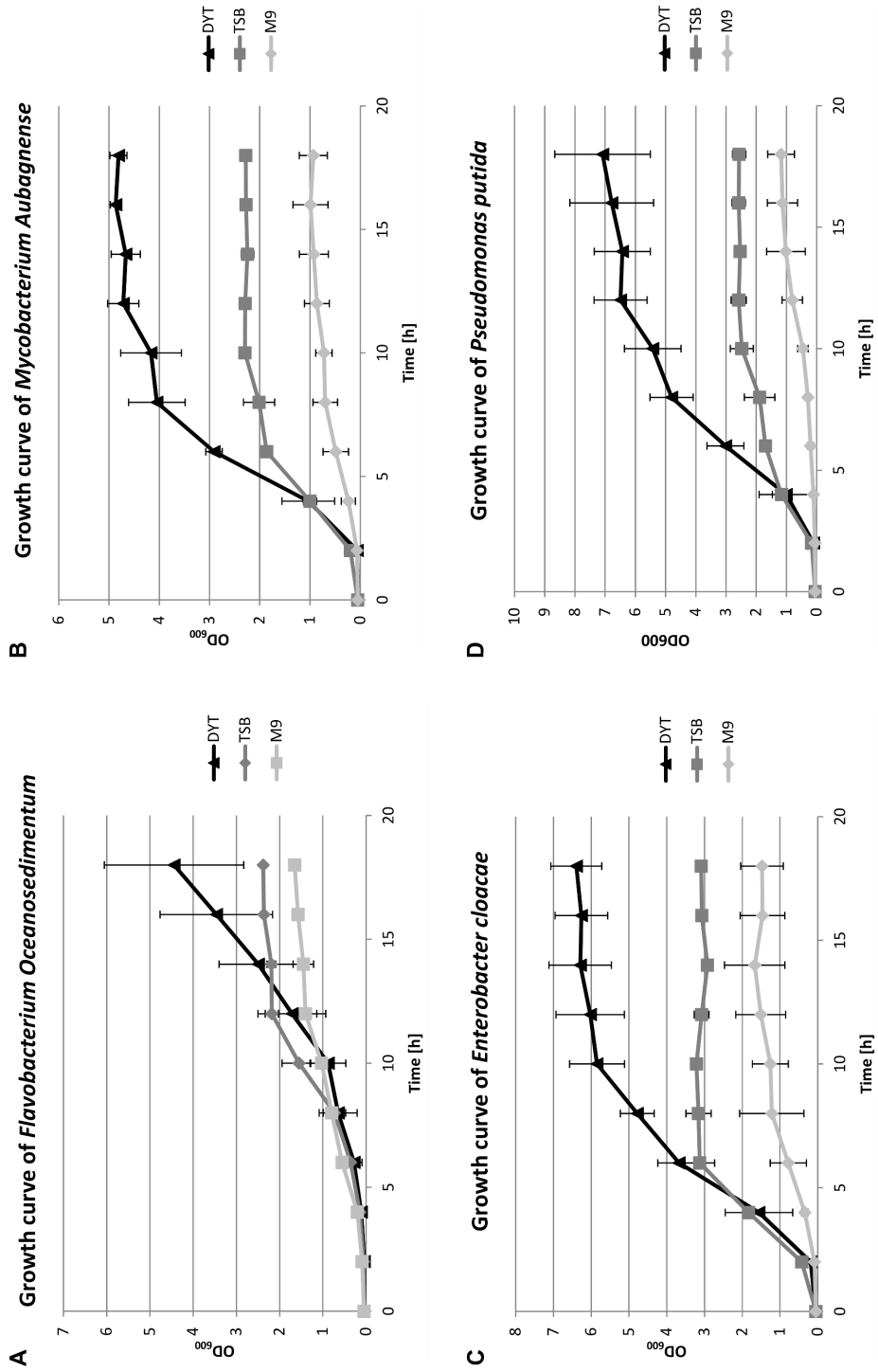
Figure 6.19: **Growth rates of bacterial candidates.**

Growth assays of *F. oceanosedimentum* (**A**), *M. aubagnense* (**B**), *E. cloacae* (**C**) and *P. putida* (**D**) in dYT- and TSB-full media as well as in M9-minimal media. Bacteria were grown in the respective media overnight and set to a starting OD_{600} equal to 0.05. Growth was determined by measuring OD_{600} every two hours in a period of 18 h.
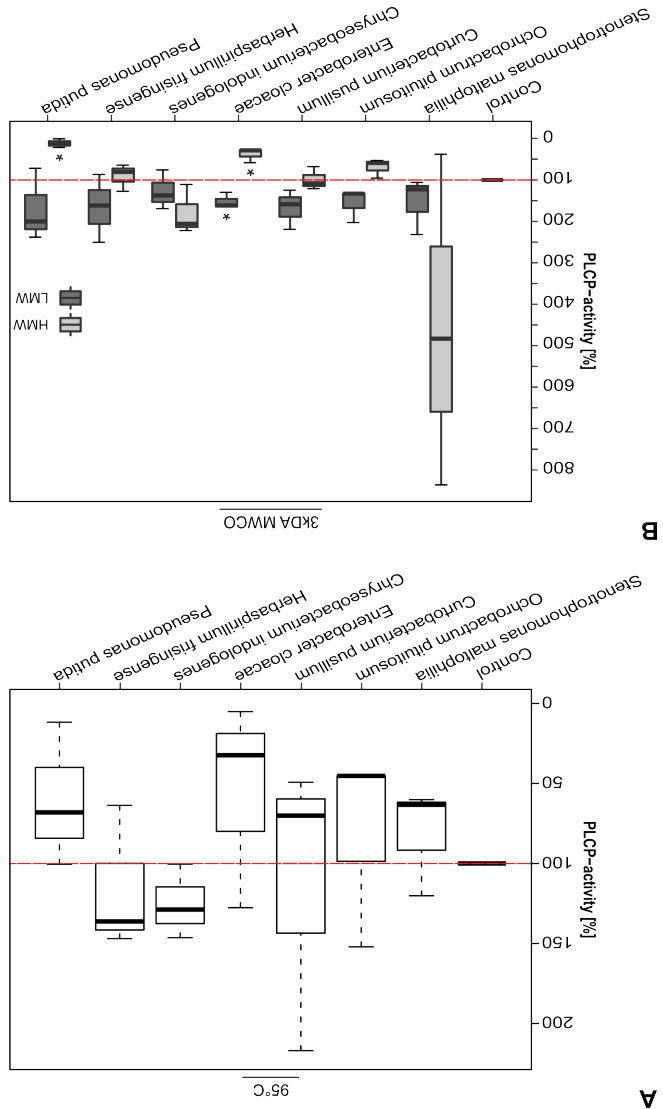
Figure 6.20: Microbial PLCP modulation of SynCom bacteria is protein-derived.
(A) The bacterial culture supernatant of the SynCom, were boiled at 95°C for 15 min in order to denaturate proteins. 60 µl of the supernatants were tested for maize PLCP-inhibition as described before (2.23A). Data was represented in a boxplot as described before. This experiment was performed using three independent biological replicates each with technical duplicates.
(B) The PLCP-inhibitory effect is due to high molecular weight fractions. Culture supernatants of the bacteria tested in (A) were subjected to size separation using a spin column with a cut-off of 3kDA to separate the supernatant into a high molecular weight (HMW) - and low molecular weight (LMW) fractions. Inhibition assays were performed as described before (2.23A). P-values were calculated with an unpaired t-test. *P<0.05.

Eidesstattliche Erklärung

Ich versichere, dass ich die von mir vorgelegte Dissertation selbständig angefertigt, die benutzten Quellen und Hilfsmittel vollständig angegeben und die Stellen der Arbeit - einschließlich Tabellen, Karten und Abbildungen -, die anderen Werken im Wortlaut oder dem Sinn nach entnommen sind, in jedem Einzelfall als Entlehnung kenntlich gemacht habe; dass diese Dissertation noch keiner anderen Fakultät oder Universität zur Prüfung vorgelegen hat; dass sie - abgesehen von unten angegebenen Teilpublikationen - noch nicht veröffentlicht worden ist, sowie, dass ich eine solche Veröffentlichung vor Abschluss des Promotionsverfahrens nicht vornehmen werde. Die Bestimmungen der Promotionsordnung sind mir bekannt. Die von mir vorgelegte Dissertation ist von Prof. Dr. Gunther Döhlemann betreut worden.

Datum: _____ Unterschrift: _____

Publications

Teile dieser Arbeit wurden in folgendem Artikel veröffentlicht:

Schulze Hüynck, J., Kaschani, F., van der Linde, K., Ziemann, S., Müller, A. N., Colby, T., Kaiser, M., Misas Villamil, J. C. & Doehlemann, G. (2019). Proteases underground: Analysis of the maize root apoplast identifies organ specific papain-like cysteine protease activity. Frontiers in Plant Science, 10, 473. doi:10.3389/fpls.2019.00473

Weitere Veröffentlichungen:

Eitzen, K., Schulze Hüynck, J., Schurack, S. & Döhlemann, G. (2019). Krieg und frieden: Molekulares ping-pong zwischen pilzen und pflanzen. BIOspektrum, 25(4), 378–381. doi:10.1007/s12268-019-1064-4

Misas Villamil, J. C., Mueller, A. N., Demir, F., Meyer, U., Okmen, B., Schulze Hüynck, J., Breuer, M., Dauben, H., Win, J., Huesgen, P. F. & Doehlemann, G. (2019). A fungal substrate mimicking molecule suppresses plant immunity via an inter-kingdom conserved motif. Nat Commun, 10(1), 1576. doi:10.1038/s41467-019-09472-8

Abgrenzung der Eigenleistung

Die in dieser Arbeit präsentierten Ergebnisse wurden von mir selbständig ohne andere als die hier aufgeführte Hilfe erarbeitet. Dabei erfolgte die Konzipierung der Experimente und die Erstellung der Publikation „Proteases Underground: Analysis of the Maize Root Apoplast Identifies Organ Specific Papain-Like Cysteine Protease Activity" in Zusammenarbeit mit meinem Betreuer Prof. Dr. Gunther Döhlemann und weiteren in der Publikation aufgeführten Personen. Im Folgenden werden weitere an dieser Arbeit beteiligten Personen sowie deren experimentellen Beiträge genannt:

Dr. Andre Müller und Dr. Stefanie Glaeser
isolierten wurzel-endophytische Bakterien aus Mais der unter Freilandbedingungen kultiviert wurde. Dr. Stefanie Glaeser führte mittels 16s-RNA-Sequenzierung eine Identifizierung der isolierten Bakterien durch. Diese Bakterien sind in 4.1.7.3 aufgeführt und wurden zur Durchführung der Versuche in 2.23C - 2.25 verwendet.

Dr. Andre Müller, Dr. Sebastian Ziemann und Dr. Karina van der Linde
isolierten apoplastische Fluide aus Mais-Blättern und -Wurzeln und führten die IEC-Experimente durch, die zur Anfertigung von 2.2A & B führten.

Dr. Karina van der Linde und Dr. Farnusch Kaschani
führten die DCG-04 pull-down Experimente der IEC-Proben durch, die zur Anfertigung von 2.2C führten.

Dr. Fanusch Kaschani, Prof. Dr. Markus Kaiser und Dr. Thomas Colby
führten die massenspektrometrischen Analysen des Proteomes im Mais Apoplasten durch. Ebenso erfolgte durch sie der anschließende Abgleich mit öffentlichen Datenbanken zur Identifikation der apoplastischen Proteine. Diese Arbeiten führten zur Anfertigung folgender Abbildungen: 2.2D-E, 2.4D-E, 2.5, 2.6.

Nick Dunken
behandelte im Rahmen seiner Bachelorarbeit Wurzeln von *A. thaliana* mit Salicylsäure, isolierte Wurzelextrakt, und führte ABPP-Experimente zur Bestimmung der PLCP-Aktivität durch, die zur Anfertigung von 2.21 führten.

Dr. Jasper Depotter und Henriette Läßle
erstellten die phylogenetischen Stammbäume der Mais PLCPs (2.7) und der Cystatine (2.18B).

Acknowledgement

At first, I would like to express my gratitude to Prof. Dr. Gunther Döhlemann for the opportunity to work in his marvellous group. It was a pleasure to work with such a pleasant and supportive group of people and therefore I have never lacked motivation to come to the lab early in the morning. The work on this project was interesting, motivating, challenging, sometimes exhausting but highly satisfying. Thanks for this project, the freedom to develop it myself, the constructive criticism and enlightening ideas.

A big thank you goes to Dr. Johana Misas-Villamil, who took care of me in the lab. Especially in the beginning you helped me find my way around in the workplace and get used to new methods. Over time, when I eventually mastered lab-work, we started to have more and more fruitful but relaxed discussions about my project over a cup of tea or coffee. Thanks for an always open door and open ear. You contributed a lot to this project and my development as a scientist and I cannot thank you enough for this.

Thank you Prof. Dr. Stanislav Kopriva, for being so kind to be the second examiner for my thesis!

As the people who had a critical look on my work from a different angle, I would like to thank the members of my thesis advisory committee Prof. Dr. Eric Kemen and Prof. Dr. Marcel Bucher. Together with Gunther and Johana, you helped me to set priorities when the project was getting beyond the scope of its investigation and gave advice on the next steps to take.

Apart from all that time of working in the lab, the CEPLAS-graduate school and the GSfBS offered a great mix of excursions, scientific courses and workshops for personal development. I want to thank Justine and Isabell for the programs they prepare every year and for nice chats during one or the other events.

Without Farnusch, there would be no CP1C and no SA-activated PLCP. Thank you for your amazing work on identifying AF proteomes, the friendly phone calls to help me out with Perseus and the great opportunity to be involved in sample preparation in your lab in Essen.
Thanks to the "Hackermann" in our lab, the great wizard of bioinformatics Jasper for lending me the processing power of his precious "Martha" and teaching Henni your wisdom so she could prepare the cystatin tree.
The guys with the green thumbs should not be forgotten here. Thanks to the gardener for watering all our plants and making life so much easier!

Now the time has come to talk about the people who went with me through thick and thin and had to endure all my swearing when Excel/Powerpoint/Word/Firefox/PyMol/Perseus/etc., crashed again. When I am around strangers, I try not to swear but only do so when I am feeling comfortable, so take all the swearing as a compliment! :D
I had a great time with all the members of the Döhlemann group during the past four years and would not swap you for another group. Thanks Bilal, for developing from the grumpy "Morgenmuffel" to a great person to have a chat about science or private stuff, for your weird stories about dead birds or the magic man in Turkey and for a lot of friendly insults and crappy puns.
Thanks to the people who keep the lab running and always offer a helping hand. Thank you Ute, Raphael, and Gudrun! A big thank you goes to Jasper, Malaika and Weiliang for nice chats, a lot

199

of cake-eating and scientific advice! Cheers to Andrea, the new queen of ABPP and cookie eating! Have fun with your grass ;)

What would Charlie have been without his three angels? Luckily, I had the chance to work with three incredible ladies as well. Thanks Elaine, Kathi and Selma for all the funny moments in the lab and beyond. For keeping up with my humour and sweets-addiction and for always having time for a nice cup of coffee :) You have the ability to make work fun and were a big factor in the process that lead to this thesis.

It is great to have people in the lab that you can go for a run with to release some stress. Thanks to Selma for starting to run with me and to Melanie, Japser and Henni that joined in for some time. Cheers to the new generation of PhD-students in this lab, Priyamedha, Luyao, Anna and Yoon Joo! Good luck with your projects and enjoy your time in this marvellous lab!

Since I was talking about the future of the lab, now it is time to talk about people that left already but made the time they were there memorable. Thanks to Zippi, Basti, Elaine and Ali who were there when I started and gave me a hearty welcome. A special thanks goes to Daniel who's sense of humour was perfectly in line with mine, which led to a bunch of amazing times full of stupid jokes. Although in the exile on the other side of the lab, I would like to thank Melanie who was always open for any kind of joke although accompanied with some jabbering ;)

Over the past years I had the chance to meet a lot of great students and try to teach some of them about what I was doing. Fritz and Julio, I hope I could teach you something that you might be able to use in the future. It was a pleasure to work with you!

A special mentioning is reserved for Nick, who was my bachelor-student for several months. It was amazing to see how fast you learned new techniques and started thinking for yourself about your work. I am glad that I did not scare you away from science but that you still stick around AG Döhlemann and stayed in the field. I am looking forward to see your scientific career develop!

It is a rare thing to keep friends for such a long time even though you have been moving a lot and only meet each other once in a while. I am glad to always be able to meet you and feel like nothing really changed! Thanks for great friendships, good parties and amazing festivals, Philip, Erik, Vehlken and all the others!

Never to forget the one and only "Piano man" Konstantin! Another old friend who was willing to read this thesis and gave advise to make it readable! I am looking forward to our next Christmas-meeting. Beer is on me!

Thank you Michelle, for all your understanding and patience especially during the last months when I started writing this thesis. Thank you for providing coffee, distraction and encouraging words, when needed and for all the lovely conversations and moments we had together.

At last I would like to thank my family, especially my mother for all their support. Although, from my Bachelor studies on you lost track of what I was actually doing (something with biology...), you still supported me without any hesitation. During all different steps I took and all the moving from one place to another, you never questioned me but rather asked if I need help on the way. Thanks for your trust in me and my decisions no matter what I was doing.